NICOLAUS COPERNICUS
UNIVERSITY
IN TORUŃ
Centre for Modern
Interdisciplinary Technologies

UNIWERSYTET
MIKOŁAJA KOPERNIKA
W TORUNIU
Wydział Chemii

Novel approach for Low Molecular Weight Compounds analysis using nanomaterials-assisted Laser Desorption/Ionization Mass Spectrometry and Solid-Phase Microextraction

by Radik Mametov, MSc

Thesis submitted for the degree of

Doctor of Philosophy

Supervisor: dr. hab. Paweł Pomastowski, NCU Prof.
Co-supervisor: dr. hab. Aleksandra Radtke, NCU Prof.

Centre for Modern Interdisciplinary Technologies

Faculty of Chemistry, Department of Inorganic and Coordination Chemistry

Nicolaus Copernicus University in Toruń

Toruń 2024

Nowe podejście do analizy związków o niskiej masie cząsteczkowej przy użyciu spektrometrii masowej z jonizacją laserową i desorpcją (Laser Desorption/Ionization Mass Spectrometry) wspomaganej nanomateriałami oraz mikroekstrakcji na stałej fazie (Solid-Phase Microextraction).

The study was financed within the framework of PRELUDIUM-18 grant entitled: "Development of selective coating materials based on conductive polymers for SPME fibers for analysis of VOCs as potential colorectal cancer biomarkers" (Nr. 2019/35/N/ST4/04363) awarded by National Science Center (Poland). In addition, the study was supported by University Center of Excellence , "Towards Personalized Medicine". Where Radik Mametov and Paweł Pomastowski are members.

I would like to dedicate the thesis to my beloved parents, Reshat Mametov and Kulbarshin Mametova, for their unwavering love and belief in me. For extremely high support and for living without restrictions and with limitations that have helped me and were the best choices for me. I am grateful for their suggestions to read certain books that have expanded my understanding of science and technology, as well as for introducing me to movies that broadened my worldview.

I am also thankful for my younger brother, Amir Mametov, who has inspired me to strive to be an example for him. My heartfelt gratitude extends to my extended family, whose support has been a constant throughout my scientific endeavors.

Special appreciation goes to my supervisor, Dr. hab. Pawel Pomastowski, for his reliable support and guidance throughout which enabled me to continue and complete my PhD program. I am also grateful to Dr. hab. Aleksandra Radtke, my co-supervisor, for her understanding, assistance, and support during my studies.

I am also indebted to Prof. Boguslaw Buszewski for providing me with the opportunity to embark on my PhD journey at NCU, and for his motivation and unique but effective supervisory style.

I extend my thanks to Dr. hab. Miroslav Sprynskyy for his support and insightful scientific discussions, particularly during the early stages of my research, and for his expertise in describing sorption processes.

Dr. hab. Małgorzata Szultka-Młyńska deserves my gratitude for assisting me in my initial exploration of conductive polymers.

I am deeply appreciative of my friends in Kazakhstan, especially Timur Akizhanov, his wife Altynay Kuskulova, and their children, for their remote support and interest in my work, as well as for their unwavering friendship.

I am grateful to Dr. Fernanda Monedeiro and Dr. Maciej Monedeiro-Milanowski for their support and friendship, both within and outside the academic sphere.

To my wife, Dr. Gulyaim Sagandykova, my scientific partner, collaborator, and best friend, I owe an immeasurable debt of gratitude for her unwavering belief in me, her incredible support, and her boundless love.

Furthermore, I am appreciative of my colleagues and the administration of ICNT and the Department of Environmental Chemistry and Bioanalytics at the Chemistry Faculty of NCU for their readiness to help and support, as well as for engaging in discussions and providing answers to numerous scientific and life-related questions.

List of contents

Contents **Page**

Acronyms:

LWM – low-molecular-weight

VOC – volatile organic compounds

SPME – solid-phase microextraction

GC-MS – gas chromatography-mass spectrometry

LDI-MS – laser desorption/ionization mass spectrometry

MOF – metal-organic frameworks

ZIF-8 - Zeolitic Imidazolate Framework-8

CP – conductive polymers

PPy – polypyrrole

MALDI – matrix assisted laser desorption/ionization

SALDI – surface assisted laser desorption/ionization

SPR – surface plasmon resonance

LSPR – local surface plasmon resonance

TLC - thin-layer chromatography

LC – liquid chromatography

PCA – principal component analyses

NTD – needle-trap device

NMR - nuclear magnetic resonance

TGA – thermal gravimetric analyses

FTIR - Fourier Transform Infrared Spectroscopy

CVD – chemical vapor deposition

SEM – scanning electron microscopy

TEM – transmission electron microscopy

DLS - dynamic light scattering

Analytical techniques involved for the realization of the aims of the study:

1. Gas chromatography – mass spectrometry
2. Gas chromatography with flame ionization detector
3. Matrix-Assisted Laser Desorption/Ionization Time-of-Flight Mass Spectrometry
4. Surface-Assisted Laser Desorption/Ionization Time-of-Flight Mass Spectrometry
5. Fourier Transform Infrared Spectroscopy
6. Thermogravimetry
7. Scanning Electron Microscopy
8. Transmission Electron Microscopy
9. X-ray Diffraction
10. UV-Vis spectroscopy
11. Dynamic Light Scattering

1. Introduction

Low-molecular-weight compounds (LMW) represent a diverse array of chemical substances characterized by their relatively low molecular weights, typically falling below 1500 Daltons. Within this category, LMW compounds encompass a broad range of molecules, including amino acids, sugars, VOCs, lipids, fatty acids, and hormones, among others. Their significance in chemistry and analytical chemistry stems from their fundamental roles in biological systems, their abundance in natural and synthetic materials, and their utility as building blocks for more complex structures.

In chemistry, LMW compounds serve as essential components in numerous chemical reactions and processes. Their small size and simple molecular structures make them versatile and highly reactive, allowing them to participate in various chemical transformations, such as synthesis, degradation, and modification reactions. Furthermore, LMW compounds often act as precursors or intermediates in the synthesis of larger molecules, including polymers, natural products, and pharmaceutical compounds, making them indispensable in organic chemistry and material science.

In analytical chemistry, LMW compounds are of paramount importance due to their abundance, diversity, and biological significance. Analytical techniques such as chromatography, mass spectrometry, and spectroscopy are routinely employed to detect, quantify, and characterize LMW compounds in complex samples. Their analysis provides valuable information about chemical composition, molecular structure, and functional properties, facilitating research in fields such as environmental science, pharmaceuticals, food science, and biotechnology.

Moreover, LMW organic compounds are mostly represented as metabolites of living organisms including bacteria. Considering modern medicine and allied science' pursuit of personalized medicine, the study of low-molecular-weight compounds is paramount. The main principle of personalized medicine, from an analytical chemistry perspective, involves tailoring medical treatments based on individual characteristics. This involves the use of advanced analytical techniques such as mass spectrometry, chromatography, and spectroscopy to analyze biological samples and identify specific molecules associated with disease states, drug responses, and patient outcomes. By integrating analytical data with clinical information and patient characteristics, personalized medicine aims to optimize

therapeutic outcomes, minimize adverse effects, and improve overall healthcare outcomes on an individualized basis.

Analytical chemistry plays a critical role by providing precise measurements of biomarkers and molecules, enabling tailored diagnosis and treatment for each patient.

There are a lot of analytical techniques for analyses of LMW compounds. Techniques such as gas chromatography-mass spectrometry (GC-MS), liquid chromatography-mass spectrometry (LC-MS), laser/desorption ionization mass-spectrometry (LDI-MS) and nuclear magnetic resonance spectroscopy (NMR) can analyze a broad spectrum of compounds, including polar, nonpolar, volatile, and nonvolatile substances. All mentioned techniques have advantages and disadvantages. The dissertation summarizes four publications aimed at addressing existing limitations and developing new approaches to contribute to research problems related to the analysis of LWM compounds. The articles have been published in journals belonging to Journal Citation Report (JCR) list:

[P1] Mametov R.; Sagandykova G.; Monedeiro-Milanowski M.; Gabryś D.; Pomastowski P. 'Electropolymerized Polypyrrole-MOF Composite as a Coating Material for SPME Fiber for Extraction VOCs Liberated by Bacteria'. *Scientific Reports.* 2023, *13* (1), 1–10. **IF = 4.6 MP = 140.**

[P2] Sagandykova G., Pryshchepa O., Rafinska K., **Mametov R**., Madajski P., Pomastowski P. 'LDI-MS performance of gold nanostars as an inorganic matrix for low molecular weight analytes' *International Journal of Mass Spectrometry*, 478, 116872 (2022). **IF = 1.934 MP = 70.**

[P3] Sagandykova G.; Piszczek P.; Radtke A.; **Mametov R**.; Pryshchepa O.; Gabryś D.; Kolankowski M.; Pomastowski P. 'Silver Nanostructured Substrates in LDI-MS of Low Molecular Weight Compounds'. *Materials (Basel).* 2022, *15* (13). **IF = 3.748 MP = 140.**

[P4] Mametov R.; Sagandykova G.; Monedeiro F.; Florkiewicz A.; Piszczek P.; Radtke A. and Pomastowski P. 'Metabolic Profiling of Bacteria with the Application of Polypyrrole-MOF SPME fibers and Plasmonic Nanostructured LDI-MS Substrates' *Scientific Reports.* 2024, *14, 5562.* **IF = 4.6 MP = 140.**

The cumulative impact factor of the publications included in the thesis: **14.882**.

1.1. Low molecular weight compounds

Low molecular weight (LMW) compounds, also referred to as 'small molecules', are compounds with the molecular weight less than 1500 Da. Due to lack of the common definition, the cutoff limit varies depending on the field, and in some cases can be defined to the value of 1000 Da. LMW compounds include lipids, monosaccharides, second messengers, other natural products and metabolites, drugs and other xenobiotics [1].

In some cases, low molecular weight compounds are volatile. According to definition introduced by European communities [2], the term 'volatile organic compound' (VOC) is any organic compound having, at 293.15 K, a vapor pressure of 0.01 kPa or more, or having corresponding volatility under the particular condition of use'.

Analysis of LMW compounds, their distribution and interactions are of interest in various disciplines, such as chemical biology [3], drug discovery [4], metabolomics [3], food [5] and environmental research [6]. This requires sensitive analytical techniques, since in some cases, they can be found at extremely low concentrations. Additionally, rich chemical composition of the real sample may interfere their analysis via the effect of the matrix. In analytical chemistry, IUPAC defined the matrix effect as 'combined effect of all components of sample other than analyte on the measurement of the quantity. If a specific component can be identified as causing an effect then this is referred to as interference' [7].

Furthermore, since composition of complex real samples include volatile and non-volatile compounds, researchers in various disciplines have to address analysis of both groups. Besides, diversity of structures of low molecular weight compounds may create challenges in their detection by single analytical technique [8]. Therefore, complementary use of analytical techniques is essential for comprehensive characterization of low molecular weight compounds in the real sample of interest.

1.2. Advanced analytical techniques for analysis of LMW compounds: solid-phase microextraction and laser desorption/ionization mass spectrometry assisted with nanomaterials.

1.2.1. Solid-phase microextraction

In addition to importance of sensitive detection, emergence of sample preparation techniques should not be underestimated, especially for overcoming the matrix effect. Traditional sample

pretreatment techniques such as liquid-liquid, Soxhlet, distillation, centrifugation, filtration have multiple limitations such as elevated use of organic solvents, low selectivity. Moreover, they are time- and labor-consuming.

Solid phase microextraction (SPME) – is a sampling technique, used for the extraction and preconcentration mostly of volatile and semi-volatile organic compounds. The method was developed and introduced by Pawliszyn in 1990 [9]. The basic principle of SPME involves the use of a fiber coated with an extracting phase, typically a polymer or a sorbent material, which selectively absorbs the target analytes from the sample matrix. The basic principles of SPME rely on the partition coefficient (K) between the sample matrix and the extracting phase, which is based on Henry's Law:

$$K=Cf/Cs$$

where Cf is the concentration of the analyte in the fiber coating and Cs is the concatenation of the analyte in the sample matrix. The partition coefficient is affected by factors such as the analyte's nature, the sample matrix composition, and the extraction phase properties. The amount of extracted analyte by SPME fiber may be described by the following equation:

$$Q=K\cdot V\cdot Cs$$

where Q is the amount of analyte extracted (in mass or moles), V – volume of the sample matrix, Cs is the concentration of the analytes in the sample matrix.

Typical commercially available SPME fiber consists of a septum-piercing needle (protective needle), sealing septum, ferrule, fiber-attachment needle, screw-hub, and coated SPME fused silica fiber. Nowadays, a few types of coatings are available on the market such as polydimethylsiloxane (PDMS), divinylbenzene (DVB), polyacrylate (PA), polyethylene glycol (PEG), Carboxen (Car), and combination of them. In addition, each type of fiber has several basic coating thicknesses up to 100 micrometers [10]. Commercially produced fibers have some limitations as well. Stability, including thermal and mechanical, compatibility with some matrix types, limited selectivity, and reusability after numbers of cycle sorption/desorption. Moreover, certain types of SPME fibers may be less readily available or more expensive, limiting access for some users or applications.

To evade these limitations, laboratories are developing new coating materials for the production of custom-made SPME fibers. In the last decades, a number of materials were proposed, characterized, and tested [11].

Conductive polymers [12,13], metal-organic frameworks (MOFs) [14,15], ionic liquids [16], nanomaterials, and nanoparticles [17] are the most widespread and used for SPME fibers preparation.

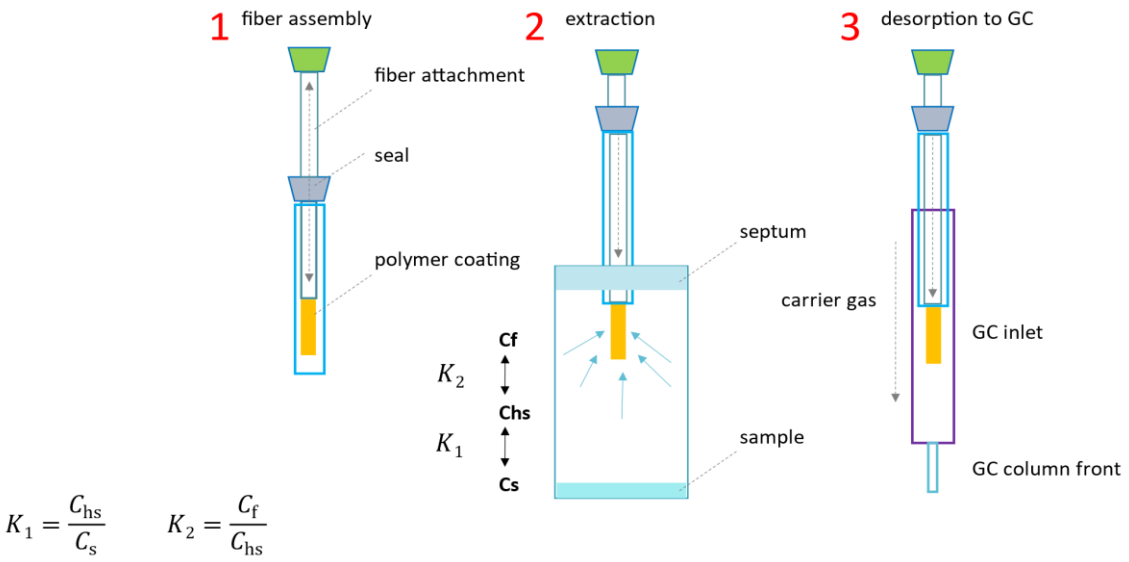

Figure 1. Working principle of Solid-Phase Microextraction

1.2.2. Laser desorption/ionization mass spectrometry

Laser desorption/ionization mass spectrometry (LDI-MS) is a family of analytical techniques used in combination with mass spectrometry. It involves desorbing molecules from a solid or liquid sample by irradiating it with a laser beam, resulting in the formation of ions that a mass spectrometer can analyze. The principle of LDI-MS involve the use of laser energy to vaporize and ionize molecules without significant fragmentation, allowing for the detection and characterization of compounds based on their mass-to-charge ratio (m/z). This technique is particularly useful for the analysis of large biomolecules such as proteins, peptides, and polymers, as well as small organic compounds. LDI was introduced by Hillenkamp and Karas, and independently by Koichi Tanaka, who was awarded the Nobel Prize in 2002 [18].

Nowadays, there are two analytical techniques in LDI-MS field: Matrix-Assisted Laser Desorption/Ionization and Surface-Assisted Laser Desorption/Ionization mass spectrometry. In the case of MALDI, organic matrix absorbs laser energy facilitating desorption and ionization of analytes in the sample by absorption of laser energy. The matrix absorbs the laser energy and facilitates the desorption and ionization of the analyte molecules. MALDI matrices are typically organic compounds such as widely used α-cyano-4-hydroxycinnamic acid (CHCA) or 2,5-dihydroxybenzoic acid (DHB).

In the case of SALDI, rather than relying on organic matrices, desorption and ionization occur through direct interaction with the surface of the target plate. SALDI involves utilization surfaces with specific properties. These surfaces can be metallic [19], metal oxides, MOFs [20], nano- and microstructures with a different sizes and shapes [21,22]. SALDI terminology was proposed by Sunner et al. in 1995 to underscore the significance of the nano substrate in the laser desorption/ionization mechanism [23]. Another fundamental work in the field is development of desorption/ionization on porous silicon (DIOS) introduced by Wei [24]. Due to numerous abbreviations introduced by authors developing LDI-MS methods based on various nanomaterials, there is a need in application of one abbreviation to avoid misunderstanding in the literature since name of the technique is expected to reflect the mechanism of desorption/ionization. Definitions of DIOS and SALDI proposed by IUPAC: ‘DIOS is soft ionization technique alternative to matrix-assisted desorption/ionization involving laser desorption/ionization of a sample deposited on a porous silicon surface’; ‘SALDI is class of matrix-free laser desorption/ionization techniques for biological macromolecules’ [25]. Since

DIOS is a specific case of SALDI, inclusion of those definitions appears unnecessary [26]. However, the use of unified abbreviation, which includes techniques that are cases of SALDI, is paramount. Nevertheless, application of term NALDI in the presented work is necessary since NALDI is LDI technique assisted with nanomaterials, while SALDI include also microstructures. Since nanostructured materials were utilized in the current work, the term NALDI was applied.

Special attention is drawn to metallic nanoparticles of noble metals, such as gold and silver, due to their unique surface plasmon resonance (SPR) properties [22,27]. When metallic nanoparticles are exposed to light, the free electrons on their surface collectively oscillate, leading to localized surface plasmon resonances (LSPRs) [28]. These excited electrons undergo ultrafast relaxation processes, generating a significant amount of heat. This surface-generated heat plays a key role in the desorption process by activating analyte molecules to break bonds in the gas phase and increase analyte desorption efficiency. At the same time, surface electrons above the Fermi level are excited and become hot electrons, which freely transfer to the lowest unoccupied molecular orbital of the absorbed analyte molecule. This process promotes the formation and release of $[M-H]^-$ (neutral hydrogen free radicals), which can enhance analyte ionization efficiency.

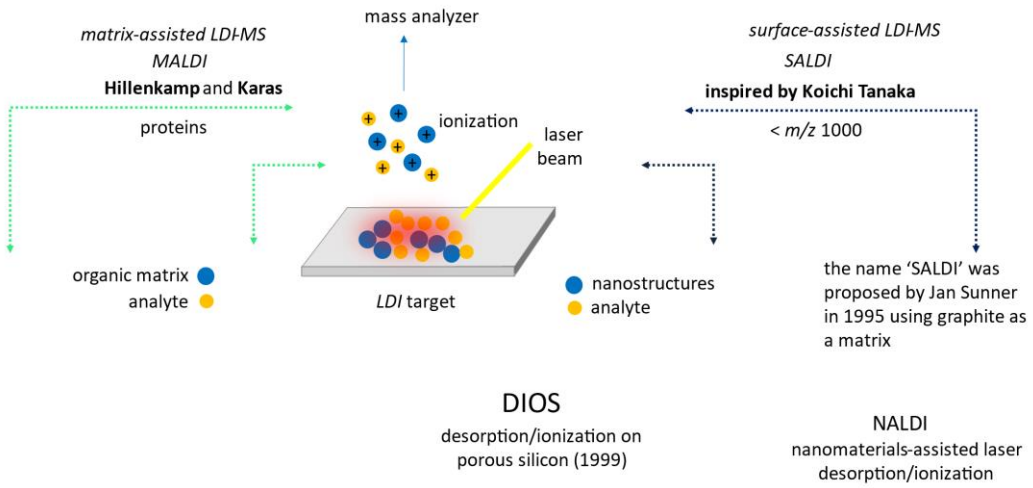

Figure 2. Laser desorption/ionization mass spectrometry

2. Aims and tasks

The main aim of presented research was to fabricate innovative analytical devices for analysis of volatile and non-volatile low molecular weight compounds and investigate potential of their complementary application for metabolic profiling of bacterial strains.

To achieve the aim of research, the following tasks were accomplished:

1. Synthesis, characterization and fabrication of SPME fibers based on modification of the polypyrrole coating material with metal organic frameworks (ZIF-8) for analysis of low molecular weight volatile organic compounds;

2. Synthesis, characterization and investigation of LDI-MS performance of gold anisotropic nanoparticles for analysis of low molecular weight analytes;

3. Synthesis, characterization and fabrication of silver nanostructured LDI-MS substrates for analysis of low molecular weight analytes;

4. Application of polypyrrole@ZIF-8 SPME fibers and silver nanostructured LDI-MS substrates for metabolic profiling of bacterial strains.

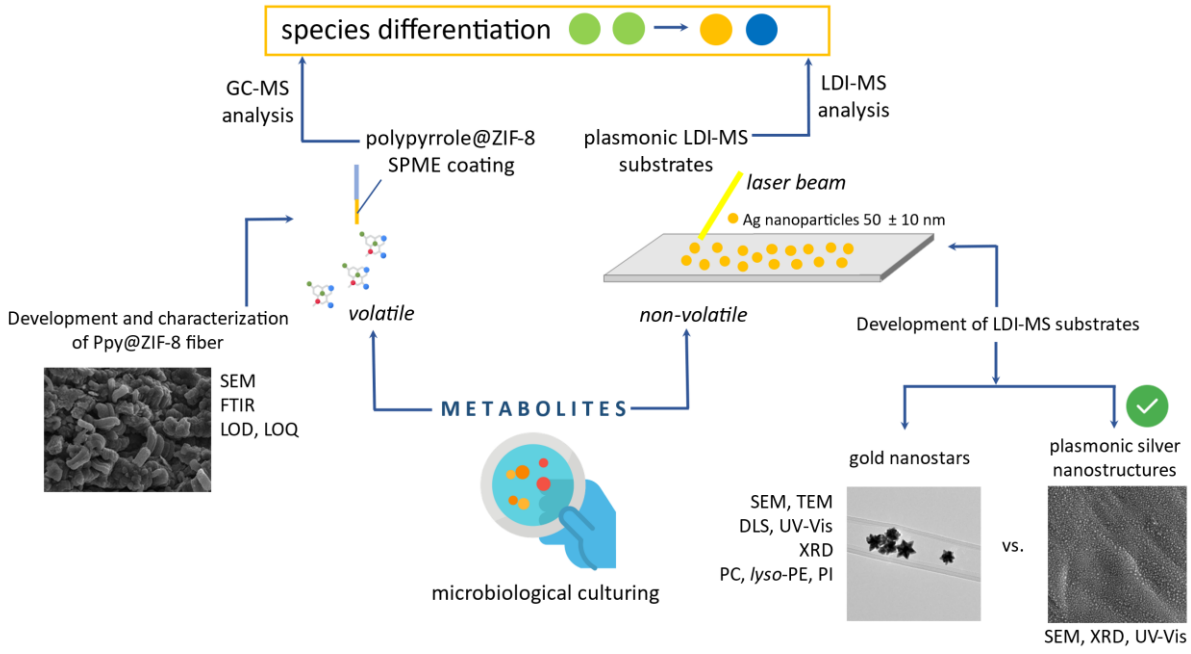

Figure 3. Schematic representation of the workflow of the study.

3. Research problems

3.1. Investigation of the effect of modification of polypyrrole coating material for SPME fibers by metal organic frameworks (ZIF-8) on the efficiency of extraction of low molecular weight compounds;

According to classification, conductive polymers (CP) are materials with a highly π-conjugated polymeric chain, which has the mechanical properties of organic polymers and both electronic properties of metals [29]. Due to the multifunctionality of conductive polymers and their stability, they become more attractive as efficient sorbents for sample preparation purposes. Despite high specific surface areas and the other advantages offered by the commercially available hydrophobic sorbents, they suffer from a basic drawback. Mostly due to their hydrophobic nature, they have poor interaction and retention in the extraction of polar compounds. A wise alternative can be proposed for preparing hydrophilic sorbents by copolymerizing monomers containing suitable functional groups or by introducing a functional group to the existing hydrophobic polymers. This was the basic ideology behind the application of the CPs as a robust sorbent for SPME. CP-based SPME coatings can be categorized into four groups: polypyrrole, polyaniline, polythiophene, and their composites with other materials.

There are a few methods of synthesis of CP, and electrochemical polymerization offer advantages such as relative simplicity and opportunity for synthesis of simultaneously doped conductive polymers, which has an effect on morphology of the coating. Additionally, extended array of cations and anions as dopant ions is available for electropolymerization. Different techniques, such as potentiostatic (constant potential), galvanostatic (constant current), and potentiodynamic (i.e., cyclic voltammetry) methods, can be used for electrochemical polymerization of CPs. Electrochemical synthesis usually results in the deposition of films of conductive polymers to the surface of the supporting electrode by anode oxidation (electropolymerization) of the corresponding monomer. When a positive potential is applied to the working electrode, oxidation begins with the formation of a radical cation. Delocalized cation-radicals induce a radical-radical connection, forming first dimmers during deprotonation at α-position. The expanded polymer coupling results in a reduction in the oxidative potential compared to the monomer. The process of electrochemical oxidation and radical binding is repeated continuously, and finally, the CP film is deposited on the

working electrode. The polymer is usually alloyed at the same time by incorporating an alloying anion into the polymer to ensure the electrical neutrality of the film [30].

In my previous work, I have synthesized, characterized and applied polypyrrole-based coating material for SPME. The obtained fibers exhibited sufficient stability for their utilization in combination with a gas chromatographic system, where the fibers are required to be thermally stable at temperatures > 250 °C. This is particularly important due to the thermal desorption in the GC injector, which operates at high temperatures. Furthermore, the introduction of two counter ions simultaneously enables the production of a stable film with high adhesion to the metallic substrate and a non-homogeneous surface with a surface area of about 220 m^2/g [13].

Given that CP, especially polypyrrole, offers an elevated capacity for modification during one-step synthesis, we selected it as the polymer for subsequent modification with a metal-organic framework in our study.

Metal-organic frameworks (MOFs) are structured three-dimensional polymers formed by the self-assembly of metal clusters or centers with organic ligands using coordinative bonds. These substances possess enduring porosity and retain their crystalline structure even after the removal of solvent molecules, demonstrating thermal stability > 500°C. Due to their crystalline nature, the constituent molecules are organized, ensuring that the pores and cavities maintain uniform diameters within the framework. This is accomplished through a reticular synthesis approach, where metal clusters act as secondary building units (SBUs) that can be linked via suitable organic spacers to create a distinct topology of the coordination network. Consequently, MOFs are customizable materials capable of being tailored to exhibit specific pore sizes and surface environments [31,32].

It is supposed that it is feasible to synthesize an almost unlimited variety of MOF types. For my study, commercially available ZIF-8 was selected for modification of polypyrrole. ZIF-8, or Zeolitic Imidazolate Framework-8, is a type of metal-organic framework known for its unique structure and properties. It is composed of tetrahedral zinc ions (Zn^{2+}) coordinated with imidazolate linkers to form a three-dimensional porous framework. The structure of ZIF-8 resembles zeolites, which are crystalline aluminosilicate materials widely used in industrial applications for their high surface area and porosity. One of the key properties of ZIF-8 is its high surface area (up to 2000 m^2/g), which results from its porous structure. This high surface area makes ZIF-8 suitable for various applications, including separation, catalysis, drug

delivery, and extractions. Additionally, ZIF-8 exhibits exceptional thermal and chemical stability, making it resistant to harsh conditions such as high temperatures and acidic or basic environments [33].

To the best of our knowledge, modification of polypyrrole with MOFs with applications for SPME was not reported previously. Therefore, this research gap was addressed by investigation of the effect of parameters of synthesis (mass of MOF, electropolymerization time) on the analytes' responses aiming at development one-step copolymerization approach for fabrication of SPME fibers. Additionally, after investigation of extraction performance using standard solutions of analytes, polypyrrole-MOF SPME fibers were applied for extraction of VOCs emitted by bacteria. The results were published in a form of research paper entitled '*Electropolymerized polypyrrole-MOF composite as a coating material for SPME fiber for extraction VOCs liberated by bacteria'*.

3.2. Investigation of performance of gold anisotropic nanoparticles in laser desorption/ionization mass spectrometry of low molecular weight compounds;

Various nanomaterials, assisting laser desorption/ionization, such as nanoparticles of noble metals [34,35] and their alloys [36], metal oxides [37], carbon nanoparticles [38] (diamond, colloidal graphite, graphene oxide), core-shell [39], silicon-based [40], metal-organic frameworks and their composites [41] were introduced for analysis of low molecular weight compounds.

Plasmonic nanomaterials such as noble metals nanoparticles, demonstrate optical resonances under the light irradiation, and has attracted much attention as inorganic matrices for LDI-MS. Despite plethora of research papers on the LDI-MS efficiency of nanoparticles of noble metals, the aspect of plasmonic properties has not been addressed.

Occurrence of LSPRs is determined by various factors, such as size, shape, the wavelength of the incident light. Previously, it was suggested that silver is more favorable for demonstrating optical resonances in LDI-MS due to the closeness of resonant wavelength to the UV-laser of the commercially available LDI instruments. In contrast, gold of the nearly spherical shape was suggested to demonstrate the resonant wavelength in the NIR region, which was suggested not to be compatible with the LDI instruments. Plasmonic gold nanoparticles has been investigated only with application of IR-wavelength of the laser [42], not widely available in laboratories, and is considered rather sophisticated. However, tuning of the shape of gold nanostructures may create opportunities for occurrence of LSPRs. According to the theory of Mie, isotropic metal nanoparticles possess a single plasmonic band, while the extinction spectra is dependent on diameter, composition and dielectric environment [43]. Anisotropic metal nanoparticles, which are nanostructures with the shape other than nearly spherical, possess two distinct plasmon bands at longitudinal and transverse directions. Reduced symmetry may provide a plasmonic nanostructure with multiple plasmon bands [44], which potentially extend the window of wavelength to promote oscillation of the valence electrons. However, this particular aspect has not been addressed in the literature. Therefore, presented research was aimed to fill the gap concerning the LDI-MS performance of gold anisotropic nanoparticles for analysis of low molecular weight compounds. For the first time, gold anisotropic nanoparticles, namely gold nanostars, has been investigated as an inorganic matrix assisting LDI of low molecular weight compounds such as biologically active adonitol and lipids. Lipids included 18:0/20:3 phosphatidylinositol, 18:0 *lyso*-

phosphatidylethanolamine and 18:3/20:3 phosphatidylcholine at nanomolar concentrations. Gold nanostars, were synthesized with wet chemical method, and characterized using SEM, TEM, DLS and XRD. Application of gold nanostars showed high sensitivity towards low molecular weight analytes. The results were published in a form of research paper entitled '*LDI-MS performance of gold nanostars as an inorganic matrix for low molecular weight analytes*'.

3.3. Investigation of the effect of mass of precursor on performance of silver nanostructured substrates in laser desorption/ionization mass spectrometry of low-molecular-weight compounds;

In laser desorption/ionization mass spectrometry assisted with nanomaterials, the fabrication technique also has a crucial role in performance. In case of fabrication of inorganic matrix in a form of a solid substrate, synthesis of the nanomaterial is carried out *in-situ* on the target. Inorganic matrix in a form of colloidal nanoparticles suffer from the following drawbacks: (i) reducing and stabilizing agents used in the synthesis may create background interference in the low mass region; (ii) 'coffee-ring' effect may result in inconsistent analytical signal.

Chemical vapor deposition has proven to serve as a versatile technique for synthesis of nanomaterials with defined morphology. In case of fabrication of LDI-MS nanostructured substrates, CVD may bring numerous advantages. First of all, CVD does not require application of additional chemical compounds except for the precursor, which results in its clean decomposition and reduced chemical background not interfering the analysis of low molecular weight compounds. Furthermore, CVD may prevent high costs of substrates' fabrication as compared to nanolithography and sputtering techniques, while not compromising the performance of synthesis. Besides, engineering of substrates with desired morphology and investigation of their LDI-MS performance open new horizons for further development of the research field, different from the 'trial-and-error' approach.

LDI-MS substrates based on silver nanostructures with various size and morphology of particle were largely investigated in the field. Plasmonic properties of silver nanostructures were also addressed, although not receiving as much attention as other groups of inorganic matrices. However, synthesis and fabrication of silver nanostructured substrates using CVD, was not addressed in the literature.

Therefore, this research gap has been addressed in a form of the research paper entitled '*Silver nanostructured substrates in LDI-MS of low molecular weight compounds*'. The results showed that variation in the mass of silver precursor allowed for fabrication of LDI-MS nanostructured substrates with tunable size and morphology. The variation in size and morphology of silver nanostructures resulted in tunable LDI-MS activity. The substrates were characterized using SEM and XRD analyses. The most sensitive substrate resulted from synthesis using 5 mg of silver precursor, resulting in deposition of nanostructures with size 50

$\pm$ 10 nm and nearly homogeneous distribution on the surface of substrate. Besides high sensitivity towards various biologically active low molecular weight compounds, interesting empirical evidence has been collected. All substrates showed fragmentation of polar lipids (phospholipids) as compared to enhanced sensitivity towards non-polar triacylglycerols. On one hand, such fragmentation could be a result of photocatalytic activity of silver, but on the other hand, interaction between non-polar lipids and hydrophobic silver nanostructures also could be a reason. Interaction between the solid LDI-MS substrate and analytes play crucial role [26] in its MS performance, however this aspect is often underestimated. Such performance could be valuable in analysis of real samples, with non-polar lipids, since their analysis represents an analytical challenge and, in many cases, only fractions of polar lipids are characterized.

3.4. Investigation of the potential of polypyrrole@ZIF-8 SPME fibers and silver nanostructured LDI-MS substrates for differentiation of bacterial species and gaining insights into their metabolism with their complementary application.

Metabolomics is a field within the '-omics' sciences that focuses on studying small-molecule metabolites. The complete set of metabolite molecules in a biological sample (cells, tissues, organs, organisms) is known as the metabolome. The metabolome is characterized by a diverse range of chemical structures and varying abundance of small molecules. Due to the dynamic nature of the metabolome, which reflects the continuous flow of metabolic and signaling pathways, multiple analytical platforms are required. Mass spectrometry is the primary technology used in metabolomic research, allowing for determining metabolite spatial distribution in tissues [45]. Nowadays, investigation of bacteria metabolome is one of the promising approaches for identification and differentiation between species, study of antibacterial resistance. Moreover, it may benefit to diagnosis and treatment of numerous diseases caused by pathogenic bacteria.

The metabolites produced by bacteria can be broadly categorized into two groups: volatile and non-volatile. Non-volatile metabolites encompass a diverse range of compounds produced by bacteria that do not readily evaporate into the gas phase under typical analytical conditions. These metabolites play integral roles in various bacterial functions, including energy production, cell growth, communication, and environmental adaptation. They include amino acids, nucleotides, carbohydrates, exopolysaccharides, and lipids, which are commonly analyzed using techniques like liquid chromatography-mass spectrometry (LC-MS) or nuclear magnetic resonance (NMR) spectroscopy. Notably, LDI techniques are finding applications in the analysis of non-volatile bacterial metabolites, promising a streamlined and efficient approach. Among these metabolites, lipids are promising compounds for the investigation of bacteria metabolism. To the best of our knowledge, bacteria contain lipids in their structure, which serve as essential components of their cell membranes, stabilizing the cell membrane, providing cell surface rigidity, participating in metabolic and signaling pathways, and acting as an energy and storage material. Furthermore, besides their passive functions, bacterial lipids also support various cellular functions such as targeted protein transport, DNA replication, and signal transduction [46].

Traditional lipid analysis methods are based on chromatographic techniques, primarily liquid (LC) and thin-layer chromatography (TLC). However, both these widely used techniques

require expertise (LC) or are limited by low resolution (TLC) [47]. Another method used to determine the chemical composition of phospholipid mixtures is nuclear magnetic resonance, which provides information about both composition and structure [48]. Given that the extraction process of lipids is inevitable [49], elimination of the separation step can minimize time and costs of analysis with application of LDI techniques. Besides, due to extreme diversity of lipids' molecules, lipidomic characterization of the sample requires application of several complementary analytical techniques. Furthermore, usually techniques may be limited based on polarity of lipids, for e.g., one of the most widely used techniques such as electrospray ionization mass spectrometry is mostly suitable for polar lipids. Characterization of membrane lipids of bacterial species is relatively new research field, and due to this reason and complexity of the sample matrix, diversity of bacterial species, mostly polar lipids were characterized. In addition, lipidomic characterization has been carried out only for few bacterial species.

Volatile metabolites, conversely, are released into the environment, and their detection and analysis offer valuable insights into bacterial physiology, metabolism, and interactions. Bacteria emit a diverse range of volatile organic compounds, including hydrocarbons, ketones, aldehydes, and esters. These compounds serve various purposes, such as signaling molecules, defense mechanisms, and metabolic byproducts. The study of volatile metabolites paints a vivid picture of bacterial metabolic activity, their interactions with other organisms, and adaptation to ever-changing environments [50]. For the analysis of these metabolites, the following techniques can be employed: solid-phase micro-extraction (SPME), thermal desorption with sorbent tubes (TDTs), and needle trap devices (NTDs). SPME plays a crucial role in *in-vitro* analysis of bacterial VOCs, while TDTs are more commonly used for *in-vivo* applications, including breath analysis to detect bacterial infections [51]. Each of these techniques offers flexibility in selectivity and sensitivity, making it crucial to adapt them to the specific requirements of the study. By exploring these diverse aspects of bacteria identification, metabolomics, and the intricacies of bacterial metabolism, scientists can gain a more holistic understanding of bacterial behavior and its far-reaching implications on human health and disease management.

In my latest publication, the main focus was on demonstrating the potential of complementary application of LDI plates and PPy@ZIF-8 SPME fibers for differentiation and characterization of eight strains of bacteria. This involved metabolic profiling of both volatile and non-volatile

low molecular weight compounds for eight bacterial species and employing data processing techniques such as principal component analysis (PCA), random forest (RF), hierarchical cluster analysis (HCA), and canonical correlation analysis (CCA). Devices demonstrated their potential for differentiation of species of bacteria and complementary use for gaining insights into metabolism. To the best of our knowledge, complete characterization of both volatile and non-volatile metabolites of bacteria has been carried out for the first time. Additionally, application of innovative devices such as silver nanostructured substrates and PPy@ZIF-8 fibers was not reported in the literature beforehand.

The results of investigation were published in a form of research paper entitled '*Metabolic profiling of bacteria with the application of polypyrrole-MOF SPME fibers and plasmonic nanostructured LDI-MS substrates'*.

4. Publications

[P1] Mametov, R.; Sagandykova, G.; Monedeiro-Milanowski, M.; Gabryś, D.; Pomastowski, P. 'Electropolymerized Polypyrrole-MOF Composite as a Coating Material for SPME Fiber for Extraction VOCs Liberated by Bacteria'. *Sci. Rep.* 2023, *13* (1), 1–10. IF = 4.6 MP = 140.

scientific reports

Check for updates

OPEN

Electropolymerized polypyrrole-MOF composite as a coating material for SPME fiber for extraction VOCs liberated by bacteria

Radik Mametov[1]✉, Gulyaim Sagandykova[1], Maciej Monedeiro-Milanowski[1], Dorota Gabryś[2] & Paweł Pomastowski[1]

The synthesis of efficient and low-cost coatings for solid-phase microextraction attracted much attention. Conductive polymers are excellent candidates for this purpose due to the possibility of electropolymerization, which results in the reproducible synthesis of films. A plethora of studies reported in the literature concluded that modification of conductive polymers with innovative materials could lead to an increase in sensitivity toward specific analytes. In this work, the metal–organic framework-polypyrrole composite was electrodeposited in one step directly onto a stainless-steel substrate. The effect of synthesis parameters on extraction efficiency was investigated. The obtained PPy@ZIF-8 coating was subjected to physical–chemical characterization using electron microscopy and Fourier-transform IR spectroscopy. The main finding of the study was that the values of the limit of detection and intra- and inter-day reproducibility for analytes with different chemical structures were found to be lower as compared to pure polypyrrole coating. Furthermore, the obtained polypyrrole-MOF coating was applied for the collection of profiles of volatile organic compounds liberated by bacteria. Hence, the polypyrrole@ZIF-8 coating synthesized using a low-cost and facile approach presented in this study can be useful for the profiling of VOCs liberated by bacteria.

Solid-phase microextraction (SPME) techniques are facile and solvent-free in comparison to exhaustive traditional sample preparation technologies[1,2]. Since its first introduction in 1990, developing analytical methods based on SPME for various applications is a constantly evolving research area. Diverse SPME tools were successfully introduced, such as in-tube SPME, needle trap, and single-drop microextraction[3].

SPME is useful in many fields, such as environmental research, food chemistry, and pharmaceutical and biomedical analysis[4]. One of the relatively recent applications of SPME concerns the analysis of volatile organic compounds emitted by bacteria.

Traditional methods for the identification of pathogens, such as culturing and biochemical tests, suffer from numerous limitations. The major disadvantage is that the procedure is laborious and time-consuming[5]. Nucleic-based and matrix-assisted laser desorption/ionization techniques tackle the limitations of traditional methods offering rapid and accurate identification[6]. However, there is a constant demand for the development of analytical techniques for bacterial identification since metabolic alterations of bacterial species complicate identification.

To the best of our knowledge, the identification of volatile organic compounds (VOCs) is an opportunistic approach to the detection of pathogenic bacteria[7] and a way to understand different metabolomic processes[8]. The advantage of VOCs' profiling is uncomplicated sample preparation. Extraction methods such as headspace solid-phase microextraction (HS-SPME), thermal desorption, purge-and-trap, and needle trap are used for profiling bacterial VOCs[9]. Headspace solid-phase microextraction (HS-SPME) is a popular extraction method for profiling bacterial VOCs, combining extraction and pre-concentration in one step.

[1]Centre for Modern Interdisciplinary Technologies, Nicolaus Copernicus University in Toruń, Wileńska 4, 87-100 Toruń, Poland. [2]Radiotherapy Department, Maria Sklodowska-Curie National Research and Institute of Oncology, Gliwice, Poland. ✉email: mametov.radik@gmail.com

However, the application of SPME in biomedical research requires low values of a limit of detection. This leads to the development of SPME fibers based on various materials. A few types of materials were presented, such as ionic liquids, metal–organic frameworks (MOF), conductive polymers, nanomaterials, and their composites[10]. In addition, commercially available fibers have some disadvantages, such as lack of thermal stability, high price, and fragility. For this reason, developing new types of SPME fibers on the stainless steel wire with new sorbent types is actual[11].

Hence, the study aims to report a facile, low-cost method for the electropolymerization of polypyrrole-MOF composite as a coating material for SPME fiber. The new-coated SPME fibers will be used to extract VOCs emitted by bacteria.

Conductive polymers are favourable for application as a coating material for SPME. The materials' multifaceted properties include polar functional groups, electroactivity, π–π interactions, and hydrophobicity[12]. The most widely used representatives are polypyrrole, polyaniline, polythiophene, and composites based on them[11]. For the study, polypyrrole was chosen as a base for the new coatings, since our research team has already reported about electropolymerized PPY-coating for SPME fibers[13].

The metal–organic framework Basolite Z1200 (ZIF-8) was used as a modification agent to improve the extraction efficiency of PPy-based fibers.

MOFs are hybrid inorganic–organic materials constructed from organic ligands and metal ions. Various metal ions and organic linkers make it possible to synthesize massive types of new MOFs with different structures, surface area, porosity, etc. Nowadays, MOFs are used for various applications in analytical chemistry[14]. In particular, there is a considerable amount of studies on applications of MOFs as sorbent materials for the different extraction and separation techniques. Examples are applications in the solid-phase extraction as a sorbent, the filling/support materials for the chromatographic columns, the microextraction techniques, etc.[15].

Zeolite imidazole's frameworks (ZIFs) are a subclass of MOF materials. ZIFs are formed by the transition of metal ions (Zn) and imidazolates linkers[16]. In particular, ZIF-8[16] has high thermal and mechanical stability and a surface area > 2000 $cm^2 g^{-1}$. In addition, ZIF-8 is a water-stable MOF, which prevents loss of sensitivity since water occupies the sorption sites interfering with analytes. Furthermore, this allows for applications of the coating not only for headspace SPME, but also for direct immersion SPME from solution, thus extending the application field.

Notably, the adhesion of MOFs towards metallic substrate is a limitation for its use as the coating for SPME fibers. Few studies addressed the problem by synthesis of polydimethylsiloxane (PDMS)[16]. This means that hybrid composites can tackle the limitations of a single material.

Rare efforts have been made to synthesize SPME fibers based on conductive polymers with metal–organic frameworks. Bagheri et al.[17] reported headspace-SPME fibers based on polyaniline-MOF nanocomposite synthesized with electropolymerization in one step.

Experimental

Reagents and materials. Basolite Z1200 (2-Methylimidazole zinc salt, ZIF-8), Pyrrole (98%), Brain Heart Infusion Agar (BHIA), sodium dodecylbenzene sulfonate, sodium perchlorate, acetonitrile (≥ 99.9%), methanol (≥ 99.9%), acetone (≥ 99.5%), hydrofluoric acid (48%), benzene, toluene, p-xylene, ethylbenzene, dodecane, phenol and 1-bromo-4-fluorobenzene (BFB) as analytical standards were all purchased from Sigma-Aldrich. Water was obtained using the Milli-Q RG apparatus by Millipore (Millipore Intertech, Bedford, MA, USA). Stainless steel wire (d = 0.1 mm) was purchased from a commercial source (BS Nižpol, Przemyśl, Poland).

Gas chromatographic analyses for standard solutions were performed with a gas chromatograph GC 7820A coupled to a flame ionization detector (Agilent, Santa Clara, CA, USA). The GC was equipped with an HP-5 analytical column (30 m × 0.32 mm i.d. and film thickness 0.25 µm). Helium (99.99%) and air were used as carrier and make-up gases, respectively. Injections were performed in the splitless mode. GC injector port operated at 220 °C. The initial oven temperature was 30 °C (held for 3 min), ramped at a rate of 4 °C min^{-1} to 50 °C (held for 1 min), then increased to 70, 100 (held for 1 min), and 200 °C at the rates of 5 °C min^{-1}, 7 °C min^{-1} and 40 °C min^{-1}, respectively. The final oven temperature was kept for 3 min. Make-up gas, hydrogen, and synthetic air flow were maintained at 30 mL/min, 30 mL/min, and 300 mL/min, respectively. The carrier gas flow rate was 2.4 mL/min. The detector operated at 300 °C.

Gas chromatographic analyses for the VOCs liberated by bacteria were carried out with a gas chromatograph GC 7820A coupled with a mass spectrometer Agilent 5977B MSD (Agilent Technologies, Waldbronn, Germany). The GC was equipped with a DB-5 MS capillary column (30 m × 0.25 mm × 0.25 µm). Helium was used as the carrier gas in constant flow mode at 1 ml/min. Injections were performed in spitless mode. GC injector port operated at 220 °C. The initial oven temperature was 40 °C (held for 4 min), ramped at a rate of 7 °C min^{-1} to 150 °C (held for 2 min), then increased to 250 °C at a rate 10 °C min^{-1}. The final oven temperature was kept for 5 min.

The mass spectrometer was operating in the EI (70 eV) mode. The ion source temperature was set to 230 °C, and the transfer line was set to 250 °C; acquisition frequency was set at 2.9 scans/s, and the mass range was 35–550 a.m.u. Compounds were identified by comparing their mass spectra with those contained in the NIST mass spectral library version 2017; each peak was searched manually (including baseline subtraction and averaging over a peak).

Electrochemical synthesis of the PPY@ZIF-8 coating. Stainless-steel wire was etched with hydrofluoric acid for 30 min at 40 °C to increase the surface area, consequently improving the adhesion between substrate and coatings[15]. Then it was washed with distilled water and dried for 30 min at room temperature. In the next step, the wire was immersed in the beaker with methanol and placed in the ultrasonic bath for 10 min. The procedure was repeated with acetone, followed by drying in nitrogen flow. Polypyrrole-MOF composite was directly electrodeposited on the prepared stainless steel substrate. An electrochemical cell consists of a working

electrode (etched SS wire) and a counter electrode SS wire twisted into a circle. To the best of our knowledge, MOFs are insoluble in our working media[17]. A specific amount of the MOF was dispersed in the 0.1 M pyrrole solution and stirred in the ultrasonic bath for 10 min to obtain the homogenous suspension. In the next step, the suspension was added to the electrolyte mixture consists acetonitrile/water (50:50), $NaClO_4$ (7 mM), $C_{18}H_{29}NaO_3S$ (7 mM), 0.1 M pyrrole monomer, and 0.006 g of MOF. Then SS wire (13 mm) was inserted into the reactive solution as the working electrode. A constant potential of 5 V was applied for different times from 15 to 45 min. After deposition, the fiber was sequentially washed with methanol and distilled water to remove excess of the reaction mixture and dried at room temperature for 2 h. Then the coated polypyrrole-MOF wire was connected to a lab-made SPME holder. Further, the fiber was conditioned in the GC injector port for 2 h at 200 °C using a 25 mL/min helium flow and then for 2 h more at 220 °C using a 35 mL/min helium flow. After this procedure, a clean blank was obtained, and analyses of blank samples were repeated after every three runs of standard samples to ensure the absence of contaminants.

Physico-chemical characterization of synthesized coating material. *Scanning electron microscopy.* Surface morphology characterization of the polypyrrole-MOF coating was carried out by scanning electron microscope (SEM, LEO 1430 VP, Leo Electron Microscopy Ltd., Cambridge, United Kingdom).

Fourier-transform infrared spectroscopy. FTIR spectra of synthesized coating material were obtained by using an FTIR spectrophotometer with attenuated total reflectance (FTIR-ATR) using a Nicolet FT-IR apparatus (Thermo Fisher Scientific, Avatar 360 Omnic Sampler) from 4000 to 500 cm^{-1}.

Utilization of obtained fiber for extraction of VOCs from standard solution. A stock solution containing benzene, toluene, ethylbenzene, *p*-xylene, phenol, dodecane, and BFB was prepared in methanol with a concentration of 1 mg mL^{-1} for each compound. 50 µL of stock solution was spiked in 2950 µL of distilled water to rich approximate concertation of each analyte 16.66 µg mL^{-1}. All extraction procedures were performed in 20-mL headspace vials with PTFE septa. Initially, a magnetic stirring bar (10 mm) and 1 g of sodium chloride were added to each vial and closed to prevent sample losses. The vials were then placed on the magnetic stirrer with the heating plate. Extraction parameters included a temperature of 30 °C, a pre-incubation time of 17 min, an extraction time of 49 min, stirring at 750 rpm, and the addition of 1 g of sodium chloride. Desorption was carried out at a temperature 220 °C for 5 min. The parameters of extraction for the selected group of VOCs were optimized in our previous work by using Box–Behnken design response surface method[13]. This method allowed us to compare the efficiency of the new composite coating with different synthesis parameters, as well as to understand the affinity of the coatings for different groups of analytes and the potential relationships between them.

Determination of limit of detection, intra-, and inter-assay reproducibility. The limit of detection (LOD) values were determined by analysis of standard solutions with decreasing concentrations of analytes. The solutions were prepared by successive dilutions of a stock solution at a concentration of 17 µg mL^{-1} for each analyte in triplicate. Detection limits were defined as the lowest concentration that provided a signal-to-noise ratio of at least 3 and was significantly different from the blank. Inter-assay reproducibility was determined by analysis of the stock solution for three consecutive days. Intra-assay reproducibility was determined by analysis of the stock solution in triplicate.

Application of the obtained fiber for extraction of VOCs emitted by bacteria. Three species of bacteria (*Hafnia alvei, Proteus mirabilis, Enterococcus faecalis and Morganella morgani*) were isolated from feces samples of patients with diagnosed colorectal cancer. Biological material was plated on Petri dishes with Brain Heart Infusion Agar (BHIA) using sterile loops, and after growing in an incubator for 24 h under CO_2, the pure cultures were obtained using the streaking method. The bacteria were identified using Bruker MALDI Biotyper® software on the ultrafleXtreme MALDI-TOF/TOF mass spectrometer (Bruker Daltonics, Bremen, Germany) equipped with a modified Nd:YAG laser (Smartbeam IITM) operating at the wavelength of 355 nm and the frequency of 2 kHz and used to acquire spectra from strains of bacteria. Identified bacterial strains were deposited at − 80 °C using Microbank®, which is a unique cryovial system incorporating treated beads and a special cryopreservation solution.

After deposition, all three investigated bacteria were cultivated in headspace 20 mL vials with magnetic polytetrafluoroethylene/silicon screw caps. First of all, the vials were filled with autoclaved BHIA (4 mL) under a laminar chamber and stood in a diagonal position to obtain slants with a solid medium. Then, the slants were inoculated with a sterile loop holding one of the beads with selected bacteria. The vials were closed with screw caps, previously treated with UV light to pre-sterilize the surface. The vials with content were placed in an incubator for 24 h at 37 °C.

After incubation, the vial was placed in the heater with a set temperature of 37 °C for the extraction procedure. Later, lab-made fiber was inserted into the vial for the headspace extraction for 20 min. Next, fiber was immediately transferred to the GC injector for 5 min of desorption at 220 °C. Such procedure was repeated for the three types of bacteria and extraction of VOCs from the pure media[18].

Human subject research. Ethical approval for this study was received by Institutional Review Board of Maria Sklodowska-Curie National Institute of Oncology in Gliwice (agreement number code KB/430-78/22,

date of approval 26 June 2022). The study was conducted according to the approved guidelines outlined in the Declaration of Helsinki. Informed consent was obtained from all participants prior to enrolment in the study.

Results and discussion

Previously, we reported the synthesis of SPME fiber based on polypyrrole[13]. The fiber showed adequate reproducibility and values of the limit of detection in the range 0.59–283.33 ng mL^{-1} for standard solutions of VOCs. Yet, further progress can be made beyond this point. Conductive polymers, in particular polypyrrole, are flexible materials for modifications[10].

There are two ways to introduce modifications into the structure of conductive polymers. Firstly, it is the incorporation of different counter ions. It has been shown that even the size of the incorporated ion may affect the morphology of the polymer coating and, subsequently, its selectivity[19]. The second way is the introduction of applicable functional groups or co-deposition of nanomaterials, MOFs, ionic liquids, or other monomers to the polymer[11].

Metal–organic frameworks possess high porosity and surface area, which is favourable for the preparation of extraction coatings. Besides, the chemical structure of MOFs may enable additional interactions between analytes and coating, which can contribute to the specificity of the fiber towards some analytes/groups of analytes and thus decrease the limit of detection. Hence, we hypothesized that introducing MOFs as modifications to the structure of polypyrrole may decrease the limit of detection. To the best of our knowledge, pure PPy coatings have different porosity and morphology depending on synthesis parameters[19]. The surface area of PPy films can reach more than 220 m^2/g[13].

Surface characterization of the PPy@ZIF-8 coating. *SEM.* SEM analysis showed the porous and nonhomogeneous structure of the obtained PPy@ZIF-8 film (Fig. 1b). Figure 1 demonstrated the differences in morphology of the coatings based on PPy and PPy@ZIF-8. Therefore, the incorporation of ZIF-8 into the polymer probably affected its structure (Fig. 1).

Since the film thickness of the coating may affect the extraction efficiency, the value of film thickness was estimated based on the SEM pictures and the well-known diameter of the stainless-steel substrate (Fig. 1c). The value of film thickness varied within the range between 65 and 72 μm.

FTIR-ATR spectroscopy. The results of FTIR-ATR spectroscopy displayed the pyrrole ring band at $\nu = 1520\ cm^{-1}$ for both PPy and PPy@ZIF-8 coatings (Fig. 4). Vibrations at $\nu = 1455\ cm^{-1}$ for coatings (i) and (ii) may correspond to the formation of sulphonamides since vibrations in the range 1420–1370 cm^{-1} are characteristic of mono-n-substituted sulphonamide bond ($-SO_2-NH-$)[20]. The spectra of PPy@ZIF-8 coating showed distinct bands at 1165, 695 and 758 cm^{-1} (Fig. 2). The band at 1165 cm^{-1} corresponds to the C–N bonds, the band at 758 cm^{-1} corresponds to the Zn–O bonds, and 695 cm^{-1} corresponds to Zn–N bonds in the imidazole group[21]. Hence, the spectra suggest the incorporation of ZIF-8 into PPy polymer.

The study of the effect of parameters on the analytes' responses. Crucial parameters that affect the electrochemical synthesis of nanocomposite based on polypyrrole and MOF are time, amount of MOF, and voltage. Variation of the voltage resulted in a loss of mechanical stability, which was observed by the loss of the coating in an attempt to insert it into the GC inlet. Hence, the effect of time and amount of MOF was studied at a constant value of voltage.

According to obtained results (Fig. 3), the time of the synthesis affected the extraction performance of the coating based on polypyrrole and ZIF-8. The increase in time of synthesis improved the extraction efficiency for all analytes except phenol. The highest value of extraction performance was achieved at a time 35 min. A decreasing trend in signal intensity was observed for all analytes at a time 45 min. The highest response for phenol was obtained at a time 35 min (Fig. 3). In addition, even the synthesis time 15 min provided higher response as compared to previously reported PPy fiber[13].

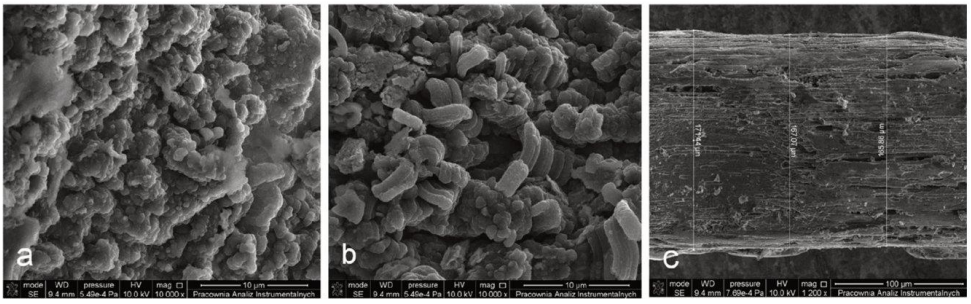

Figure 1. SEM images of the synthesized coatings: (**a**) PPy, (**b**) PPy@ZIF-8, (**c**) stainless steel support coated by PPy@ZIF-8.

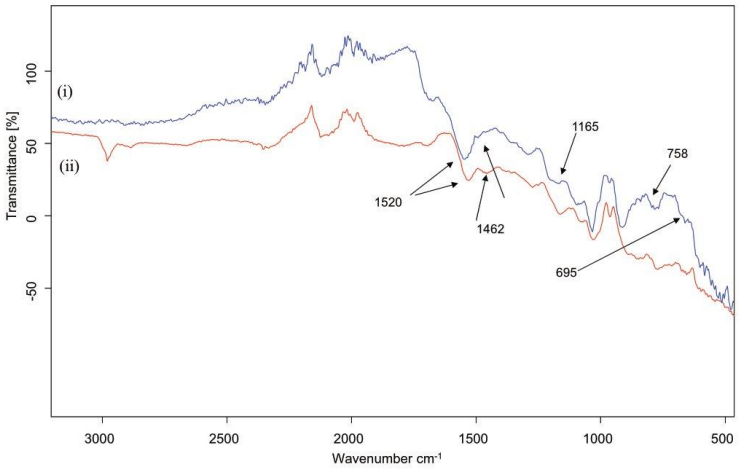

Figure 2. FTIR-ATR spectra of the synthesized coatings: (i) PPy@ZIF-8 and (ii) PPy.

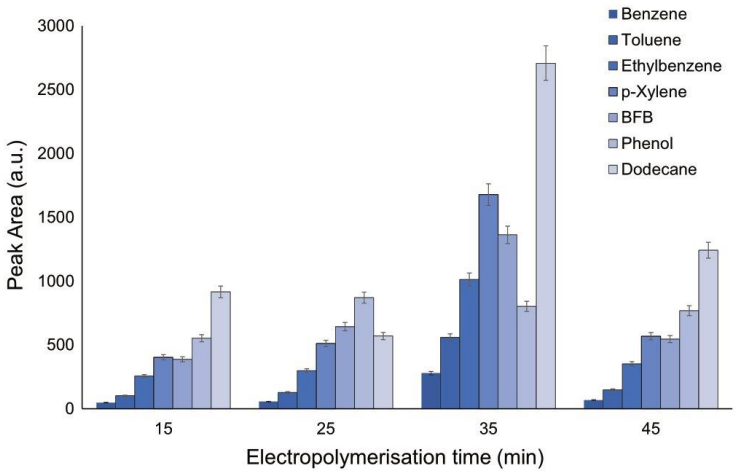

Figure 3. The effect of time of synthesis on responses of analytes extracted by coating based on PPy@ZIF-8.

The following parameter that affected the extraction performance is the amount of ZIF-8 that was added to the electrolyte-monomer solution. According to obtained results (Fig. 4), variation in the amount of added MOF provided significant differences in the extraction efficiency of resulting coating for some of the analytes. Figure 2 showed that 6 mg provided the highest responses for all analytes. The lowest values of RSDs were also obtained in case of addition of 6 mg of ZIF-8 to the reaction solution (Fig. 4).

The mass of ZIF-8 > 9 mg added to the reaction solution resulted in poor adhesion of the coating towards the stainless-steel wire. The mass < 3 mg resulted in the analytes responses similar to pure PPy coating, which probably indicated that ZIF-8 did not participate in composite formation.

Hence, the following parameters were selected for synthesis of PPy@ZIF-8: time 35 min, 6 mg of ZIF-8 and applied voltage 5 V.

Utilization of obtained fiber for extraction of VOCs from standard solution. To the best of our knowledge, it is challenging to measure the mechanical stability of the fiber, and in particular, the adhesion

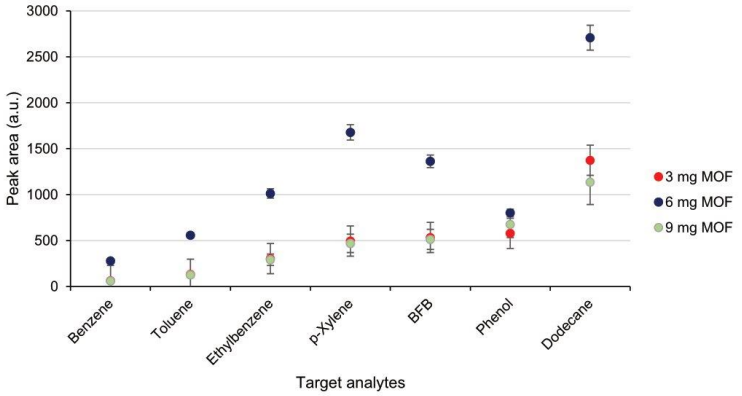

Figure 4. The effect of the amount of ZIF-8 added to the reaction mixture on responses of analytes extracted by coating based on PPy@ZIF-8.

	PPy	PPy@ZIF-8	$logk_{ow}$
Analyte	LOD, ng mL^{-1}		[ref.]
Benzene	102.55	12.73	2.13[22]
Toluene	107.4	18.47	2.54[22]
Ethylbenzene	96.7	1.67	90.5[22]
p-Xylene	52.2	4.99	45.0[22]
BFB	0.71	0.09	0.59[23]
Phenol	298.68	18.14	8.0[24]
Dodecane	7.55	0.73	0.59[25]

Table 1. The values of LOD for PPY and PPY@ZIF-8 coatings.

	PPy@ZIF-8		PPy	
	Intra-assay	Inter-assay	Intra-assay	Inter-assay
Analyte	RSD, %		RSD, %	
Benzene	3.71	4.10	2.1	5.11
Toluene	3.95	2.66	1.1	6.58
Ethylbenzene	4.50	5.70	3.08	4.12
p-Xylene	4.43	5.82	5.74	6.08
BFB	6.94	11.65	4.22	3.18
Phenol	9.26	11.69	4.54	10.85
Dodecane	11.83	9.47	11.54	12.87

Table 2. Intra- and inter-assay reproducibility for selected VOCs extracted using PPy@ZIF-8 coating.

between coating and support. For this reason, the responses of analytes and the corresponding value of standard deviation were considered for the assessment of fiber stability.

The values of the limit of detection (Table 1) and intra- and inter-assay reproducibility (Table 2) were calculated for PPy@ZIF-8 and PPy coatings. In order to assess the effect of PPy modification on LOD value, extraction of selected VOCs has been carried out at the same conditions that were optimized previously for PPy coating.

Table 1 showed significant differences in the values of LOD for extracted VOCs with the utilization of pure PPy and PPy@ZIF-8 coatings. The lowest value of the limit of detection was found for dodecane (Table 1). Such differences probably can be caused by the higher volatility of dodecane and the smallest value of its log k_{ow}. In

addition, Chang et al.[26] suggested that the selectivity of ZIF-8 coatings for the *n*-alkanes probably can be explained by the suitability of the pores' aperture.

Notably, the LOD values of selected VOCs for PPy@ZIF-8 coatings were found to be lower than those obtained for PPy coating, even at extraction conditions optimized for pure PPy coating. This means that the LOD value of PPy@ZIF-8 coating potentially can be found to be even lower than the values presented in Table 1.

The values of LOD for benzene homologs such as toluene, *p*-xylene extracted by PPy@ZIF-8 were found to be lower than for pure PPy coatings (Table 1). This probably can be explained by the general affinity of polypyrrole to benzene homologs due to π–π interactions[10] and π–π stacking owing to the imidazole group of ZIF-8[26].

Table 2 demonstrated that the values of relative standard deviation were found to be less than 12%. The data in Tables 1 and 2 indicated that modification of the PPy coating with ZIF-8 resulted in an increase in sensitivity for different groups of VOCs. The RSD value of the fiber-to-fiber reproducibility (inter-batch studies) is less than 15% for each chosen analyte. Reduction in extraction efficiency of PPy@ZIF-8 fibers was observed to the values in the range of 15–20% after 30 cycles (sorption/desorption) depending on analyte.

The linear range has also been investigated within PPy@ZIF-8 fibers (Fig. 5). The linear range for all analytes accounted for 1–20 μg mL^{-1}, except for dodecane. It can be explained by higher volatility of dodecane as compared to the rest of analytes as can be demonstrated by the value of $logk_{ow}$ (Table 1).

Extraction of VOCs emitted by bacteria with the utilization of the PPy@ZIF-8 coating. Literature data indicated that comparison of profiles of VOCs liberated by bacteria might assist in the identification and differentiation between the species[27,28]. In addition, monitoring of VOC profiles liberated by bacteria was reported as an alternative method to assess changes occurring in bacterial metabolism[29]. Therefore, we aimed to investigate the extraction performance of the PPy@ZIF-8 coating for VOCs liberated by three bacterial species.

Before starting the sample analysis, pre-conditioned fibers were exposed to the headspace of empty sterile vials, and blank analyses were carried out. In addition, culture media used for bacteria inoculation was also analysed. All signals originating from blank analyses (potentially fiber material) and culture media were excluded from identification and were not considered.

However, the effect of extraction time on VOCs' responses emitted by bacteria was not studied in the current study since standard conditions used (extraction time 20 min) in case of PPy@ZIF-8 fibers provided reliable extraction performance. Since such parameters have a significant effect on extraction performance, the results obtained at standard extraction conditions potentially indicated that study of the effect of parameters on extraction performance for selected bacterial species may show improvement in extraction performance for those species, which emit VOCs at low concentration levels.

A total number of 405 volatile organic compounds were observed for three bacterial species and culture media. After the removal of signals originating from blank analyses and culture media, a total of 140 compounds was observed for 3 species such as *Hafnia alvei, Proteus mirabilis* and *Enterococcus faecalis*. After separation, different groups of VOCs were identified, and the predominant groups of volatiles were: hydrocarbons, ketones, alcohols, short-chain fatty acids, and sulphur-containing compounds.

Chromatogram corresponding to *Enterococcus faecalis* is presented in Fig. 6 as an example.

The list of identified compounds in the case of *Enterococcus faecalis* is shown in Table 3. The complete list of compounds including those originating from culture media and blank analyses is shown in Table S1. GC–MS

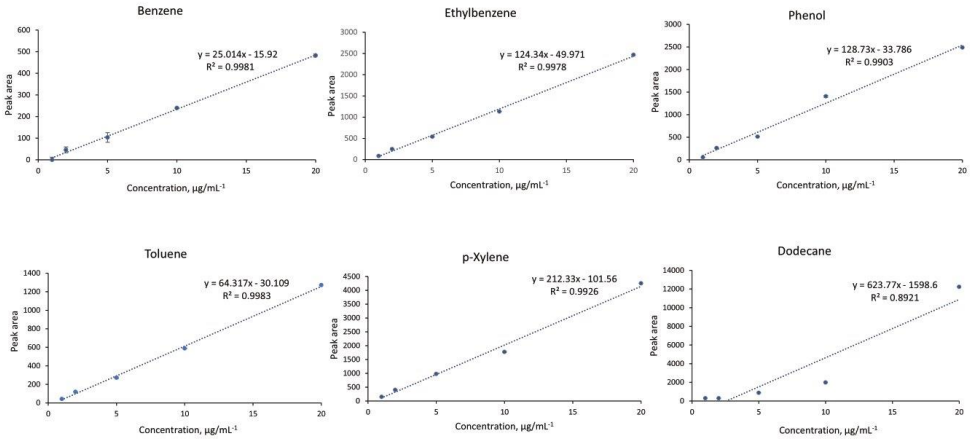

Figure 5. Calibration curves for 6 studied analytes extracted with utilization of PPy@ZIF-8 coating at the following parameters: 30 C, magnetic stirring at 750 rpm, 1 g of NaCl, pre-incubation time 17 min, extraction time 49 min.

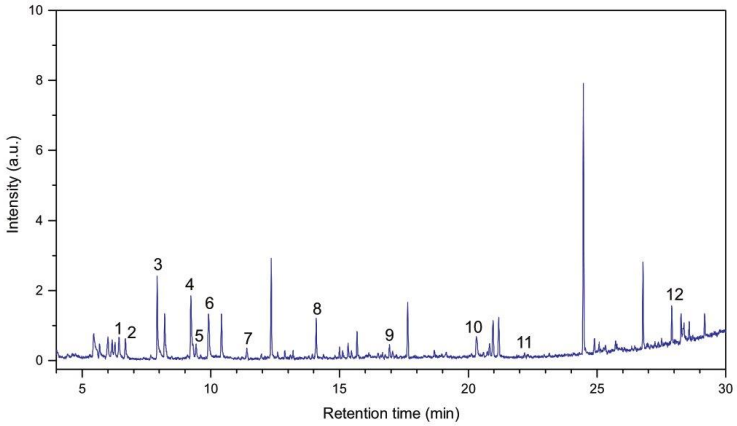

Figure 6. GC–MS chromatogram of VOCs liberated by *Enterococcus faecalis* extracted with the utilization of PPy@ZIF-8 coating.

Peak	Compound	RT, min	Area
1	Ethylbenzene	6.425	106,199.3
2	*p*-Xylene	6.684	101,417.6
3	Cyclobutanol	7.666	21,150.53
4	Benzaldehyde	9.225	367,384.2
5	Dimethyl trisulfide	9.425	69,062.53
6	Phenol	9.907	273,315.6
7	Cathinone	11.966	19,642.11
8	1-Octanamine, N-methyl-	14.378	19,088.77
9	D-Alanine	16.489	17,278.31
10	2,4-Di-tert-butylphenol	21.183	165,678.2
11	Ethyne, fluoro-	23.148	10,694.75
12	Heptacosane	27.906	126,643.2

Table 3. Volatile organic compounds liberated by *Enterococcus faecalis*.

chromatograms of VOCs liberated by *Hafnia alvei*, *Proteus mirabilis* and *Morganella morgani* can be found in Supplementary Information (Figs. S1–S3).

To the best of our knowledge, it is challenging to determine specific VOCs for bacterial species for several reasons. However, despite differences in culture media and methods, VOCs identified in this study partially agree with previously conducted research.

Nowadays is no recognized specific volatile compound dedicated to *Enterococcus faecalis*. However, several research groups proposed sets of VOCs, which were distinct and hence, potentially may serve as biomarkers for *Enterococcus faecalis* differentiation. Storer and co-authors measured VOCs liberated by bacteria in urine samples by SIFT-MS. Such VOCs as 2-pentanone, acetone, 2-methylbutanal, ammonia, dimethyl disulphide, dimethyl sulphide, ethyl butanoate, formaldehyde, hydrogen suphide, methyl mercaptan and propyl acetate were proposed as potential biomarkers[27].

Another study has described the application of IMR-MS coupled with a headspace autosampler as a system to identify VOC liberated by *Enterococcus faecalis*. They carried out the measurements after incubation for 4, 8, and 24 h. Propanal, propanol, acetone, ethanol, isoprene and 1,3-butadiene were detected[28].

Conclusion

In this study, we presented a facile, cost- and labour-effective method for the synthesis of SPME fiber based on polypyrrole@ZIF-8 composite. The effect of the time of synthesis and mass of ZIF-8 on the sensitivity and stability of the coating was investigated. Direct electropolymerization of the PPy@ZIF-8 coating onto stainless steel wire allowed for the synthesis of the composite in one step. Such an approach prevented time-consuming and laborious synthesis protocols described in the literature.

Physical–chemical characterization of PPy@ZIF-8 coating has been carried out with utilization of scanning electron microscopy and FTIR-ATR spectroscopy. The values of limit of detection and intra- and inter-day reproducibility were found to be lower as compared to pure PPy coating for different groups of analytes, suggesting the validity of the main hypothesis of the current investigation. Furthermore, a significant increase in the sensitivity of PPy@ZIF-8 coating allowed for the profiling of VOCs liberated by bacteria.

Hence, PPy@ZIF-8 showed potential to be applied as a tool for the study of bacteria VOCs profiles.

Data availability

The datasets used and/or analysed during the current study available from the corresponding author on reasonable request.

Received: 31 March 2023; Accepted: 29 May 2023
Published online: 01 June 2023

References

1. Reyes-Garcés, N. *et al.* Advances in solid phase microextraction and perspective on future directions. *Anal. Chem.* **90**, 302–360 (2018).
2. Arthur, C. L. & Pawliszyn, J. Solid phase microextraction with thermal desorption using fused silica optical fibers. *Anal. Chem.* **62**, 2145–2148 (1990).
3. Piri-Moghadam, H., Alam, M. N. & Pawliszyn, J. Review of geometries and coating materials in solid phase microextraction: Opportunities, limitations, and future perspectives. *Anal. Chim. Acta* **984**, 42–65 (2017).
4. Zheng, J. *et al.* Fabrications of novel solid phase microextraction fiber coatings based on new materials for high enrichment capability. *TrAC Trends Anal. Chem.* **108**, 135–153 (2018).
5. Tait, E., Perry, J. D., Stanforth, S. P. & Dean, J. R. Use of volatile compounds as a diagnostic tool for the detection of pathogenic bacteria. *TrAC Trends Anal. Chem.* **53**, 117–125 (2014).
6. Carbonnelle, E. *et al.* MALDI-TOF mass spectrometry tools for bacterial identification in clinical microbiology laboratory. *Clin. Biochem.* **44**, 104–109 (2011).
7. Lough, F., Perry, J. D., Stanforth, S. P. & Dean, J. R. Detection of exogenous VOCs as a novel in vitro diagnostic technique for the detection of pathogenic bacteria. *TrAC Trends Anal. Chem.* **87**, 71–81 (2017).
8. Schulz, S. & Dickschat, J. S. Bacterial volatiles: The smell of small organisms. *Nat. Prod. Rep.* **24**, 814–842 (2007).
9. Franchina, F. A., Purcaro, G., Burklund, A., Beccaria, M. & Hill, J. E. Evaluation of different adsorbent materials for the untargeted and targeted bacterial VOC analysis using GC×GC-MS. *Anal. Chim. Acta* **1066**, 146–153 (2019).
10. Lashgari, M. & Yamini, Y. An overview of the most common lab-made coating materials in solid phase microextraction. *Talanta* https://doi.org/10.1016/j.talanta.2018.08.077 (2019).
11. Bagheri, H., Ayazi, Z. & Naderi, M. Conductive polymer-based microextraction methods: A review. *Anal. Chim. Acta* **767**, 1–13 (2013).
12. Bagheri, H. & Mohammadi, A. Pyrrole-based conductive polymer as the solid-phase extraction medium for the preconcentration of environmental pollutants in water samples followed by gas chromatography with flame ionization and mass spectrometry detection. *J. Chromatogr. A* **1015**, 23–30 (2003).
13. Mametov, R., Sagandykova, G., Monedeiro, F. & Buszewski, B. Development of controlled film of polypyrrole for solid-phase microextraction fiber by electropolymerization. *Talanta* **232**, 122394 (2021).
14. Bazargan, M., Ghaemi, F., Amiri, A. & Mirzaei, M. Metal–organic framework-based sorbents in analytical sample preparation. *Coord. Chem. Rev.* **445**, 214107 (2021).
15. Omarova, A., Bakaikina, N. V., Muratuly, A., Kazemian, H. & Baimatova, N. A review on preparation methods and applications of metal–organic framework-based solid-phase microextraction coatings. *Microchem. J.* **175**, 107147 (2022).
16. Liu, X., Fu, J., Wang, L. & Wang, C. Polydimethylsiloxane/ZIF-8@GO sponge headspace solid-phase extraction followed by GC-MS for the analysis of lavender essential oil. *Anal. Biochem.* **622**, 114167 (2021).
17. Bagheri, H., Javanmardi, H., Abbasi, A. & Banihashemi, S. A metal organic framework-polyaniline nanocomposite as a fiber coating for solid phase microextraction. *J. Chromatogr. A* **1431**, 27–35 (2016).
18. Milanowski, M. *et al.* Profiling of VOCs released from different salivary bacteria treated with non-lethal concentrations of silver nitrate. *Anal. Biochem.* **578**, 36–44 (2019).
19. Wu, J. & Pawliszyn, J. Solid-phase microextraction based on polypyrrole films with different counter ions. *Anal. Chim. Acta* **520**, 257–264 (2004).
20. Socrates, G. *Infrared and Raman Characteristic Group Frequencies. Tables and Charts* (Wiley, 2001).
21. Huang, D. *et al.* Synergistic effects of zeolite imidazole framework@graphene oxide composites in humidified mixed matrix membranes on CO_2 separation. *RSC Adv.* **8**, 6099–6109 (2018).
22. Šoštarić, A., Stojić, A., StanišićStojić, S. & Gržetić, I. Quantification and mechanisms of BTEX distribution between aqueous and gaseous phase in a dynamic system. *Chemosphere* **144**, 721–727 (2016).
23. Health, S., Technical, R. & Agency, U. S. E. P. Provisional Peer-Reviewed Toxicity Values for Azodicarbonamide. (2014).
24. Makovskaya, V., Dean, J. R., Tomlinson, W. R. & Comber, M. Octanol-water partition coefficients of substituted phenols and their correlation with molecular descriptors. *Anal. Chim. Acta* **315**, 193–200 (1995).
25. Souza, E. S. *et al.* Estimating the octanol/water partition coefficient for aliphatic organic compounds using semi-empirical electrotopological index. *Int. J. Mol. Sci.* **12**, 7250–7264 (2011).
26. Chang, N., Gu, Z. Y., Wang, H. F. & Yan, X. P. Metal-organic-framework-based tandem molecular sieves as a dual platform for selective microextraction and high-resolution gas chromatographic separation of n-alkanes in complex matrixes. *Anal. Chem.* **83**, 7094–7101 (2011).
27. Storer, M. K., Hibbard-Melles, K., Davis, B. & Scotter, J. Detection of volatile compounds produced by microbial growth in urine by selected ion flow tube mass spectrometry (SIFT-MS). *J. Microbiol. Methods* **87**, 111–113 (2011).
28. Dolch, M. E. *et al.* Volatile organic compound analysis by ion molecule reaction mass spectrometry for Gram-positive bacteria differentiation. *Eur. J. Clin. Microbiol. Infect. Dis.* **31**, 3007–3013 (2012).
29. Reese, K. L., Rasley, A., Avila, J. R., Jones, A. D. & Frank, M. Metabolic profiling of volatile organic compounds (VOCs) emitted by the pathogens *Francisella tularensis* and *Bacillus anthracis* in liquid culture. *Sci. Rep.* **10**, 1–17 (2020).

Acknowledgements

The study was financed by The National Science Centre (Poland) in a framework of the Preludium 18 project No. 2019/35/N/ST4/04363 (2020–2022). The authors would like to acknowledge dr. Katarzyna Rafińska for technical support and Oleksandra Pryshchepa for the scientific criticism and discussion.R.M. and P.P. are members of

Toruń Center of Excellence "Towards Personalized Medicine" operating under Excellence Initiative-Research University (Torun, Poland).

Author contributions

Conceptualization: R.M., G.S.; Data curation: R.M.; Formal analysis: R.M., S.G., M.M., D.G.; Funding acquisition R. M.; Investigation R.M., G.S., M.M., D.G., P.P.; Methodology: R.M., G.S., M.M., P.P.; Project administration: R. M., P. P.; Resources: R. M.; Supervision: R. M., P.P., G.S.; Validation: R.M., M.M.; Writing—original draft: R.M. S.G.; Writing—review & editing: R.M., G.S., M.M., D.G., P.P.

Competing interests

The authors declare no competing interests.

Additional information

Supplementary Information The online version contains supplementary material available at https://doi.org/10.1038/s41598-023-36081-9.

Correspondence and requests for materials should be addressed to R.M.

Reprints and permissions information is available at www.nature.com/reprints.

Publisher's note Springer Nature remains neutral with regard to jurisdictional claims in published maps and institutional affiliations.

Electronic supplementary information

Electropolymerized polypyrrole-MOF composite as a coating material for SPME fiber for extraction VOCs liberated by bacteria

Radik Mametov [a,*], Gulyaim Sagandykova [a], Maciej Monedeiro-Milanowski [a], Dorota Gabryś [b] and Paweł Pomastowski [a]

[a] Centre for Modern Interdisciplinary Technologies, Nicolaus Copernicus University in Toruń, Wileńska 4, 87-100 Toruń, Poland

[b] Radiotherapy Department, Maria Sklodowska-Curie National Research and Institute of Oncology, Gliwice, Poland

*****corresponding author: mametov.radik@gmail.com; tel.: +48 56 665 60 01

Table of contents

Table S1. The complete list of volatile organic compounds liberated by *Enterococcus faecalis*

#	Compound	*RT, min*	Area
1	Carbon dioxide	1.178	29161134
2	Acetic acid ethenyl ester	1.525	43362.78
3	Acetic acid	1.69	304000.4
4	unknown	2.066	2081327
5	1-Butanol	2.196	169935.3
6	4-Fluorohistamine	2.584	13022.96
7	Ethanol, 2-(vinyloxy)-	2.825	150875.8
8	Propanedioic acid	3.114	33640.5
9	Dextroamphetamine	3.831	30346
10	4-Fluorohistamine	3.908	26884.6
11	unknown	4.002	32725.73
12	unknown	4.443	33749.66
13	Propanedioic acid, propyl-	4.608	18519.68
14	2-Hexanamine, 4-methyl-	4.749	10720.93
15	Cyclotrisiloxane, hexamethyl-	5.449	245736.3
16	Cyclotrisiloxane, hexamethyl-	5.672	60856.85
17	Propanedioic acid, propyl-	6.007	98621.59
18	Propanedioic acid, propyl-	6.166	66512.75
19	Butanoic acid, 2-methyl-	6.278	62352.25
20	Ethylbenzene	6.425	106199.3
21	p-Xylene	6.684	101417.6
22	Cyclobutanol	7.666	21150.53
23	Oxime-, methoxy-phenyl-	7.913	374213.8
24	p-Bromofluorobenzene	8.207	211543.2
25	unknown	8.472	4799.06
26	unknown	9.101	12439.67
27	Benzaldehyde	9.225	367384.2
28	Dimethyl trisulfide	9.425	69062.53
29	Norpseudoephedrine	9.607	9738.16
30	Phenol	9.907	273315.6
31	Cyclotetrasiloxane, octamethyl-	10.407	202931.7
32	Amphetamine	11.395	50521.98
33	Cathinone	11.966	19642.11
34	Cyclotrisiloxane, hexamethyl-	12.342	338050.5
35	2-Hexanamine, 4-methyl-	12.589	20441.72
36	unknown	12.872	27296.15
37	unknown	13.095	14798.06
38	2,4-Dihydroxybenzaldehyde, 2TMS derivative	13.195	26162.09
39	Benzeneethanamine, N-methyl-	13.936	12360.14
40	Cyclopentasiloxane, decamethyl-	14.095	158207.7
41	1-Octanamine, N-methyl-	14.378	19088.77
42	2-Hexanamine, 4-methyl-	14.825	6835.65
43	Piperazine, 2-methyl-	15.001	35131.62
44	unknown	15.125	29181.77
45	unknown	15.336	56443.19

46	2-Pyrrolidinone, 4-hydroxy-5-methyl- (isomer 1)	15.466	25624.03
47	Cyclotetrasiloxane, octamethyl-	15.678	96311.66
48	unknown	16.136	23473.91
49	D-Alanine	16.489	17278.31
50	unknown	16.672	12023.46
51	R-(-)-Cyclohexylethylamine	16.777	13133.77
52	unknown	16.942	40786.19
53	1-Octanamine, N-methyl-	17.066	22490.58
54	2-Hexanamine, 4-methyl-	17.213	9221.67
55	Cyclohexasiloxane, dodecamethyl-	17.648	194395.5
56	unknown	18.689	24895.21
57	(+)-2-Aminoheptane	18.971	9842.74
58	Carbamic acid, monoammonium salt	19.148	21915.87
59	Imidazole, 2-amino-5-[(2-carboxy)vinyl]-	20.313	151372.8
60	R-(-)-Cyclohexylethylamine	20.595	14830.48
61	Phenethylamine, p,α-dimethyl-	20.748	20108
62	1-Octadecanamine, N-methyl-	20.83	54771.64
63	Cycloheptasiloxane, tetradecamethyl-	20.966	164018.6
64	2,4-Di-tert-butylphenol	21.183	165678.2
65	Cycloheptasiloxane, tetradecamethyl-	22.189	15622.62
66	Ethyne, fluoro-	23.148	10694.75
67	unknown	24.071	22670.02
68	Cyclooctasiloxane, hexadecamethyl-	24.471	951955.5
69	1-Octadecanamine, N-methyl-	24.901	51689.36
70	N-dl-Alanylglycine	25.083	24888.63
71	unknown	25.324	19467.15
72	unknown	25.718	30994.18
73	unknown	25.777	21091.79
74	unknown	26.048	11778.77
75	unknown	26.348	5859.37
76	Cyclononasiloxane, octadecamethyl-	26.789	298096.8
77	unknown	26.953	15714.04
78	unknown	26.989	8679.1
79	unknown	27.253	13150.25
80	unknown	27.383	23925.87
81	unknown	27.518	23147.88
82	Heptacosane	27.906	126643.2
83	unknown	28	5689
84	Benzeneethanamine, 2,5-difluoro-β,3,4-trihydroxy-N-methyl-	28.265	87941.69
85	Pterin-6-carboxylic acid	28.377	118690.3
86	Octasiloxane, 1,1,3,3,5,5,7,7,9,9,11,11,13,13,15,15-hexadecamethyl-	28.583	58191.11
87	unknown	28.718	11829.61
88	Cyclic octaatomic sulfur	29.183	78684.46
89	unknown	29.459	4502.86

90	unknown	30.124	39304.5
91	unknown	31.477	35453.79
92	unknown	34.535	388527.5

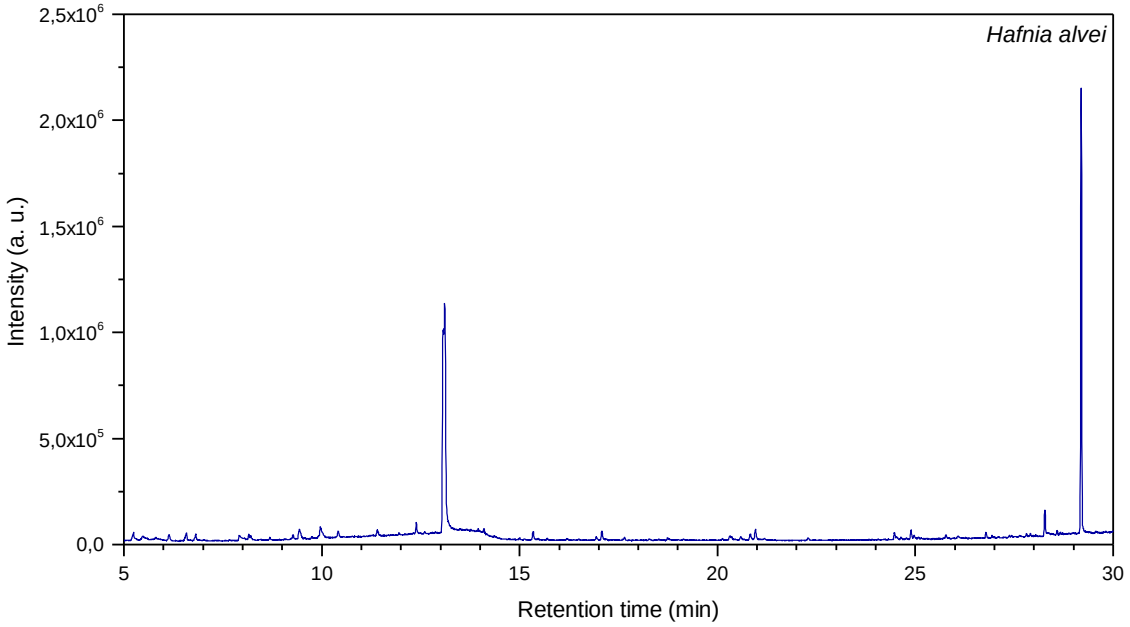

Figure S1. GC-MS chromatogram of VOCs liberated by *Hafnia alvei* extracted with the utilization of PPy@ZIF-8 coating

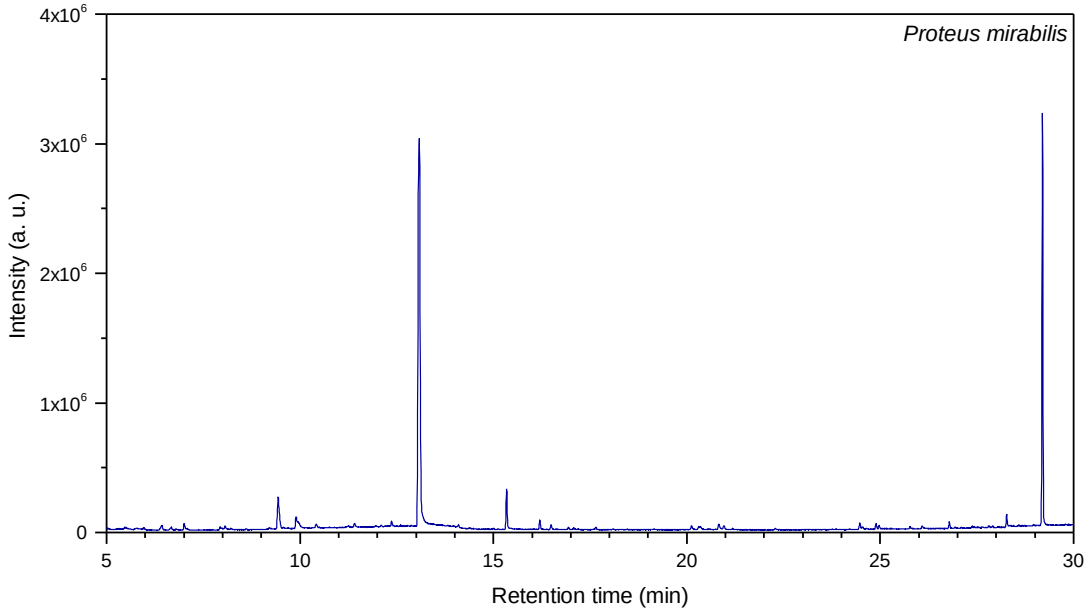

Figure S2. GC-MS chromatogram of VOCs liberated by *Proteus mirabilis* extracted with the utilization of PPy@ZIF-8 coating

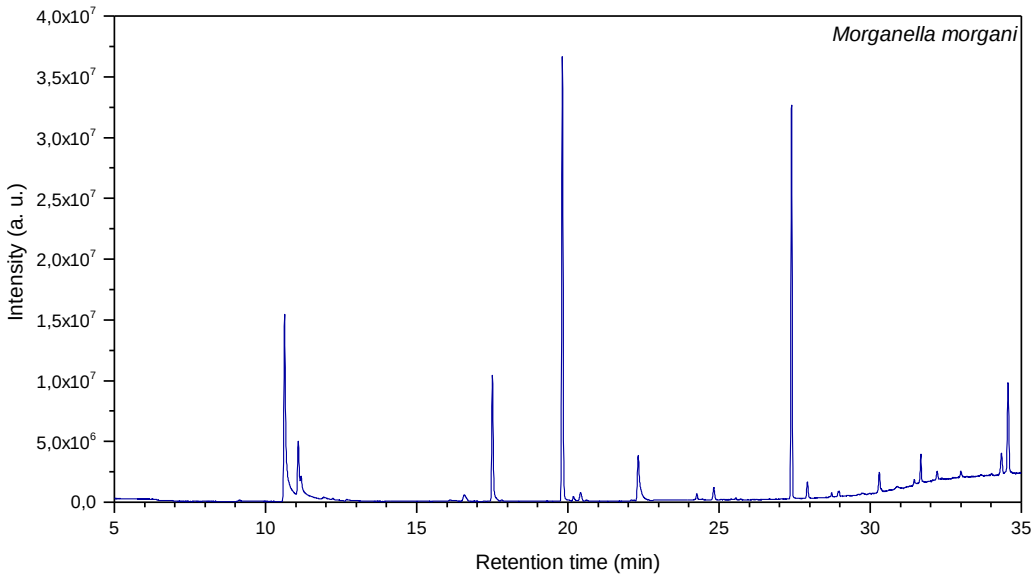

Figure S3. GC-MS chromatogram of VOCs liberated by *Morganella morgani* extracted with the utilization of PPy@ZIF-8 coating

[P2] Sagandykova G., Pryshchepa O., Rafinska K., **Mametov R**., Madajski P., Pomastowski P. 'LDI-MS performance of gold nanostars as an inorganic matrix for low molecular weight analytes' International Journal of Mass Spectrometry, 478, 116872 (2022). IF = 1.934 MP = 70.

International Journal of Mass Spectrometry 478 (2022) 116872

Contents lists available at ScienceDirect

International Journal of Mass Spectrometry

journal homepage: www.elsevier.com/locate/ijms

LDI-MS performance of gold nanostars as an inorganic matrix for low molecular weight analytes

Gulyaim Sagandykova [a, *], Oleksandra Pryshchepa [a, b], Katarzyna Rafińska [b], Radik Mametov [a, b], Piotr Madajski [c], Paweł Pomastowski [a]

[a] Centre for Modern Interdisciplinary Technologies, Nicolaus Copernicus University in Toruń, Wileńska 4, 87-100 Toruń, Poland
[b] Department of Environmental Chemistry and Bioanalytics, Faculty of Chemistry, Nicolaus Copernicus University in Toruń, Gagarina 7, 87-100 Toruń, Poland
[c] Department of Chemistry of Materials Adsorption and Catalysis, Faculty of Chemistry, Nicolaus Copernicus University in Toruń, Gagarina 7, 87-100 Toruń, Poland

ARTICLE INFO

Article history:
Received 15 March 2022
Received in revised form
27 April 2022
Accepted 2 May 2022
Available online 16 May 2022

Keywords:
Laser desorption ionization
Gold nanostars
Lipidomics
Low molecular weight compounds
Mass spectrometry

ABSTRACT

Anisotropy at the nanoscale fascinates researchers in various areas of science and technology. Well-known applications of anisotropic nanoparticles include biosensors and catalysis. However, utilization of gold nanostars in analytical chemistry is limited to surface enhanced Raman spectroscopy. LDI-MS assisted with gold nanostars has not been addressed for low molecular weight compounds. Herein, we report LDI-MS performance of phospholipids at nanomolar concentrations with application of gold nanostars for the first time. Intense signals of molecular ions were detected as metal adduct ions with relatively low fragmentation and signals of interferences in low-mass region. Nanostars were characterized with utilization of electron microscopic, X-Ray powder diffraction and dynamic light scattering techniques. The results showed that gold nanostars can serve as a bright perspective for new inorganic matrices in LDI-MS of low molecular weight compounds.

1. Introduction

Laser desorption ionization mass spectrometry (LDI-MS) offers detection of compounds in low-mass region (<1000 *m/z*). Being firstly introduced by Hillenkamp and Tanaka et al. awarded with the Nobel Prize in 2002 [1], LDI-MS found many applications in analysis of various biologically active compounds utilizing targeted and untargeted approaches. In the era of lipidomics and metabolomics, development of LDI-MS techniques may contribute to analysis of samples of biological origin to collect data with relative ease of instrument operation and low sample volume. Although LDI-MS techniques have not been widely adopted for quantitative analysis, screening of low molecular weight compounds in biological sample also provides important information since they participate in biochemical pathways and perform biological functions [2]. As compared to liquid chromatographic techniques, which are considered as gold standard for analysis of biological samples in many areas of research, LDI-MS requires no sample preparation and separation of analytes.

Classical technique in LDI-MS family, namely matrix-assisted laser desorption ionization (MALDI), utilizes organic molecules with light absorbing properties for desorption and ionization of analytes. As compared to MALDI-MS, LDI requires no organic matrices, which eliminates the main disadvantages of the classical technique in analysis of small compounds. The use of organic matrix generates chemical background in the low mass region and multiple adducts with analyte, thus substantially complicating the spectra. LDI-MS matrices also possess non-volatility thus being stable under conditions of high vacuum [3] and large surface area offering high molecular loading capacity [4].

Great endeavors were undertaken to develop efficient LDI MS platforms in recent years. Though advances in synthesis of LDI systems based on noble metals such as gold and silver, clusters (e.g. Au_n^+) may interfere with detection of low molecular weight compounds [5]. Zhao et al. reported self-assembled sandwich-like Au@MSN@Ag nanomatrices based on mesoporous silica nanocomposite for detection of small biomolecules [6]. Core-shell structure has benefits for easy functionalization and diverse properties that shows it as powerful candidate as LDI matrix, while

* Corresponding author.,
E-mail address: sagandykova.gulyaim1@gmail.com (G. Sagandykova).

https://doi.org/10.1016/j.ijms.2022.116872

mesoporous structure brings advantages due its high specific area and pore volume. In addition, UV—Vis absorption properties showed that Au@MSN@Ag nanomatrices has superior performance in MALDI-TOF-MS [6]. Dou et al. reported application of Au nanoparticles/ZnO nanorods for detection of glutathione. The Au—ZnO hybrid nanostructures may promote the hot electrons transfer at gold-zinc oxide nanorods interface and enhancement of LDI efficiency [7]. Enrichment of analytes on-target by selective capturing and isolating was also one of the advantages of the system for analysis of biological samples [7].

LDI platforms with utilization of various nanomaterials were reported in several worthwhile studies. Multi-shelled hollow Cr_2O_3 spheres were applied for bio-fluid metabolic analysis for clinical diagnostics of schizophrenia [8]. Due to multi-shelled hollow structure and semi-conducting properties with a band gap energy of 3.4 eV. Integration of these parameters demonstrated significant enhancement of detection efficiency [8]. Cao et al. designed Pd—Au alloys supported by a core shell structure constructed from magnetic core particles as a LDI matrix [9]. Enhanced LDI efficiency allowed to achieve direct detection of biofluids in seconds with low sample consumption (100 nL in serum) for diagnosis of medulloblastoma and evaluation of radiotherapy. The success of utilization of Pd—Au alloys can be explained by high salt and protein tolerance and contribution to efficient electron transfer and surface stability due to plasmonic and alloying effects [9]. A trimetallic plasmonic alloy with mesoporous morphology allowed direct metabolic profiling in seconds with low sample volume (500 nL of native plasma) and no enrichment and purification. The platform enabled to reveal a distinct metabolic phenotype for early gastric cancer [10]. On the other hand, Pei et al. reported utilization of FeOOH@ZIF-8 nanocomposite for analysis of metabolites in serum for diagnosis of gynecological cancers [11]. The LDI system showed enhanced ionization efficiency without sample pretreatment due to size-exclusion effect [11]. Vedarethinam et al. designed vanadium core-shell nanorods for evaluation of metabolic changes of diabetic retinopathy [12]. Mesoporous structures provided the hollow space accessible for guest molecules contributing to trapping of metabolites in bio-fluids. Moreover, negatively charged surface led to cation attachment and electron transfer in ion-positive mode [12]. Zhang et al. designed ferrous nanoparticles and a deep stabilizer for ultra-fast, label- and antibody-free MS method for metabolic diagnosis of coronary heart disease in trace serum [13]. Finally, Sun et al. [14] studied fragmentation and cation adduction of small molecules using nanoparticle-assisted LDI system that may find implications in identification towards profiling and can assist in advanced analysis of small metabolites.

LDI-MS with application of metal nanoparticles instead of matrix was introduced by application of 30-nm cobalt nanopowder dispersed in glycerol for analysis of peptides and proteins [1]. Although, not only substrates based on metal nanomaterials are successfully used instead of classical matrix, metal nanoparticles have unique optical properties in addition to relative inertness and physico-chemical characteristics assisting desorption and ionization of analytes. Although there is no generally accepted mechanism for LDI, it also depends on several parameters of the system, in particular analyte properties such as molecular weight, polarity, presence of functional groups, hydrophilicity and hydrophobicity. Furthermore, the interplay between analyte, nanoparticles and laser would be important to consider, however it remains challenging [15] and requires multi-disciplinary approach. Various suggestions have been made in attempt to explain the nature of LDI being a subject for numerous review papers [2,15,16]. One group of the suggestions addressed the thermal nature of ionization, which had been subject of multiple investigations. However, one of the propositions for non-thermal processes assisting ionization included surface plasmon resonances (SPRs). Surface plasmons, which are collective oscillations of free electrons on the surface of plasmonic metals, sometimes are taken for granted and not taken into consideration in LDI studies. However, such feature of noble metal nanoparticles may serve as a source of signal enhancement since their interaction with light excites surface plasmons of the metal. Such excitement leads to activation of local surface plasmon resonances (LSPRs), where the light energy is concentrated in small volume [17].

Despite perspectives for enhancement of the LDI efficiency, SPR-based LDI methods were not so much discussed probably due to the challenges in experimental design [17—23]. The central problem in wide application of this phenomenon is that resonances can work at specific wavelength and angle of excitation. In addition, resonant wavelength and SPR intensity depend also on the surface chemistry, size and shape of nanomaterial [24]. Since angle and wavelength considerations were not made in most of LDI research, it was discussed that surface plasmon resonance cannot be considered as main ionization mechanism, but it may provide plasmonic effects assisting energy transfer, optical processes and subsequent signal enhancement [16]. On the other hand, plasmonic nanostructures can enhance efficiency of energy absorption in the UV-region, which also shows potential for signal enhancement.

Nevertheless, the solution of the problem of application of SPR in LDI can be in anisotropic nanoparticles since according to Mie's theory, isotropic metal nanoparticles have single plasmon band and the extinction spectra depend on diameter, composition and dielectric environment [25]. In contrast, anisotropic noble metal nanoparticles, which can be defined as nanostructures with the shape other than spherical, have two distinct plasmon bands at longitudinal and transverse directions owing to difference in surface energies and strains on the crystal facets. Moreover, reduced symmetry provides nanoparticles with multiple plasmonic bands corresponding to number of symmetric planes in the structure [25,26]. Presence of the single plasmonic band of isotropic nanoparticles limits the possibilities for widespread applications for signal enhancement and requires optimization of wavelength and angle. Multiple plasmonic bands of anisotropic nanoparticles potentially can provide a wide window for the wavelength to induce resonant oscillation of the valence electrons. Although anisotropic nanoparticles previously have been studied in terms of LDI-efficiency [20], they were not discussed from the point of view of potential SPR-based signal enhancement. However, little interest was dedicated to gold nanostars, which are star-shaped plasmonic nanoparticles with multiple sharp tips. Experimental and theoretical studies revealed that star-shaped nanoparticles showed resonances in a very wide range of wavelengths [27]. For e.g., interesting study by Hao et al. applied finite-difference time-domain method and reported that the gold nanostar core play role as nanoscale antenna thus significantly increasing excitation cross section and electromagnetic field enhancements of the plasmons at tips [28]. This unique feature of star-shaped plasmonic nanoparticles such as presence of multiple sharp tips is advantageous also from the point of view of the effect of the substrate on LDI-efficiency. Studies showed that plasmon resonances at tips were sensitive to local dielectric environment [29], which means that adjustment of the substrate for LDI plate can bring more potential for further enhancement of LDI efficiency. What is also important for inorganic matrices is that gold nanostars have strong light absorption in the visible spectrum [30].

All the mentioned above, indicates that gold nanostars have properties suitable to serve as inorganic matrix in LDI, but also perspectives for potential enhancement of LDI efficiency. Along with the mentioned properties and significant advances in precise shape control in synthesis of anisotropic nanoparticles [31], gold

nanostars can serve as a bright candidate to represent new generation of inorganic matrices in LDI-MS analysis. Nonetheless, only few authors addressed application of gold nanostars in LDI analysis. Gamez et al. reported UV–Vis LDI-MS of synthetic polymers assisted by gold nanospheres, nanorods and nanostars [32]. Nishi et al. addressed reproducible ionization of gold nanospheres and nanostars in gelatin sections [33]. Interesting paper of Kolářová et al. [34] reported application of flower-like and polyhedral gold nanoparticles in LDI-MS analysis of bioactive molecules. However, studied nanoparticles were rather similar to one aggregate structure without sharp edges as compared to gold nanostars.

The aim of this work was to study and report LDI performance of gold nanostars as inorganic matrix in analysis of low molecular weight analytes for the first time. The synthesis of gold nanostars has been carried out by seed-mediated growth without application of surfactants, which can lead to signal suppression, surface passivation thus blocking optical properties of nanoparticles. Synthetic approach used in the current paper allowed efficient shape control of gold nanostars, which were successfully applied for LDI-MS analysis of low molecular weight compounds. The results showed intense signals of molecular ion of three various phospholipids at nanomolar concentrations, which can contribute to analytes identification in samples of biological origin.

2. Materials and methods

2.1. Reagents and materials

All solvents used in the study such as water, methanol and chloroform were of LC-MS grade quality (≥99.9%) and purchased from Sigma Aldrich (Steinheim, Germany). Precursor salt such as gold (III) chloride hydrate (99.995%) as well as sodium citrate dihydrate (≥99%), hydrogen peroxide (30% solution, pure for analysis) and sodium hydroxide (in powder, pure for analysis) were purchased from Sigma-Aldrich. Standards of phospholipids such as phospatidylcholine (from egg yolk, European Pharmacopeia standard) and L-α-phosphatidylinositol (from Glycine max, soybean, ~50% by TLC) were purchased from Sigma-Aldrich. Standard of L-α-lyso-phosphatidylcholine (from egg yolk, ≥ 99%) was purchased from Avanti-Polar lipids (Alabaster, Alabama, USA). The standard of adonitol was purchased from Sigma Aldrich (Steinheim, Germany). Stock solutions of phospholipids were prepared by dissolving powder of standards in a 1.5-mL amber glass vials in methanol (phospatidylcholine and *lyso*-phosphatidylethanolamine) and chloroform (phosphatidylinositol). Respective dilutions were carried out in 1.5-mL vials using manual glass syringes for sample preparation (Agilent, USA).

2.2. Synthesis of anisotropic nanoparticles

Gold nanostars were synthesized using the protocol of seed-mediated growth described in the study of Wall et al. [35]. All solutions were prepared freshly before the synthesis of each portion using volumetric flasks. Sodium borohydride solution and water were kept in ice for 20 min. Solution of NaOH dissolved in 0.3% H_2O_2 was prepared immediately prior to addition. The stock solution of the precursor was prepared by dissolving salt in 4 mL of water to the final concentration of 125 mg/mL. Due to the hygroscopic properties of $HAuCl_4$, the stock solution was prepared by dissolving the salt directly in the ampoule [36]. Furthermore, stock solution was diluted to the final concentration of 25 mM in 1.5-mL dark Eppendorf tube. For preparation of the seed solution, 100 μL of the stock solution of the precursor (25 mM) and 100 μL of sodium citrate at concentration 25 mM were added to 9.8 mL of water poured to the 20-mL glass vial. The next step was addition of 300 μL of ice-cold $NaBH_4$ under vigorous stirring. The color of the solution turned orange-brown. For synthesis of gold nanostars, the growth solution was prepared by addition of 30 μL of seeds solution to 9.97 mL of ice-cold water, which was followed by addition of 150 μL of stock solution of the precursor (25 mM). The reaction was initiated by addition of 50 μL of 1 M solution of sodium hydroxide dissolved in 1 mL of 0.3% H_2O_2. The color of the solution changed immediately to intensive blue (Fig. S2). LC-MS grade water was utilized for the preparation of all solutions. Dialysis has been performed using Spectra/Por dialysis membrane with a cut-off value of 3500 Da (Spectrum Laboratories, California, USA). Preparation of seed solution was carried out in a 20-mL glass vial (Sigma-Aldrich). Preparation of growth solution was performed in a 50-mL glass beaker with a total volume of solution 29.9 mL. Concentration of gold after the dialysis was determined using Shimadzu ICP-MS 2030 instrument with gold standard purchased from Sigma Aldrich (Steinheim, Germany) as an internal standard.

2.3. LDI-MS analysis of phospholipids with the utilization of gold nanostars

LDI-MS analysis of phospholipids has been performed in positive ion-reflectron mode with the utilization of laser power value 60% in the mass range of *m/z* 0–2000. The value of the global attenuator offset accounted for 42%. Analysis was carried out using ultraFlextreme MALDI-TOF-MS apparatus (Bruker Daltonics, Bremen, Germany) equipped with a modified neodymium-doped yttrium aluminium garnet (Nd:YAG) laser operating at 355 nm and frequency 2 kHz. All spectra were acquired and processed using Flex Control and Flex Analysis software (Bruker Daltonics, Bremen, Germany). For analysis of phospholipids, 1 μL of gold nanostars after dialysis was deposited to commercial MTP ground steel target (Bruker Daltonics, Bremen, Germany) and allowed to dry, following deposition of 1 μL of standards of lipids. Mass calibration was carried out using gold signals and cubic enhanced calibration model individually for each spectrum. Analysis was carried out using phospholipids standard solutions, which were prepared by respective dilutions of stock solution of each lipid at concentration 1 mg/mL. The number of laser shots accounted for 1500 (3 x 500 shots) for each spot. Reflector voltages were 26.64 and 13.54 kV. The first accelerating voltage accounted for 25.08 kV, while the value for second ion source voltage was 22.43 kV. The structures of fragments of lipids were proposed using ChemSketch program (version 12.01, Advanced Chemistry Development, Toronto, Canada). Theoretical *m/z* values of analyzed compounds were calculated by using ChemCalc program [37]. Disposable low-cost lab-made target was prepared by cutting the list of the stainless steel (H17) without any additional processing to pieces with size 2.5 × 7.5 cm. The prepared target was washed with solvents (methanol, *iso*-propanol and acetonitrile) and inserted to MTP Slide-Adapter II (Bruker Daltonics, Bremen, Germany).

2.4. XRD analysis

X-Ray powder diffraction method was utilized to determine crystalline structure and size of crystal grain. The X'Pert Pro Analytical (Philips, Erlangen, Germany) instrument equipped with CuKα (λ equal to 1.54056 Å) radiation source and nickel filter was applied.

2.5. Size distribution and zeta-potential of synthesized nanoparticles

Zeta potential of synthesized nanostars was measured using Malvern Zetasizer Nano ZS (Malvern, Worcestershire, UK)

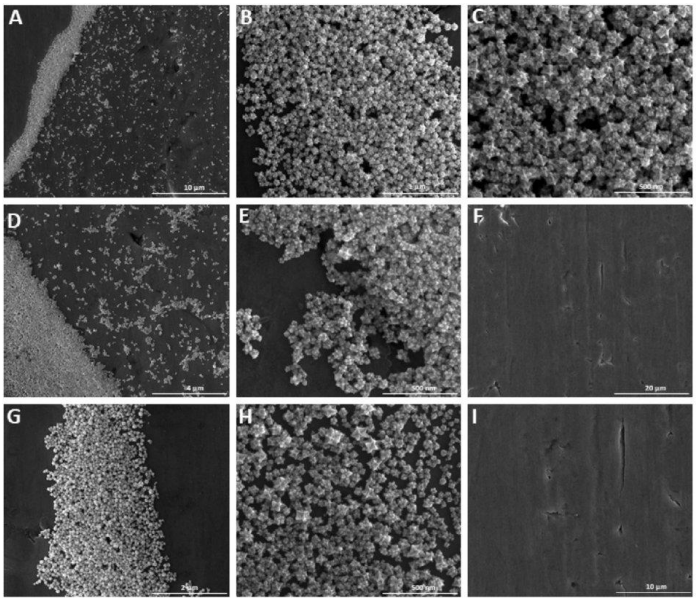

Fig. 1. SEM images of gold nanostars deposited to lab-made LDI target after storage during 2 months and 12 days: A, B and C – portion 1; D and E – portion 2, G and H – portion 3; F and I – images of the empty plate as a control image; D and G – images at the edges of spot.

reproducibility of synthesis in general. For assessment of stability of dispersions (Fig. S7, g,h and k), we repeated the size distribution analysis after 2 months and 12 days after synthesis storing the dispersions at 4 °C. The values were as follows: 84.96 ± 0.33, 62.11 ± 0.31 and 73.55 ± 0.54 (average sizes) versus 98.00 ± 1.76, 74.15 ± 1.15 and 87.87 ± 0.32 (peak maximum). The differences between freshly synthesized batches and those stored during 2 months and 12 days can be considered as insignificant (in the range of standard deviation) and indicates on stability of dispersions.

In addition, we measured zeta-potential (ZP) values for all synthesized batches and the values were as follows: 34.47 ± 1.22, −26.80 ± 0.26 and −28.13 ± 0.40 mV. It is generally accepted that the system with absolute values of zeta-potential in the range of ±20−30 mV or higher can be considered as stable [41]. The obtained values fell in the indicated range and are complementary to data on stability during 2 months and 12 days storage.

Furthermore, the DLS technique enabled the observation of the evidence of purification of nanoparticles using dialysis during 24 and 48h. Separate experiment with three samples was carried out: freshly synthesized, dialyzed during 24 and 48h. The measured values were as follows: 60.78 ± 1.14 nm for freshly prepared solution, 69.04 ± 0.03 and 69.47 ± 0.23 nm for NPs after 24 and 48h of dialysis respectively. Zeta potential (ZP) measurements showed the values −55.20 ± 1.41 mV for freshly prepared AuNPs in contrast to −36.57 ± 0.12 and −35.2 ± 1.12 mV for NPs after 24 and 48 h of dialysis, respectively. The decrease in the ZP value indicates on the desorption of ions from the surface, while increase in the NPs size is connected with the decrease of ionic strength of the solution. The obtained data both from size distribution and ZP measurements indicated that 48h dialysis was suitable for purification of nanoparticles since only insignificant differences were observed for nanoparticles dialyzed during 24 and 48h. MS spectra recorded for nanostars purified with 24 and 48h dialysis time can be found in Supplementary material (Fig. S3).

3.2. TEM and XRD analysis

TEM analysis (Fig. 2) revealed that synthesized gold nanostars had multiple branches with sharp edges, and had similar size and shape in all portions. EDX spectra showed that gold nanostars consisted mainly from gold (Fig. S6). Unlike in EDX spectra, the signals corresponding to K^+ and Na^+ were observed in LDI-MS spectra of controls and lipids. Since trace amounts of sodium and potassium can present in water even after purification, the signals were expected in case of LDI-MS and adducts of analytes with sodium and potassium. The absence of sodium and potassium in EDX spectra probably could be explained by limit of detection (<0.01 % wt.) of this technique [42], which could be achieved after purification with dialysis during 48h.

Selected area electron diffraction (SAED) analysis confirmed the crystalline nature of the particles (Fig. S6). The average sizes of gold nanostars from each portion were determined from corresponding TEM images and accounted for 70.0 ± 19.9 nm (portion 1), 94.6 ± 26.7 nm (portion 2) and 66.0 ± 16.8 nm (portion 3). Sizes of nanostars in portions 1 and 2 were found to be similar, while portion 2 had higher difference in sizes with portions 1 and 3. Since only the first one was applied for the evaluation of LDI efficiency, the study of the effect of size of gold nanostars can be worthy of future investigation. In addition, difference in sizes in portion 2 was in agreement with the results obtained by DLS technique (Section 'Size distribution and zeta-potential'). This means that DLS technique is complementary to TEM analysis in the study of gold nanostars and can be applied for future fast evaluation of reproducibility of synthesis between the batches for application in LDI.

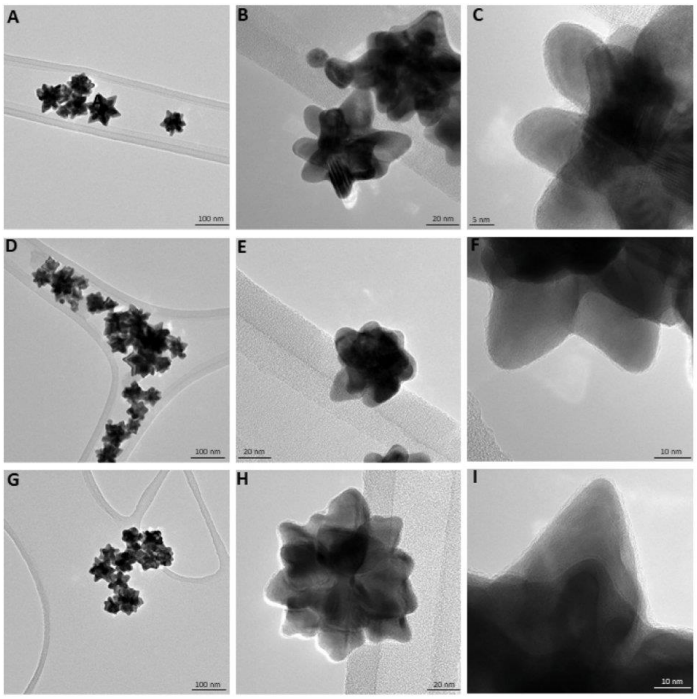

Fig. 2. TEM images of gold nanostars: A, B and C for portion 1; D, E and F for portion 2; G, H and I for portion 3.

X-Ray powder diffraction method was applied to characterize the crystalline nature of gold nanostars. XRD spectra for 3 portions (Fig. 3) showed similar patterns: sharp and intense peaks at 38.2°, 44.4°, 64.6°, 77.6° and 81.9°, which can be assigned to the (111), (200), (220), (311) and (222) planes of the face-centered cubic (fcc) structure of the particles. This is in good agreement with the literature reported previously [43,44]. In addition, diffraction peaks are in good agreement with those reported for the gold standard [45]. Furthermore, we determined the size of crystallite with Scherrer equation [46]. The values for all batches accounted for 29.8 nm, while value of nanoparticles size obtained from TEM images was higher. This may indicate that there is more than one crystal boundary on the surface of nanostars and XRD is not able to distinguish between two boundaries [41]. In addition, this may indicate that there are number of crystallites constructing a nanoparticle as units. The results showed that particles consisted of well-crystallized gold nanocrystals with preferential growth along the (111) planes.

3.3. LDI performance of gold nanostars for analysis of phospholipids

According to obtained results, the laser power 60% provided molecular ions for three phospholipids: phospatidylcholine, *lyso*-phospatidylethanolamine and phosphatidylinositol (Figs. 4-6). All the species were registered as adducts with sodium and potassium. To the best of our knowledge, gold nanoparticles have photocatalytic properties [47], which potentially can cause fragmentation of the analyte, complicating identification. Moreover, due to the anisotropic shape, gold nanostars showed light-induced catalytic properties higher as compared to spherical nanoparticles [48]. However, the literature on photocatalytic activity of gold nanostars in the UV–Vis region was not found. In addition, for some of the analytes, fragments can be not specific to enable reliable identification. Therefore, detection of the molecular ion was preferable and it was important to analyze fragmentation pathways that were proposed below.

Molecular ion of phosphatidylinositol was observed as sodium adduct $[M+Na]^+$ at *m/z* 911.42 at concentration of 1 nmol/μL, which corresponds to PI 18:0/20:3 (Fig. 4). Along with sodium adduct, the signal at *m/z* 939.45 corresponds to adduct with sodium and proton $[M + H+2Na]^+$. Fragments were observed in three ranges of the spectra: *m/z* < 200, 400–500, 700–800. The signal at *m/z* 179.99 correspond to the cleavage of inositol moiety, while signal at *m/z* 86.04 $[C_6H_{14}]^+$ corresponds to cleavage of the part linolenic acid. Fragment at *m/z* 455.20 was registered as sodium adduct and corresponds to the cleavage of stearic acid and part of linolenic acid with cleavage of the double bond. Fragments in the region at *m/z* 700–800 correspond to cleavage of different parts of linolenic acid with reduction of double bonds. Some of them were registered as sodium adducts (*m/z* 749.42, 816.47, 818.49, 820.50). The signals at *m/z* 754.46, 778.46 and 792.47 correspond to reduction of one double bond in addition to fragmentation of fatty acid chain, while signals at *m/z* 794.45, 816.42, 820.46 and 822.46 correspond to reduction of two double bonds. In contrast, the signal at *m/z* 818.44 correspond to reduction of three double bonds. Interesting observation has been made in the region > *m/z* 1000. The signals with

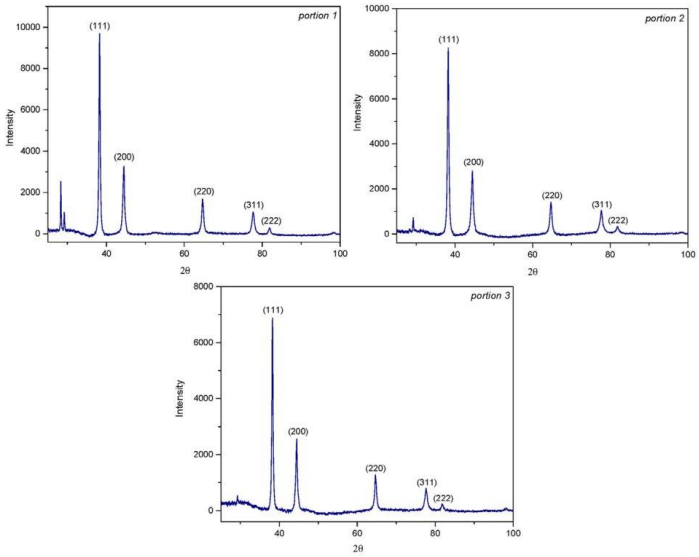

Fig. 3. X-Ray powder diffraction spectra for 3 portions of gold nanostars.

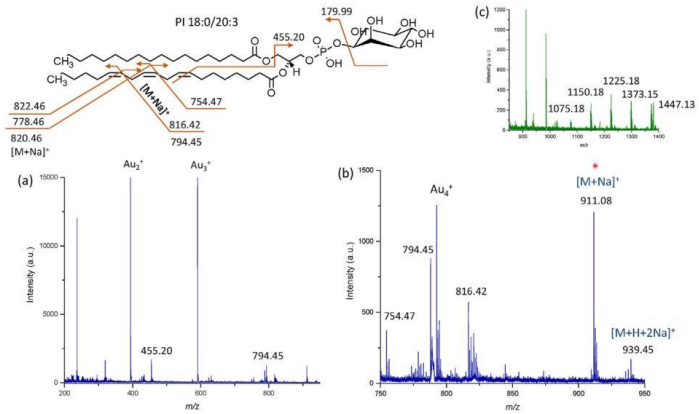

Fig. 4. LDI-TOF-MS spectra of phosphatidylinositol at concentration of 1 nmol/μL and proposed fragmentation pathway; (a) full spectrum with signals from gold used for mass calibration; (b) enhanced spectrum in the range at *m/z* 750–950 with S/N value for MS equal to 57; (c) enhanced spectrum in the range at *m/z* 900–1400.

intensities <200 a.u. were registered as adducts with sodium and water as well as addition of OH-group (Fig. 4c). For e.g., the differences in mass between the signals at *m/z* 1075.18 and 1150.18 accounted for 75.00 Da, which corresponds to one sodium, two molecules of water and OH-group with replacement of one hydrogen. Further mass difference between the signals at *m/z* 1150.18 and 1225.18 was also 75.00 Da. Such difference led to the suggestion that PI formed multiple adducts with sodium corresponding to thirteen signals. The number of signals allows to suggest that all of the oxygen atoms in PI were occupied with sodium since inositol moiety has six additional oxygen atoms. However, the stability of such adducts might have been low, which resulted in the signals with low intensity. The differences in mass for other signals was 72.98, 74.93, 73.93, 74.96 and 73.98 Da. The difference of 72.98 Da corresponds to addition of one sodium, one water and two OH-groups with replacement of two hydrogen atoms and the value 73.97 Da corresponds to the same addition with replacement of one hydrogen. In contrast, values 74.93 and 74.96 Da correspond to similar addition without changes in the number of hydrogen atoms in the structure. The replacement of hydrogen could occur at the cyclitol moiety or fatty acid chains. Therefore, the signals at *m/z* 1075.18, 1150.18, 1225.18, 1298.16, 1373.15, 1447.13, 1521.11, 1595.09

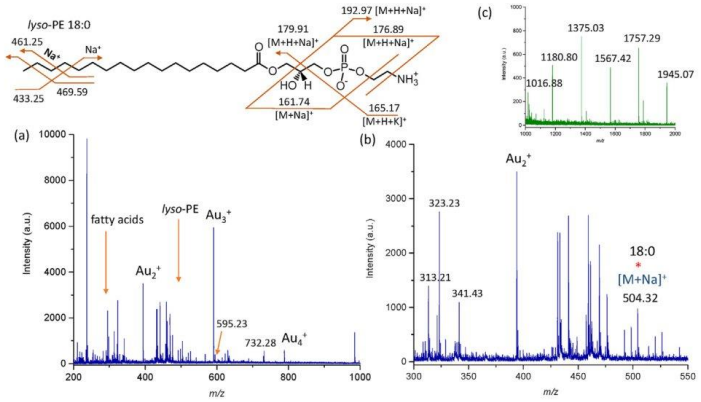

Fig. 5. LDI-TOF-MS spectra of *lyso*-phosphatidylethanolamine at concentration of 2 nmol/μL and proposed fragmentation pathway; (a) full spectrum with signals from gold used for mass calibration; (b) enhanced spectrum in the range at *m/z* 300–550 with S/N value for MI equal to 18; (c) enhanced spectrum in the range at *m/z* 1000–2000.

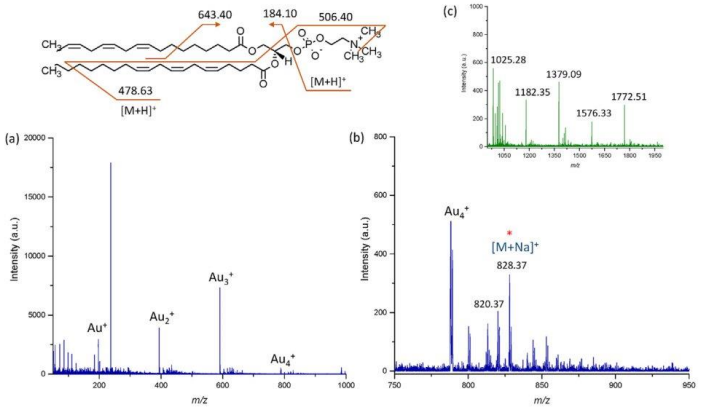

Fig. 6. LDI-TOF-MS spectra of phosphatidylcholine at concentration of 0.02 nmol/μL and proposed fragmentation pathway; (a) full spectrum with signals from gold used for mass calibration; (b) enhanced spectrum in the range at *m/z* 750–950, S/N value for MI is equal to 16; (c) enhanced spectrum in the range at *m/z* 1000–2000.

and 1670.05 correspond to adducts of PI with different number of sodium atoms, water molecules and OH-groups. Presence of double bonds in one of the fatty acids in the structure of PI could determine the ionization patterns. First of all, multiple fragmentation occurred probably at the place of double bonds. Moreover, double bonds are attractive sites for alkali metals. Furthermore, cyclitol moiety provided additional sites for sodium addition, while phosphate group provided negative charge that could be compensated by sodium [49]. In addition, preferable mechanism of ion formation assisted by gold nanoparticles in positive mode is cationization with alkali metals. Hence, all the mentioned factors could result in the appearance of signals as adducts with multiple atoms of sodium.

In case of *lyso*-phosphatidylethanolamine (Fig. 5), molecular ion was detected as sodium adduct at *m/z* 504.32, which corresponds to *lyso*-PE 18:0. The manufacturer (Avanti Polar Lipids, Alabaster, Alabama, USA) indicated that fatty acid 18:0 was dominant, while also 16:0, 16:1 and 18:1 were present. However, they did not present similar ionization pattern since only adduct with sodium was observed for *lyso*-PE 16:0 at *m/z* 476.30. In contrast, *lyso*-PE 16:1 demonstrated adduct with two atoms of sodium and proton $[M + H+2Na]^+$ at *m/z* 498.27 and adduct with sodium and water $[M + H_2O + Na]^+$ at *m/z* 492.27. Similar to 16:1, *lyso*-PE 18:1 was observed as adduct with sodium and water at *m/z* 520.30. Similar to phosphatidylinositol, *lyso*-phospatidylethanolamine showed the adduct with seven atoms of sodium and five molecules of water at *m/z* 732.29 with intensity <600 a.u. In addition, *lyso*-PE 16:0 and 18:0 were registered as adducts with two atoms of potassium and two molecules of water at *m/z* 567.17 and 595.23, respectively. The presence of *lyso*-PE 16:1 and 18:1 was confirmed by signals at *m/z* 282.25 and 254.22, which corresponds to palmitoleic and oleic acids, respectively. The signals corresponding to cleavage of fatty acids from the lipid can assist in its identification. However, in contrast to phosphatidylinositol, *lyso*-PE was more susceptible to cleavage of fatty acids. Oleic acid also was registered as adduct with potassium at *m/z* 321.21. Palmitic acid, which was prevailing acid in the standard, was registered as adduct with potassium at *m/z*

295.34 $[M+K]^+$ and adduct with potassium and water $[M+2H_2O+2K]^+$ at *m/z* 313.42. Intense signal at *m/z* 298.03 corresponds to adduct of palmitic acid with one atom of sodium, hydrogen and one molecule of water $[M + H + H_2O + Na]^+$. Stearic acid also was registered as adduct $[M+K]^+$ with potassium at *m/z* 323.23 and adduct with potassium and water $[M + H_2O + K]^+$ at *m/z* 341.24. The signal at *m/z* 308.26 also corresponds to adduct of stearic acid with sodium and hydrogen $[M + H + Na]^+$. Fragmentation also was observed by signals in the range *m/z* < 200. Signals at *m/z* 162.00, 164.97 and 177.02 were potentially originated from cleavage of fatty acid and $(CH_2)_2NH_3^+$ moiety and were registered as $[M+Na]^+$, $[M + H + K]^+$ and $[M + H + Na]^+$. Signals coming from adducts with proton generally were not expected, since metal nanoparticles as a source of proton are not well established [32] and acidic groups immobilized on the surface [50] or application of buffers [51] may reduce alkali metals adducts. However, organic compounds used in synthesis and adsorbed on the surface potentially could be a source of proton, but not sufficient to produce higher number of protonated ions. In addition, the signal at *m/z* 161.74 was suggested to show similar fragmentation pathway with exception of addition of hydrogen potentially at negatively charged oxygen in phosphate group. Similar to PI, charge compensation mechanism could be responsible for multiple addition of hydrogen and alkali metals. Signals at *m/z* 176.89, 179.91 and 192.97 also were supposed to present due to addition of hydrogen and sodium. Little fragmentation also occurred in fatty acid chain, which was evidenced by signals at *m/z* 433.25, 461.25 and 469.59, and two of them were registered as sodium adducts. Such little fragmentation can be helpful in identification since fragments at *m/z* < 200 showed the lipid structure apart from fatty acid chain.

Enhanced spectrum (Fig. 5c) showed signals after *m/z* 1000 and some of them were observed to be close to the gold signals by mass. Therefore, we attempted to calibrate the same spectrum using signals of Au^+, Au_2^+, Au_4^+, Au_6^+ and cubic enhanced calibration strategy to check whether it will provide more precise masses in this region. It appeared that the signals of interest after such calibration were at *m/z* 1016.84, 1181.77, 1378.61, 1575.49, 1804.24 and 1969.00. This means that all of the signals except those at *m/z* 1016.84 and 1804.24 corresponds to gold: Au_6^+ (1181.77), Au_7^+ (1378.61), Au_8^+ (1575.73) and Au_{10}^+ (1969.00). This was interesting observation since signals of gold after *m/z* 1000 appeared not in all spectra, which probably can be the evidence of processes taking place during the ionization. Moreover, since one of the well-known advantages of application of gold nanoparticles is their relative inertness and absence of adducts with analytes, the signals not corresponding to gold were not expected. This means that spectrum interpretation after *m/z* 1000 should be carried out carefully. The signal at *m/z* 1016.84 appeared to correspond to $Au_5O_2^+$, while the signal at *m/z* 1804.24 corresponds to $Au_9O_2^+$. The study by Shi et al. reported that formation of neutral complex Au_5O_2 can be provided via charge transfer and subsequent chemisorption of oxygen [52]. Experiments showed that adsorption of molecular oxygen of cationic cluster Au_n^+ ($n \leq 6$) was not observed [53]. Moreover, theoretical results by Ding et al. demonstrated a monotonic decrease in adsorption energy with the increase of size of the cluster for cationic systems [54]. In addition, it was previously reported that small gas-phase gold clusters are not reactive to molecular oxygen [53]. Formation of anionic complex could not be possible in positive reflector mode. This means that neutral Au_n cluster could interact with oxygen in the gas phase with its subsequent chemisorption that was followed by ionization.

In case of phosphatidylcholine, intensity of the molecular ion was not as abundant as for PI and *lyso*-PE (Fig. 6). The most prominent candidates for molecular ion are the signals at *m/z* 828.37 and 820.37 correspond to sodium adduct of PC 18:3/20:3 ($C_{46}H_{80}NO_8P$) and $C_{44}H_{80}NO_8P$ as potassium adduct or $C_{45}H_{84}NO_8P$ as sodium adduct. The signal at *m/z* 820.37 was observed only at concentration 0.02 nmol, being less abundant than the signal at *m/z* 828.37. Based on the mass error, an option with PC registered at *m/z* 820.37 as sodium adduct is more probable (183.86 ppm for sodium vs 253.75 ppm for potassium). The signal at *m/z* 828.37 may correspond to the main phosphatidylcholine in the standard since it was detected at all concentrations except 1 nmol. Signals corresponding to fragments were less abundant at concentration 0.02 nmol. In contrast, spectrum of PC at the highest concentration showed more abundant signals of fragments (Fig. S4). The signals at *m/z* 295.23, 319.23, 321.24 and 323.26 were the most abundant at concentration of 1 nmol and can be evident on cleavage of fatty acids from the structure of lipids. The signal at *m/z* 295.23 corresponds to potassium adduct of C16:0 and adduct of 16:1 with sodium and water. The signal at *m/z* 319.23 corresponds to potassium adduct of 18:2/sodium and potassium adduct of 18:3, while signals at *m/z* 321.24 and 323.26 correspond to potassium adduct of 18:1/sodium and water adduct of 18:2 and potassium adduct of 18:0/sodium and water adduct of 18:1, respectively. Based on the values of the mass error, the most prominent candidates to be presented in the standard were 18:3 (25.25 vs. 91.04 ppm for 18:2), 18:2 (23.16 vs. 88.44 ppm for 18:1) and 18:1 (27.19 vs. 92.07 ppm). Together with observation of the fragment at *m/z* 506.40, which corresponds to cleavage of 20:3 and one CH_3-group, the initial proposition on the presence of PC 18:3/20:3 seems to be relevant. The fragment at *m/z* 643.40 corresponds to fragmentation of 20:3, the fragment at *m/z* 478 correspond to cleavage of 20:3 followed by fragmentation of 18:3 with reduction of two double bonds and hydrogen adduct. In turn, based on the signals coming from fatty acids, the signal at *m/z* 820.37 correspond to PC 18:2/18:2 and 18:1/18:3. In addition, the signals at *m/z* 86 and 184, specific for phosphatidylcholines, were observed at all concentrations (Fig. S4). The mass region > *m/z* 1000 (Fig. 6c) showed several signals: 997.44, 1009.40, 1017.35, 1041.38 as well as signals corresponding to gold clusters. Interesting that the signal at *m/z* 1017.35 also correspond to $Au_5O_2^+$ as it was observed for *lyso*-phosphatidylethanolamine. However, in contrast to *lyso*-PE, the signal at *m/z* 1041.38 correspond to $Au_5(CO)_2^+$. The cleavage of CO-groups of lipids and organic compounds adsorbed on the surface of nanoparticles could be potential source of CO molecules. The study of rate constants determined for CO adsorption on gold clusters revealed that for all cluster sizes except Au_5^+, Au_8^+ and Au_9^+, adsorption of the first CO molecule occurred with higher rate constant than subsequent CO adsorption [55]. This is in agreement with the obtained MS spectrum, since other signals corresponding to $Au_m(CO)_n^+$ were not observed. Furthermore, the intensity of the signal was half the size of the signal corresponding to $Au_5O_2^+$. This probably can be explained by potential loss of CO molecule since such complexes could be metastable [56,57]. The signals at *m/z* 997.44 and 1009.40 correspond to adducts of PC with sodium: addition of six atoms of sodium with three molecules of water and eight atoms of sodium with two molecules of water followed by reduction of one double bond. Formation of adducts with multiple atoms of sodium can be indicative on its incomplete removal during the dialysis. The experimental details and data interpretation on the LDI efficiency of gold nanostars for phosphatidylcholine at different concentrations are presented in the section of Supporting Information (with corresponding Fig. S4).

4. Conclusion

We report the LDI-MS performance of gold nanostars for analysis of low molecular weight compounds for the first time. Gold nanostars synthesized by seed-mediated growth without addition

of surfactants was successfully applied for analysis of lipid standards. All of them were registered as adducts with sodium at concentration range 0.02–2 nmol/spot. MS spectra showed signals corresponding to the fragments of analytes, however not interfering lipids identification. In addition, fatty acids were registered in the region *m/z* 300–400 that also assisted identification. All of the lipids showed adducts with multiple atoms of sodium. This potentially can be explained by relatively high content of sodium in the synthesis system as well as affinity of lipids to alkali metals. Intense molecular ions of studied analytes were obtained with application of 1500 shots of the laser with power 60%. Microscopic analysis of synthesized nanostars did not show changes in shape and size, thus allowing the storage of LDI plates. Finally, the obtained results showed a bright perspective for gold nanostars to be applied as a new inorganic matrix in LDI-MS analysis of low molecular weight compounds. This potentially can allow analysis of low molecular weight analytes in metabolomics and lipidomics.

Authors' contributions

Sagandykova G.: conceptualization; data curation; formal analysis; funding acquisition; investigation; methodology; project administration; validation; visualization; writing – original draft preparation; writing – review & editing.

Pryshchepa O.: investigation; writing – original draft preparation; data curation; conceptualization.

Rafińska K.: investigation; data curation; visualization; formal analysis; validation.

Mametov R.; investigation; data curation; visualization; formal analysis.

Madajski P.: data curation; formal analysis.

Pomastowski P.: resources; supervision; writing – review & editing; conceptualization.

Declaration of competing interest

The authors declare that they have no known competing financial interests or personal relationships that could have appeared to influence the work reported in this paper.

Acknowledgements

This study was financially supported by the National Science Center (Kraków, Poland) in a framework of Preludium 16 grant no. 2018/31/N/ST4/02210 (2019–2022). Authors would like to thank Dr. Justyna Walczak-Skierska for her kind help with MS spectra interpretation, Ewelina Masłak for technical assistance and Jolanta Wółkiewicz for preparation of SEM figures. In addition, authors are grateful to Bogusław Buszewski for consulting in technical questions of the grant realization.

Appendix A. Supplementary data

Supplementary data to this article can be found online at https://doi.org/10.1016/j.ijms.2022.116872.

References

[1] K. Tanaka, H. Waki, Y. Ido, S. Akita, Y. Yoshida, T. Yoshida, Protein and polymer analyses up to m/z 100 000 by laser ionization time-of-flight mass spectrometry, Rapid Commun. Mass Spectrom. 2 (1988) 151–153, https://doi.org/10.1002/rcm.1290020802.

[2] W.H. Müller, A. Verdin, E. De Pauw, C. Malherbe, G. Eppe, Surface-assisted laser desorption/ionization mass spectrometry imaging: a review, Mass Spectrom. Rev. (2020), https://doi.org/10.1002/mas.21670.

[3] R.L. Hansen, M.E. Dueñas, Y.J. Lee, Sputter-coated metal screening for small molecule analysis and high-spatial resolution imaging in laser desorption ionization mass spectrometry, J. Am. Soc. Mass Spectrom. 30 (2019) 299–308, https://doi.org/10.1007/s13361-018-2081-0.

[4] H.N. Abdelhamid, Nanoparticle assisted laser desorption/ionization mass spectrometry for small molecule analytes, Microchim. Acta 185 (2018) 1–16, https://doi.org/10.1007/s00604-018-2687-8.

[5] L.Z. Samarah, A. Vertes, Mass spectrometry imaging based on laser desorption ionization from inorganic and nanophotonic platforms, View 1 (2020), 20200063, https://doi.org/10.1002/viw.20200063.

[6] D. Zhao, C. Ma, M. Gao, Y. Li, B. Yang, H. Li, R. Zhang, M. Hao, J. Huang, K. Liang, P. Chen, L. Xie, R. Rong, B. Kong, Super-assembled sandwich-like Au@MSN@Ag nanomatrices for high-throughput and efficient detection of small biomolecules, Nano Res. 15 (2022) 2722–2733, https://doi.org/10.1007/s12274-021-3741-0.

[7] S. Dou, J. Du, Q. Zhu, Z. Wang, Y. Wang, Q. Chen, N. Lu, Au nanoparticles/ZnO nanorods as SALDI-MS substrate for on-plate enrichment and detection of glutathione in real samples, Sensor. Actuator. B Chem. 335 (2021), 129709, https://doi.org/10.1016/j.snb.2021.129709.

[8] R. Li, Y. Zhou, C. Liu, C. Pei, W. Shu, C. Zhang, L. Liu, L. Zhou, J. Wan, Design of multi-shelled hollow Cr2O3 spheres for metabolic fingerprinting, Angew. Chem. Int. Ed. 60 (2021) 12504–12512, https://doi.org/10.1002/anie.202101007.

[9] J. Cao, X. Shi, D.D. Gurav, L. Huang, H. Su, K. Li, J. Niu, M. Zhang, Q. Wang, M. Jiang, K. Qian, Metabolic fingerprinting on synthetic alloys for medulloblastoma diagnosis and radiotherapy evaluation, Adv. Mater. 32 (2020), https://doi.org/10.1002/adma.202000906.

[10] H. Su, X. Li, L. Huang, J. Cao, M. Zhang, V. Vedarethinam, W. Di, Z. Hu, K. Qian, Plasmonic alloys reveal a distinct metabolic phenotype of early gastric cancer, Adv. Mater. (2021), https://doi.org/10.1002/adma.202007978.

[11] C. Pei, C. Liu, Y. Wang, D. Cheng, R. Li, W. Shu, C. Zhang, W. Hu, A. Jin, Y. Yang, J. Wan, FeOOH@Metal–Organic framework core–satellite nanocomposites for the serum metabolic fingerprinting of gynecological cancers, Angew. Chem. Int. Ed. 59 (2020) 10831–10835, https://doi.org/10.1002/anie.202001135.

[12] V. Vedarethinam, L. Huang, M. Zhang, H. Su, H. Hu, H. Xia, Y. Liu, B. Wu, X. Wan, J. Shen, L. Xu, W. Liu, J. Ma, K. Qian, Vanadium core–shell nanorods inspect metabolic changes of diabetic retinopathy, Adv. Funct. Mater. 30 (2020) 1–10, https://doi.org/10.1002/adfm.202002791.

[13] M. Zhang, L. Huang, J. Yang, W. Xu, H. Su, J. Cao, Q. Wang, J. Pu, K. Qian, Ultrafast label-free serum metabolic diagnosis of coronary heart disease via a deep stabilizer, Adv. Sci. 8 (2021) 1–11, https://doi.org/10.1002/advs.202101333.

[14] S. Sun, W. Liu, J. Yang, H. Wang, K. Qian, Nanoparticle-assisted cation adduction and fragmentation of small metabolites, Angew. Chem. Int. Ed. 60 (2021) 11310–11317, https://doi.org/10.1002/anie.202100734.

[15] H.N. Abdelhamid, Nanoparticle-based surface assisted laser desorption ionization mass spectrometry: a review, Microchim. Acta 186 (2019), https://doi.org/10.1007/s00604-019-3770-5.

[16] K. Song, Q. Cheng, Desorption and ionization mechanisms and signal enhancement in surface assisted laser desorption ionization mass spectrometry (SALDI-MS), Appl. Spectrosc. Rev. 55 (2020) 220–242, https://doi.org/10.1080/05704928.2019.1570519.

[17] Y. Li, X. Cao, L. Zhan, J. Xue, J. Wang, C. Xiong, Z. Nie, Hot electron transfer promotes ion production in plasmonic metal nanostructure assisted laser desorption ionization mass spectrometry, Chem. Commun. 54 (2018) 10905–10908, https://doi.org/10.1039/c8cc05793a.

[18] E.T. Castellana, R.C. Gamez, M.E. Gómez, D.H. Russell, Longitudinal surface plasmon resonance based gold nanorod biosensors for mass spectrometry, Langmuir 26 (2010) 6066–6070, https://doi.org/10.1021/la904467b.

[19] S. Owega, E.P.C. Lai, A.D.O. Bawagan, Surface plasmon resonance-laser desorption/Ionization-Time-of-Flight mass spectrometry, Anal. Chem. 70 (1998) 2360–2365, https://doi.org/10.1021/ac971166u.

[20] L.C. Chen, J. Yonehama, T. Ueda, H. Hori, K. Hiraoka, Visible-laser desorption/ionization on gold nanostructures, J. Mass Spectrom. 42 (2007) 346–353, https://doi.org/10.1002/jms.1165.

[21] M.T. Spencer, H. Furutani, S.J. Oldenburg, T.K. Darlington, K.A. Prather, Gold nanoparticles as a matrix for visible-wavelength single-particle matrix-assisted laser desorption/ionization mass spectrometry of small biomolecules, J. Phys. Chem. C 112 (2008) 4083–4090, https://doi.org/10.1021/jp076688k.

[22] K. Shibamoto, K. Sakata, K. Nagoshi, T. Korenaga, Laser desorption ionization mass spectrometry by using surface plasmon excitation on gold nanoparticle, J. Phys. Chem. C 113 (2009) 17774–17779, https://doi.org/10.1021/jp9020432.

[23] M. Inuta, R. Arakawa, H. Kawasaki, Protein-modified silver nanoplates for the complementary analytical method of localised surface plasmon resonance and matrix assisted laser desorption/ionisation mass spectrometry, Anal. Methods 5 (2013) 5031–5036, https://doi.org/10.1039/c3ay40708j.

[24] S. Linic, P. Christopher, D.B. Ingram, Plasmonic-metal nanostructures for efficient conversion of solar to chemical energy, Nat. Mater. 10 (2011) 911–921, https://doi.org/10.1038/nmat3151.

[25] G. Paramasivam, N. Kayambu, A.M. Rabel, A.K. Sundramoorthy, A. Sundaramurthy, Anisotropic noble metal nanoparticles: synthesis, surface functionalization and applications in biosensing, bioimaging, drug delivery and theranostics, Acta Biomater. 49 (2017) 45–65, https://doi.org/10.1016/j.actbio.2016.11.066.

[26] H. Wang, D.W. Brandl, P. Nordlander, N.J. Halas, Plasmonic nanostructures: artificial molecules, Acc. Chem. Res. 40 (2007) 53–62.

[27] C. Noguez, Surface plasmons on metal nanoparticles: the influence of shape and physical, J. Phys. Chem. C 111 (2007) 3806–3819.
[28] F. Hao, C.L. Nehl, J. Hafner, P. Nordlander, Plasmon resonances of a gold nanostar, Nano Lett. 7 (2007) 729–732, https://doi.org/10.1021/nl062969c.
[29] C.L. Nehl, H. Liao, J.H. Hafner, Optical properties of star-shaped gold nanoparticles, Nano Lett. 6 (2006) 683–688.
[30] H. Puig, J.O. Tam, C.-W. Yen, L. Gehrke, K. Hamad-Schifferli, Extinction coefficient of gold nanostars, J. Phys. Chem. C 119 (2015) 17408–17415, https://doi.org/10.1021/acs.jpcc.5b03624.
[31] A.K. Pearce, T.R. Wilks, M.C. Arno, R.K. O'Reilly, Synthesis and applications of anisotropic nanoparticles with precisely defined dimensions, Nat. Rev. Chem 5 (2021) 21–45, https://doi.org/10.1038/s41570-020-00232-7.
[32] F. Gámez, P. Hurtado, P.M. Castillo, C. Caro, A.R. Hortal, P. Zaderenko, B. Martínez-Haya, UV-Vis-NIR laser desorption/ionization of synthetic polymers assisted by gold nanospheres, nanorods and nanostars, Plasmonics 5 (2010) 125–133, https://doi.org/10.1007/s11468-010-9125-z.
[33] T. Nishi, D. Muko, J.B. Rabor, Y. Niidome, Reproducible ionization of gold nanospheres and nanostars in gelatin sections, Bull. Chem. Soc. Jpn. 93 (2020) 58–64, https://doi.org/10.1246/bcsj.20190267.
[34] L. Kolářová, L. Kučera, P. Vaňhara, A. Hampl, J. Havel, Use of flower-like gold nanoparticles in time-of-flight mass spectrometry, Rapid Commun. Mass Spectrom. 29 (2015) 1585–1595, https://doi.org/10.1002/rcm.7265.
[35] M.A. Wall, S. Harmsen, S. Pal, L. Zhang, G. Arianna, J.R. Lombardi, C.M. Drain, M.F. Kircher, Surfactant-free shape control of gold nanoparticles enabled by unified theoretical framework of nanocrystal synthesis, Adv. Mater. 29 (2017), https://doi.org/10.1002/adma.201605622.
[36] L. Scarabelli, A. Sánchez-Iglesias, J. Pérez-Juste, L.M. Liz-Marzán, A "tips and tricks" practical guide to the synthesis of gold nanorods, J. Phys. Chem. Lett. 6 (2015) 4270–4279, https://doi.org/10.1021/acs.jpclett.5b02123.
[37] L. Patiny, A. Borel, ChemCalc: a building block for tomorrow's chemical infrastructure, J. Chem. Inf. Model. 53 (2013) 1223–1228, https://doi.org/10.1021/ci300563h.
[38] H. Kawasaki, T. Sugitani, T. Watanabe, T. Yonezawa, H. Moriwaki, R. Arakawa, Layer-by-layer self-assembled mutilayer films of gold nanoparticles for surface-assisted laser desorption/ionization mass spectrometry, Anal. Chem. 80 (2008) 7524–7533, https://doi.org/10.1021/ac800789t.
[39] J.B. Hu, Y.C. Chen, P.L. Urban, Coffee-ring effects in laser desorption/ionization mass spectrometry, Anal. Chim. Acta 766 (2013) 77–82, https://doi.org/10.1016/j.aca.2012.12.044.
[40] S. Bhattacharjee, DLS and zeta potential – what they are and what they are not? J. Contr. Release 235 (2016) 337–351, https://doi.org/10.1016/j.jconrel.2016.06.017.
[41] S. Mourdikoudis, R.M. Pallares, Characterization techniques for nanoparticles: comparison and complementarity upon studying, Nanoscale 10 (2018) 12871–12934, https://doi.org/10.1039/c8nr02278j.
[42] J.I. Goldstein, D.E. Newbury, J.R. Michael, N.W.M. Ritchie, J.H.J. Scott, D.C. Joy, Scanning Electron Microscope (SEM) Instrumentation, 2018, https://doi.org/10.1007/978-1-4939-6676-9_5.
[43] Q. Cui, B. Xia, S. Mitzscherling, A. Masic, L. Li, M. Bargheer, H. Möhwald, Preparation of gold nanostars and their study in selective catalytic reactions, Colloids Surfaces A Physicochem. Eng. Asp. 465 (2015) 20–25, https://doi.org/10.1016/j.colsurfa.2014.10.028.
[44] J. Depciuch, M. Stec, A. Maximenko, M. Pawlyta, J. Baran, M. Parlinska-Wojtan, Control of arms of au stars size and its dependent cytotoxicity and photosensitizer effects in photothermal anticancer therapy, Int. J. Mol. Sci. 20 (2019), https://doi.org/10.3390/ijms20205011.
[45] L. Cheng, X. Li, J. Dong, Size-controlled preparation of gold nanoparticles with novel pH responsive gemini amphiphiles, J. Mater. Chem. C. 3 (2015) 6334–6340, https://doi.org/10.1039/c5tc00624d.
[46] P. Scherrer, Bestimmung der Größe und der inneren Struktur von Kolloidteilchen mittels Röntgenstrahlen, Nachrichten von Der Gesellschaft Der Wissenschaften Zu Göttingen, Math. Klasse. (1918) 98–100, n.d. https://eudml.org/doc/59018#.YWAWtuyx4lE.mendeley. (Accessed 8 October 2021).
[47] J. Zhao, S.C. Nguyen, R. Ye, B. Ye, H. Weller, G.A. Somorjai, A.P. Alivisatos, F. Dean Toste, A comparison of photocatalytic activities of gold nanoparticles following plasmonic and interband excitation and a strategy for harnessing interband hot carriers for solution phase photocatalysis, ACS Cent. Sci. 3 (2017) 482–488, https://doi.org/10.1021/acscentsci.7b00122.
[48] Y. Zhang, C. Zhao, X. Wang, S. Sun, D. Zhang, L. Zhang, Y. Fang, P. Wang, Plasmon-driven photocatalytic properties based on the surface of gold nanostar particles, Spectrochim. Acta Part A Mol. Biomol. Spectrosc. 264 (2022), 120240, https://doi.org/10.1016/j.saa.2021.120240.
[49] J. Schiller, J. Arnhold, S. Benard, M. Müller, S. Reichl, K. Arnold, Lipid analysis by matrix-assisted laser desorption and ionization mass spectrometry: a methodological approach, Anal. Biochem. 267 (1999) 46–56, https://doi.org/10.1006/abio.1998.3001.
[50] E.T. Castellana, D.H. Russell, Tailoring nanoparticle surface chemistry to enhance laser desorption ionization of peptides and proteins, Nano Lett. 7 (2007) 3023–3025, https://doi.org/10.1021/nl071469w.
[51] T. Yonezawa, H. Kawasaki, A. Tarui, T. Watanabe, R. Arakawa, T. Shimada, F. Mafuné, Detailed investigation on the possibility of nanoparticles of various metal elements for surface-assisted laser desorption/ionization mass spectrometry, Anal. Sci. 25 (2009) 339–346, https://doi.org/10.2116/analsci.25.339.
[52] H.X. Shi, W.G. Sun, X.Y. Kuang, C. Lu, X.X. Xia, B. Le Chen, A. Hermann, Probing the Interactions of O 2 with Small Gold Cluster Au nQ (N = 2 – 10 , Q = 0 , – 1): A Neutral Chemisorbed Complex Au5O2 Cluster Predicted, 2017, pp. 24886–24893, https://doi.org/10.1021/acs.jpcc.7b09022.
[53] D.M. Cox, R. Brickman, K. Creegan, A. Kaldor, Gold clusters: reactions and deuterium uptake, Z. Physik D Atoms, Mol. Clust. 19 (1991) 353–355, https://doi.org/10.1007/BF01448327.
[54] X. Ding, Z. Li, J. Yang, J.G. Hou, Q. Zhu, Adsorption energies of molecular oxygen on Au clusters, J. Chem. Phys. 120 (2004) 9594–9600, https://doi.org/10.1063/1.1665323.
[55] M. Neumaier, F. Weigend, O. Hampe, M.M. Kappes, Binding energies of CO on gold cluster cations Aun+ (n=1-65): a radiative association kinetics study, J. Chem. Phys. 122 (2005), https://doi.org/10.1063/1.1854619.
[56] A. Zavras, G.N. Khairallah, R.A.J. O'Hair, Gas Phase Formation, Structure and Reactivity of Gold Cluster Ions, 2014, https://doi.org/10.1007/430_2014_140.
[57] W.T. Wallace, R.L. Whetten, Metastability of gold-carbonyl cluster complexes, AuN(CO)-M, Eur. Phys. J. D. 16 (2001) 123–126, https://doi.org/10.1007/s100530170075.

Supplementary material for manuscript entitled ‘LDI-MS performance of gold nanostars as an inorganic matrix for low molecular weight analytes’

by Gulyaim Sagandykova[§], Oleksandra Pryshchepa, Katarzyna Rafińska, Radik Mametov, Piotr Madajski and Paweł Pomastowski

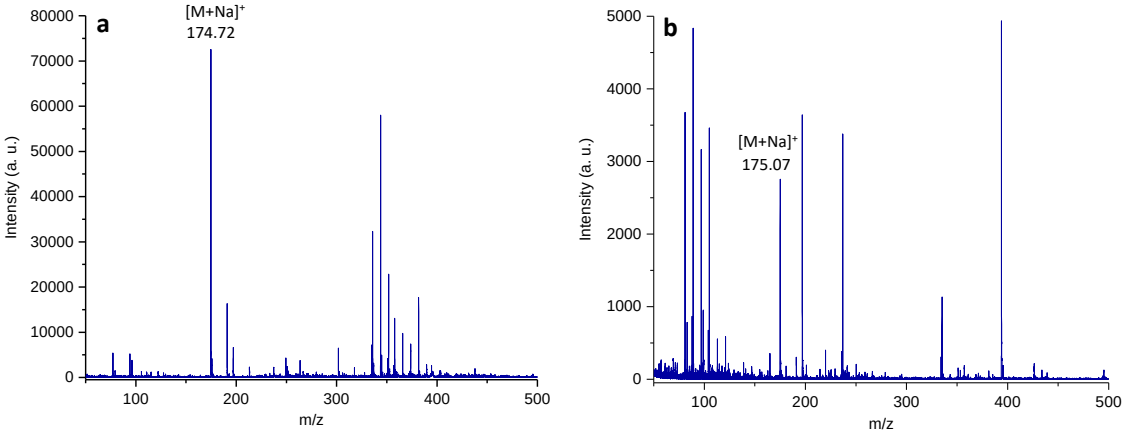

Figure S1. LDI-TOF-MS spectra of adonitol with application of gold nanostars: (a) classical commercial ground steel target; (b) lab-made target from stainless steel

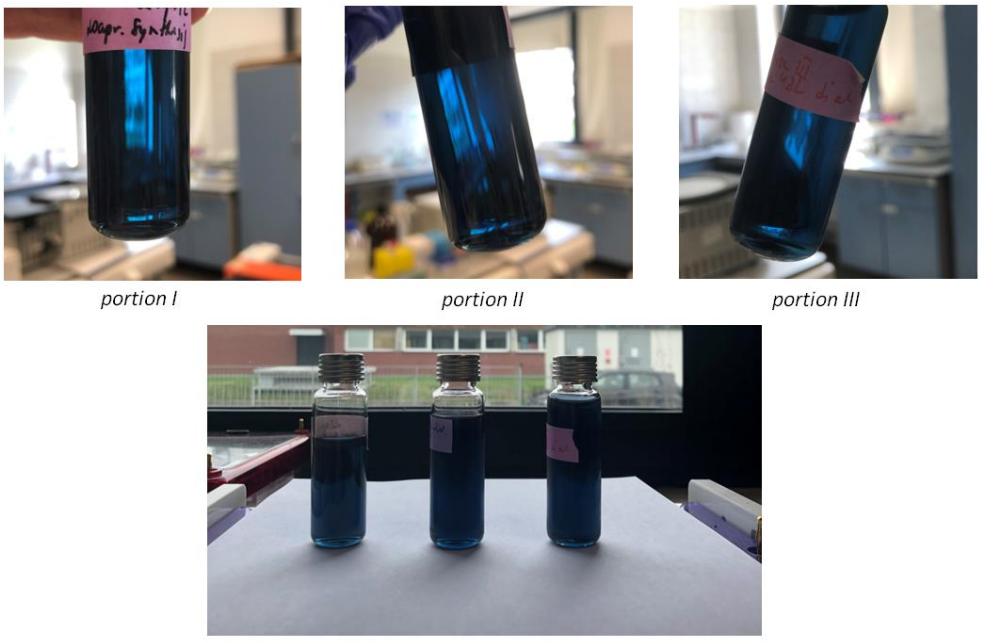

Figure S2. Color accents of three portions of gold nanostars after 48 hours of dialysis

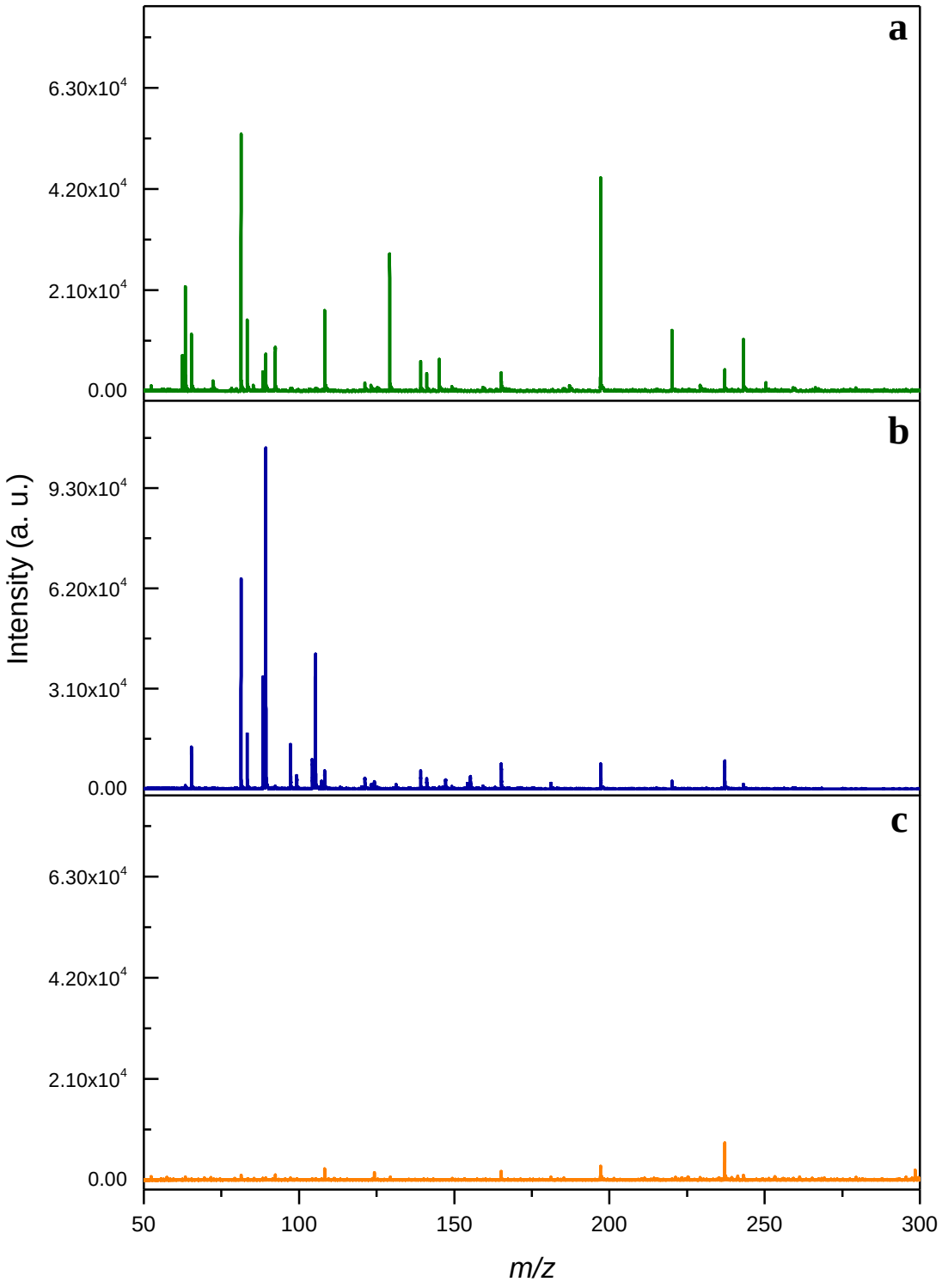

Figure S3. Comparison of ionization of gold nanostars: (a) freshly synthesized nanoparticles, (b) dialyzed for 24 hours and (c) dialyzed for 48 hours.

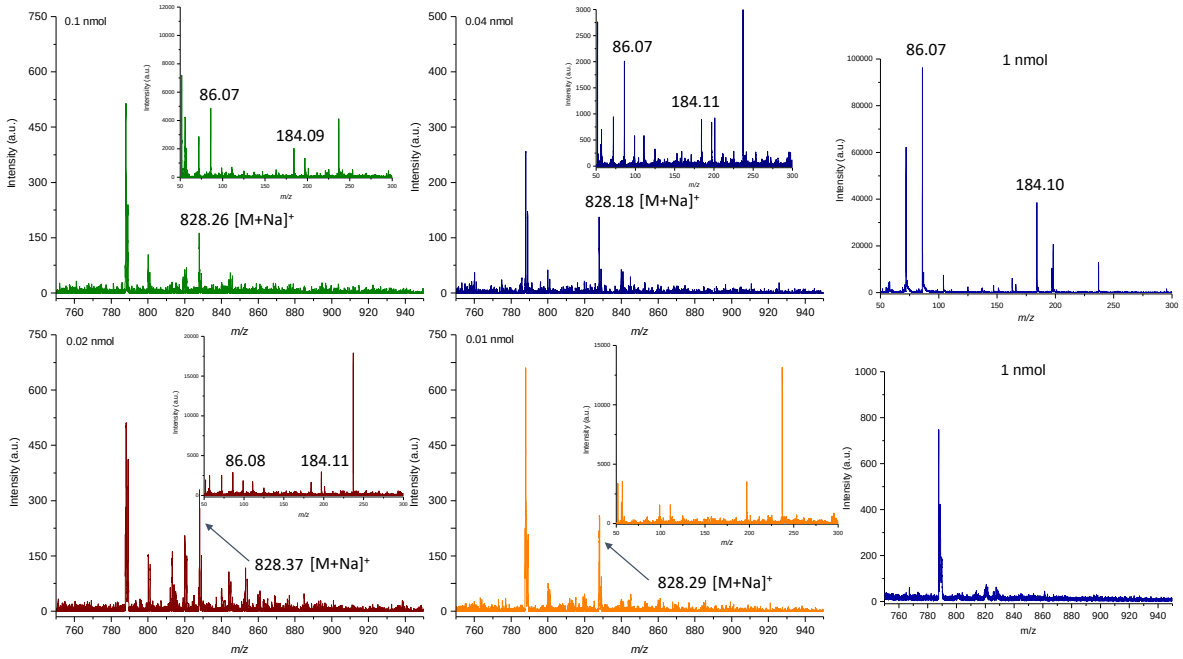

Figure S4. LDI-TOF-MS spectra of phospatidylcholine at concentrations 0.1, 0.01, 0.02, 0.04, 0.1 and 1 nmol

As evidenced from the spectra of PC (Fig. S4), an increase in concentration led to the absence of the signal of molecular ion, while lower concentration resulted in higher intensity. In contrast, intensity of fragments was observed to be higher for higher concentrations. However, in case of PI and *lyso*-PE, the same trend was not observed. Firstly, this can be probably explained by different tendency for fragmentation depending on the structure. In addition, such differences could be provided by different distribution of analytes on the surface depending on their hydrophobicity and affinity. Since the present study shows the performance of gold nanostars without control of the assembly on the plate, it seems that depending on the analytes, the assembly of analytes on the surface of nanoparticles is also an important aspect. Due to irregular shape, it could be interesting to study the adsorption of different analytes on gold nanostars. At the beginning of the study, different spotting techniques were applied to assess its effect on the analyte responses: (i) sample (1 ul) allowed to dry with further deposition of nanoparticles (1 ul), (ii) nanoparticles allowed to dry with further deposition of sample, (iii) nanoparticles allowed to dry with further deposition of sample and nanoparticles, (iv) mixing of the

analyte and nanoparticles (1:1) prior to deposition. Data (Fig. S5) showed that the response of adonitol by spotting method (iii) was the highest and the lowest response was obtained for spotting method (ii). Interesting thing is that application of metal nanoparticles instead of matrix generally involved pre-mixing of the sample with nanoparticles before deposition to the plate. It was suggested that in this case transfer of thermal energy can be more efficient, which may contribute to more efficient analyte desorption[52]. Since mechanisms of desorption and ionization may also depend on physico-chemical properties of the analyte, for different analytes such mechanisms can differ significantly. Therefore, it is interesting whether this is an indicator of non-thermal signal enhancement for cyclitols with utilization of gold nanostars as a matrix. On the other hand, this also can be explained by higher concentration of deposited nanostars with spotting method (iii), since this parameter was not controlled in this study.

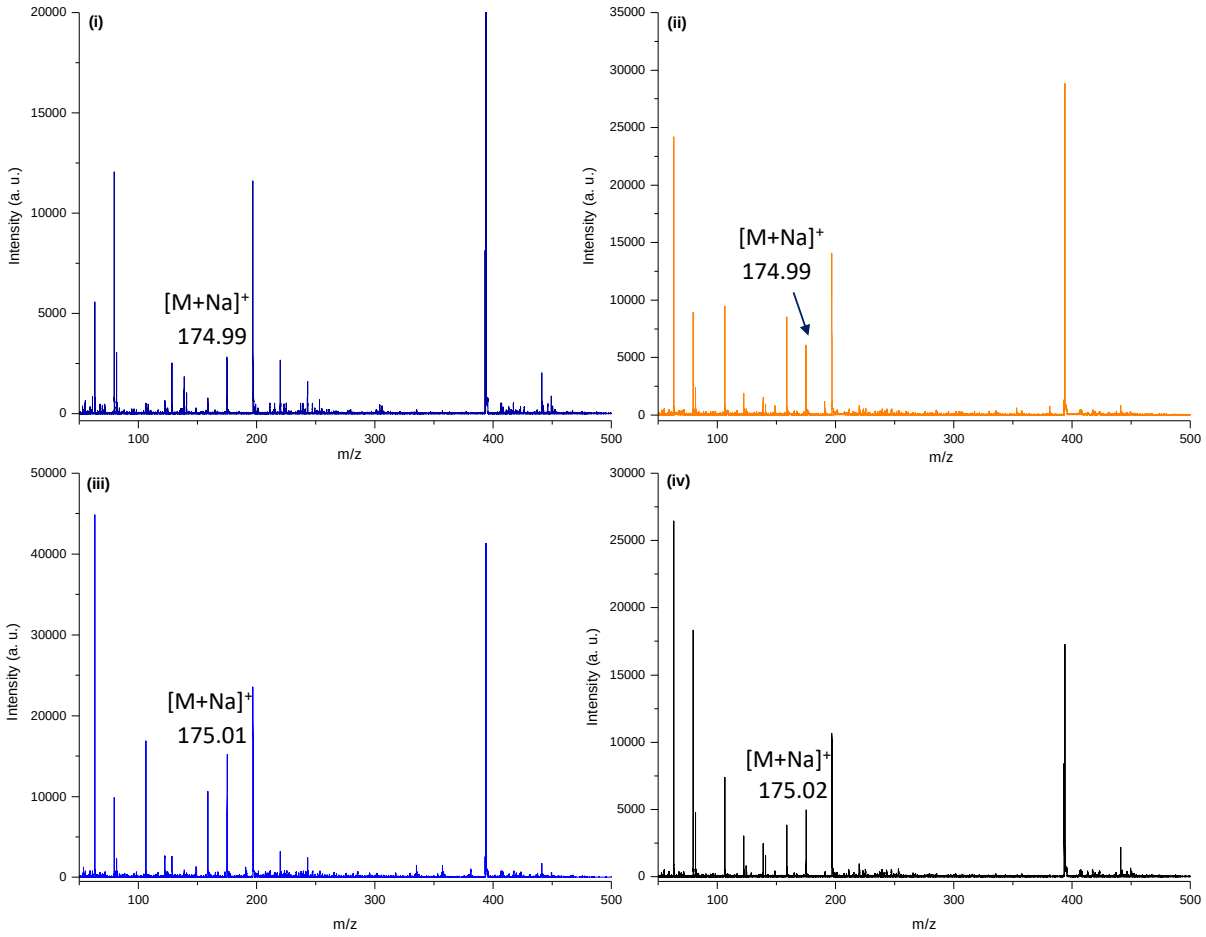

Figure S5. LDI-TOF-MS spectra of adonitol using different spotting techniques: i) sample (1 ul) allowed to dry with further deposition of nanoparticles (1 ul), (ii) nanoparticles allowed to dry with

further deposition of sample, (iii) nanoparticles allowed to dry with further deposition of sample and nanoparticles, (iv) mixing of the analyte and nanoparticles (1:1) prior to deposition

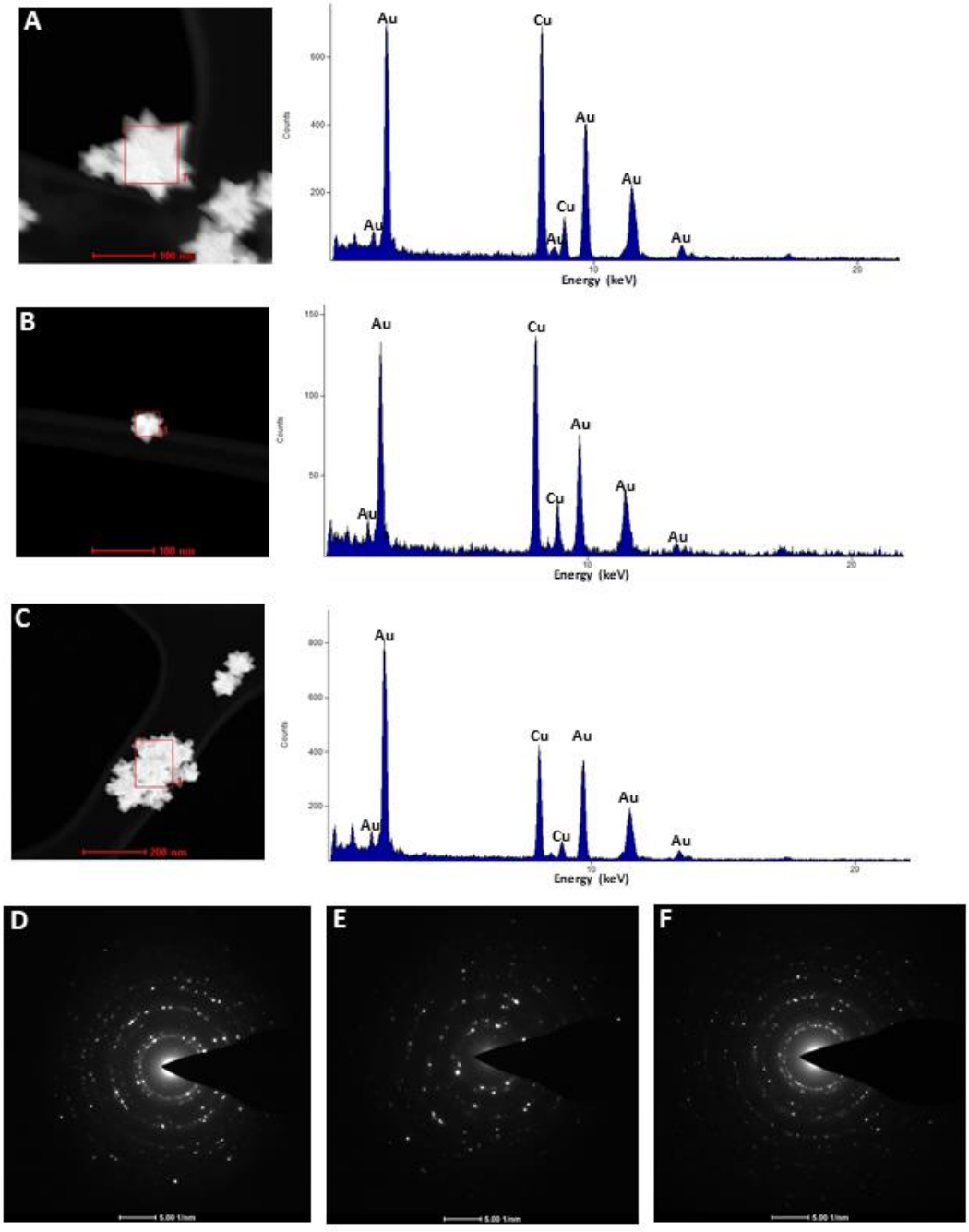

Figure S6. TEM-EDX spectra of gold nanostars; A, B and C – TEM pictures with corresponding EDX spectra for portions 1, 2 and 3, respectively; D, E and F – SAED images for portions 1, 2 and 3, respectively

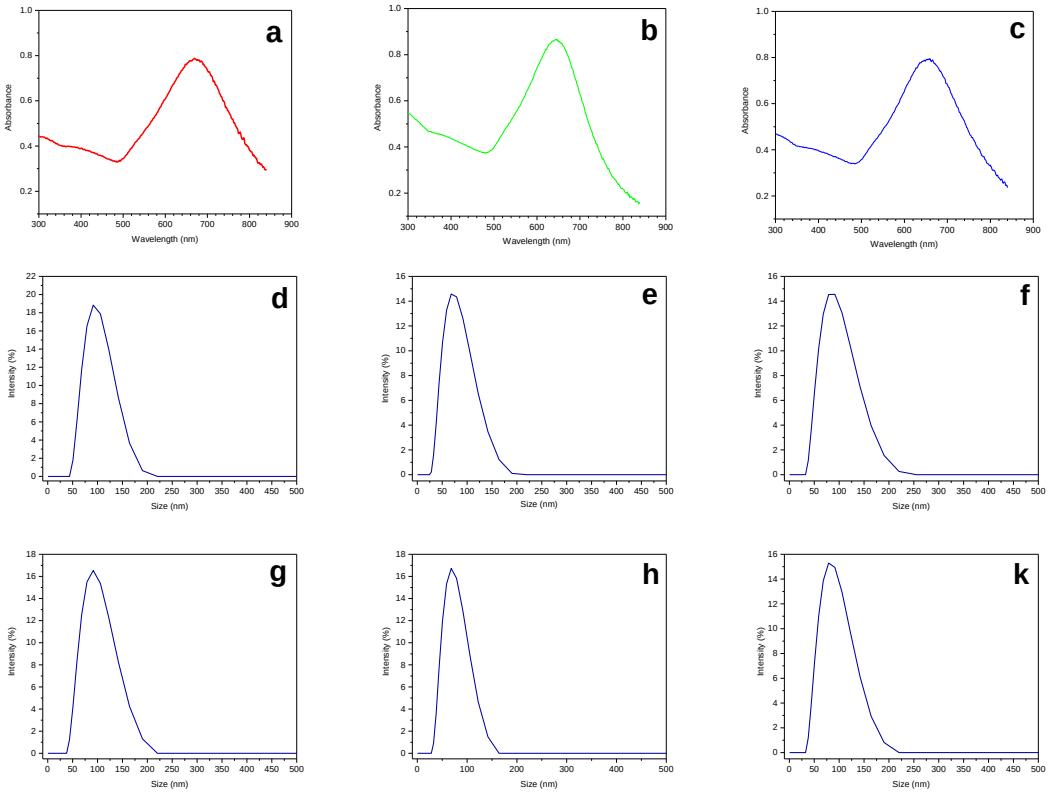

Figure S7. UV-Vis spectra and size distribution of gold nanostars: a – UV-Vis spectrum of freshly synthesized portion I, b and c – UV-Vis spectrum of freshly synthesized portions II and III, respectively; d, e and f – size distribution of freshly synthesized portions I, II and III, respectively; g, h and k – size distribution of portions I, II and III after storage during 2 months and 12 days at 4 ºC.

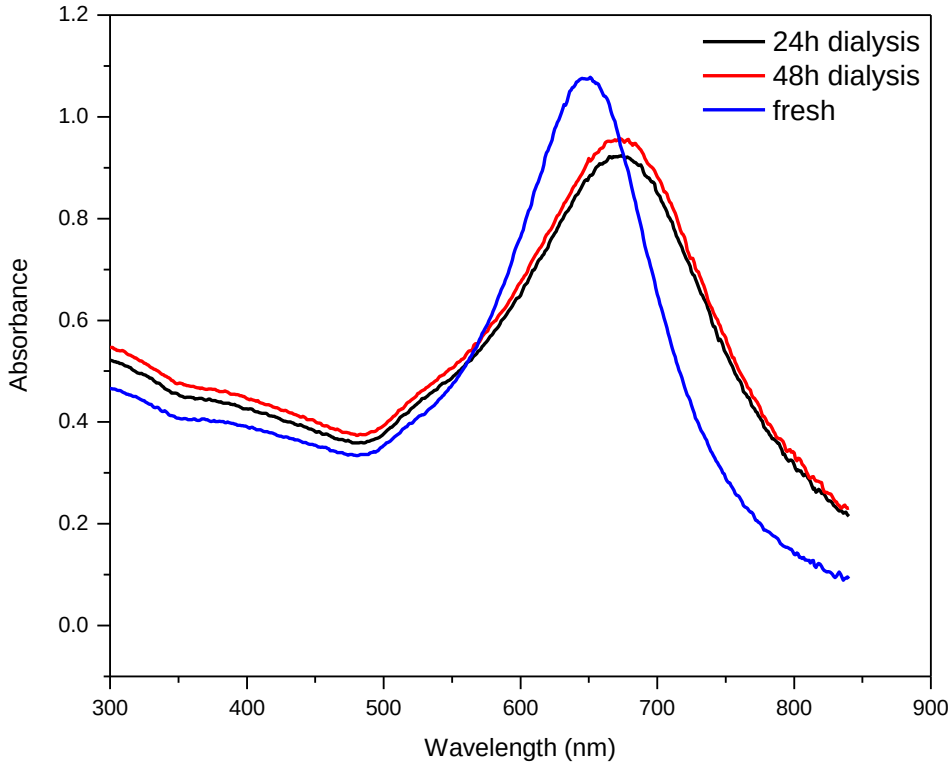

Figure S8. UV-Vis spectra of freshly synthesized gold nanostars as compared to dialyzed for 24 and 48 h

[P3] Sagandykova, G.; Piszczek, P.; Radtke, A.; **Mametov, R**.; Pryshchepa, O.; Gabryś, D.; Kolankowski, M.; Pomastowski, P. 'Silver Nanostructured Substrates in LDI-MS of Low Molecular Weight Compounds' *Materials (Basel).* 2022, *15* (13). IF = 3.748 MP = 140.

materials

MDPI

Communication

Silver Nanostructured Substrates in LDI-MS of Low Molecular Weight Compounds

Gulyaim Sagandykova [1,*], Piotr Piszczek [2], Aleksandra Radtke [2], Radik Mametov [1,3], Oleksandra Pryshchepa [1,3], Dorota Gabryś [4], Mateusz Kolankowski [1] and Paweł Pomastowski [1]

[1] Centre for Modern Interdisciplinary Technologies, Nicolaus Copernicus University in Toruń, Wileńska 4, 87-100 Toruń, Poland; mametov.radik@gmail.com (R.M.); pryshchepa.alexie@gmail.com (O.P.); mate.kola@hotmail.com (M.K.); pomastowski.pawel@gmail.com (P.P.)
[2] Department of Inorganic and Coordination Chemistry, Faculty of Chemistry, Nicolaus Copernicus University in Toruń, Gagarina 7, 87-100 Toruń, Poland; piszczek@umk.pl (P.P.); aradtke@umk.pl (A.R.)
[3] Department of Environmental Chemistry and Bioanalytics, Faculty of Chemistry, Nicolaus Copernicus University in Toruń, 87-100 Toruń, Poland
[4] Radiotherapy Department, Maria Sklodowska-Curie National Research Institute of Oncology, Gliwice Branch, Wybrzeże Armii Krajowej 15, 44-101 Gliwice, Poland; dorota.gabrys@io.gliwice.pl
* Correspondence: sagandykova.gulyaim1@gmail.com; Tel.: +48-56-665-60-01

Abstract: Mass spectrometric techniques can provide data on the composition of a studied sample, utilizing both targeted and untargeted approaches to solve various research problems. Analysis of compounds in the low mass range has practical implications in many areas of research and industry. Laser desorption ionization techniques are utilized for the analysis of molecules in a low mass region using low sample volume, providing high sensitivity with low chemical background. The fabrication of substrates based on nanostructures to assist ionization with well-controlled morphology may improve LDI-MS efficiency for silver nanoparticles with plasmonic properties. In this work, we report an approach for the preparation of silver nanostructured substrates applied as laser desorption ionization (LDI) plates, using the chemical vapor deposition (CVD) technique. Depending on the mass of used CVD precursor, the approach allowed the synthesis of LDI plates with tunable sensitivity for various low molecular weight compounds in both ion-positive and ion-negative modes. Reduced chemical background and sensitivity to small biomolecules of various classes (fatty acids, amino acids and water-soluble metabolites) at nanomolar and picomolar detection levels for lipids such as triacylglycerols, phosphatidylethanolamines and lyso-phosphatidylcholines represent an emerging perspective for applications of LDI-MS plates for the collection of molecular profiles and targeted analysis of low molecular weight compounds for various purposes.

Keywords: laser desorption/ionization mass spectrometry; small biomolecules; silver nanostructures; chemical vapor deposition

Citation: Sagandykova, G.; Piszczek, P.; Radtke, A.; Mametov, R.; Pryshchepa, O.; Gabryś, D.; Kolankowski, M.; Pomastowski, P. Silver Nanostructured Substrates in LDI-MS of Low Molecular Weight Compounds. *Materials* **2022**, *15*, 4660. https://doi.org/10.3390/ma15134660

Academic Editor: Andres Sotelo

Received: 19 May 2022
Accepted: 28 June 2022
Published: 2 July 2022

1. Introduction

Low molecular weight (LMW) compounds are targeted in various research fields with the aims of (i) searching for potential diseases biomarkers, e.g., gastric or prostate cancers [1,2], (ii) safety control of food products [3], (iii) environmental assessment [4] and (iv) applications in forensic science [5]. The 'gold standard' in the analysis of low molecular weight volatile organic compounds in various matrices is gas chromatography (GC) coupled to mass spectrometric (MS) techniques. Liquid chromatography mass spectrometry (LC-MS) also serves for the analysis of small molecules, including non-volatile compounds, providing high throughput in complex mixtures. However, the separation of samples with complex chemical composition complicates the analysis of large number of samples to collect the molecular profiles. The optimization of separation conditions is a laborious and time-consuming procedure, even though the required amount of sample remains to

be accounted in milliliters. In contrast, an untargeted approach in the application of MS techniques can be informative depending on the goal of the research, with low sample volume and providing fast data acquisition. In addition, mass spectrometry can serve as a versatile technique for the characterization of metal nanoclusters [6,7].

Laser desorption ionization/mass spectrometry (LDI-MS) was firstly utilized for the analysis of proteins with cobalt nanoparticles as an inorganic matrix by Tanaka et al. [8]. Noble metal nanoparticles are excellent candidates to assist ionization due to their UV-absorbing properties, chemical stability and reduced chemical background.

Many developments in the fabrication of various nanostructures based on noble metals such as gold and silver have been reported in the last decade [9]. One of the group of techniques employed for the fabrication of LDI nanoparticles-based substrates include wet and dry chemical methods. The wet chemical method is relatively simple and inexpensive; however, an uncontrolled aggregation of colloidal particles may occur, resulting in nonhomogeneous structures and thus significant signals inconsistency. Furthermore, the coffee ring effect can lead to a nonhomogeneous distribution of the analytes on the surface of nanostructures, resulting in poor reproducibility. To avoid aggregation, the preparation of the LDI substrates using wet chemical methods requires the application of stabilizers and reducing agents, which may complicate the spectra. On the other hand, dry methods such as electron beam lithography have provided well-controlled nanostructures and highly reproducible LDI performance [10]. However, these nanofabrication techniques require highly sophisticated and high-cost devices, as well as time-consuming and complicated procedures. Therefore, it is essential to prepare flexible, low-cost, time-saving and well-controlled nanostructured substrates for the analysis of low molecular weight profiles, with high sensitivity and reproducibility. Stainless steel is advantageous for the preparation of LDI-MS substrates due to its inexpensive price and relative chemical inertness. Moreover, H17 steel is available for commercial purchase in a wide variety of sheets of various thicknesses and sizes, which also simplifies its use as a substrate.

Chemical vapor deposition technique allows the synthesis of nanolayers of inorganic materials on the surface of 3D substrates [11]. The success of the deposition is dependent on the precursor utilized for synthesis; highly volatile, thermally stable compounds enable clean decomposition, potentially resulting in reduced chemical background when used in LDI-MS. Moreover, since the procedure is computer-controlled, it allows for the synthesis of well-controlled substrates and it is beneficial for target-to-target reproducibility [12]. Notably, well-controlled morphology may enhance the plasmonic properties of noble metals [13], potentially leading to the enhancement of LDI efficiency.

Despite the utilization of the CVD technique for fabrication of a nanostructured layer on various substrates, rare efforts have been focused on its application in LDI-MS. The CVD technique has been used previously for fabrication of carbon nanotubes [14] that were applied in the LDI-MS analysis of carbohydrates and amino acids. In addition, it has been utilized for synthesis of carbon nanowalls to be applied in analysis of fatty acids, lipids, saccharides, peptides [15], amino acids [16]; and graphene for analysis of carbohydrates [17]. To the best of our knowledge, metal nanostructures synthesized using the CVD technique have not yet been reported in LDI-MS analysis.

The aim of this study was to study the effect of the mass of the precursor on morphology and the LDI-MS efficiency of the obtained silver nanostructures towards low molecular weight analytes with utilization of chemical vapor deposition techniques. The LDI-MS plates synthesized with the proposed approach showed tunable sensitivity in both ion-positive and ion-negative modes. The plates can be used for the collection of molecular profiles and the analysis of small biomolecules with targeted approach at nanomolar and picomolar detection levels.

2. Materials and Methods

2.1. Reagents and Materials

Standards of low molecular weight compounds such as adonitol, glucose, fructose, shikimic acid, oleic acid, palmitic acid, cholesterol, methionine, serine, alanine and phenylalanine, all of the highest available purity, were purchased from Sigma Aldrich (Steinheim, Germany). Standards of various classes of lipids were purchased from Avanti Polar Lipids (Alabaster, AL, USA), including phosphatidylcholine 18:0 (<99%), lyso-PC, PE, PI and TG internal standard mixture (Ultimate SPLASH™, Avanti Polar Lipids, Alabaster, AL, USA). Solvents for the preparation of stock solutions of LC-MS grade quality (≥99.9%), such as water and chloroform, were purchased from Sigma Aldrich (Steinheim, Germany).

2.2. Synthesis and Characterization of LDI-MS Plates

For the synthesis of the LDI plates, stainless steel (H17) was cut to pieces 2.5 × 7.5 cm. The surfaces of the steel samples (substrates) were covered by the silver coating, consisting of densely packed silver nanoparticles and microparticles (AgPs). For this purpose, a chemical vapor deposition (CVD) technique was used under conditions described in Table 1. In our CVD experiments, $Ag_5(O_2CC_2F_5)_5(H_2O)_3$ has been used as a precursor, the synthesis and physicochemical properties of which were earlier described [11,18–21]. The $[Ag_5(O_2CC_2F_5)_5(H_2O)_3]$ compound has also been used as a precursor in our CVD experiments; the synthesis and physicochemical properties of the compound were described earlier [11,21]. The fast and cheap synthesis of this precursor are among its advantages, as well as high structural stability of the silver(I) compound, allowing for long storage at room temperature without the access of light. The substrate surface preparation for the CVD process consisted of washing in an ultrasonic bath with distilled water containing a non-ionic surfactant for degreasing for 45 min (twice). Then, the substrate was immersed in the acetone (analytical grade) for 30 min, then distilled water for 10 min and, after drying in an Ar stream, it was placed in a CVD reactor. The morphology of created coatings was studied using a scanning electron microscope (SEM, Quanta 3D FEG, Houston, TX, USA). The structure of the AgPs films was investigated using an energy-dispersive X-ray diffractometer (Quantax 200 XFlash 4010) with a copper monochromator and CuKα radiation (λ = 0.15418 nm). XRD patterns were collected in the 2Θ range 10–80°, step 0.02° and time 20 sec. The Sartorius MCA2.7S-2S00-M microbalance (Sartorius Lab Instruments GmbH & Co. KG, Goettingen, Germany) has been applied to determine the weight of the reference sample before and after the CVD process. The stainless steel (H17) reference samples of sizes 1 × 1 cm were placed in the CVD reactor together with the investigated sample to obtain similar deposition conditions.

Table 1. Deposition parameters of AgNPs' coatings.

Precursor	$Ag_5(O_2CC_2F_5)_5(H_2O)_3$
Precursor weight (mg)	2.5, 5, 10, 15, 35, 50, 70, 100
Vaporization temperature (T_V) (°C)	230
Carrier gas	Ar
Total reactor pressure (p) (mbar)	3.0
Substrate temperature (T_D) (°C)	290
Substrates	stainless steel (H17)
Deposition time (min)	60
Sample heating time (min)	30 (Ar/H_2 (3:1%))

For the purposes of the MALDI experiments, Ag films were prepared in real time, and the storage time of samples (in a closed box, at room temperature and with limited access to light) was not longer than 2–3 days.

2.3. LDI-MS Analysis

The LDI-MS performance of the synthesized plates was evaluated by using stock solutions at concentration of 1 mg/mL and standard mixtures of various lipids. Stock solutions of adonitol, glucose, fructose, shikimic acid, methionine, serine, alanine and phenylalanine were prepared by dissolving a powder of each standard in water using 1.5 mL Eppendorf tubes. Stock solutions of cholesterol, oleic acid, palmitic acid and PC were prepared by dissolving a powder of each standard in chloroform using 1.5-mL amber glass vials and glass syringes for manual sample preparation (Agilent, Santa Clara, CA, USA). The standard mixtures of the various lipids were sonicated for 5 min prior to spotting to the target plate to avoid precipitation of lipids during storage. Subsequently, 1 µL of the stock solution of each compound and standard mixture was spotted to the synthesized LDI plates. LDI-MS analysis of low molecular weight compounds was carried out in both positive and negative ion-reflectron modes with the utilization of laser power at 80% in the mass range of m/z 60–1500. Analysis was performed using an UltrafleXtreme II MALDI-TOF-MS apparatus (Bruker Daltonics, Bremen, Germany) equipped with a modified neodymium-doped yttrium aluminium garnet (Nd:YAG) laser operating at 355 nm and frequency 2 kHz. The value of global attenuator offset was 30%, with a parameter set '5_ultra' and the detector gain for reflector was 2.51× for all low molecular weight compounds except lipids. The following parameters were used for lipids: global attenuator offset 25%, with parameter set '4_large' and the value of detector gain set to 30×. Mass calibration was performed using signals of silver using quadratic and cubic enhanced calibration methods individually for each spectrum. Reflector voltages accounted for 26.64 and 13.54 kV with first accelerating voltage set to 25.08 kV and the value for the second ion source voltage was 22.43 kV for the ion-positive mode. Reflector voltages for the ion-negative mode were 21.31 and 10.82 kV, with 20.07 kV as the first accelerating voltage and 17.97 kV as the second ion source voltage. Theoretical m/z values of the analyzed compounds were calculated by using ChemCalc program [22]. The number of laser shots was 2000 (4 × 500 shots) for each compound. LDI-MS targets were inserted into an MTP Slide-Adapter II (Bruker Daltonics, Bremen, Germany) and utilized for the collection of data. Heatmaps were prepared using GraphPad Prism software (version 8.0.1., San-Diego, CA, USA).

3. Results and Discussion

3.1. Characterization of LDI Plates

Our main idea was to study the dependency between the size of the deposited silver particles (AgPs), the coatings' surface morphology and the LDI plates' sensitivity to various low molecular weight compounds. For this purpose, the plates were subjected to characterization using scanning electron microscopy (SEM) and X-ray diffraction (XRD) techniques. The obtained results are presented in Table 2 and Figures 1 and 2. The produced coatings consisted of densely packed metallic silver nano- and microparticles uniformly covering the entire surface of the LDI plates (Figure 1). The use of different masses of solid Ag precursor and similar deposition conditions (Table 1) enabled controlling the surface morphology of the deposited layers as well as controlling the size of the AgPs deposited. The analysis of SEM images revealed that the produced coatings could be divided into three groups from a morphological point of view (Figure 1). The use of the high Ag precursor concentrations (precursor weight: 35–100 mg) and accompanying coalescence effects led to a deposition of mainly micro-AgPs with irregular shapes. Films, which consisted of densely packed silver nanoparticles similar in shape to a sphere, were produced in the case of low precursor concentrations in vapors (precursor weight: 5–15 mg). Medium grain sizes of AgPs ranged from 50 to 240 nm for coatings produced using 5 and 15 mg of the precursor, respectively (Table 2, Figure 1). The further reduction in the applied precursor weight (up to 2.5 mg) caused a layer formation consisting of dispersed AgPs of dimeter ca. 150 nm. The registration of XRD patterns for studied samples confirmed the deposition of a pure form of metallic silver nanoparticles on the surface of steel substrates (Figure 2).

Table 2. AgNPs films deposited by CVD technique.

Sample	Precursor Weight (mg)	Percentage Substrate Mass Increase after the CVD Process (wt.%)	AgPs Medium Grain Size (μm)
AgPs 0.20	100	0.20	0.7–2.8 ± 0.2–0.9
AgPs 0.19	75	0.19	0.5–1.7 ± 0.2–1.0
AgPs 0.17	50	0.17	0.2–0.7 ± 0.09–0.2
AgPs 0.11	35	0.11	0.33 ± 0.09
AgPs 0.06	15	0.06	0.24 ± 0.08
AgPs 0.04	10	0.04	0.15 ± 0.05
AgPs 0.03	5	0.03	0.05 ± 0.01
AgPs 0.02	2.5	ca. 0.02	0.15 ± 0.08

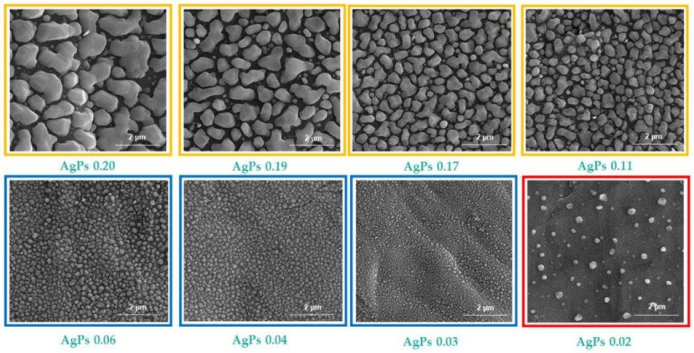

Figure 1. SEM images of AgPs films deposited on the surface of stainless steel (H17) substrates using CVD technique.

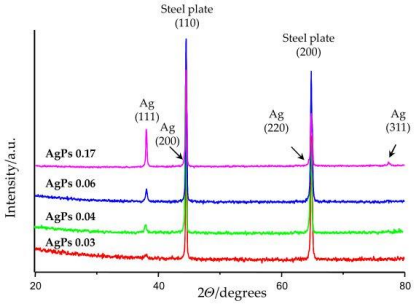

Figure 2. X-ray diffraction patterns of AgPs films deposited using CVD technique. A number of Bragg reflection peaks were observed at 2θ values of 38.2°, 44.3°, 64.3° and 77.6°, which are indexed to (111), (200), (220) and (311), respectively.

3.2. LDI-MS Performances of Silver Nanostructures for Low Molecular Weight Biomolecules

According to obtained results (Figure 3), all of the synthesized plates showed sensitivity to various low molecular weight compounds in both ion-positive and ion-negative modes. Low molecular weight analytes are biological molecules fulfilling various functions in the human organism and, thus, may serve as biomarkers of pathological processes, as has been suggested in numerous studies [1,23–25]. The studied compounds can be divided into three groups: water-soluble compounds, fatty acids and lipids, and amino acids. All compounds except lipids were ionized at nanomolar concentrations, while lipids showed sensitivity in both positive and negative modes at the picomolar level.

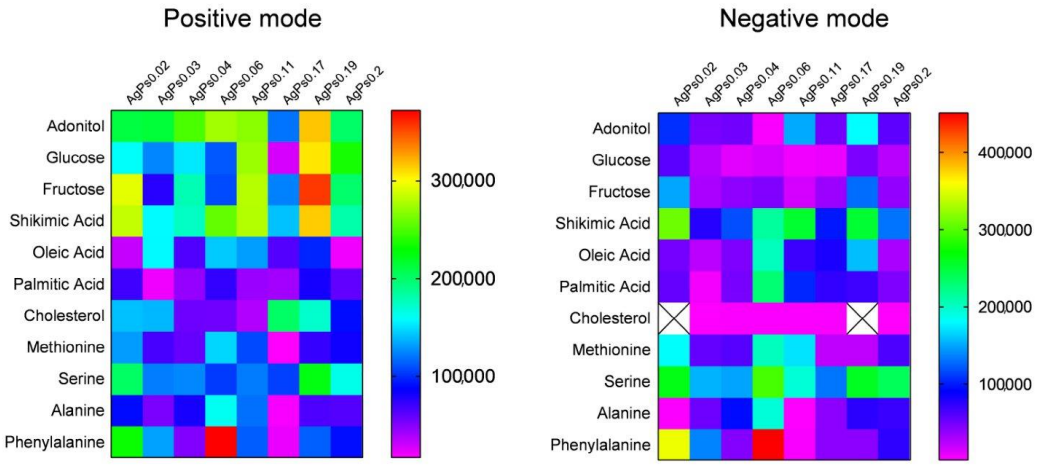

Figure 3. LDI-MS performances of the LDI-MS plates with various masses of silver for the analysis of low molecular weight compounds; molecular ions for all the compounds in positive mode were assigned as $[M + {}^{107}Ag]^+$.

LDI-MS intensity has been shown to be different for various compounds depending on the mass of the precursor for both ion-positive and ion-negative modes. The differences in LDI-MS dependent on the applied mass of the precursor probably could be explained by the amount of deposited silver and the differences in the affinity of compounds towards silver nanostructures. Interactions of the analytes with nanostructured substrates may affect LDI-MS efficiency, and they can be characterized by complementary analytical techniques. A good example of such work was reported by Mandal et al. [26].

Figure 3 shows that the proposed approach allows for the synthesis of LDI plates with tunable sensitivity towards low molecular weight analytes. Water-soluble compounds such as adonitol, glucose and fructose showed higher intensity in the positive mode for all plates, as compared to shikimic acid, which demonstrated comparable intensities for plates AgPs0.02, AgPs0.11 and AgPs0.19 in the negative mode. Cholesterol was more efficiently ionized in the positive mode (Figure 3). Fatty acids showed LDI-MS intensity $<2 \times 10^5$ a.u. for all plates in both modes, except palmitic acid for plate AgPs0.06. In addition, the plates AgPs0.03, AgPs0.06 and AgPs0.11 in positive mode, in addition to AgPs0.06 and AgPs0.19, showed LDI-MS intensities close to 2×10^5 a.u. for oleic acid. The plate AgPs0.06 was shown to be the most efficient for phenylalanine in both modes. Serine showed efficient ionization with intensity $>2 \times 10^5$ a.u for plates AgPs0.02 and AgPs0.19 in positive mode and AgPs0.02, AgPs0.06, AgPs0.19 and AgPs0.2 in negative mode. The ionization of methionine occurred with similar intensities $<2 \times 10^5$ a.u for all the plates in positive mode and intensities close to 2×10^5 for the plates AgPs0.02, AgPs0.06 and AgPs0.11 in negative mode.

Notably, all of the compounds were detected in negative mode as $[M]^-$ radical ions for all plates with high abundance. For some of the analytes, $[M - H]^-$ species were also detected, as well as signals that may correspond to the fragments. Ionization in negative mode could occur via transfer of the hot electrons, as was suggested by Li et al., and hot electrons could be a source of charges in plasmonic metal nanostructures [27]. The occurrence of hot electrons can probably be explained by the well-controlled morphology of the silver nanostructures deposited by the CVD technique. To the best of our knowledge, hot electrons can be generated via localized surface plasmon resonance (LSPR) and interband transition [28]. Since LSPR depends strictly on the shape and size of the nanostructure, and all the plates showed sensitivity in ion-negative mode, the occurrence of hot electrons

could also be related to interband transition. The occurrence of the signals corresponding to Ag_n^-, which were observed for all the plates, also could be related to hot electrons [29].

Interestingly, the synthesized plates showed comparable efficiencies in both ion-positive and ion-negative modes, which might indicate an advantage for further applications of the plates. One possible interpretation is that the plates possess mechanisms of ion formation for both ion-positive and ion-negative modes. Substrate morphology allows for occurrence of both mechanisms: hot electrons transfer in negative mode and the cationization of silver in positive mode. The versatility of the obtained substrates for applications in ion-positive and ion-negative modes can be seen as potentially advantageous for the selective ionization of lipids in samples with rich composition. This may bring advantages for particular applications where selected classes of lipids are of interest; however, other classes of lipids with similar structures create interferences in mass spectra. Moreover, the selective isolation of lipids from samples with rich chemical compositions also represents an analytical challenge.

3.3. LDI-MS Performances of Silver Nanostructures for Lipids

The LDI-MS efficiency of the plates for lipids was evaluated using deuterated standard mixtures. Phosphatidylethanolamines (PEs) and triacylglycerols (TG) were detected in ion-negative mode at the picomolar level. Signals corresponding to $[M-2H]^-$ and $[M-3H]^-$ were assigned to molecular ions of PEs in negative mode (Figure 4). The plate AgPs0.02 provided the lowest intensities for PEs as compared to the plates AgPs0.11 and AgPs0.2, corresponding to 35 and 100 mg of precursor, respectively. In addition, plates AgPs0.02 and AgPs0.03 showed molecular ions as $[M-3H]^-$ and plate AgPs0.11 showed $[M-2H]^-$ for all PEs in the mixture. Plate AgPs0.2 provided $[M-2H]^-$ for PEs with the highest values of monoisotopic mass (Figure 4; signals 4,5) and $[M-3H]^-$ for PEs assigned to 1, 2 and 3 (Figure 4). It could be suggested that such differences are related to the morphology and size of the obtained nanostructures. For example, ionization patterns of PEs were similar for the plates AgPs0.02 and AgPs0.03, both of which have specific features as compared to other plates, such as size (50 ± 10 nm) in the case of AgPs0.02, and morphology, i.e., isolated nanostructures, in the case of AgPs0.03. In contrast, plates AgPs0.11 and AgPs0.2, which showed higher intensities for PEs, consisted of microparticles with irregular shape. Moreover, affinities of lipids towards the nanostructured substrates also affect LDI-MS performance. It has been suggested that the high affinity of the analyte molecules towards the substrate can lead to reduced ionization efficiency, since it can decrease analyte desorption [30]. On the other hand, interactions between analyte molecules and substrate can promote selective and sensitive LDI ionization, as for example, was reported for olefins and silver nanoparticles [31]. Furthermore, the surface adsorption of the analytes may also play a role, thus suggesting that differences between the substrates could be also explained by differences in the surface area [32].

Triacylglycerols (TGs) were detected for the plate Ag0.11 in negative mode (Figure 5). All plates showed signals assigned to $[M-2H]^-$ for all triacylglycerols. Only the TG with mass 929.84 Da was not detected in negative mode.

Triacylglycerols were also detected for all plates in ion-positive mode (Figure 6). The heatmap (Figure 6) presents intensities for molecular ions assigned as an adduct such as $[M+Ag]^+/[M+Na]^+/[M+K]^+$, selected as those with the highest values of LDI-MS efficiency. The complete list of the values of m/z is presented in Table S1. According to obtained results (Figure 6, Table S1), plate AgPs0.02 provided signals corresponding to mostly $[M+Ag]^+$ with the exception of TGs 18:1-17:1:18:1 and 18:1-19:2-18:1, which were detected as $[M+H]^+$ assigned to m/z 984.70 and 1010.71, respectively. The other plates showed signals corresponding to $[M+Na]^+$ in most cases, and only selected plates showed signals corresponding to $[M+Ag]^+$ and $[M+H]^+$ (Table S1).

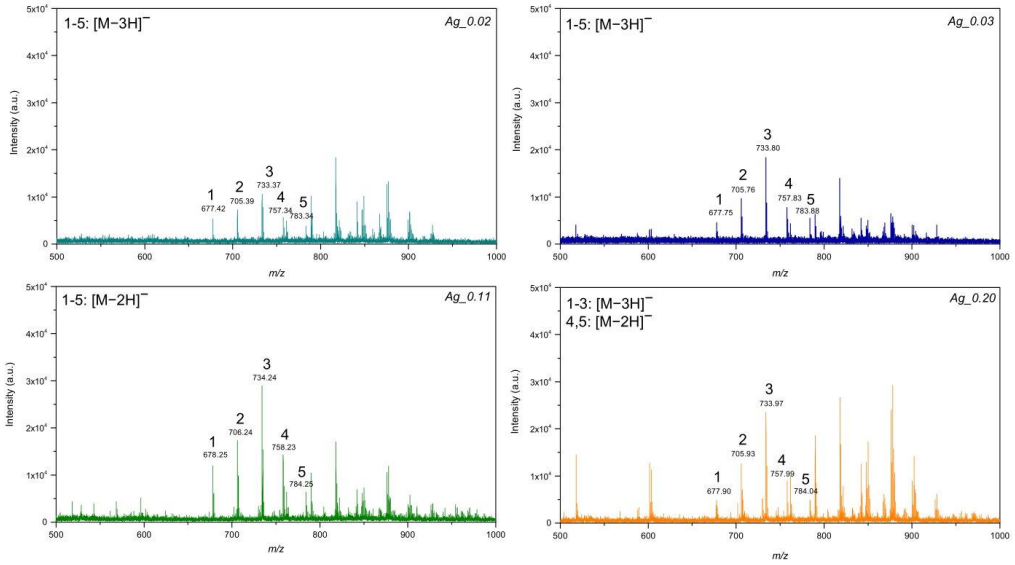

Figure 4. LDI-MS spectra of the standard mixture of phosphatidylethanolamines, where 1—17:0-14-1 PE (25 µg/mL); 2—17:0-16:1 PE (50 µg/mL); 3—17:0-18:1 PE (75 µg/mL); 4—17:0-20:3 PE (50 µg/mL); 5—17:0-22:4 PE (25 µg/mL), for the LDI plates AgPs0.02, AgPs0.03, AgPs0.11 and AgPs0.2.

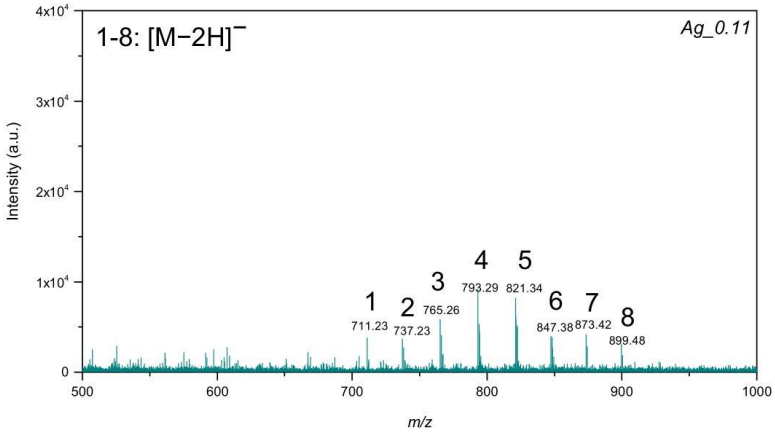

Figure 5. LDI-MS spectra of the standard mixture of triacylglycerols, where 1—14:0-13:0-14:0 TG (25 µg/mL); 2—14:0-15:1-14:0 TG (50 µg/mL); 3—14:0-17:1-14:0 TG (75 µg/mL); 4—16:0-15:1-16:0 TG (100 µg/mL); 5—16:0-17:1-16:0 TG (125 µg/mL); 6—16:0-19:2-16:0 (100 µg/mL); 7—18:1-17:1-18:1 TG (75 µg/mL); 8—18:1-19:2-18:1 TG (50 µg/mL).

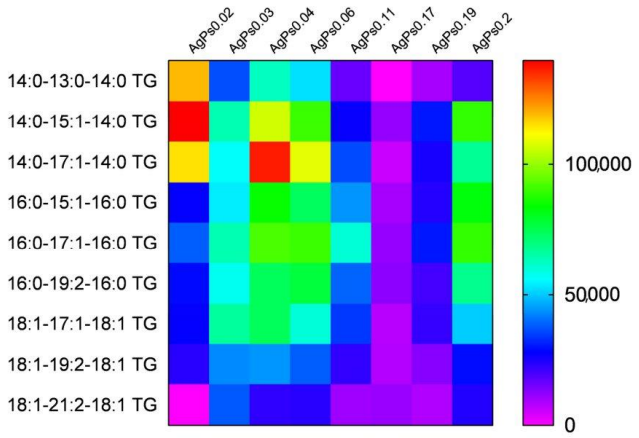

Figure 6. LDI-MS performance of LDI-MS plates with various masses of silver for analysis of standard mixture of triacylglycerols.

All of the lyso-PCs of the standard mixture were detected using plate AgPs0.04 (Figure 7). The signal at m/z 487.11 was assigned to $[M + H]^+$ and the signal at m/z 524.88 was assigned to $[M + K]^+$ corresponding to 15:0 lyso-PC. Other lyso-PCs such as 17:0 and 19:0 were detected as $[M + H]^+$ at m/z 515.02 and 543.02, respectively. The other plates, such as AgPs0.06 and AgPs0.11, provided molecular ions for only selected lyso-PCs. For example, the plate AgPs0.06 allowed to register 15:0 lyso-PC as $[M + Na]^+$ at m/z 598.90 and $[M + K]^+$ at m/z 524.90, only where the value of global attenuator was 25% and parameter set '4_large', while for plate AgPs0.04, registered molecular ions for all lyso-PCs and such conditions were not necessary. The plate AgPs0.11 provided molecular ions assigned to $[M + K]^+$ at m/z 524.83 corresponding to lyso-PC 15:0. The plate AgPs0.2 showed that the signal at m/z 525.35 was assigned to $[M + K]^+$ (15:0 *lyso*-PC), and the signal at m/z 538.66 probably corresponds to $[M + Na + H]^+$ with relatively low intensity (S/N value equal to 6). $[M + Na + H]^+$ species were probably less stable in the gas phase from the thermodynamic point of view.

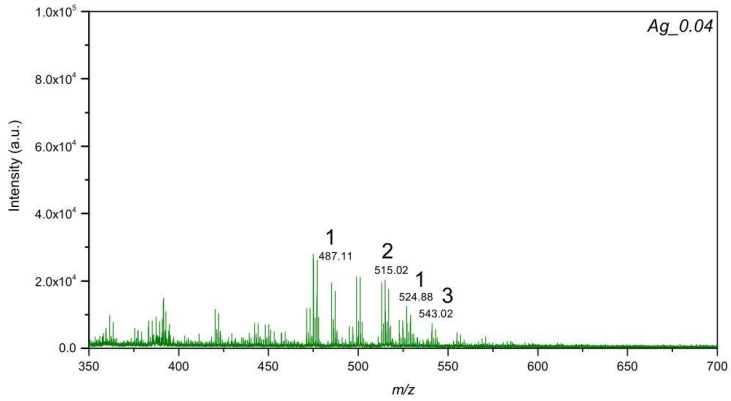

Figure 7. LDI-MS spectra of the standard mixture of lyso-phosphatidylcholines, where 1—15:0 LPC (25 µg/mL); 2—17:0 LPC (50 µg/mL); 3—19:0 LPC (25 µg/mL).

The other classes of lipids (PC, PE and PI) might have undergone fragmentation, since their molecular ions were not detected. Due to the plasmonic properties of noble metal nanostructures, an excess of energy could lead to an enhanced fragmentation of lipids, which may complicate identification. A decrease in laser power did not result in obtaining signals corresponding to molecular ions. However, the plates could be used in the future for the collection of molecular profiles of samples, with an aim to reveal the differences and similarities between the samples, since fragments of various classes of lipids also can be characteristic.

4. Conclusions

The presented approach allows for the synthesis of LDI plates with tunable sensitivity for various classes of small biomolecules. The utilization of a chemical vapor deposition technique with various values of the mass of the precursor resulted in the formation of structures with sizes 50–330 nm and up to 1 µm with irregular shapes. Small biomolecules were detected at nanomolar concentrations, while lipids were detected at the picomolar level with a reduced chemical background. Sensitivity towards low molecular weight analytes in both ion-positive and ion-negative modes is an advantage for the applications of the plates for the collection of molecular profiles as well as targeted analysis.

Supplementary Materials: The following supporting information can be downloaded at: https://www.mdpi.com/article/10.3390/ma15134660/s1, Table S1: The m/z values for compounds detected using LDI-MS nanostructured substrates.

Author Contributions: Conceptualization, G.S., P.P. (Piotr Piszczek), A.R., O.P., D.G. and P.P. (Paweł Pomastowski); methodology, G.S., P.P. (Piotr Piszczek), A.R.; validation, G.S.; formal analysis, G.S., P.P. (Piotr Piszczek), R.M., M.K., investigation, G.S., P.P. (Piotr Piszczek), A.R., R.M., O.P., D.G., M.K., P.P. (Paweł Pomastowski); resources, P.P. (Paweł Pomastowski); data curation, G.S., P.P. (Piotr Piszczek), R.M. and O.P.; writing—original draft preparation, G.S., P.P. (Piotr Piszczek), O.P.; writing—review and editing, G.S., P.P., A.R., D.G. and P.P.; visualization, G.S., P.P. (Piotr Piszczek) and O.P.; supervision, P.P. (Paweł Pomastowski); project administration, G.S.; funding acquisition, G.S. All authors have read and agreed to the published version of the manuscript.

Funding: This study was financially supported by the National Science Center (Kraków, Poland) within a framework of Preludium 16 grant no. 2018/31/N/ST4/02210 (2019–2022).

Institutional Review Board Statement: Not applicable.

Informed Consent Statement: Not applicable.

Data Availability Statement: All data generated or analyzed during this study are included in this published article (and its Supplementary Information files).

Acknowledgments: The authors would like to thank Nano Implant Ltd. for mechanical and technical processing of stainless-steel plates, and Justyna Walczak-Skierska, Adrian Arendowski and Ewelina Maślak for their help with technical questions. In addition, the authors are grateful towards Bogusław Buszewski for consulting on technical questions of grant realization.

Conflicts of Interest: The authors declare no conflict of interest.

References

1. Su, H.; Li, X.; Huang, L.; Cao, J.; Zhang, M.; Vedarethinam, V.; Di, W.; Hu, Z.; Qian, K. Plasmonic Alloys Reveal a Distinct Metabolic Phenotype of Early Gastric Cancer. *Adv. Mater.* **2021**, *33*, 2007978. [CrossRef] [PubMed]
2. Ossoliński, K.; Nizioł, J.; Arendowski, A.; Ossolińska, A.; Ossoliński, T.; Kucharz, J.; Wiechno, P.; Ruman, T. Mass Spectrometry-Based Metabolomic Profiling of Prostate Cancer—A Pilot Study. *J. Cancer Metastasis Treat.* **2019**, *5*, 1–12. [CrossRef]
3. Marin, V.R.; Moreno, M.C.; Villasenor, M.C.G.; Hernandez, E.A.G.; Mendoza, A.G. Presence of Aflatoxin Carcinogens in Fresh and Mature Cheeses. *Pharm. Anal. Acta* **2018**, *9*, 1000581. [CrossRef]
4. Kerimray, A.; Baimatova, N.; Ibragimova, O.P.; Bukenov, B.; Kenessov, B.; Plotitsyn, P.; Karaca, F. Assessing Air Quality Changes in Large Cities during COVID-19 Lockdowns: The Impacts of Traffic-Free Urban Conditions in Almaty, Kazakhstan. *Sci. Total Environ.* **2020**, *730*, 139179. [CrossRef] [PubMed]

5. Lim, A.Y.; Ma, J.; Boey, Y.C.F. Development of Nanomaterials for SALDI-MS Analysis in Forensics. *Adv. Mater.* **2012**, *24*, 4211–4216. [CrossRef]
6. Qin, Z.; Hu, S.; Han, W.; Li, Z.; Xu, W.W.; Zhang, J.; Li, G. Tailoring Optical and Photocatalytic Properties by Single-Ag-Atom Exchange in Au13Ag12(PPh3)10Cl8 Nanoclusters. *Nano Res.* **2022**, *15*, 2971–2976. [CrossRef]
7. Liu, Z.; Qin, Z.; Cui, C.; Luo, Z.; Yang, B.; Jiang, Y.; Lai, C.; Wang, Z.; Wang, X.; Fang, X.; et al. In-Situ Generation and Global Property Profiling of Metal Nanoclusters by Ultraviolet Laser Dissociation-Mass Spectrometry. *Sci. China Chem.* **2022**, *65*, 1196–1203. [CrossRef]
8. Tanaka, K.; Waki, H.; Ido, Y.; Akita, S.; Yoshida, Y.; Yoshida, T. Protein and Polymer Analyses up to m/z 100,000 by Laser Ionization Time-of-flight Mass Spectrometry. *Rapid Commun. Mass Spectrom.* **1988**, *2*, 151–153. [CrossRef]
9. Yagnik, G.B.; Hansen, R.L.; Korte, A.R.; Reichert, M.D.; Vela, J.; Lee, Y.J. Large Scale Nanoparticle Screening for Small Molecule Analysis in Laser Desorption Ionization Mass Spectrometry. *Anal. Chem.* **2016**, *88*, 8926–8930. [CrossRef]
10. Xiao, Y.; Scott, T.R.; Darrell, K.T.; Jia-Yuan, T.; Lin, H. Impacts of Surface Morphology on Ion Desorption and Ionization in Desorption Ionization on Porous Silicon (DIOS) Mass Spectrometry. *J. Phys. Chem. C* **2009**, *113*, 3076–3083. [CrossRef]
11. Piszczek, P.; Radtke, A. Silver Nanoparticles Fabricated Using Chemical Vapor Deposition and Atomic Layer Deposition Techniques: Properties, Applications and Perspectives: Review. In *Noble and Precious Metals–Properties, Nanoscale Effects and Applications*; InTech: Hong Kong, China, 2018; pp. 187–213.
12. Silina, Y.E.; Volmer, D.A. Nanostructured Solid Substrates for Efficient Laser Desorption/Ionization Mass Spectrometry (LDI-MS) of Low Molecular Weight Compounds. *Analyst* **2013**, *138*, 7053–7065. [CrossRef] [PubMed]
13. Wang, H.; Brandl, D.W.; Nordlander, P.; Halas, N.J. Plasmonic Nanostructures: Artificial Molecules. *Acc. Chem. Res.* **2007**, *40*, 53–62. [CrossRef] [PubMed]
14. Wang, C.; Li, J.; Yao, S.; Guo, Y.; Xia, X. High-Sensitivity Matrix-Assisted Laser Desorption/Ionization Fourier Transform Mass Spectrometry Analyses of Small Carbohydrates and Amino Acids Using Oxidized Carbon Nanotubes Prepared by Chemical Vapor Deposition as Matrix. *Anal. Chim. Acta* **2007**, *604*, 158–164. [CrossRef]
15. Hosu, I.S.; Sobaszek, M.; Ficek, M.; Bogdanowicz, R.; Drobecq, H.; Boussekey, L.; Barras, A.; Melnyk, O.; Boukherroub, R.; Coffinier, Y. Carbon Nanowalls: A New Versatile Graphene Based Interface for the Laser Desorption/Ionization-Mass Spectrometry Detection of Small Compounds in Real Samples. *Nanoscale* **2017**, *9*, 9701–9715. [CrossRef] [PubMed]
16. Sakai, R.; Ichikawa, T.; Kondo, H.; Ishikawa, K.; Shimizu, N.; Ohta, T.; Hiramatsu, M.; Hori, M. Effects of Carbon Nanowalls (Cnws) Substrates on Soft Ionization of Low-Molecular-Weight Organic Compounds in Surface-Assisted Laser Desorption/Ionization Mass Spectrometry (Saldi-Ms). *Nanomaterials* **2021**, *11*, 262. [CrossRef] [PubMed]
17. Merino, J.P.; Serna, S.; Criado, A.; Centeno, A.; Napal, I.; Calvo, J.; Zurutuza, A.; Reichardt, N.; Prato, M. Mass Spectrometry of Carbohydrate-Protein Interactions on a Glycan Array Conjugated to CVD Graphene Surfaces. *2D Mater.* **2020**, *7*, 024003. [CrossRef]
18. Szlyk, E.; Piszczek, P.; Chaberski, M.; Goliński, A. Studies of Thermal Decomposition Process of Ag(I) Perfluorinated Carboxylates with Temperature Variable IR and MS. *Polyhedron* **2001**, *20*, 2853–2861. [CrossRef]
19. Szłyk, E.; Piszczek, P.; Grodzicki, A.; Chaberski, M.; Goliński, A.; Szatkowski, J.; Błaszczyk, T. CVD of AgI Complexes with Tertiary Phosphines and Perfluorinated Carboxylates—A New Class of Silver Precursors. *Chem. Vap. Depos.* **2001**, *7*, 111–116. [CrossRef]
20. Piszczek, P.; Szłyk, E.; Chaberski, M.; Taeschner, C.; Leonhardt, A.; Bała, W.; Bartkiewicz, K. Characterization of Silver Trimethylacetate Complexes with Tertiary Phosphines as CVD Precursors of Thin Silver Films. *Chem. Vap. Depos.* **2005**, *11*, 53–59. [CrossRef]
21. Radtke, A.; Grodzicka, M.; Ehlert, M.; Muzioł, T.M.; Szkodo, M.; Bartmański, M.; Piszczek, P. Studies on Silver Ions Releasing Processes and Mechanical Properties of Surface-Modified Titanium Alloy Implants. *Int. J. Mol. Sci.* **2018**, *19*, 3962. [CrossRef]
22. Patiny, L.; Borel, A. ChemCalc: A Building Block for Tomorrow's Chemical Infrastructure. *J. Chem. Inf. Model.* **2013**, *53*, 1223–1228. [CrossRef] [PubMed]
23. Li, R.; Zhou, Y.; Liu, C.; Pei, C.; Shu, W.; Zhang, C.; Liu, L.; Zhou, L.; Wan, J. Design of Multi-Shelled Hollow Cr2O3 Spheres for Metabolic Fingerprinting. *Angew. Chem. Int. Ed.* **2021**, *60*, 12504–12512. [CrossRef] [PubMed]
24. Pei, C.; Liu, C.; Wang, Y.; Cheng, D.; Li, R.; Shu, W.; Zhang, C.; Hu, W.; Jin, A.; Yang, Y.; et al. FeOOH@Metal–Organic Framework Core–Satellite Nanocomposites for the Serum Metabolic Fingerprinting of Gynecological Cancers. *Angew. Chem. Int. Ed.* **2020**, *59*, 10831–10835. [CrossRef] [PubMed]
25. Cao, J.; Shi, X.; Gurav, D.D.; Huang, L.; Su, H.; Li, K.; Niu, J.; Zhang, M.; Wang, Q.; Jiang, M.; et al. Metabolic Fingerprinting on Synthetic Alloys for Medulloblastoma Diagnosis and Radiotherapy Evaluation. *Adv. Mater.* **2020**, *32*, 2000906. [CrossRef] [PubMed]
26. Mandal, G.; Moráň, L.; Pečinka, L.; Vaňhara, P.; Havel, J. Matrix Enrichment by Black Phosphorus Improves Ionization and Reproducibility of Mass Spectrometry of Intact Cells, Peptides, and Amino Acids. *Sci. Rep.* **2022**, *12*, 1175. [CrossRef]
27. Li, Y.; Cao, X.; Zhan, L.; Xue, J.; Wang, J.; Xiong, C.; Nie, Z. Hot Electron Transfer Promotes Ion Production in Plasmonic Metal Nanostructure Assisted Laser Desorption Ionization Mass Spectrometry. *Chem. Commun.* **2018**, *54*, 10905–10908. [CrossRef]
28. Zhao, J.; Nguyen, S.C.; Ye, R.; Ye, B.; Weller, H.; Somorjai, G.A.; Alivisatos, A.P.; Dean Toste, F. A Comparison of Photocatalytic Activities of Gold Nanoparticles Following Plasmonic and Interband Excitation and a Strategy for Harnessing Interband Hot Carriers for Solution Phase Photocatalysis. *ACS Cent. Sci.* **2017**, *3*, 482–488. [CrossRef]

29. Ganteför, G.; Gausa, M.; Meiwes-Broer, K.H.; Lutz, H.O. Photoelectron Spectroscopy of Silver and Palladium Cluster Anions. Electron Delocalization versus, Localization. *J. Chem. Soc. Faraday Trans.* **1990**, *86*, 2483–2488. [CrossRef]
30. Ng, K.M.; Chau, S.L.; Tang, H.W.; Wei, X.G.; Lau, K.C.; Ye, F.; Ng, A.M.C. Ion-Desorption Efficiency and Internal-Energy Transfer in Surface-Assisted Laser Desorption/Ionization: More Implication(s) for the Thermal-Driven and Phase-Transition-Driven Desorption Process. *J. Phys. Chem. C* **2015**, *119*, 23708–23720. [CrossRef]
31. Sherrod, S.D.; Diaz, A.J.; Russell, W.K.; Cremer, P.S.; Russell, D.H. Silver Nanoparticles as Selective Ionization Probes for Analysis of Olefins by Mass Spectrometry. *Anal. Chem.* **2008**, *80*, 6796–6799. [CrossRef]
32. Jin, J.M.; Choi, S.; Kim, Y.H.; Choi, M.H.; Kim, J.; Kim, S. Evaluation of Nanoporous Gold with Controlled Surface Structures for Laser Desorption Ionization (LDI) Analysis: Surface Area versus LDI Signal Intensity. *J. Am. Soc. Mass Spectrom.* **2012**, *23*, 1450–1453. [CrossRef] [PubMed]

Supplementary material for manuscript entitled 'Silver nanostructured substrates in LDI-MS of low molecular weight compounds'

by Gulyaim Sagandykova, Piotr Piszczek, Aleksandra Radtke, Radik Mametov, Oleksandra Pryshchepa, Dorota Gabryś, Mateusz Kolankowski and Paweł Pomastowski

Table S1. The *m/z* values for compounds detected using LDI-MS nanostructured substrates

Compound	*m/z*	[M]
plate AgPs0.02		
14:0-13:0-14:0 TG	820.13	$[M+^{107}Ag]^+$
14:0-15:1-14:0 TG	848.35	$[M+^{109}Ag]^+$
14:0-17:1-14:0 TG	874.54	$[M+^{107}Ag]^+$
16:0-15:1-16:0 TG	904.63	$[M+^{109}Ag]^+$
16:0-17:1-16:0 TG	932.88	$[M+^{109}Ag]^+$
16:0-19:2-16:0 TG	958.10	$[M+^{109}Ag]^+$
18:1-17:1-18:1 TG	876.57	$[M+H]^+$
18:1-19:2-18:1 TG	902.78	$[M+H]^+$
adonitol	258.98	$[M+^{107}Ag]^+$
cholesterol	493.41	$[M+^{107}Ag]^+$
alanine	195.96	$[M+^{107}Ag]^+$
fructose	286.97	$[M+^{107}Ag]^+$
glucose	286.96	$[M+^{107}Ag]^+$
methionine	255.97	$[M+^{107}Ag]^+$
palmitic acid	363.14	$[M+^{107}Ag]^+$
oleic acid	389.16	$[M+^{107}Ag]^+$
phenylalanine	271.99	$[M+^{107}Ag]^+$
serine	211.59	$[M+^{107}Ag]^+$
shikimic acid	281.00	$[M+^{107}Ag]^+$
17:0-14-1 PE	677.42	$[M-3H]^-$
17:0-16:1 PE	705.39	$[M-3H]^-$
17:0-18:1 PE	733.37	$[M-3H]^-$
17:0-20:3 PE	757.34	$[M-3H]^-$
17:0-22:4 PE	783.34	$[M-3H]^-$
adonitol	152.36	$[M]^{\bullet-}$

alanine	90.65	$[M]^{\bullet-}$
fructose	180.01	$[M]^{\bullet-}$
glucose	180.21	$[M]^{\bullet-}$
palmitic acid	255.41	$[M]^{\bullet-}$
oleic acid	281.31	$[M]^{\bullet-}$
phenylalanine	165.44	$[M]^{\bullet-}$
serine	106.07	$[M]^{\bullet-}$
shikimic acid	173.94	$[M]^{\bullet-}$
plate AgPs0.03		
14:0-13:0-14:0 TG	736.03	$[M+Na]^+$
14:0-15:1-14:0 TG	846.74	$[M+^{107}Ag]^+$
14:0-17:1-14:0 TG	790.90	$[M+Na]^+$
16:0-15:1-16:0 TG	818.82	$[M+Na]^+$
16:0-17:1-16:0 TG	846.74	$[M+Na]^+$
16:0-19:2-16:0 TG	872.65	$[M+Na]^+$
18:1-17:1-18:1 TG	898.89	$[M+Na]^+$
18:1-19:2-18:1 TG	924.44	$[M+Na]^+$
18:1-21:2-18:1 TG	968.54	$[M+K]^+$
adonitol	258.98	$[M+^{107}Ag]^+$
cholesterol	493.38	$[M+^{107}Ag]^+$
alanine	195.96	$[M+^{107}Ag]^+$
fructose	286.98	$[M+^{107}Ag]^+$
glucose	286.97	$[M+^{107}Ag]^+$
methionine	255.92	$[M+^{107}Ag]^+$
palmitic acid	363.13	$[M+^{107}Ag]^+$
oleic acid	389.15	$[M+^{107}Ag]^+$
phenylalanine	271.99	$[M+^{107}Ag]^+$
serine	211.91	$[M+^{107}Ag]^+$
shikimic acid	280.97	$[M+^{107}Ag]^+$
17:0-14-1 PE	677.75	$[M-3H]^-$
17:0-16:1 PE	705.76	$[M-3H]^-$
17:0-18:1 PE	733.80	$[M-3H]^-$
17:0-20:3 PE	757.83	$[M-3H]^-$
17:0-22:4 PE	783.88	$[M-3H]^-$
adonitol	152.34	$[M]^{\bullet-}$

cholesterol	385.83	$[M]^{\bullet-}$
alanine	89.97	$[M]^{\bullet-}$
fructose	180.01	$[M]^{\bullet-}$
glucose	180.29	$[M]^{\bullet-}$
methionine	149.63	$[M]^{\bullet-}$
palmitic acid	256.58	$[M]^{\bullet-}$
oleic acid	281.31	$[M]^{\bullet-}$
phenylalanine	165.46	$[M]^{\bullet-}$
serine	105.96	$[M]^{\bullet-}$
shikimic acid	174.00	$[M]^{\bullet-}$
plate AgPs0.04		
14:0-13:0-14:0 TG	736.20	$[M+Na]^+$
14:0-15:1-14:0 TG	762.11	$[M+Na]^+$
14:0-17:1-14:0 TG	790.00	$[M+Na]^+$
16:0-15:1-16:0 TG	818.87	$[M+Na]^+$
16:0-17:1-16:0 TG	846.73	$[M+Na]^+$
16:0-19:2-16:0 TG	872.56	$[M+Na]^+$
18:1-17:1-18:1 TG	898.38	$[M+Na]^+$
18:1-19:2-18:1 TG	924.17	$[M+Na]^+$
18:1-21:2-18:1 TG	952.81	$[M+H]^+$
adonitol	258.97	$[M+^{107}Ag]^+$
cholesterol	493.28	$[M+^{107}Ag]^+$
alanine	195.97	$[M+^{107}Ag]^+$
fructose	286.96	$[M+^{107}Ag]^+$
glucose	286.97	$[M+^{107}Ag]^+$
methionine	255.98	$[M+^{107}Ag]^+$
palmitic acid	363.44	$[M+^{107}Ag]^+$
oleic acid	389.09	$[M+^{107}Ag]^+$
phenylalanine	272.00	$[M+^{107}Ag]^+$
serine	211.83	$[M+^{107}Ag]^+$
shikimic acid	280.97	$[M+^{107}Ag]^+$
15:0 LPC	487.12	$[M+H]^+$
17:0 LPC	515.47	$[M+H]^+$
19:0 LPC	543.01	$[M+H]^+$
adonitol	152.24	$[M]^{\bullet-}$

cholesterol	385.83	$[M]^{\bullet-}$
alanine	90.16	$[M]^{\bullet-}$
fructose	180.36	$[M]^{\bullet-}$
glucose	180.32	$[M]^{\bullet-}$
methionine	149.57	$[M]^{\bullet-}$
palmitic acid	255.51	$[M]^{\bullet-}$
oleic acid	281.38	$[M]^{\bullet-}$
phenylalanine	165.41	$[M]^{\bullet-}$
serine	106.01	$[M]^{\bullet-}$
shikimic acid	173.96	$[M]^{\bullet-}$
plate AgPs0.06		
14:0-13:0-14:0 TG	736.24	$[M+Na]^{+}$
14:0-15:1-14:0 TG	846.78	$[M+^{107}Ag]^{+}$
14:0-17:1-14:0 TG	790.05	$[M+Na]^{+}$
16:0-15:1-16:0 TG	818.93	$[M+Na]^{+}$
16:0-17:1-16:0 TG	846.78	$[M+Na]^{+}$
16:0-19:2-16:0 TG	872.62	$[M+Na]^{+}$
18:1-17:1-18:1 TG	898.44	$[M+Na]^{+}$
18:1-19:2-18:1 TG	924.25	$[M+Na]^{+}$
18:1-21:2-18:1 TG	952.02	$[M+Na]^{+}$
adonitol	258.97	$[M+^{107}Ag]^{+}$
cholesterol	493.65	$[M+^{107}Ag]^{+}$
alanine	195.96	$[M+^{107}Ag]^{+}$
fructose	286.97	$[M+^{107}Ag]^{+}$
glucose	286.96	$[M+^{107}Ag]^{+}$
methionine	255.96	$[M+^{107}Ag]^{+}$
palmitic acid	363.45	$[M+^{107}Ag]^{+}$
oleic acid	389.03	$[M+^{107}Ag]^{+}$
phenylalanine	271.99	$[M+^{107}Ag]^{+}$
serine	211.97	$[M+^{107}Ag]^{+}$
shikimic acid	280.95	$[M+^{107}Ag]^{+}$
adonitol	152.36	$[M]^{\bullet-}$
cholesterol	385.82	$[M]^{\bullet-}$
alanine	90.34	$[M]^{\bullet-}$
fructose	180.11	$[M]^{\bullet-}$

glucose	180.15	$[M]^{\bullet-}$
methionine	149.42	$[M]^{\bullet-}$
palmitic acid	255.41	$[M]^{\bullet-}$
oleic acid	281.03	$[M]^{\bullet-}$
phenylalanine	165.46	$[M]^{\bullet-}$
serine	106.04	$[M]^{\bullet-}$
shikimic acid	174.07	$[M]^{\bullet-}$
plate AgPs0.11		
14:0-13:0-14:0 TG	736.71	$[M+Na]^{+}$
14:0-15:1-14:0 TG	762.72	$[M+Na]^{+}$
14:0-17:1-14:0 TG	790.75	$[M+Na]^{+}$
16:0-15:1-16:0 TG	818.74	$[M+Na]^{+}$
16:0-17:1-16:0 TG	846.81	$[M+Na]^{+}$
16:0-19:2-16:0 TG	872.77	$[M+Na]^{+}$
18:1-17:1-18:1 TG	898.81	$[M+Na]^{+}$
18:1-19:2-18:1 TG	924.83	$[M+Na]^{+}$
18:1-21:2-18:1 TG	952.85	$[M+Na]^{+}$
adonitol	258.45	$[M+^{107}Ag]^{+}$
cholesterol	493.62	$[M+^{107}Ag]^{+}$
alanine	195.98	$[M+^{107}Ag]^{+}$
fructose	286.99	$[M+^{107}Ag]^{+}$
glucose	286.96	$[M+^{107}Ag]^{+}$
methionine	255.96	$[M+^{107}Ag]^{+}$
palmitic acid	363.11	$[M+^{107}Ag]^{+}$
oleic acid	389.35	$[M+^{107}Ag]^{+}$
phenylalanine	271.99	$[M+^{107}Ag]^{+}$
serine	211.81	$[M+^{107}Ag]^{+}$
shikimic acid	280.95	$[M+^{107}Ag]^{+}$
adonitol	152.38	$[M]^{\bullet-}$
cholesterol	385.43	$[M]^{\bullet-}$
alanine	89.78	$[M]^{\bullet-}$
fructose	180.24	$[M]^{\bullet-}$
glucose	180.20	$[M]^{\bullet-}$
methionine	149.40	$[M]^{\bullet-}$
palmitic acid	255.38	$[M]^{\bullet-}$

oleic acid	281.29	$[M]^{\bullet-}$
phenylalanine	165.22	$[M]^{\bullet-}$
serine	105.27	$[M]^{\bullet-}$
shikimic acid	174.06	$[M]^{\bullet-}$
17:0-14-1 PE	678.25	$[M-2H]^{-}$
17:0-16:1 PE	706.24	$[M-2H]^{-}$
17:0-18:1 PE	734.24	$[M-2H]^{-}$
17:0-20:3 PE	758.23	$[M-2H]^{-}$
17:0-22:4 PE	784.25	$[M-2H]^{-}$
14:0-13:0-14:0 TG	711.23	$[M-2H]^{-}$
14:0-15:1-14:0 TG	737.23	$[M-2H]^{-}$
14:0-17:1-14:0 TG	765.26	$[M-2H]^{-}$
16:0-15:1-16:0 TG	793.29	$[M-2H]^{-}$
16:0-17:1-16:0 TG	821.34	$[M-2H]^{-}$
16:0-19:2-16:0 TG	847.38	$[M-2H]^{-}$
18:1-17:1-18:1 TG	873.42	$[M-2H]^{-}$
18:1-19:2-18:1 TG	899.48	$[M-2H]^{-}$
plate AgPs0.17		
14:0-15:1-14:0 TG	846.35	$[M+^{107}Ag]^{+}$
14:0-17:1-14:0 TG	874.26	$[M+^{107}Ag]^{+}$
16:0-15:1-16:0 TG	818.27	$[M+Na]^{+}$
16:0-17:1-16:0 TG	846.72	$[M+Na]^{+}$
16:0-19:2-16:0 TG	872.42	$[M+Na]^{+}$
18:1-17:1-18:1 TG	898.53	$[M+Na]^{+}$
18:1-19:2-18:1 TG	902.38	$[M+H]^{+}$
18:1-21:2-18:1 TG	930.55	$[M+H]^{+}$
adonitol	259.00	$[M+^{107}Ag]^{+}$
cholesterol	493.20	$[M+^{107}Ag]^{+}$
alanine	195.96	$[M+^{107}Ag]^{+}$
fructose	286.99	$[M+^{107}Ag]^{+}$
glucose	286.99	$[M+^{107}Ag]^{+}$
methionine	255.98	$[M+^{107}Ag]^{+}$
palmitic acid	363.14	$[M+^{107}Ag]^{+}$
oleic acid	389.06	$[M+^{107}Ag]^{+}$
phenylalanine	272.01	$[M+^{107}Ag]^{+}$

serine	211.76	$[M+^{107}Ag]^+$
shikimic acid	280.99	$[M+^{107}Ag]^+$
adonitol	152.54	$[M]^{\bullet-}$
cholesterol	385.79	$[M]^{\bullet-}$
alanine	90.46	$[M]^{\bullet-}$
fructose	180.14	$[M]^{\bullet-}$
glucose	180.11	$[M]^{\bullet-}$
methionine	149.55	$[M]^{\bullet-}$
palmitic acid	255.37	$[M]^{\bullet-}$
oleic acid	281.30	$[M]^{\bullet-}$
phenylalanine	165.39	$[M]^{\bullet-}$
serine	106.20	$[M]^{\bullet-}$
shikimic acid	174.07	$[M]^{\bullet-}$
plate AgPs0.19		
14:0-13:0-14:0 TG	736.63	$[M+Na]^+$
14:0-15:1-14:0 TG	846.76	$[M+^{107}Ag]^+$
14:0-17:1-14:0 TG	790.69	$[M+Na]^+$
16:0-15:1-16:0 TG	818.72	$[M+Na]^+$
16:0-17:1-16:0 TG	846.76	$[M+Na]^+$
16:0-19:2-16:0 TG	872.78	$[M+Na]^+$
18:1-17:1-18:1 TG	898.79	$[M+Na]^+$
18:1-19:2-18:1 TG	924.81	$[M+Na]^+$
18:1-21:2-18:1 TG	952.85	$[M+Na]^+$
adonitol	259.00	$[M+^{107}Ag]^+$
cholesterol	493.22	$[M+^{107}Ag]^+$
alanine	195.77	$[M+^{107}Ag]^+$
fructose	286.98	$[M+^{107}Ag]^+$
glucose	286.98	$[M+^{107}Ag]^+$
methionine	255.97	$[M+^{107}Ag]^+$
palmitic acid	363.12	$[M+^{107}Ag]^+$
oleic acid	389.05	$[M+^{107}Ag]^+$
phenylalanine	271.98	$[M+^{107}Ag]^+$
serine	211.80	$[M+^{107}Ag]^+$
shikimic acid	280.95	$[M+^{107}Ag]^+$
adonitol	152.39	$[M]^{\bullet-}$

alanine	90.15	$[M]^{\bullet-}$
fructose	180.03	$[M]^{\bullet-}$
glucose	180.41	$[M]^{\bullet-}$
methionine	149.55	$[M]^{\bullet-}$
palmitic acid	255.44	$[M]^{\bullet-}$
oleic acid	281.32	$[M]^{\bullet-}$
phenylalanine	165.41	$[M]^{\bullet-}$
serine	106.17	$[M]^{\bullet-}$
shikimic acid	174.51	$[M]^{\bullet-}$
plate AgPs0.2		
14:0-13:0-14:0 TG	736.66	$[M+Na]^{+}$
14:0-15:1-14:0 TG	762.68	$[M+Na]^{+}$
14:0-17:1-14:0 TG	790.71	$[M+Na]^{+}$
16:0-15:1-16:0 TG	818.74	$[M+Na]^{+}$
16:0-17:1-16:0 TG	846.77	$[M+Na]^{+}$
16:0-19:2-16:0 TG	872.78	$[M+Na]^{+}$
18:1-17:1-18:1 TG	898.80	$[M+Na]^{+}$
18:1-19:2-18:1 TG	924.81	$[M+Na]^{+}$
18:1-21:2-18:1 TG	952.83	$[M+Na]^{+}$
adonitol	258.99	$[M+^{107}Ag]^{+}$
cholesterol	493.36	$[M+^{107}Ag]^{+}$
alanine	195.95	$[M+^{107}Ag]^{+}$
fructose	286.99	$[M+^{107}Ag]^{+}$
glucose	286.99	$[M+^{107}Ag]^{+}$
methionine	255.97	$[M+^{107}Ag]^{+}$
palmitic acid	363.16	$[M+^{107}Ag]^{+}$
oleic acid	389.11	$[M+^{107}Ag]^{+}$
phenylalanine	272.00	$[M+^{107}Ag]^{+}$
serine	211.76	$[M+^{107}Ag]^{+}$
shikimic acid	280.99	$[M+^{107}Ag]^{+}$
adonitol	152.30	$[M]^{\bullet-}$
alanine	90.36	$[M]^{\bullet-}$
fructose	180.45	$[M]^{\bullet-}$
glucose	180.41	$[M]^{\bullet-}$
methionine	149.36	$[M]^{\bullet-}$

palmitic acid	255.42	$[M]^{\bullet-}$
oleic acid	281.33	$[M]^{\bullet-}$
phenylalanine	165.15	$[M]^{\bullet-}$
serine	106.08	$[M]^{\bullet-}$
shikimic acid	174.45	$[M]^{\bullet-}$
17:0-14-1 PE	677.90	$[M-3H]^{-}$
17:0-16:1 PE	705.93	$[M-3H]^{-}$
17:0-18:1 PE	733.97	$[M-3H]^{-}$
17:0-20:3 PE	757.99	$[M-2H]^{-}$
17:0-22:4 PE	784.04	$[M-2H]^{-}$

[P4] Mametov R.; Sagandykova G.; Monedeiro F.; Florkiewicz A.; Piszczek P.; Radtke A. and Pomastowski P. 'Metabolic Profiling of Bacteria with the Application of Polypyrrole-MOF SPME fibers and Plasmonic Nanostructured LDI-MS Substrates' *Scientific Reports.* 2024, *14, 5562.* IF = 4.6 MP = 140.

scientific reports

Check for updates

OPEN

Metabolic profiling of bacteria with the application of polypyrrole-MOF SPME fibers and plasmonic nanostructured LDI-MS substrates

Radik Mametov[1]✉, Gulyaim Sagandykova[1], Fernanda Monedeiro[2], Aleksandra Florkiewicz[1], Piotr Piszczek[3], Aleksandra Radtke[3] & Pawel Pomastowski[1]

Here we present application of innovative lab-made analytical devices such as plasmonic silver nanostructured substrates and polypyrrole-MOF solid-phase microextraction fibers for metabolic profiling of bacteria. For the first time, comprehensive metabolic profiling of both volatile and non-volatile low-molecular weight compounds in eight bacterial strains was carried out with utilization of lab-made devices. Profiles of low molecular weight metabolites were analyzed for similarities and differences using principal component analysis, hierarchical cluster analysis and random forest algorithm. The results showed clear differentiation between Gram positive (G+) and Gram negative (G−) species which were identified as distinct clusters according to their volatile metabolites. In case of non-volatile metabolites, differentiation between G+ and G− species and clustering for all eight species were observed for the chloroform fraction of the Bligh & Dyer extract, while methanolic fraction failed to recover specific ions in the profile. Furthermore, the results showed correlation between volatile and non-volatile metabolites, which suggests that lab-made devices presented in the current study might be complementary and therefore, useful for species differentiation and gaining insights into bacterial metabolic pathways.

Infectious diseases pose a global health concern. Development of rapid and accurate identification methods plays a pivotal role in safeguarding public health.

Mass spectrometric platforms such as MALDI Biotyper[1] and VITEK MS[2] have been developed as efficient alternative for microbiological culturing with subsequent biochemical identification. The underlying principle of these platforms revolves around the profiling of bacterial membrane proteome and their comparison with a database with application of matrix-assisted laser desorption/ionization (MALDI). In addition to proteomic profiling, profiling of low molecular weight (LMW) volatile organic compounds and non-volatile metabolites has also received increased attention.

Bacterial membrane lipids possess rich structural diversity[3], which can be useful in species differentiation. For the purpose of profiling of bacterial membrane lipids, application of laser desorption/ionization (LDI) techniques for profiling of membrane lipids offers advantage in terms of sensitivity, simplicity of use, low sample volume and relatively fast time of analysis.

Leung et al.[4] reported that bacterial membrane glycolipids were specific for different clinically significant pathogens with application of MALDI coupled to time-of-flight mass spectrometry (TOF–MS). Similar approach was applied in the study reported by Liang et al.[5] with the exception of sample preparation method, where authors proposed aqueous sodium acetate buffer for efficient extraction of lipids. The applied approach allowed for identification of four clinically relevant bacterial strains in < 1 h. Another LDI technique, promising for rapid profiling of bacterial membrane lipids, is nanomaterials-assisted LDI mass spectrometry (NALDI-MS),

[1]Centre for Modern Interdisciplinary Technologies, Nicolaus Copernicus University in Toruń, Wileńska 4, 87-100 Toruń, Poland. [2]Department of Chemistry, Faculty of Philosophy, Sciences and Letters of Ribeirão Preto, University of São Paulo, Av. Bandeirantes 3900, Ribeirão Preto 14040-901, Brazil. [3]Department of Inorganic and Coordination Chemistry, Faculty of Chemistry, Nicolaus Copernicus University in Toruń, Gagarina 7, 87-100 Toruń, Poland. ✉email: mametov.radik@gmail.com

where nanomaterials are utilized for desorption and ionization of analytes in the sample[6]. NALDI demonstrated enhanced sensitivity towards various low molecular weight analytes including lipids[7], especially with utilization of plasmonic nanostructures. Plasmonic LDI-MS substrates demonstrated utility for analysis of clinically relevant biomolecules[8,9] owing to localized surface plasmon resonances (LSPRs) upon interaction of the nanomaterials with light. However, there have been no studies reporting the application of plasmonic LDI-MS substrates in attempt to differentiate between bacterial species.

Efforts to differentiate bacterial species utilizing profiling of volatile organic compounds (VOCs) have been in progress for more than three decades. Initial studies utilized bacterial VOCs collection techniques, like traps made from a sorbent material such as Tenax[10]. Nowadays, gold standard in the bacteria VOCs profile collection is headspace solid-phase microextraction (HS-SPME) coupled with gas chromatography (GC)[11]. SPME was introduced in 1990 and received wide recognition as a simple and solvent-free method[12]. Recent studies by Reese[13] and Fitzgerald[14] reported volatile profiles of various pathogenic bacteria, demonstrating potential of utility of VOCs profiling in genus- and species-level discrimination. It is worth mentioning that all of the mentioned works reported application of commercially available SPME fibers. Introduction of new materials as extraction coating might be helpful in revealing specific bacterial metabolites due to the changes in affinity and therefore, specificity of analysis. Numerous papers exploring the application of novel materials as extraction coating for SPME were reported in the literature[15]. However, there is a lack of studies reporting application of lab-made SPME fibers based on new materials as extraction coatings for detection and profiling of bacterial volatile metabolites.

While previous studies have extensively explored volatile or non-volatile metabolites, rare efforts were dedicated to metabolic profiling of bacteria with an emphasis on both groups aiming at species differentiation. To the best of our knowledge, only one study by Wang et al.[16] has been carried out with utilization of silver nanostructured substrates for surface enhanced Raman spectroscopy to detect both volatile and non-volatile metabolites aiming at bacterial quantification and growth monitoring.

Hence, we introduce here alternative innovative lab-made analytical devices for metabolic profiling of bacteria. Analytical devices encompass polypyrrole-MOF (PPy@ZIF-8) HS-SPME fiber and plasmonic silver nanostructured LDI-MS substrates, and their simultaneous use allowed for comprehensive profiling of both volatile and non-volatile bacterial metabolites of eight strains of bacteria.

Materials and methods

Reagents and materials

All reagents and solvents used in the current study were of the highest available purity and purchased from Sigma Aldrich (Steinheim, Germany). Organic matrices for matrix-assisted laser desorption/ionization mass spectrometry (MALDI-MS) such as hydroxycinnamic acid (HCCA) and dihydroxybenzoic acid (DHB) were purchased from Bruker Daltonics (Bremen, Germany). Brain Heart Infusion Agar (BHIA) was purchased from Sigma Aldrich (Steinheim, Germany). Water was obtained using the Milli-Q RG apparatus by Millipore (Millipore Intertech, Bedford, MA, USA). Commercial SPME fiber, namely 75 µm carboxen/polydimethylsiloxane (CAR/PDMS) was purchased from Agilent Technologies, California, USA).

Culturing of bacteria

Eight strains of bacteria, namely *Morganella morganii* (MM), *Staphylococcus warneri* (SW), *Lactobacillus plantarum* (LP), *Enterococcus faecium* (EF), *Enterococcus durans* (ED), *Lactococcus garvieae* (LG), *Staphylococcus epidermidis* (SE), and *Escherichia coli* (EC) were obtained from Microbank® cryovials (Pro-Lab Diagnostics, UK) deposited at −80 °C[17] and grown using a modified method previously described by our research team[18]. In order to confirm the identification of selected species of microorganisms, one bead was inoculated on Petri dishes (Alchem, Poland) with solid Mueller Hinton Agar medium (Sigma Aldrich, Germany). A microbial loop (1 µL) of bacterial biomass was applied directly to the plate, according to the procedure recommended by the manufacturer. A further procedure consisting of a bacterial protein extraction protocol using microorganism identification analysis using the MALDI-TOF–MS technique and the MALDI Biotyper 3.0 platform (Bruker Daltonics, Bremen, Germany) has been described in previous works of our team[18,19].

Extraction of lipids

For collection of non-volatile metabolic profiles, extraction has been carried out using the standard Bligh & Dyer[20] (B & D) method with modifications. In the attempt of sampling standardization, 100 mg of bacterial biomass was collected from five separate Petri dishes. After separation of chloroform and methanol phases, solvents were evaporated and 1.5-mL Eppendorf vials were weighted to determine the mass of the dry residue. Stock solution for each phase was prepared by addition of corresponding solvent (chloroform and methanol) in microliters to final ratio between the dry residue and solvent 1:1.

Growth curves experiment

In order to determine the growth curves for the selected microorganisms, we transplanted fresh bacterial colonies that had been grown in MHA culture medium into glass tubes containing Mueller Hinton Broth (MHB). This process aimed to achieve a 0.50 McFarland (McF) standard, measured at a wavelength of $\lambda = 565 \pm 15$ nm using a DEN-1B Densitometer, which operates based on turbidity approaches (Biosan, Józefów, Poland). For the McFarland 0.5 Standard, the approximate OD at 600 nm is between 0.08 and 0.13[21]. Additionally, measurements of optical density (OD) values at $\lambda = 600 \pm 1$ nm were conducted using a Thermo Scientific™ Varioskan™ LUX, with further details provided in the supplementary data (Fig. S17). The control used in the experiment was MHB medium alone. The prepared bacterial suspensions were incubated at 37 °C under aerobic conditions,

with measurements taken hourly for approximately 32 h. Each experiment was conducted with at least three replicates to ensure consistency and reliability.

HS–SPME–GC–MS profiles

All bacteria species were inoculated and grown in disposable culture tubes with round-bottom and screw caps to enable measurement of concentration directly before the extraction of VOCs. Septa from disposable culture tubes were exchanged to silicone/PTFE 18 mm from the classical 20-mL headspace vials to prevent losses of volatile compounds. All tubes, septa, caps and medium were autoclaved for sterilization. For extraction of VOCs of bacteria, lab-made PPy@ZIF-8 coated SPME fiber was utilized.

Prior to performing the sample analysis, pre-conditioned fibers were exposed to the headspace of empty sterile culture tubes, and blank analyses were carried out. Furthermore, we also performed an analysis of the culture media used for bacteria inoculation. Any signals originating from blank analyses (potentially fiber material) and culture media were excluded from identification and were not considered. After each three runs the blank of the SPME fibers was taken to ensure the absence of contaminants.

For extraction of VOCs, the following parameters were used: equilibration time was dependent on certain types of bacteria species. Extraction temperature was set as 37 °C and time of extraction set as 40 min. The desorption process was performed in the GC-inlet at 220 °C for 5 min.

Gas chromatographic analyses of VOCs released by bacteria were conducted using a GC 7820A gas chromatograph coupled with an Agilent 5977B mass spectrometer MSD (Agilent Technologies, Waldbronn, Germany). The GC system was equipped with a ZB-624 capillary column (30 m × 0.25 mm × 1.4 µm). Helium was employed as the carrier gas, flowing continuously at a rate of 1 mL/min. Injections were carried out using the splitless mode, and the GC injector port was maintained at a temperature of 220 °C. HS–SPME–GC–MS profiles of all strains were collected with consideration of growth phases.

The temperature program for the GC oven initiated at 30 °C and was held for 4 min, after which it was ramped at a rate of 7 °C min^{-1} to reach 150 °C (maintained for 2 min). Subsequently, the temperature was raised to 250 °C at a rate of 10 °C min^{-1}. The final oven temperature was held constant for 5 min. The mass spectrometer was operated in the electron impact (EI) mode with an energy of 70 eV. The ion source temperature and the transfer line temperature were set to 230 °C and 250 °C, respectively. Data acquisition was performed at a frequency of 2.9 scans per second, covering a mass range of 35 to 550 atomic mass units (a.m.u.). Compound identification was processed by searching the obtained mass spectrum in the NIST11 mass spectral library. The criterion for peak detection was a signal-to-noise of at least 3, and peak integration was performed manually. Spectrum search encompassed baseline subtraction and averaging over a peak. Each peak was searched manually, including baseline subtraction and averaging over a peak. Forward match quality of at least 700/1000 was applied as the lower match threshold. Peaks detected in samples corresponding to pure culture media were deleted from the total dataset, for the obtainment of signals attributed solely to bacteria sample. Chromatographic data was processed using the software MassHunter Qualitative analysis 10.0. Signal integration step was based on the total ion current (TIC) of the peak, as the employed methodology set-up was ideal for an optimized separation of the compounds of interest, only significant peaks were considered, and deconvolution procedures were not performed. A table containing bacterial VOCs identified in each culture is provided in the Supplementary Material (Table S1). To ensure reliability of identification, it has been carried out with consideration of several parameters, such as probability of match (minimal threshold was set to 75%), retention index and retention time, peak shape and spectra compared to a reference standard.

For comparison of extraction performance of PPy@ZIF-8 and commercial carboxen/polydimethylsiloxane (CAR/PDMS) fibers, standard solution of compounds with distinct structures was prepared. The solution was prepared in methanol with the final concentration 17 µg/mL for each analyte. Commercial fiber was pre-conditioned prior to extraction, following the guidelines of the manufacturer. Extraction has been carried out at 30 °C for 49 min with stirring 750 rpm. The solution was pre-incubated for 17 min at room temperature. The sample volume accounted for 3 mL. 1 g of NaCl was added to solution prior to extraction. GC analyses of standard solution after extraction were carried out with a gas chromatograph GC 7820A coupled to a flame ionization detector (Agilent, Santa Clara, CA, USA). The instrument was equipped with HP-5 analytical column (30 m × 0.32 mm i. d. and film thickness 0.25 µm). Carrier and make-up gases were helium (99.99%) and air. Analyses were performed in the splitless mode, injector port operated at 220 °C. Detector operated at 300 °C and the carrier gas flow rate was 2.4 mL/min. The initial oven temperature was 30 °C (held for 3 min), ramped at a rate of 4 °C min^{-1} to 50 °C (held for 1 min), then increased to 70, 100 (held for 1 min), and 200 °C at the rates of 5 °C min^{-1}, 7 °C min^{-1} and 40 °C min^{-1}, respectively. The final oven temperature was kept for 3 min. Make-up gas, hydrogen, and synthetic air flow were maintained at 30 mL/min, 30 mL/min, and 300 mL/min, respectively.

NALDI-MS profiles

NALDI-MS profiles of bacterial extracts were collected using silver nanostructured substrates with size of nanoparticles 50 ± 10 nm[22], and organic matrices (HCCA and DHB) as a reference technique. In case of MALDI, organic matrices were prepared at concentration 10 mg/mL in TA30 solution. Deposition of samples was performed using dried droplet technique: 2.5 µL of matrix solution was mixed with 2.5 µL of sample, and 1 µL was deposited onto the target plate (ground steel target, Bruker Daltonics, Bremen, Germany).

To consider the differences in concentration of lipids, stock solutions and dilutions (10, 10^2 and 10^3 times) were analyzed using MALDI and NALDI to determine the dilution providing with intense signals in the lipid region (*m/z* 400–1500) in MS spectra. For MALDI, all bacterial extracts were analyzed using the stock solution. In case of NALDI, all chloroform extracts were registered using dilution factor 10, except for *Enterococcus Faecium*, where stock solution was used, and stock solution was used in case of methanol fractions.

For both MALDI and NALDI, UltraFlextreme MALDI-TOF–MS instrument (Bruker Daltonics, Bremen, Germany) with a modified neodymium-doped yttrium aluminium garnet (Nd:YAG) laser operating at 355 nm and frequency 2 kHz was used. The profiles were collected in ion-positive mode in the mass range *m/z* 60–1400 and the number of shots for single MS spectrum collection accounted for 2500. Mass calibration for MALDI analyses was carried out using clusters of CsI_3: 2.5 µL of 10 mg/mL solution of CsI_3 in methanol was mixed to 2.5 µL of 10 mg/mL of DHB matrix in methanol and 1 µL was deposited onto the target plate. In case of NALDI, 1 µL of extracts were deposited directly onto the solid substrate and internal mass calibration using signals of silver was carried out. For all LDI measurements, cubic enhanced calibration method was used. For NALDI, the following instrument parameters were applied: 80% of laser power, detector gain 30×, value of global attenuator of 30% and parameter set 'ultra'. For MALDI, the same parameters were used except for detector gain value, which was set to 2.51× in case of DHB. Profiles of NALDI were collected in 5 replications. For silver nanostructured substrates, MTP slide adapter II was used (Bruker Daltonics, Bremen, Germany). The list of all detected signals is provided in the Supplementary Material (Tables S2–S17).

Data analysis

Data analysis was conducted in R environment (R v.4.2.1), using RStudio console (v. 2022.02.03, PBC, Boston, MA, USA). Principal component analysis (PCA) was performed using the packages "factoextra" and "FactoMineR". Heatmaps ("pheatmap" package) used as input the scaled average values of peak area and ion intensity, in case of VOCs and LDI-MS data, respectively. For hierarchical clustering analysis (HCA), Euclidean distance was used to measure the association between samples, and Ward's was selected as the clustering method. Normality of data distribution was verified using Shapiro–Wilk test ("stats" package). Statistical comparison between ion intensities obtained from LDI-MS using different extraction phases was carried out using Mann–Whitney test ("stats" package). Random forest (RF) model was created using "randomForest" package, employing the following parameters: number of trees = 900, number of variables randomly sampled as candidates at each split = 3, cut-off = 1/k (majority vote wins, where k is the number of classes, i.e., 8). After a random split, 60% of the data was used for model training, while the remaining 40% was employed for model testing. Canonical correlation analysis (CCA) was carried out using "vegan" package, while univariate correlation analysis (Spearman's method) was conducted using "Hmisc". Networks were built with the aid of "igraph" and "visNetwork" packages.

Results and discussion

Bacteria growth curves

To collect volatile metabolites, we carried out investigation of the growth phases for all strains.

The growth curves of selected microorganisms as a function of time are shown in Fig. 1. All isolated microorganism strains showed good ability to grow in MRS broth at 37 °C. For the temperature 37 °C, the exponential growth phase was observed between 10 and 16 h (Fig. 1).

Bacterial suspension turbidity (McF) values are shown as averages of three technical replicates ± SE. For *E. coli* cultured at 37 °C, there was an apparent exponential growth phase between 2 and 8 h, seemingly reaching a stationary phase between 6 and 12 h (Fig. 1A). Under ideal conditions, E. coli in a rich liquid broth medium is speculated to have a doubling time of approximately 20 min and may reach a cell density greater than 10^9 CFU/mL after an overnight culture[23,24]. Similarly, *L. plantarum* at 37 °C appeared to enter exponential growth between 2 and 8 h, with a presumed stationary phase from 5 to 12 h (Fig. 1B). A comparable pattern at both 37 °C and 45 °C was suggested in the study by Smetanková et al.[25]. The growth variability of *Lactobacillus plantarum*, distinct from other bacteria, is attributed to its unique nutritional needs and heightened sensitivity to environmental factors like oxygen levels, temperature, and pH. Its specific metabolic pathway, fermenting sugars into lactic acid, further contributes to this variability, especially in standard laboratory settings. Understanding these unique requirements is key to optimizing L. plantarum cultivation and offers insights into bacterial growth dynamics under varied conditions[26].

In turn, the bacterium *M. morganii* (Fig. 1C) grew exponentially up to 5 h of culture and reached stationary phase between 6 and 10 h. This bacterium is known[27] to grow in the temperature range from 4 to 45 °C, identical growth of this bacterium for 37°C was shown by the results of Minnullina et al.[28]. In the case of *E. durans* (Fig. 1D), the exponential growth phase possibly lasted up to 6 h, and a stationary phase might have occurred from 10 to 14 h. The control of the experiment, MHB medium, showed no traditional growth curve (Fig. 1E). *S. epidermidis* demonstrated specific proliferation patterns (Fig. 1F), inferred from the growth curve where the exponential phase lasted around 20 h, and a stationary phase, with minor fluctuations, was likely reached between 20 and 32 h. This is confirmed by a study by Mantripragada et al.[29], in which the exponential growth phase of *S. epidermidis* lasted up to 9 h of incubation, but the typical plateau phase was not characterized, although bacterial proliferation was no longer as intense. *E. faecium*, as shown in Fig. 1G, appeared to reach exponential phase between 2 and 8 h, and a stationary phase between 13 and 15 h, followed by a gradual decline. In a study by Zhang et al.[30], the growth curves of E. faecium strain E1162 and various mutants indicated exponential growth up to 5 h, with a plateau phase from 5 to 9 h, under incubation at 37 °C in BHI medium with ampicillin[30]. *L. garvieae* exhibited a probable exponential growth up to 9 h, and a plateau phase from 10 to 15 h. In the study by Xie et al.[31], the growth curve of *L. garvieae* was characterized by an exponential phase reached by 6 h of incubation at 37 °C in BHI medium, while the stationary phase was reached between 10 and 16 h of culture. Finally, S. warneri (Fig. 1I) seemed to reach an exponential phase by 10 h of incubation, and while a typical stationary phase was not clearly observed, it is speculated to be between 18 and 20 h. Hourly observations in TSB medium suggested that the final logarithmic or exponential phase of S. warneri MBF02-19J lasted for 17 h[32].

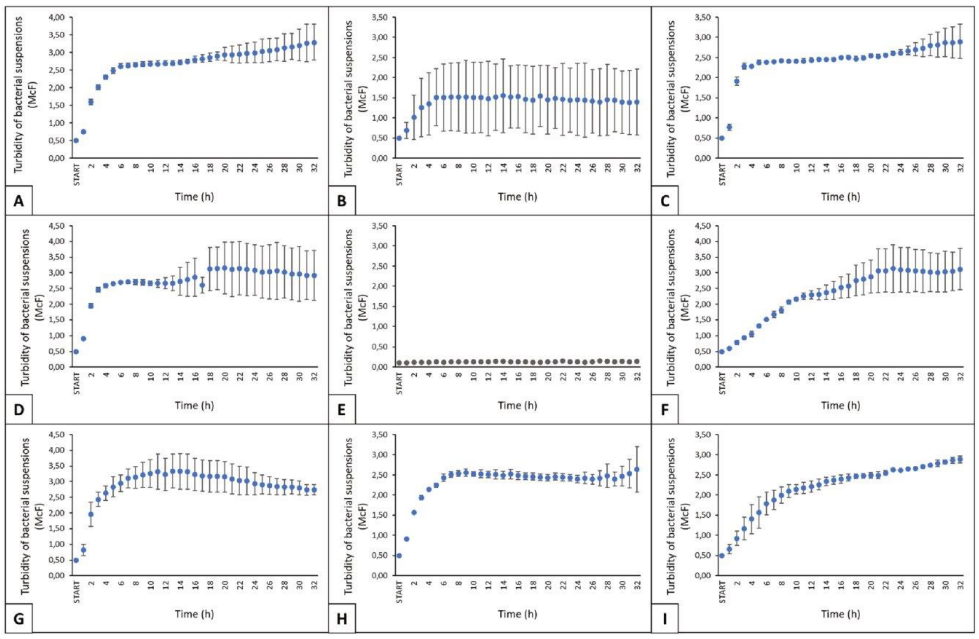

Figure 1. Microbial growth curves of bacteria grown at 37 °C for 32h. (**a**) *Escherichia coli*, (**b**) *Lactobacillus plantarum*, (**c**) *Morganella morganii*, (**d**) *Enterococcus durans*, (**d**) control, Mueller Hinton Broth medium, (**f**) *Staphylococcus epidermidis*, (**g**) *Enterococcus faecium*, (**h**) *Lactococcus garvieae*, (**i**) *Staphylococcus warneri*.

Investigation of patterns within volatile and non-volatile LMW profiles

The PPy@ZIF8 SPME fiber allowed the recovery of a total of 68 different VOCs, associated with bacteria presence in the cultures. From these, 40 VOCs could be annotated according with the compound identification criteria. Each different bacterial volatile detected across the cultures was attributed to a VOC class, and the number of unique VOCs ascribed to a given class was evaluated (in terms of percentage) in relation to the total number of bacterial VOCs (100%) (Fig. 2a, b).

Identified VOCs recovered from bacterial cultures consisted mainly of volatile nitrogen-containing compounds (VNCs, 19–32%), followed by ketones (16–19%), aldehydes (11–16%), alcohols and organic acids (8–11%). In the attempt of comparison of our data for selected compounds extracted by PPy@ZIF-8 and data reported in the literature, the following observation has been made. The previous study[33], conducted by our research group, stressed VOCs emitted by various strains, including *Staphylococcus warneri*, with utilization of the PDMS/DVB commercial fiber. In this study[33], the predominant group of detected compounds were ketones, hydrocarbons and alcohols (Fig. 3C)[33]. In our study, predominant group of compounds was nitrogen-containing compounds in case of *Staphylococcus warneri* and other species. Therefore, the affinity of PPy@ZIF-8 fiber towards nitrogen-containing compounds has been suggested, especially for the pyrrole-ring containing compounds. On the other hand, Drabińska and co-authors[34] performed the experiment for extraction of VOCs by SPME–GC–MS/MOS method and utilized CAR/PDMS commercial fiber. According to the results, detected compounds included benzaldehydes, pyrazines derivatives, xylene etc[34], and some of the compounds were similar as in the current study. In addition, it is essential to consider that the composition of VOCs' profiles depend on strain and sample matrix, culture media and growth conditions. Hence, we propose that the prevalence of nitrogen-containing compounds in the profiles may not necessarily be linked to the affinity toward nitrogen within the polypyrrole ring's structure. Moreover, the efficiency of SPME fiber in a headspace mode is a complex process influenced by various factors. The interplay between fiber properties and the chemical structures of analytes becomes particularly significant in chemically-rich sample matrices[35], such as bacteria. To exemplify the diversity of responses in complex mixtures, we examined the extraction performance of both PPy@ZIF-8 and commercial CAR/PDMS fibers using a standard mixture of compounds with distinct chemical structures (Table S18). The results indicated that the CAR/PDMS coating is the mostly non-polar, while the PPY@ZIF-8 coating is conversely more polar. Interestingly, despite non-polar nature of dodecane, PPY@ZIF-8 exhibited a high response, likely due to the affinity of polypyrrole to long-chain linear hydrocarbons[36]. Lab-made coating demonstrated approximately two times lower efficiency for extracting BTEX group analytes compared to CAR/

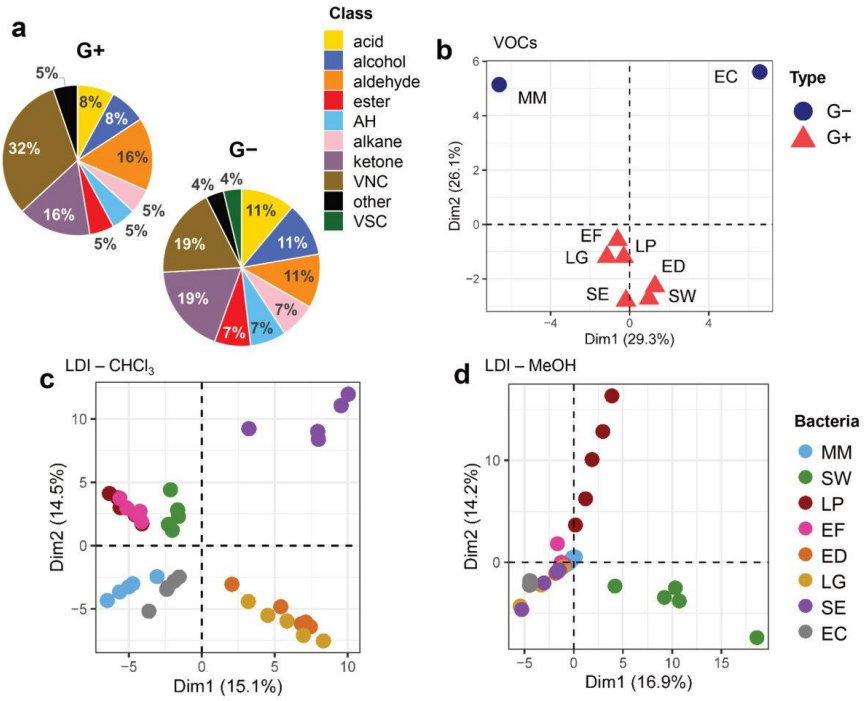

Figure 2. (**a**) Fractions of each VOC class detected among G+ and G− bacteria; PCA score plots for (**b**) VOCs data and NALDI-MS data, considering the analysis of (**c**) the chloroform phase and (**d**) the methanol phase (n = 5 per bacteria). *AH* aromatic hydrocarbon, *VNC* volatile nitrogen-containing compound, *VSC* volatile sulfur-containing compound.

PDMS, suggesting a weaker affinity of lab-made SPME fibers for non-polar analytes. This may be attributed to competition on the fiber, where binding sites was occupied by more polar compounds such as methanol.

Since many biologically active bacterial metabolites are VNCs (e.g., indole, pyrazines), the prepared fiber might be favorable for the study of microbial interactions. Here, such greater recovery of VNCs is possibly attributed to the affinity of VNCs towards nitrogen in the structure of PPy@ZIF-8 coating[17] as well as the unequal distribution of electrons leading to dipole moment. Differences were observed regarding the fraction of VOC classes prevalent in the headspace of bacteria, depending on if these were G+ or G− species (Fig. 2a). G+ presented a greater proportion of VNCs and aldehydes while G−, while G− displayed a greater percentage of ketones, alcohols and acids. Besides, dimethyl disulfide—a volatile sulfur-containing compound (VSC), was detected only in G− species. PCA score plot of VOCs data (Fig. 2b) shows a clear discrimination between G+ and G− profiles, provided by the first PC. Although very distinct from G+ , VOC profiles from G− species also presented substantial differences between themselves, being discriminated by the second PC.

PCA was also used to explore patterns related with bacterial species within the NALDI-MS datasets. Figure 2c refers to lipid ions recovered from the chloroform fraction—in this case, each experimental replicate was plotted close to each other, indicating that the performed assays displayed adequate reproducibility. Reproducibility of profiles possibly was achieved due to nearly homogeneous distribution of silver nanoparticles[22] acquired via chemical vapor deposition as compared to wet chemical synthesis, where coffee ring effect[37] can lead to formation of hot spots and profiles inconsistency.

Moreover, clusters referring to individual species of bacteria can be observed, although an overlap between LP and EF, as well as between ED and LG is present. This overlap indicates a greater similarity between the lipid composition of these pair of bacteria. It is also of notice that the two G- bacteria (MM and EC) appear confined in the third quadrant of the plot. On the other hand, NALDI-MS lipid profiles acquired in the methanolic fraction for the same bacteria were not so congruent, displaying considerable intra-variability (Fig. 2d). Furthermore, the formed PCA clusters did not characterize most of bacteria species, with only LP and SW appearing as more distinct from others.

Figure 3 shows PCA variable plots, allowing us to verify which VOCs or lipid ions are correlated with the main PCs and the previously observed clusters. In these plots, only the top 30 variables contributing the most

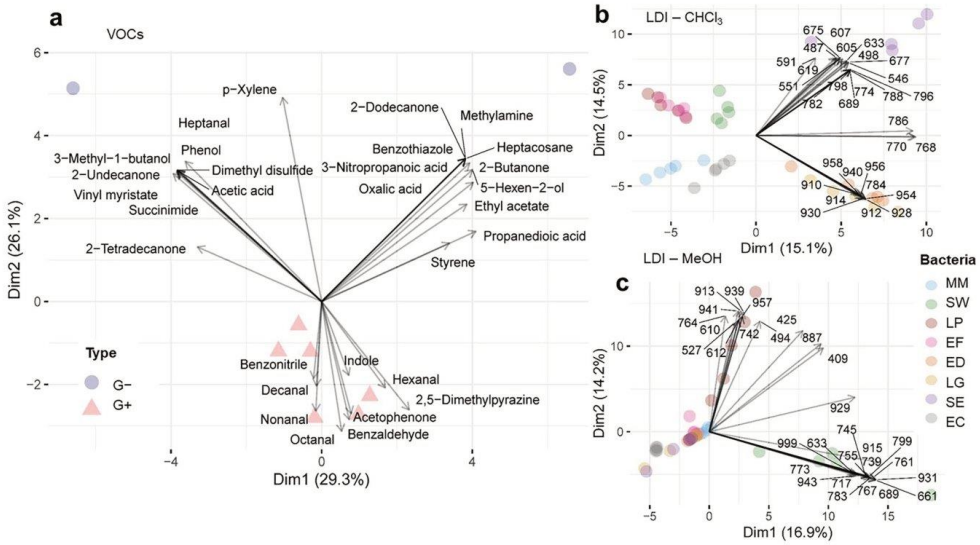

Figure 3. PCA variable plots displaying the top 30 most contributing variables, for (**a**) VOCs data, as well as NALDI-MS data obtained from the analysis of (**b**) chloroform and (**c**) methanol phases (n = 5 per bacteria).

for data variance are showed. In case of VOCs (Fig. 3a), it was shown that G+ were characterized by an increased production of fatty aldehydes (hexanal, nonanal, decanal), benzaldehyde, acetophenone, 2,5-dimethylpyrazine and indole. According to literature, nitrogen-containing compounds, including pyrroles, and derivatives of pyrazine (such as 2,5-dimethylpyrazine, 2-ethyl-3,5-dimethylpyrazine, and 3-iso-pentyl-2,5-dimethylpyrazine), can be emitted by various bacterial strains[33]. Pyrazines, in particular, are noted as a prevalent group of compounds released by bacteria, although the metabolic pathways and biosynthesis are not fully elucidated[38]. Although *p*-xylene is a volatile compound considerably abundant in the indoor air, it has been also detected in bacterial cultures[39]. Such aromatic volatiles are possibly derived from intermediates of the shikimate pathway[40]. However, the analysis of blank sample of empty vial showed the absence of *p*-xylene as well as in the blank samples of media. Therefore, it was suggested that *p*-xylene could be emitted by bacteria. Nevertheless, the interpretation of data regarding the profiles of VOCs emitted by bacteria should be approached with caution. The existing literature suggests that pyrazines may be inherent to bacterial metabolism, but their presence can also arise from interactions between compounds in culturing media and bacterial metabolism, as well as chemical reactions occurring during the autoclaving of the media. Adams and Kimpe reported that standard test showed formation of pyrazine during autoclaving upon alkalization to pH 9 or higher suggesting that lysine that was added to the media served as a precursor for chemical formation of pyrazine by Maillard reaction[41]. Formation of pyrazines was also reported earlier by DeMilo et al.[42], where authors concluded that their formation did not seem affected by bacterial action, but almost exclusively was affected by autoclaving of broth.

In the current investigation, commercial culturing media were employed, potentially accounting for the absence of pyrazines in the volatile profile of the media. This observation underscores the significance of meticulous consideration in the sample preparation of culturing media to investigate potential artifacts. Such considerations are pivotal for ensuring robust data interpretation in studies focused on bacterial metabolism.

Regarding the cultures of G- bacteria, MM presented increased levels of 3-methyl-1-butanol, 2-undecanone, phenol and dimethyl sulfide. In contrast, EC cultures displayed augmented 2-dodecanone, benzothiazole, methylamine and heptacosane. In NALDI-MS data from the chloroform fraction (Fig. 3b), SE were marked by the increased response of lipids ranging from *m/z* 487 to 798, which in turn were depleted among G- species. LG and ED presented greater responses of the lipids corresponding to signals at *m/z* 784 and *m/z* 910–958, which were decreased among EF, LP, SW. In NALDI-MS data from methanolic phase (Fig. 3c), LP displays increased intensities for the lipid ions at *m/z* 913, 939, 941 and 957, among others. For SW, the lipids at *m/z* 661, 689, 767 and 931 were those which presented higher intensities. Conversely, the remaining bacterial species were characterized by decreased responses of the same lipid ions which were enhanced in LP profile.

Correspondence between molecular profiles were also investigated using HCA. In this case, dissimilarities between samples were calculated based on the Euclidean distance. As observed in PCA, VOCs profiles obtained for G+ and G− bacteria were once more clustered separately (Fig. 4a). EC were the G− species more similar to G+, while EF appeared to be the most singular bacteria among other G+ species. Among VOCs, 6 clusters were identified based on the trends presented by these compounds across the samples of bacterial cultures. Clusters 1

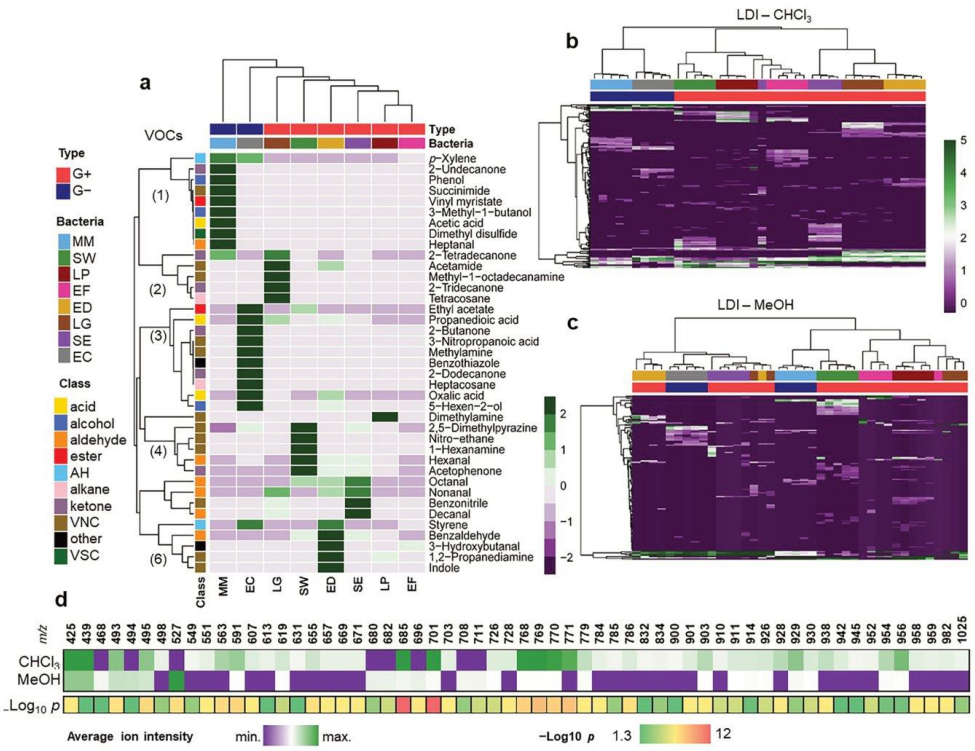

Figure 4. Hierarchical cluster analysis and associated heatmaps for (**a**) VOCs data, as well as NALDI-MS data obtained from the analysis of (**b**) chloroform and (**c**) methanol phases (n = 5 per bacteria); (**d**) chart showing the lipid ions which presented statistically significant differences in their intensities ($p < 0.05$), when comparing chloroform and methanol phases.

(composed by various VOC classes) and 3 (mainly acids, ketones and VNCs) defined G+ species. The cluster 2 (ketones and VNCs) characterizes LG, while the clusters 4, 5 and 6 (mostly VNCs and aldehydes) define SW, ED and SE. Lastly, LP and EF were not particularly enriched with any of these main clusters. In NALDI-MS using the chloroform fraction (Fig. 4b), clusters corresponding to each bacterial species are observed, in addition to a clear distinction between G− and G+ bacteria. An overlap between species was only detected in case of SE and EF, the same bacteria which also presented a greater intersection in the corresponding PCA plots. On the other hand, lipid profiles obtained using the methanolic fraction did not display such coherent clustering of species (Fig. 4c). According to this approach, LG, EF and ED were the bacteria presenting less consistent lipid profiles.

NALDI-MS profiles of lipids obtained using the chloroform and methanol fractions were compared (Fig. 4d). The vast majority of ions presenting statistically significant differences in their intensities were better recovered in chloroform. Only signals at *m/z* 468, 494, 527, 680, 682, 696, 708 and 711 were uniquely detected in the methanolic phase—possibly, these are lipids with a stronger hydrophilic pole. This reasserts the results of the previous unsupervised analyzes, which demonstrated that chloroform fraction is the most suitable for the obtaining of representative and reproducible lipid profiles. Failure of differentiation between species based on methanolic fraction of the B & D extract could be caused by fragmentation of lipids in NALDI-MS with application of silver nanostructured substrates[22]. Our previous investigation demonstrated that plasmonic silver substrates exhibited sensitivity to various lipid classes[22], which might be favorable for distinguishing between bacterial species due to the diversity of membrane lipids[3]. Nevertheless, fragmentation of phospholipids, especially polar phosphatidylcholine was observed[22], which could potentially be attributed to photocatalytic properties of silver. This is in agreement with B & D extraction method, where polar lipids are extracted into the methanolic phase[43]. On the other hand, this also could be attributed to differences in the lipid content depending on the species. In addition, both MALDI and NALDI profiles showed less signals in the lipid region of the methanolic fraction of B & D extracts (Figs. S1–S8) as compared to chloroform phase (Figs. S9–S16). This aligns with previous investigation of our research group[44], where silver nanostructured substrates enabled classification of the *Escherichia coli* strains

into cefotaxime-resistant and cefotaxime-sensitive strains, while signals attributed to organic matrix hampered classification in case of application of MALDI.

The list of *m/z* values and corresponding intensities for the signals detected in the lipids' mass region has been listed in Tables S2–S17. Since the current study was aimed at untargeted approach, and diversity of possible lipids, identification of the signals has not been performed. Nevertheless, the values of *m/z* could be compared with other data with assistance of the Lipid Maps database, which has been extended including non-mammalian sources of lipids[45]. Furthermore, due to extreme complexity of the sample matrix, identification of signals requires application of a targeted approach with a set of instrumental analytical techniques, including LC–MS with high resolution and opportunity to perform MS/MS analysis to generate specific fragments. For example, Oursel[46] and co-authors investigated the lipid composition of *Escherichia coli* membranes using LC–ESI–MS/MS. However, the authors identified only phospholipids species, which can be explained by suitability of electrospray ionization for polar lipids[47]. Nevertheless, Jaber[48] et al. reported di- and triacylglycerols detected in the lipidomic extract of *Escherichia coli* strains, however the precise data about identified species was not reported.

RF model aiming for bacteria classification

Next, a model using RF algorithm was prepared, with the objective to classify bacterial species based on their lipid profiles obtained through NALDI-MS. The top 20 variables contributing the most for model accuracy are showed in Fig. 5a, b. These can be interpreted as the ions with the most distinctive responses across species, some of them being consistently unique for a given bacteria. Multidimensional scaling (MDS) plots of RF proximity matrices indicate the level of similarity between the questioned classes (i.e., bacteria species) according to model calibration (Fig. 5c, d). A greater distance between points correlates with a higher dissimilarity between samples. Therefore, a greater proximity between the points indicates species more prone to misclassification in the model. Partition around medoids (PAM) clustering allowed the classification of samples used for calibration as members of three different clusters. For example, in the chloroform fraction (Fig. 5c), G- species display a greater distance from the remaining species. Additionally, ED and LG appear grouped very closely, indicating the correspondence between these bacteria regarding their lipid composition. Analogous conclusions were made based on PCA results. Table 1 summarize the information regarding model performance. The out-of-bag (OOB) estimate of error rate obtained for NALDI-MS from chloroform and methanolic phases were 8.33% and 58.4%,

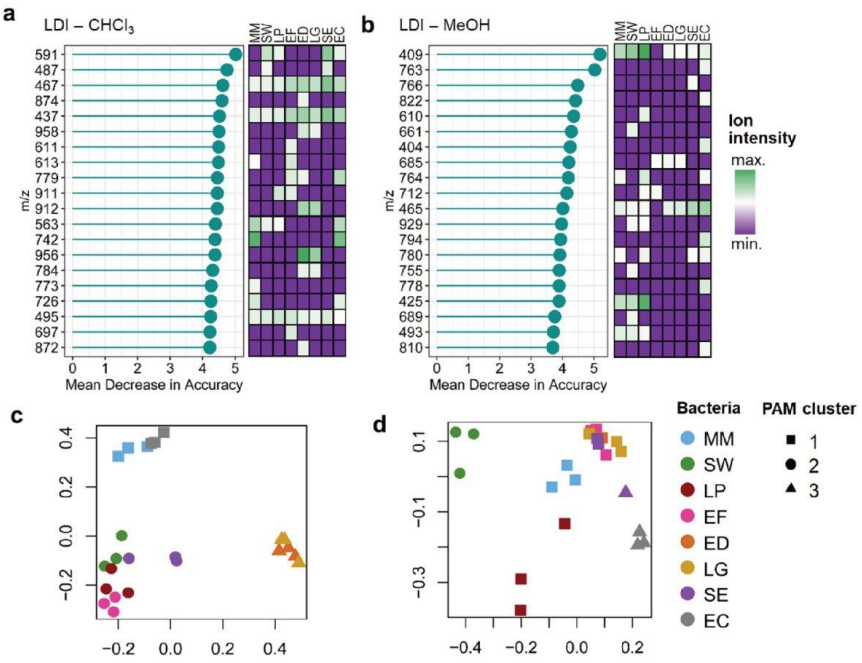

Figure 5. Variable importance rank in terms of mean decrease in accuracy, obtained according with RF model for LDI-MS in (**a**) chloroform and (**b**) methanol fractions; MDS plots built based on RF proximity matrix, applied to the calibration sets of LDI-MS data obtained from the analysis of (**c**) chloroform and (**d**) methanol phases.

Phase	Parameter Bacteria	MM (%)	SW (%)	LP (%)	EF (%)	ED (%)	LG (%)	SE (%)	EC (%)
$CHCl_3$	Sensitivity	100	100	100	100	100	100	100	100
	Specificity	100	100	100	100	100	100	100	100
	Balanced Accuracy	100	100	100	100	100	100	100	100
	Overall accuracy	100.0							
	95% CI	79.4–100							
MeOH	Sensitivity	100.0	100.0	100.0	50.0	100.0	0.0	50.0	100.0
	Specificity	100.0	100.0	100.0	85.7	85.7	100.0	100.0	100.0
	Balanced Accuracy	100.0	100.0	100.0	67.9	92.9	50.0	75.0	100.0
	Overall accuracy	75.0							
	95% CI	47.6–92.7							

Table 1. RF model performance (CI = confidence interval).

respectively. As expected, NALDI-MS from the chloroform phase provided a superior balanced accuracy in the testing step (100%, 95%CI [79.4, 100%]). The excellent accuracy obtained for this dataset highlights the usefulness of NALDI-MS lipidomics for differentiation between bacterial species. For NALDI-MS of the methanolic fraction, balanced accuracy in the testing step was 75.0% (95%CI [47.6, 92.7%]). Lipid profiles from methanol phase failed to correctly classify the species EF, ED, LG and SE, the same appearing superimposed in the correspondent MDS plot.

Correlations between volatile and non-volatile profiles

Methods of correlation analysis were used to investigate associations between lipids profiles recovered from the chloroform fraction, VOCs and bacterial species. Correlation maps presented in Fig. 6a provide an overview of the abundance and nature of all possible bicorrelations existing among VOCs (matrix X) and lipids (matrix Y). In these plots, dark blue hues denote VOCs or lipids displaying strong negative correlations, red hues refer to strong positive correlations, while cyan and green hues denote very weak/irrelevant correlations. A cross-correlation matrix (X–Y) obtained from the combination between VOCs and NALDI-MS data exhibits several strong correlations between volatiles and lipids, suggesting a relevant relationship between both datasets. Figure 6b summarizes CCA output, presenting a merging between results for site and variables scores. The orientation and length of arrows are proportional to the degree of correlation a lipid has with the VOCs and bacterial species. G− and G + bacteria were separated by the first component—a discrimination ruled mainly by the lipids at *m/z* 549 and 657, which are the most correlated with CCA1. In contrast, the ions at *m/z* 703, 768 and 770 are associated with G + bacteria and the production of nonanal, decanal, octanal and benzonitrile by them. In this line, the lipids at *m/z* 657 and 549 appear as strongly associated with the generation of acetic acid and heptanal, respectively.

Spearman correlation analysis allowed us to find connections between individual lipids and microbial VOCs, a network view of these results show 5 groups of relationships (Fig. 6c). The first one, related to the 2-butanone, styrene and benzothiazole; the second one, regarding heptanal and *p*-xylene; the third one, regarding acetic acid; the fourth one, showing the correspondences between nonanal, decanal and benzonitrile; lastly, the fifth one regards octanal trends. Overall, it showed an association between NALDI-MS lipid profiles and the metabolism of fatty acids (giving rise to the fatty aldehydes heptanal, octanal, nonanal and decanal), the metabolism of amino acids (benzonitrile and benzothiazole), fermentation pathways (acetic acid and 2-butanone) and the metabolism of aromatic hydrocarbons by microorganisms (*p*-xylene, styrene). Fatty aldehydes such as the mentioned ones can be derived from the oxidation of lipids from the cell membranes, or during fatty acid metabolism through the reduction of fatty acyl-ACP[39]. Considering this, fatty aldehydes are metabolites expected to be linked with the lipid composition of bacteria. Aromatic amino acids, which are precursors of benzonitrile (through the aldoxime–nitrile pathway) and possibly also of benzothiazole are required for lipid stabilization[39,49]. Therefore, the metabolism of aromatic amino acids may be an indicative of lipid synthesis and composition. It is known that bacteria are able to metabolize polyaromatic hydrocarbons (PAHs) from the environment. Parallelly, the switch of bacterial metabolism towards the catabolism of PAHs may lead to changes in fatty acid content or composition in bacteria[50]. Fermentative metabolic routes generate pyruvate. Pyruvate when further converted into malonyl-CoA becomes precursor in the biosynthesis of fatty acids, which can be incorporated into lipids[39].

Conclusion

The present study demonstrated specificities of the metabolic profiles for eight strains of bacteria with application of polypyrrole-MOF solid-phase microextraction fibers and plasmonic silver nanostructured substrates. Due to simultaneous application of innovative devices, comprehensive profiling based on volatile and non-volatile metabolites was carried out for the first time. The main hypothesis of the study was that presented devices would enable registration of metabolic profiles, which could be valuable for species differentiation.

Volatile profiles collected with utilization of PPy@ZIF-8 SPME fibers consisted of nitrogen-containing compounds, ketones, aldehydes, alcohols, organic acids, which probably can be explained by affinity of fiber coating towards polar analytes. This is in agreement with the structure of polypyrrole ring, where nitrogen introduces affinity towards nitrogen-containing compounds and provides unequal distribution of electrons creating a

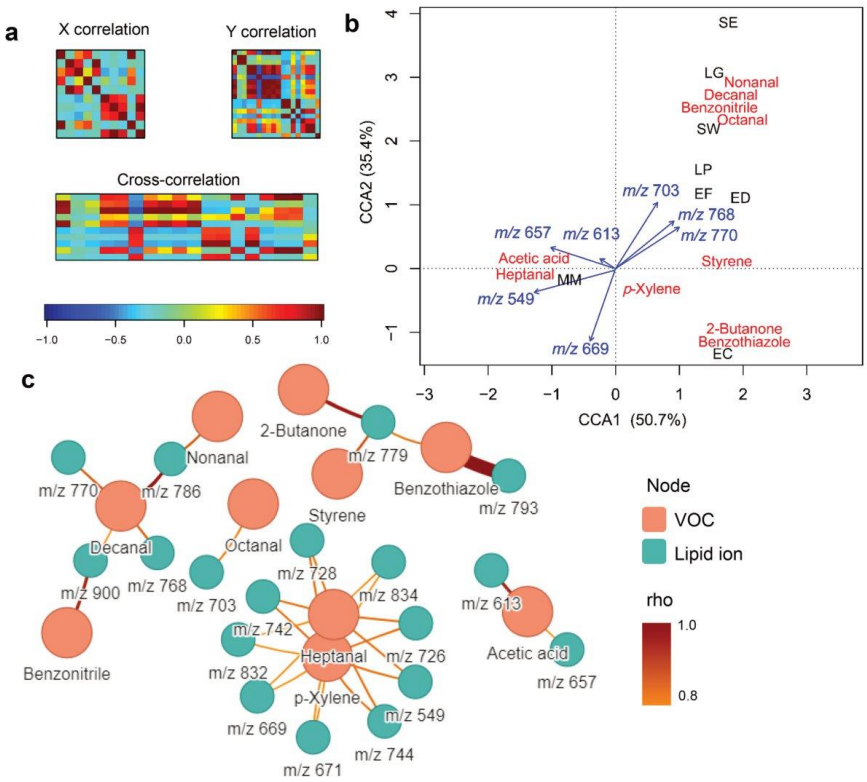

Figure 6. (**a**) Cross-correlation matrix (X–Y) obtained from combining the matrices X (VOCs) and Y (lipid ions in the chloroform fraction); (**b**) CCA biplot; (**c**) networks showing the significant associations between lipid ions and VOCs, according to Spearman correlation analysis (significance criteria: $p < 0.05$, rho = |0.8|). Edge color and thickness refers to the strength and significance ($-\mathrm{Log}_{10}\, p$) of the correlation, respectively.

permanent dipole moment. Although prevalence of nitrogen-containing compounds in collected profiles were possibly not attributed to the affinity of nitrogen in the structure of polypyrrole ring towards analytes, the results suggest that PPy@ZIF-8 fibers could serve as a cost-efficient alternative for VOCs profiling, offering relatively low cost and rapid synthesis, as well as mechanical and thermal stability.

Principal component analysis revealed distinction between G+ and G− species for both volatile and non-volatile profiles. Hierarchical cluster analysis showed discrimination between G+ and G− species and six clusters based on volatile profiles. In case of non-volatile profiles of chloroform fraction of the B & D bacterial extract, eight clusters corresponding to each species were observed in addition to distinction between G+ and G− species. Random forest model showed high accuracy (100%, 95%CI [79.4, 100%]) for classification of species using chloroform fraction of B & D extract in contrast to the methanolic fraction (95%CI [47.6, 92.7%]).

In case of non-volatile profiling, clear discrimination between eight species was achieved, potentially attributed to enhanced sensitivity of the NALDI-MS substrates towards low molecular weight metabolites due to plasmonic properties of silver nanoparticles. Failure of discrimination in case of polar phase of bacterial extracts possibly could be attributed either by fragmentation of polar lipids or their low content. Fragmentation of polar lipids in NALDI-MS analysis with application of silver nanostructured substrates could be explained by the nature of the interactions between analytes and nanoparticles.

Furthermore, methods of correlation analysis suggested relationship between volatile and non-volatile datasets, which demonstrated that complementary application of presented lab-made devices could be useful for gaining valuable insights into bacterial metabolism.

Data availability

The datasets used and/or analyzed during the current study available from the corresponding author on reasonable request.

Received: 29 September 2023; Accepted: 1 March 2024
Published online: 06 March 2024

References

1. Maier, T., Klepel, S., Renner, U. & Kostrzewa, M. Fast and reliable MALDI-TOF MS-based microorganism identification. *Nat. Methods* **3**, 113 (2006).
2. Mather, C. A., Rivera, S. F. & Butler-Wu, S. M. Comparison of the bruker biotyper and vitek MS matrix-assisted laser desorption ionization-time of flight mass spectrometry systems for identification of mycobacteria using simplified protein extraction protocols. *J. Clin. Microbiol.* **52**, 130–138 (2014).
3. Sohlenkamp, C. & Geiger, O. Bacterial membrane lipids: Diversity in structures and pathways. *FEMS Microbiol. Rev.* **40**, 133–159 (2015).
4. Leung, L. M. *et al.* Identification of the ESKAPE pathogens by mass spectrometric analysis of microbial membrane glycolipids. *Sci. Rep.* **7**, 1–10 (2017).
5. Liang, T. *et al.* Rapid microbial identification and antibiotic resistance detection by mass spectrometric analysis of membrane lipids. *Anal. Chem.* **91**, 1286–1294 (2018).
6. Tanaka, K. *et al.* Protein and polymer analyses up to *m/z* 100 000 by laser ionization time-of-flight mass spectrometry. *Rapid Commun. Mass Spectrom.* **2**, 151–153 (1988).
7. Abdelhamid, H. N. Nanoparticle assisted laser desorption/ionization mass spectrometry for small molecule analytes. *Microchim. Acta* **185**, 1–16 (2018).
8. Su, H. *et al.* Plasmonic alloys reveal a distinct metabolic phenotype of early gastric cancer. *Adv. Mater.* **33**, 2007978 (2021).
9. Huang, L. *et al.* Plasmonic silver nanoshells for drug and metabolite detection. *Nat. Commun.* **8**, 220 (2017).
10. Labows, J. N., McGinley, K. J., Webster, G. F. & Leyden, J. J. Headspace analysis of volatile metabolites of *Pseudomonas aeruginosa* and related species by gas chromatography–mass spectrometry. *J. Clin. Microbiol.* **12**, 521–526 (1980).
11. Chen, J., Tang, J., Shi, H., Tang, C. & Zhang, R. Characteristics of volatile organic compounds produced from five pathogenic bacteria by headspace-solid phase micro-extraction/gas chromatography–mass spectrometry. *J. Basic Microbiol.* **57**, 228–237 (2017).
12. Arthur, C. L. & Pawliszyn, J. Solid phase microextraction with thermal desorption using fused silica optical fibers. *Anal. Chem.* **62**, 2145–2148 (1990).
13. Reese, K. L., Rasley, A., Avila, J. R., Jones, D. & Frank, M. Metabolic profiling of volatile organic compounds (VOCs) emitted by the pathogens *Francisella tularensis* and *Bacillus anthracis* in liquid culture. *Sci. Rep.* **10**, 13 (2020).
14. Fitzgerald, S., Duffy, E., Holland, L. & Morrin, A. Multi-strain volatile profiling of pathogenic and commensal cutaneous bacteria. *Sci. Rep.* https://doi.org/10.1038/s41598-020-74909-w (2020).
15. Lashgari, M. & Yamini, Y. An overview of the most common lab-made coating materials in solid phase microextraction. *Talanta* https://doi.org/10.1016/j.talanta.2018.08.077 (2019).
16. Wang, W., Kang, S. & Vikesland, P. J. Surface-enhanced Raman spectroscopy of bacterial metabolites for bacterial growth monitoring and diagnosis of viral infection. *Environ. Sci. Technol.* https://doi.org/10.1021/acs.est.1c02552 (2021).
17. Mametov, R., Sagandykova, G., Monedeiro-Milanowski, M., Gabryś, D. & Pomastowski, P. Electropolymerized polypyrrole-MOF composite as a coating material for SPME fiber for extraction VOCs liberated by bacteria. *Sci. Rep.* **13**, 1–10 (2023).
18. Maslak, E. *et al.* A new approach to imaging and rapid microbiome identification for prostate cancer patients undergoing radiotherapy. *Biomedicines* **10**, 33 (2022).
19. Złoch, M., Pomastowski, P., Maślak, E., Monedeiro, F. & Buszewski, B. Study on molecular profiles of *Staphylococcus aureus* strains: Spectrometric approach. *Molecules* **25**, 1–20 (2020).
20. Bligh, E. G. & Dyer, W. J. A rapid method for extraction and purification. *Can. J. Biochem. Physiol.* **37**, 911 (1959).
21. Cockerill III, F.R. *et al.* & Abstract. *Methods for Dilution Antimicrobial Susceptibility Tests for Bacteria that Grow Aerobically; Approved Standard—Ninth Edition*. Vol. 32 (2012).
22. Sagandykova, G. *et al.* Silver nanostructured substrates in LDI-MS of low molecular weight compounds. *Materials (Basel).* **15**, 1–12 (2022).
23. Son, M. S. & Taylor, R. K. Growth and maintenance of *Escherichia coli* laboratory strains. *Curr. Protoc.* **1**, 5 (2021).
24. Amabilis-Sosa, L. E., Vazquez-Lopez, M., Rojas, G. J. L., Roe-Sosa, A. & Moeller-Chavez, G. E. Efficient bacteria inactivation by ultrasound in municipal wastewater. *Environments* **5**, 47 (2018).
25. Smetanková, J. *et al.* Influence of aerobic and anaerobic conditions on the growth and metabolism of selected strains of *Lactobacillus plantarum*. *Acta Chim. Slov.* **5**, 204–210 (2012).
26. Mis Solval, K., Chouljenko, A., Chotiko, A. & Sathivel, S. Growth kinetics and lactic acid production of *Lactobacillus plantarum* NRRL B-4496, *L. acidophilus* NRRL B-4495, and *L. reuteri* B-14171 in media containing egg white hydrolysates. *LWT* **105**, 393–399 (2019).
27. Emborg, J., Dalgaard, P. & Ahrens, P. *Morganella psychrotolerans* sp. nov., a histamine-producing bacterium isolated from various seafoods. *Int. J. Syst. Evol. Microbiol.* **56**, 2473–2479 (2006).
28. Minnullina, L., Kostennikova, Z., Evtugin, V., Akosah, Y. & Sharipova, M. Diversity in the swimming motility and flagellar regulon structure of uropathogenic *Morganella morganii* strains. *Int. Microbiol.* **25**, 111–122 (2022).
29. Mantripragada, V. P. & Jayasuriya, A. C. Effect of dual delivery of antibiotics (vancomycin and cefazolin) and BMP-7 from chitosan microparticles on *Staphylococcus epidermidis* and pre-osteoblasts in vitro. *Mater. Sci. Eng. C* **1**, 12 (2016).
30. Zhang, X. *et al.* Genome-wide identification of ampicillin resistance determinants in *Enterococcus faecium*. *PLoS Genet.* **8**, 1002804 (2012).
31. Xie, X. *et al.* Prevalence, virulence, and antibiotics gene profiles in *Lactococcus garvieae* isolated from cows with clinical mastitis in China. *Microorganisms* **11**, 379 (2023).
32. Baikuni, A., Hawari, F. L., Ramadon, D. & Malik, A. Untargeted LC-QTOF-MS/MS based metabolomic profile approach of bacterial ferment lysates and skin commensal bacterial cocktail ferment lysates. *Hayati J. Biosci.* **30**, 576–587 (2023).
33. Milanowski, M. *et al.* Profiling of VOCs released from different salivary bacteria treated with non-lethal concentrations of silver nitrate. *Anal. Biochem.* **578**, 36–44 (2019).
34. Drabińska, N. *et al.* Application of a solid-phase microextraction-gas chromatography-mass spectrometry/metal oxide sensor system for detection of antibiotic susceptibility in urinary tract infection-causing *Escherichia coli*—A proof of principle study. *Adv. Med. Sci.* **67**, 1–9 (2022).
35. Pawliszyn, J. Theory of solid-phase microextraction. In *Handbook of Solid Phase Microextraction*. 13–59 https://doi.org/10.1016/B978-0-12-416017-0.00002-4 (Elsevier Inc., 2012).
36. Mametov, R., Sagandykova, G., Monedeiro, F. & Buszewski, B. Development of controlled film of polypyrrole for solid-phase microextraction fiber by electropolymerization. *Talanta* **232**, 122394 (2021).
37. Hu, J. B., Chen, Y. C. & Urban, P. L. Coffee-ring effects in laser desorption/ionization mass spectrometry. *Anal. Chim. Acta* **766**, 77–82 (2013).
38. Schulz, S. & Dickschat, J. S. Bacterial volatiles: The smell of small organisms. *Nat. Prod. Rep.* **24**, 814–842 (2007).

39. Monedeiro, F., Railean-Plugaru, V., Monedeiro-Milanowski, M., Pomastowski, P. & Buszewski, B. Metabolic profiling of vocs emitted by bacteria isolated from pressure ulcers and treated with different concentrations of bio-agnps. *Int. J. Mol. Sci.* **22**, 4696 (2021).
40. Gosset, G. Production of aromatic compounds in bacteria. *Curr. Opin. Biotechnol.* **20**, 651–658 (2009).
41. Adams, A. & De Kimpe, N. Formation of pyrazines and 2-acetyl-1-pyrroline by *Bacillus cereus*. *Food Chem.* **101**, 1230–1238 (2007).
42. DeMilo, A. B., Lee, C. J., Moreno, D. S. & Martinez, A. J. Identification of volatiles derived from citrobacter freundii fermentation of a trypticase soy broth. *J. Agric. Food Chem.* **44**, 607–612 (1996).
43. Breil, C., Abert Vian, M., Zemb, T., Kunz, W. & Chemat, F. "Bligh and Dyer" and Folch methods for solid–liquid–liquid extraction of lipids from microorganisms. Comprehension of solvatation mechanisms and towards substitution with alternative solvents. *Int. J. Mol. Sci.* **18**, 1–21 (2017).
44. Maslak, E. *et al.* Silver nanoparticle targets fabricated using chemical vapor deposition method for differentiation of bacteria based on lipidomic profiles in laser desorption/ionization mass spectrometry. *Antibiotics* **12**, 874 (2023).
45. Fahy, E. *et al.* Update of the LIPID MAPS comprehensive classification system for lipids. *J. Lipid Res.* **50**, 9–14 (2009).
46. Oursel, D. *et al.* Lipid composition of membranes of Escherichia coli by liquid chromatography/tandem mass spectrometry using negative electrospray ionization. *Rapid Commun. Mass Spectrom.* **21**, 1721–1728 (2007).
47. Li, M., Yang, L., Bai, Y. & Liu, H. Analytical methods in lipidomics and their applications. *Anal. Chem.* **86**, 161–175 (2014).
48. Jaber, M. A. *et al.* Advantages of using biologically generated ^{13}C-labelled multiple internal standards for stable isotope-assisted LC–MS-based lipidomics. *Anal. Methods* **15**, 2925–2934 (2023).
49. Mbaye, M. N. *et al.* A comprehensive computational study of amino acid interactions in membrane proteins. *Sci. Rep.* **9**, 1–14 (2019).
50. Seo, J. S., Keum, Y. S. & Li, Q. X. Bacterial degradation of aromatic compounds. *Int. J. Environ. Res. Public Health* **6**, 278 (2009).

Acknowledgements
The study was financed by The National Science Centre (Poland) in a framework of the Preludium 18 project No. 2019/35/N/ST4/04363 (2020–2022). R.M. and P.P. are members of Scientific Toruń Center of Excellence "Towards Personalized Medicine" operating under Excellence Initiative Research University (Torun, Poland).

Author contributions
Conceptualization: R.M., G.S., P.P.; Data curation: R.M., A.F and G.S.; Formal analysis: R.M., G.S., A.F. F.M.; Funding acquisition R. M.; Investigation R.M., G.S., F.M., A.F.; Methodology: R.M., G.S., F.M., P.P. (Piotr Piszczek)., A.F., A.R.; Project administration: R. M., P. P. (Pawel Pomastowski); Resources: R. M., P.P. (Pawel Pomastowski); Supervision: R.M., P.P., G.S.; Validation: R.M., F.M.; Writing—original draft: R.M. G.S., F.M., A.F.; Writing—review & editing: R.M., G.S., F.M., A.F., P.P., P.P., A.R.

Competing interests
The authors declare no competing interests.

Additional information
Supplementary Information The online version contains supplementary material available at https://doi.org/10.1038/s41598-024-56107-0.

Correspondence and requests for materials should be addressed to R.M.

Reprints and permissions information is available at www.nature.com/reprints.

Publisher's note Springer Nature remains neutral with regard to jurisdictional claims in published maps and institutional affiliations.

Electronic supplementary information

Metabolic Profiling of Bacteria with the Application of Polypyrrole-MOF SPME fibers and Plasmonic Nanostructured LDI-MS Substrates

Radik Mametov [a,§], Gulyaim Sagandykova [a], Fernanda Monedeiro [b], Aleksandra Florkiewicz [a], Piotr Piszczek [c], Aleksandra Radtke [c] and Pawel Pomastowski [a]

[a] Centre for Modern Interdisciplinary Technologies, Nicolaus Copernicus University in Toruń, Wileńska 4, Toruń, 87-100, Poland

[b] Department of Chemistry, Faculty of Philosophy, Sciences and Letters of Ribeirão Preto, University of São Paulo, Av. Bandeirantes 3900, Ribeirão Preto, 14040-901, Brazil

[c] Department of Inorganic and Coordination Chemistry, Faculty of Chemistry, Nicolaus Copernicus University in Toruń, Gagarina 7, Toruń, 87-100, Poland

[§] corresponding author, e-mail: mametov.radik@gmail.com, tel. + 48 56 665 60 01

Table of contents

Figure S9. NALDI and MALDI-TOF-MS (stock solution) spectra of the methanol fraction of the Bligh & Dyer extract of *Morganella morganii* collected by application of silver nanostructured substrates (NALDI), DHB and HCCA matrices (MALDI)

Figure S10. NALDI and MALDI-TOF-MS (stock solution) spectra of the methanol fraction of the Bligh & Dyer extract of *Staphylococcus warneri* collected by application of silver nanostructured substrates (NALDI), DHB and HCCA matrices (MALDI)

Figure S11. NALDI and MALDI-TOF-MS (stock solution) spectra of the methanol fraction of the Bligh & Dyer extract of *Lactobacillus plantarum* collected by application of silver nanostructured substrates (NALDI), DHB and HCCA matrices (MALDI)

Figure S12. NALDI and MALDI-TOF-MS (stock solution) spectra of the methanol phase of the Bligh & Dyer extract of *Enterococcus faecium* collected by application of silver nanostructured substrates (NALDI), DHB and HCCA matrices (MALDI)

Figure S13. NALDI and MALDI-TOF-MS (stock solution) spectra of the methanol fraction of the Bligh & Dyer extract of *Enterococcus durans* collected by application of silver nanostructured substrates (NALDI), DHB and HCCA matrices (MALDI)

Figure S14. NALDI and MALDI-TOF-MS (stock solution) spectra of the methanolic fraction of the Bligh & Dyer extract of *Lactococcus garvieae* collected by application of silver nanostructured substrates (NALDI), DHB and HCCA matrices (MALDI)

Figure S15. NALDI and MALDI-TOF-MS (stock solution) spectra of the methanolic fraction of the Bligh & Dyer extract of *Staphylococcus epidermidis* collected by application of silver nanostructured substrates (NALDI), DHB and HCCA matrices (MALDI)

Figure S16. NALDI and MALDI-TOF-MS (stock solution) spectra of the methanol fraction of the Bligh & Dyer extract of *Escherichia coli* collected by application of silver nanostructured substrates (NALDI), DHB and HCCA matrices (MALDI)

FigureS17. Microbial growth curves of bacteria grown at 37°C for 32h represented by optical density (OD) values: (a) *Escherichia coli*, (b) *Lactobacillus plantarum*, (c) *Morganella morganii*, (d) *Enterococcus durans*, (d) Control, Mueller Hinton Broth medium, (f) *Staphylococcus epidermidis*, (g) *Enterococcus faecium*, (h) *Lactococcus garvieae*, (i) *Staphylococcus warneri*

Table S1. Detected bacterial VOCs (after medium blanks subtraction) and their respective peak areas. Missing values refer to undetected peaks

Table S2. The list of *m/z* values and corresponding intensities for detected signals in chloroform fraction of B & D extract of *Morganella morganii* collected with NALDI-MS

Table S3. The list of *m/z* values and corresponding intensities for detected signals in chloroform fraction of B & D extract of *Staphylococcus warneri* collected with NALDI-MS

Table S4. The list of *m/z* values and corresponding intensities for detected signals in chloroform fraction of B & D extract of *Lactobacillus plantarum* collected with NALDI-MS

Table S5. The list of *m/z* values and corresponding intensities for detected signals in chloroform fraction of B & D extract of *Enterococcus faecium* collected with NALDI-MS

Table S6. The list of *m/z* values and corresponding intensities for detected signals in chloroform fraction of B & D extract of *Enterococcus durans* collected with NALDI-MS

Table S7. The list of *m/z* values and corresponding intensities for detected signals in chloroform fraction of B & D extract of *Lactococcus garvieae* collected with NALDI-MS

Table S8. The list of *m/z* values and corresponding intensities for detected signals in chloroform fraction of B & D extract of *Staphylococcus epidermidis* collected with NALDI-MS

Table S9. The list of *m/z* values and corresponding intensities for detected signals in chloroform fraction of B & D extract of *Escherichia coli* collected with NALDI-MS

Table S10. The list of *m/z* values and corresponding intensities for detected signals in methanol fraction of B & D extract of *Morganella morganii* collected with NALDI-MS

Table S11. The list of *m/z* values and corresponding intensities for detected signals in methanol fraction of B & D extract of *Staphylococcus warneri* collected with NALDI-MS

Table S12. The list of *m/z* values and corresponding intensities for detected signals in methanol fraction of B & D extract of *Lactobacillus plantarum* collected with NALDI-MS

Table S13. The list of *m/z* values and corresponding intensities for detected signals in methanol fraction of B & D extract of *Enterococcus faecium* collected with NALDI-MS

Table S14. The list of *m/z* values and corresponding intensities for detected signals in chloroform fraction of B & D extract of *Enterococcus durans* collected with NALDI-MS

Table S15. The list of *m/z* values and corresponding intensities for detected signals in methanol fraction of B & D extract of *Lactococcus garvieae* collected with NALDI-MS

Table S16. The list of *m/z* values and corresponding intensities for detected signals in methanol fraction of B & D extract of *Staphylococcus epidermidis* collected with NALDI-MS

Table S17. The list of *m/z* values and corresponding intensities for detected signals in methanol fraction of B & D extract of *Escherichia coli* collected with NALDI-MS

Table S18. Comparison of the extraction performance of PPY@ZIF-8 and CAR/PDMS SPME fibers for standard mixture of VOCs by HS-GC-FID analysis

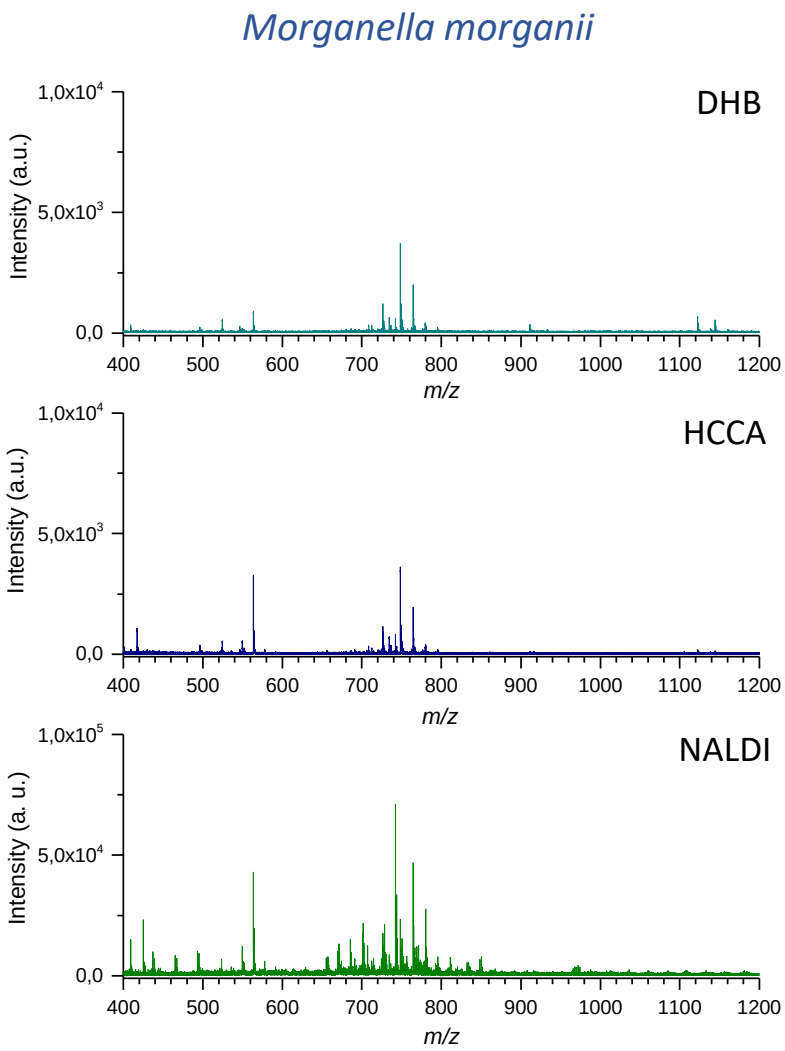

Figure S1. NALDI (dilution 1:10) and MALDI-TOF-MS (stock solution) spectra of the chloroform phase of the Bligh & Dyer extract of *Morganella morganii* collected by application of silver nanostructured substrates (NALDI), DHB and HCCA matrices (MALDI)

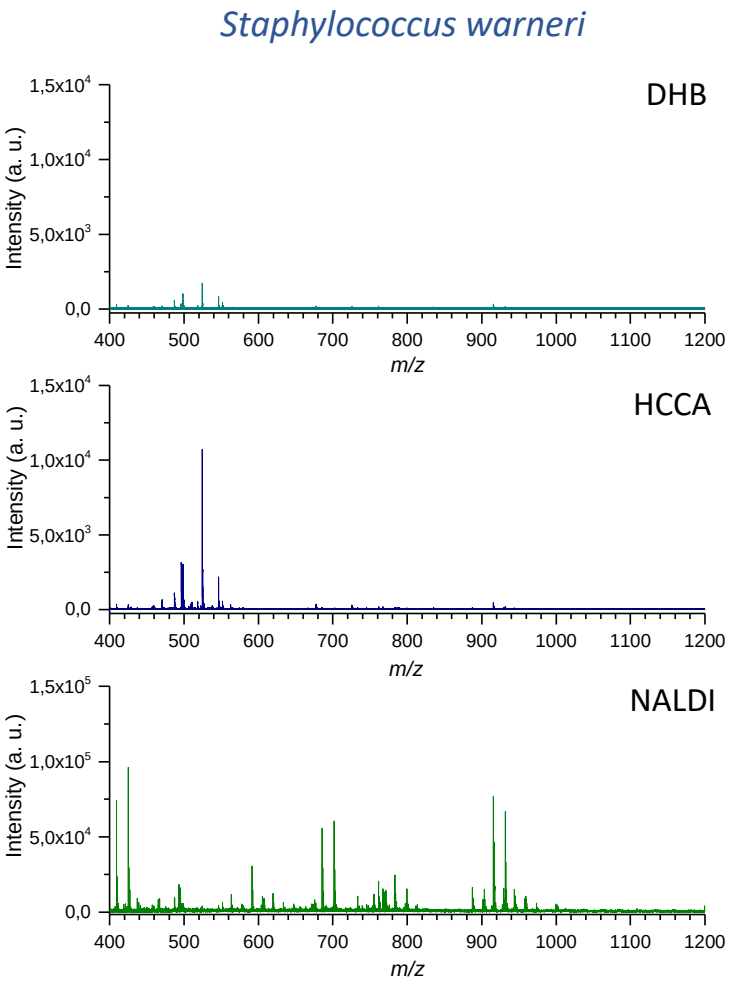

Figure S2. NALDI (dilution 1:10) and MALDI-TOF-MS (stock solution) spectra of the chloroform phase of the Bligh & Dyer extract of *Staphylococcus warneri* collected by application of silver nanostructured substrates (NALDI), DHB and HCCA matrices (MALDI)

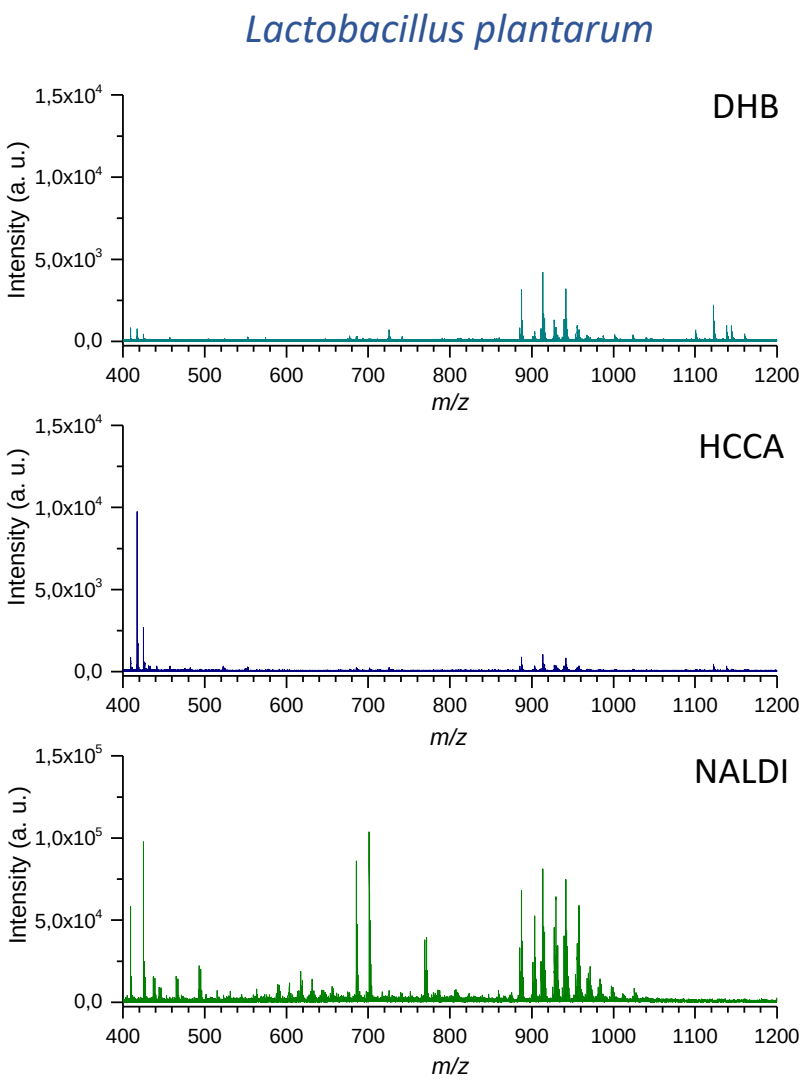

Figure S3. NALDI (dilution 1:10) and MALDI-TOF-MS (stock solution) spectra of the chloroform phase of the Bligh & Dyer extract of *Lactobacillus plantarum* collected by application of silver nanostructured substrates (NALDI), DHB and HCCA matrices (MALDI)

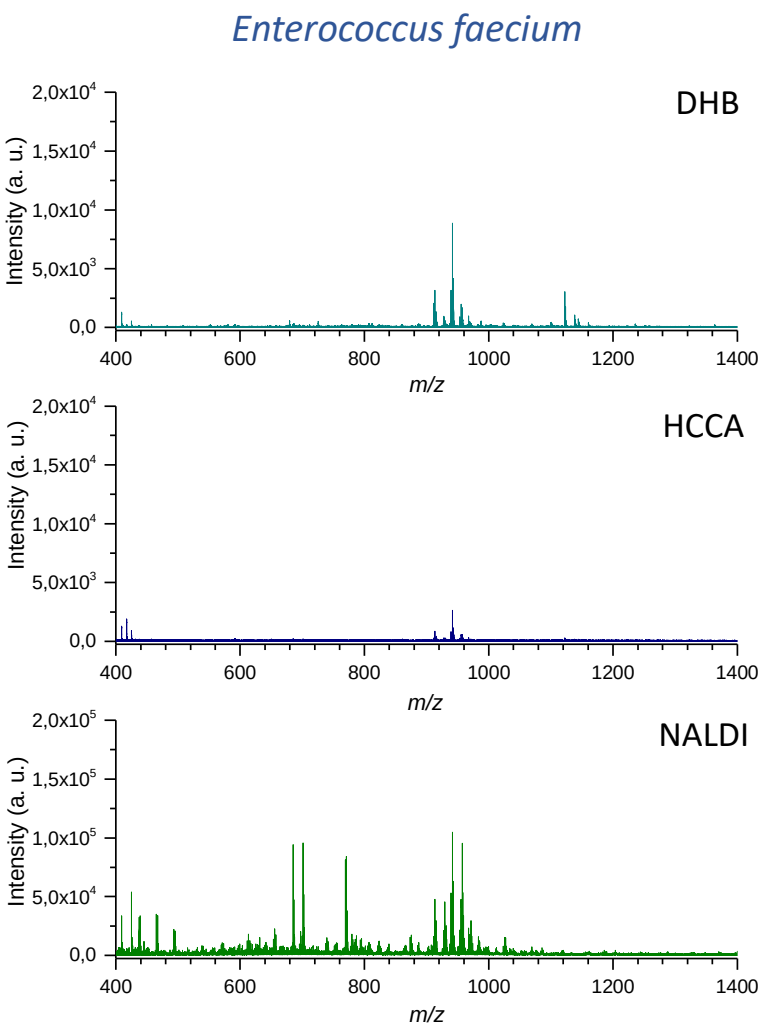

Figure S4. NALDI (stock solution) and MALDI-TOF-MS (stock solution) spectra of the chloroform phase of the Bligh & Dyer extract of *Enterococcus faecium* collected by application of silver nanostructured substrates (NALDI), DHB and HCCA matrices (MALDI)

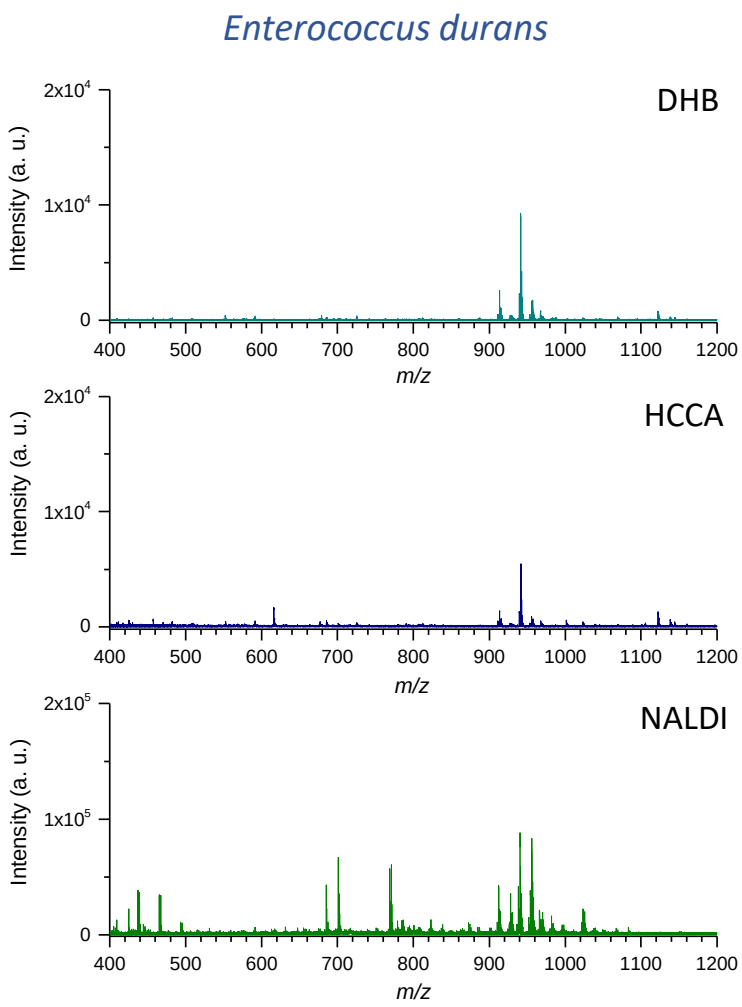

Figure S5. NALDI (dilution 1:10) and MALDI-TOF-MS (stock solution) spectra of the chloroform phase of the Bligh & Dyer extract of *Enterococcus durans* collected by application of silver nanostructured substrates (NALDI), DHB and HCCA matrices (MALDI)

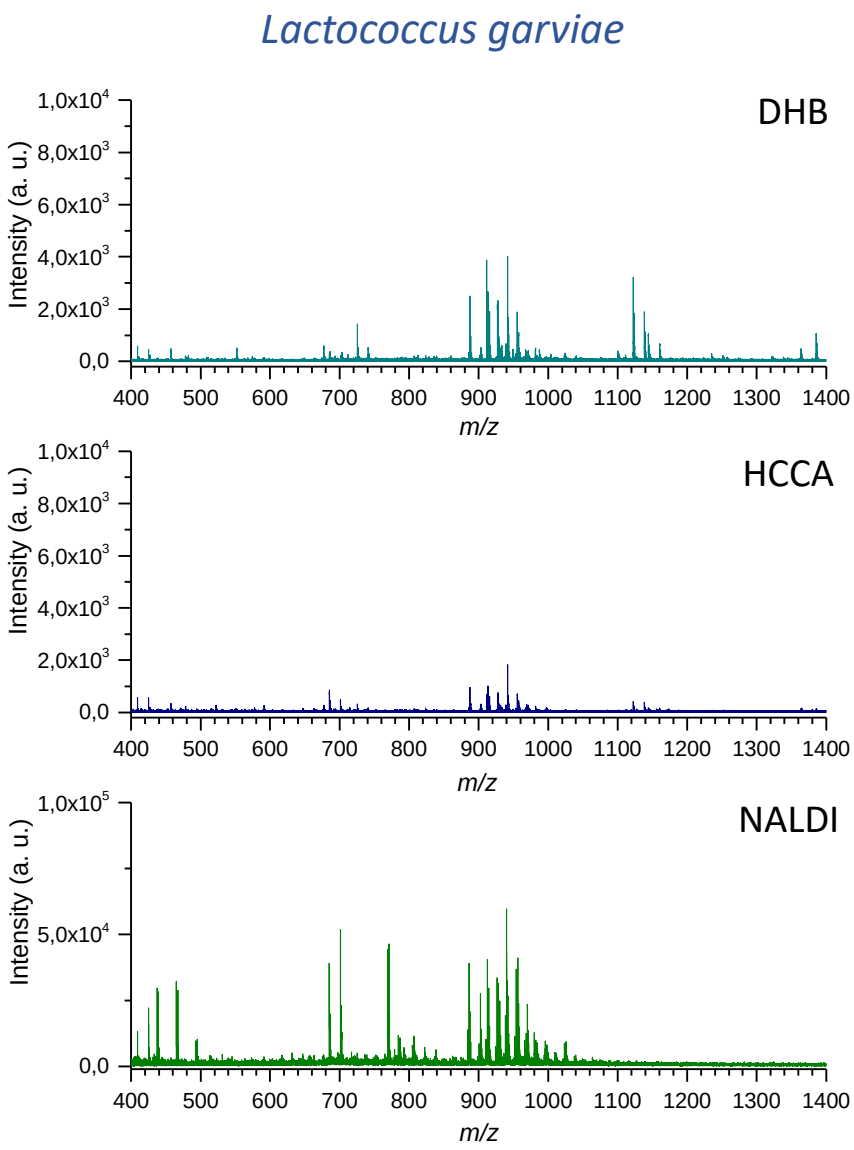

Figure S6. NALDI (dilution 1:10) and MALDI-TOF-MS (stock solution) spectra of the chloroform phase of the Bligh & Dyer extract of *Lactococcus garvieae* collected by application of silver nanostructured substrates (NALDI), DHB and HCCA matrices (MALDI)

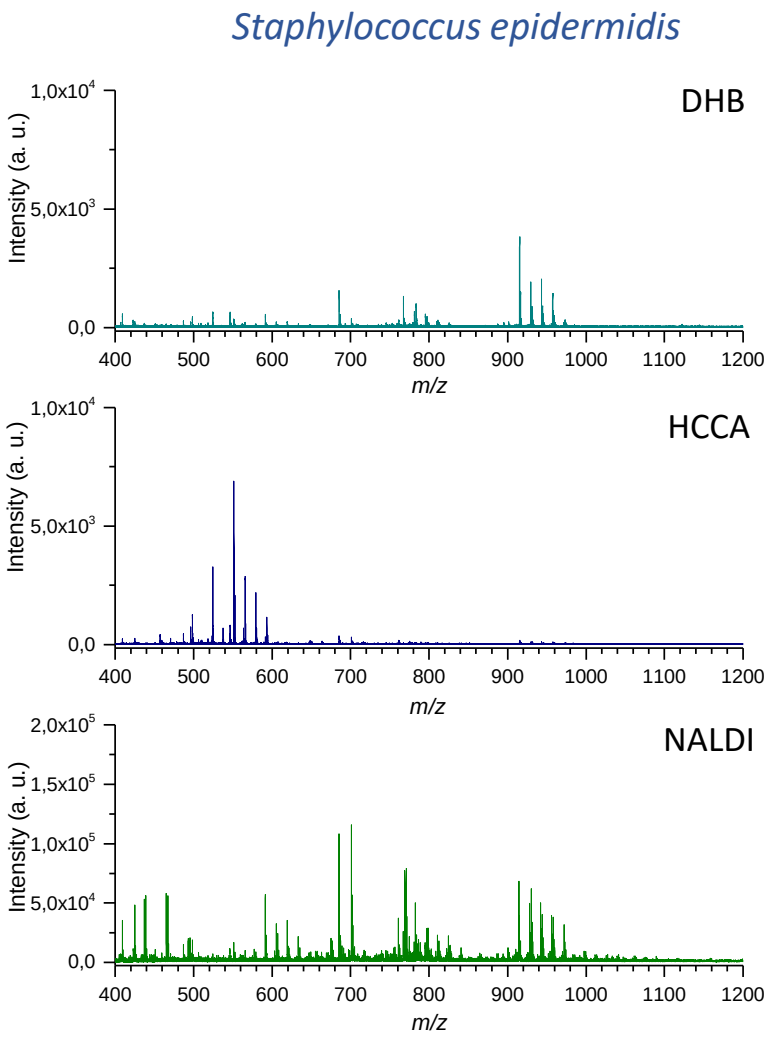

Figure S7. NALDI (dilution 1:10) and MALDI-TOF-MS (stock solution) spectra of the chloroform phase of the Bligh & Dyer extract of *Staphylococcus epidermidis* collected by application of silver nanostructured substrates (NALDI), DHB and HCCA matrices (MALDI)

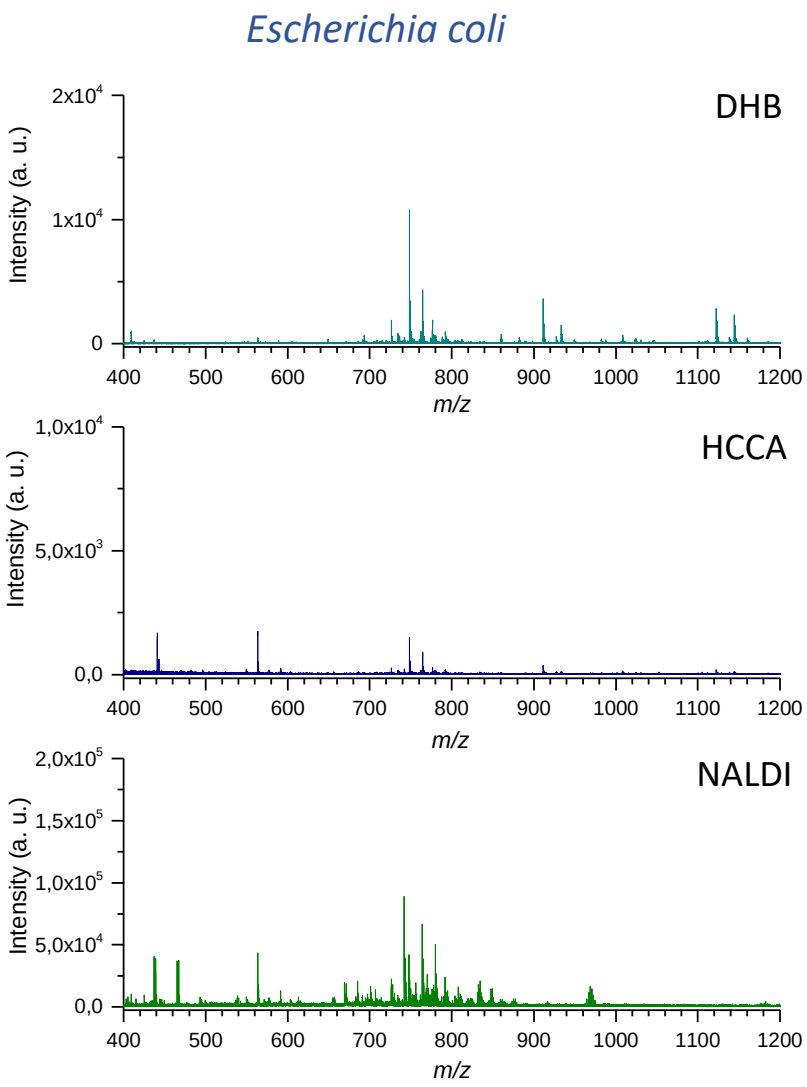

Figure S8. NALDI (dilution 1:10) and MALDI-TOF-MS (stock solution) spectra of the chloroform phase of the Bligh & Dyer extract of *Escherichia coli* collected by application of silver nanostructured substrates (NALDI), DHB and HCCA matrices (MALDI)

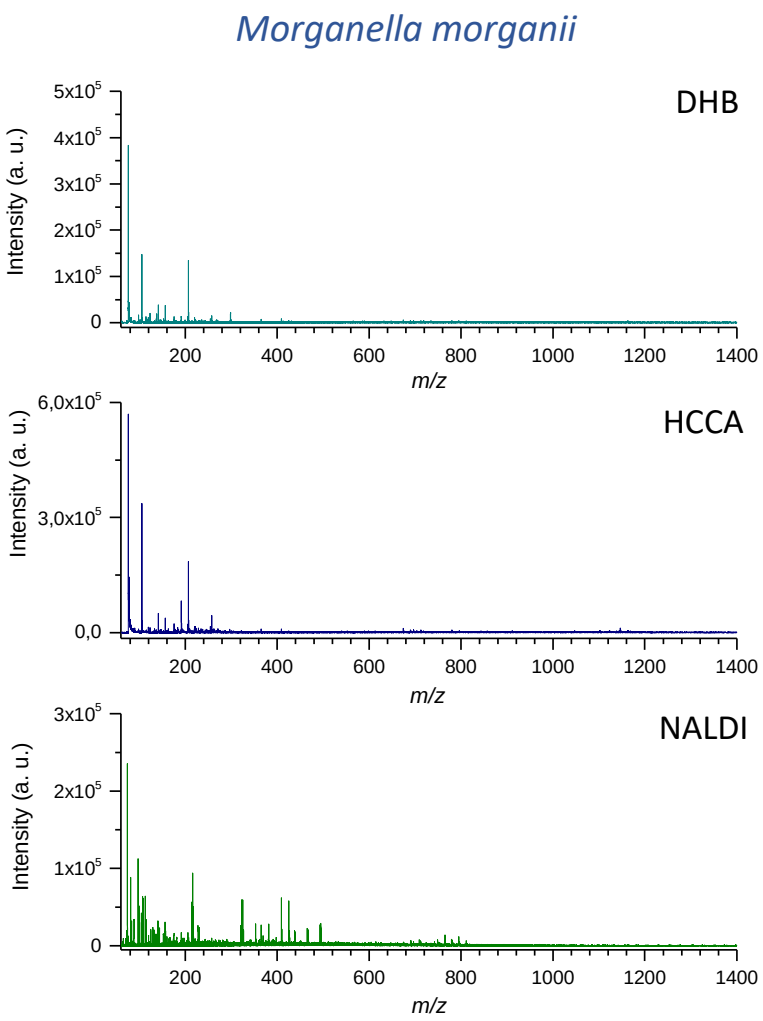

Figure S9. NALDI and MALDI-TOF-MS (stock solution) spectra of the methanol fraction of the Bligh & Dyer extract of *Morganella morganii* collected by application of silver nanostructured substrates (NALDI), DHB and HCCA matrices (MALDI)

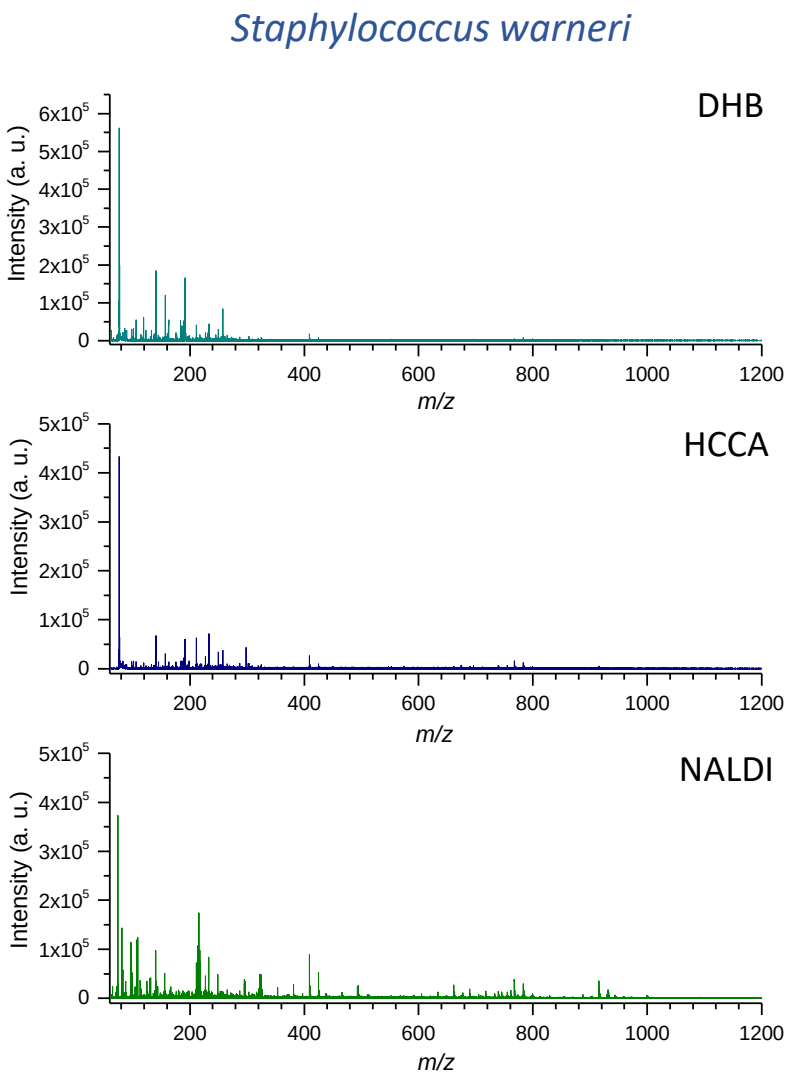

Figure S10. NALDI and MALDI-TOF-MS (stock solution) spectra of the methanol fraction of the Bligh & Dyer extract of *Staphylococcus warneri* collected by application of silver nanostructured substrates (NALDI), DHB and HCCA matrices (MALDI)

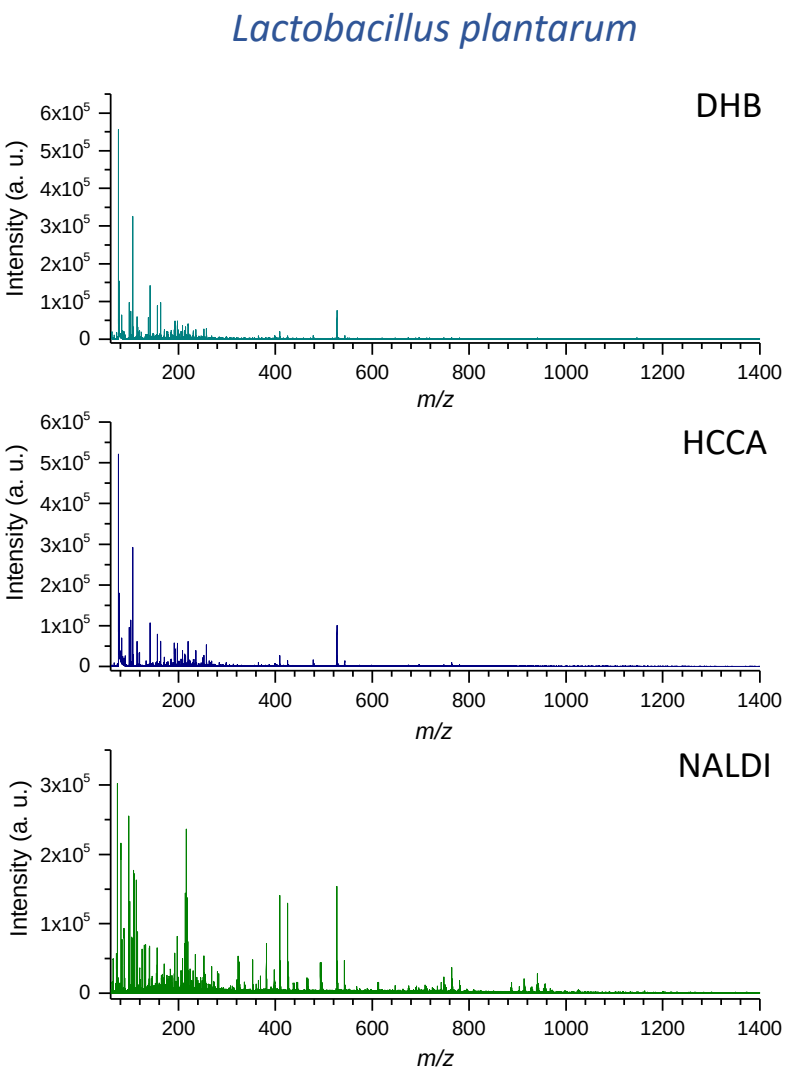

Figure S11. NALDI and MALDI-TOF-MS (stock solution) spectra of the methanol fraction of the Bligh & Dyer extract of *Lactobacillus plantarum* collected by application of silver nanostructured substrates (NALDI), DHB and HCCA matrices (MALDI)

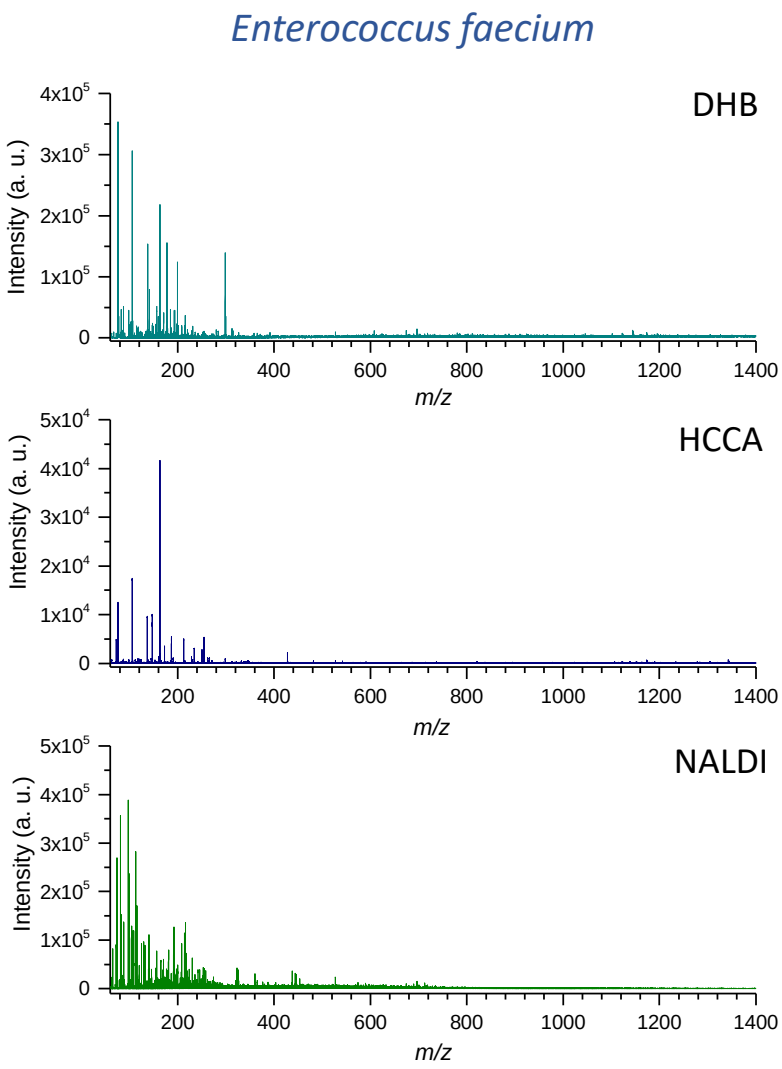

Figure S12. NALDI and MALDI-TOF-MS (stock solution) spectra of the methanol phase of the Bligh & Dyer extract of *Enterococcus faecium* collected by application of silver nanostructured substrates (NALDI), DHB and HCCA matrices (MALDI)

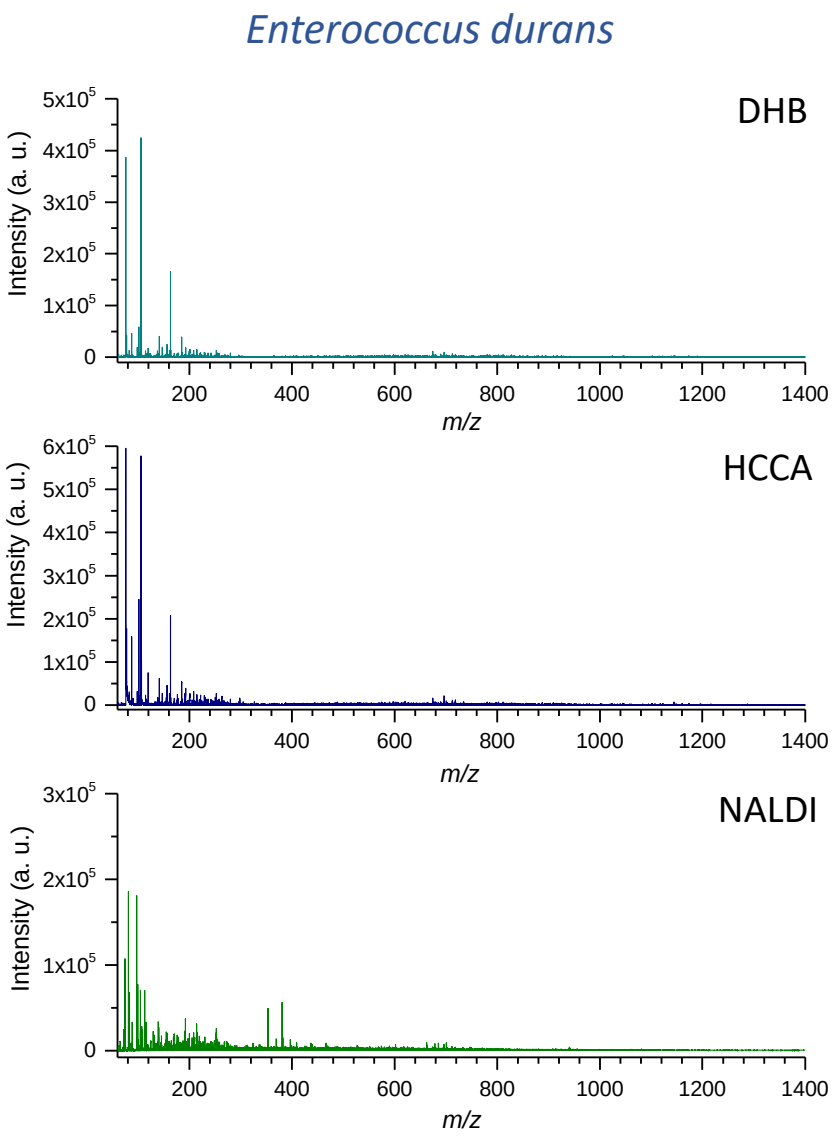

Figure S13. NALDI and MALDI-TOF-MS (stock solution) spectra of the methanol fraction of the Bligh & Dyer extract of *Enterococcus durans* collected by application of silver nanostructured substrates (NALDI), DHB and HCCA matrices (MALDI)

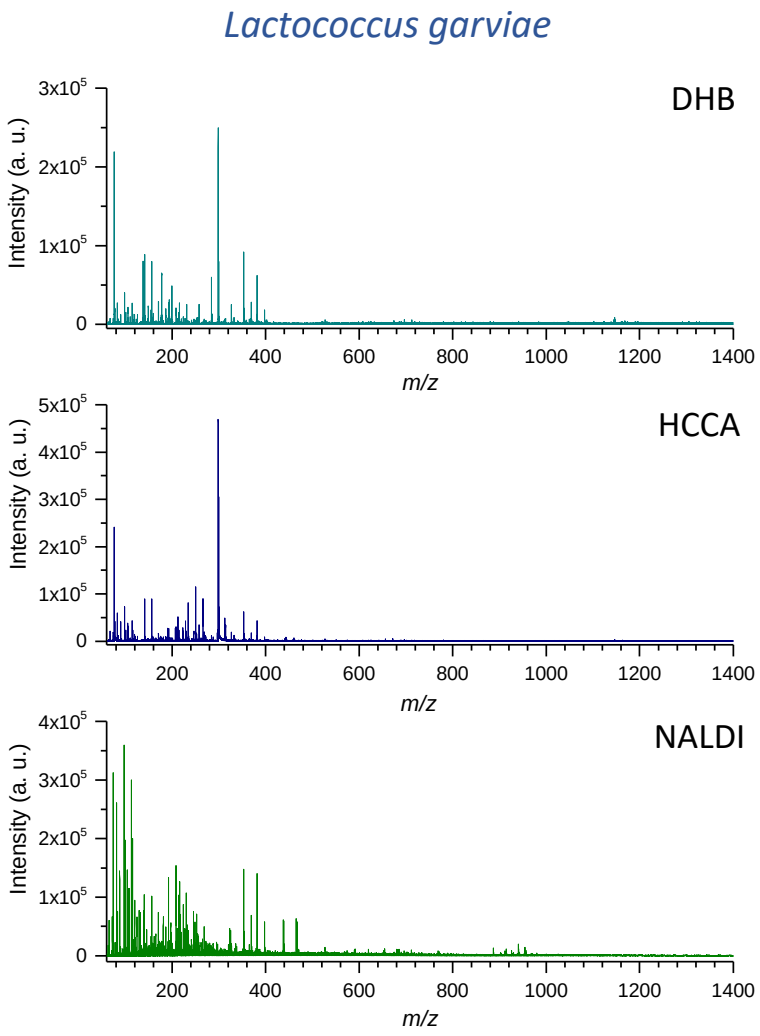

Figure S14. NALDI and MALDI-TOF-MS (stock solution) spectra of the methanolic fraction of the Bligh & Dyer extract of *Lactococcus garvieae* collected by application of silver nanostructured substrates (NALDI), DHB and HCCA matrices (MALDI)

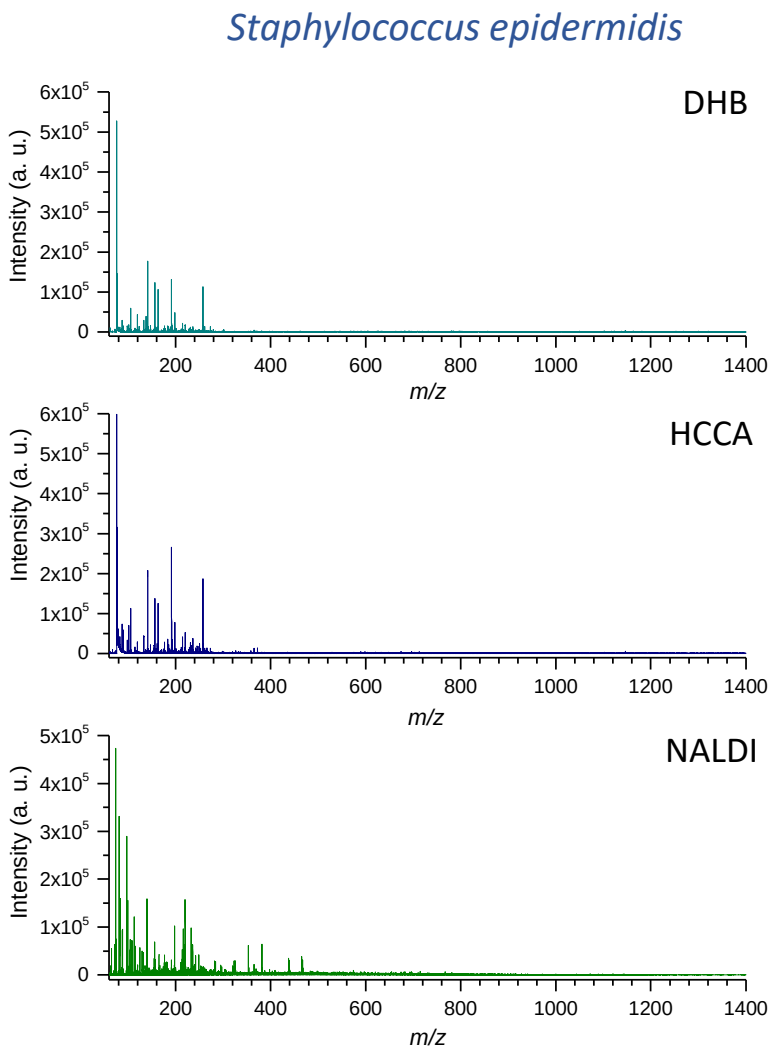

Figure S15. NALDI and MALDI-TOF-MS (stock solution) spectra of the methanolic fraction of the Bligh & Dyer extract of *Staphylococcus epidermidis* collected by application of silver nanostructured substrates (NALDI), DHB and HCCA matrices (MALDI)

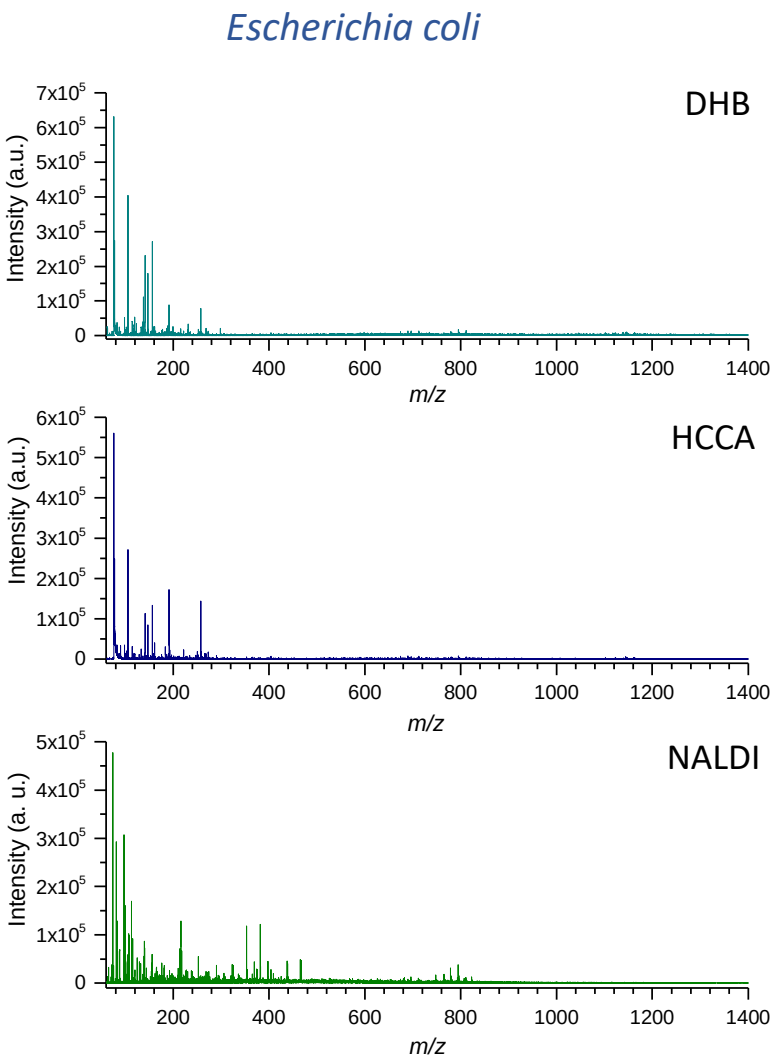

Figure S16. NALDI and MALDI-TOF-MS (stock solution) spectra of the methanol fraction of the Bligh & Dyer extract of *Escherichia coli* collected by application of silver nanostructured substrates (NALDI), DHB and HCCA matrices (MALDI

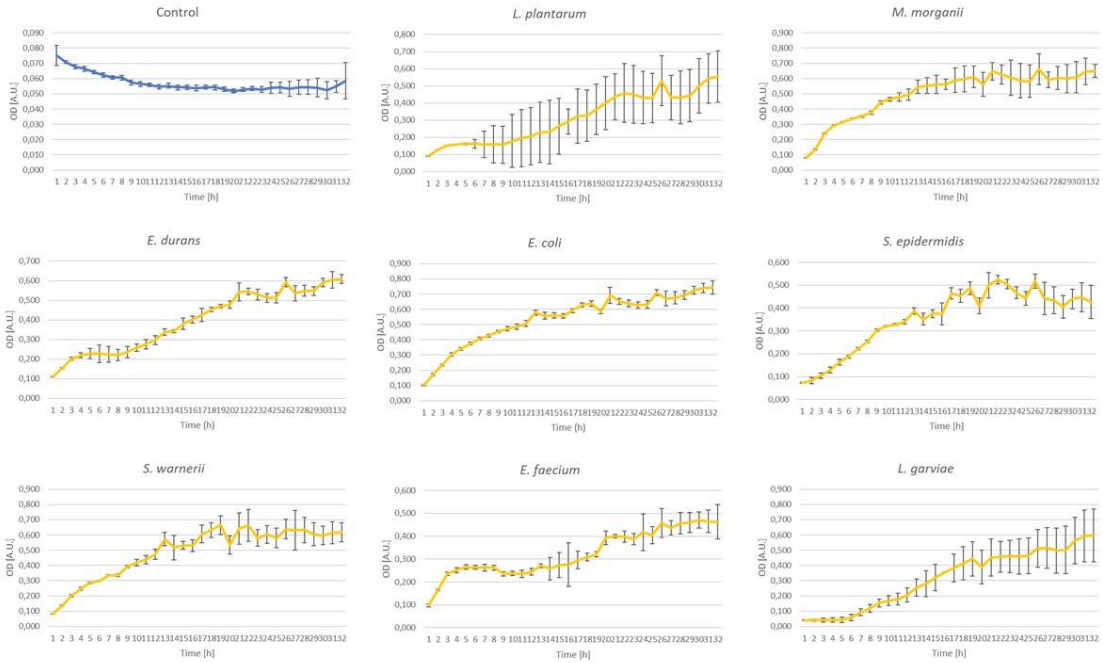

FigureS17. Microbial growth curves of bacteria grown at 37°C for 32h represented by optical density (OD) values: (a) *Escherichia coli*, (b) *Lactobacillus plantarum*, (c) *Morganella morganii*, (d) *Enterococcus durans*, (d) Control, Mueller Hinton Broth medium, (f) *Staphylococcus epidermidis*, (g) *Enterococcus faecium*, (h) *Lactococcus garvieae*, (i) *Staphylococcus warneri*

Table S1. Detected bacterial VOCs (after medium blanks subtraction) and their respective values of peak area. Missing values refer to undetected peaks and SE is Staphylococcus epidermidis, ED is Enterococcus durans, LP is Lactobacillus plantarum, SW is Staphylococcus Warneri, LG is Lactococcus garvieae, MM is Morganella morganii, EC is Escherichia coli, EF is Enterococcus Faecium

Retention time (min)	Compound	*SE*	*ED*	*LP*	*SW*	*LG*	*MM*	*EC*	*EF*
2,33	1,2-Propanediamine		1138662,92	390867,33					
3,31	Dimethylamine			4855489,4	1088816,2				
3,34	Nitro-ethane				41586791			1509158,59	
3,83	Methylamine							2426092	30346
6,28	2-Butanone		426949,28					4014983,44	62352,25
7,04	Ethyl acetate				131275,2			183678,6	
9,14	Acetic acid						1080942,21		12439,67
9,99	Hexanal	487786,08	436133,74	408817,52	1113320,7			415073,3	
10,25	Propanedioic acid	388358,4	624676,71	290123,04	502056,79	819970,11		1381876,29	
10,63	Dimethyl disulfide						72750645,8	350740,77	
11,17	3-Methyl-1-butanol					77276,77	5859607,22		
11,88	Oxalic acid		179483,75			71725,44		431193,4	
14,31	5-Hexen-2-ol		578370,51					1659721,05	
15,34	3-Hydroxybutanal		150429,81						56443,19
15,42	3-Nitropropanoic acid					44366,93		1453394,23	
16,14	p-Xylene						1980426,01	1400289,51	101417,57
16,45	Acetamide		84658,63			137588,83			
16,94	Styrene		461185,66					425513,91	40786,19
17,52	Heptanal					46680,89	33875190,9	119406,99	
17,72	2,5-Dimethylpyrazine	514852,74	393744,84	407965,28	959628,14	407882,64		439793,8	194395,47
19,45	1-Hexanamine				96361,21	23677,82			
20,08	Benzaldehyde	2349810,49	5568495,91	1707124,6	2487775,7	879167,45	704530,63	514533,83	
20,62	Octanal	181531,24	97809,01		102107,05				14830,48
21,21	Benzonitrile	461082,24				127407,61			

22,48	Phenol	486944,16	1076807,43	151849,19	2827457	2159439,09	117645838	8157424,19	273315,59
23,26	Acetophenone	174246,25	225291,87	144635,22	543144,99				
23,47	Nonanal	336589,78	194583,36			244331,51			22670,02
24,85	Benzothiazole							2830557,79	51689,36
24,98	Methyl-1-octadecanamine					113586,18			24888,63
26,57	Decanal	503386,37	100028,04			124050,86			
27,35	Succinimide	534652,17	2069917,2	516344,89	820908,3	1933478,72	87490432,8		
28,94	2-Undecanone		121503,92			317947,24	2354230,33		
30,69	Indole	1893334,03	7784875,4	1834404,49					
30,71	2-Dodecanone					3081101,15		272264116,4	
32,35	2-Tridecanone					12423808	2525640,08		
33,72	2-Tetradecanone	433722,21			642101,14	2618168,27	2300326,35		
34,34	Tetracosane					135990452	8308808,66		
34,56	Vinyl myristate	604992,9					28315923,5		
35,64	Heptacosane				426786,84			118562426,6	

Table S2. The list of *m/z* values and corresponding intensities for detected signals in chloroform fraction of B & D extract of *Morganella morganii* collected with NALDI-MS

rep 1		rep 2		rep 3		rep 4		rep 5	
m/z	Intensity	*m/z*	Intensity	*m/z*	Intensity	*m/z*	Intensity	*m/z*	Intensity
409	15255	409	12141	409	14759	409	20372	409	15242
425	22637	425	15145	425	23259	425	23622	425	23126
437	8747	437	8497	437	11115	437	13248	437	15301
439	5544	439	7472	439	7976	439	13024	439	10704
465	7812	465	6517	465	8030	465	14084	465	11359
467	6081	467	5188	467	8052	467	12302	467	11078
493	8740	493	5093	493	11448	493	15177	493	12111
495	7604	495	4161	495	8555	495	13766	495	9767
523	5709	549	4193	549	9421	549	11271	549	7297
549	11782	563	11873	563	28975	563	40410	563	29237
563	40012	669	5030	655	5961	655	8881	613	5232
655	5933	671	4372	657	6737	669	10859	655	7387
657	5717	685	16009	669	9174	671	10455	657	6013
669	8706	701	13495	671	8051	685	24510	669	9839
671	9162	702	5142	685	15130	701	20257	671	10341
685	15697	714	4714	700	5735	702	10532	674	5650
691	6196	726	9355	701	12558	707	9171	685	16915
701	19997	728	10466	702	6650	726	18653	701	19287
702	9686	730	5305	707	8795	728	22783	702	11579
707	9999	734	5235	714	6452	730	7977	707	8573
712	6136	742	40962	726	17056	734	8847	714	6283
714	6208	764	22338	728	19290	742	60788	726	16232
724	6956	769	8942	730	5672	744	6881	728	21379
726	17548	771	8772	734	5542	764	38854	730	8065
728	19471	773	4212	742	56239	769	18517	734	6076
730	7360	780	13391	744	7760	771	16852	742	67184
734	8518	795	4739	764	39588	773	6835	744	10205
742	71815			766	8615	780	23252	764	38814
764	45663			769	13290	782	6208	769	21426
769	10381			771	13019	795	6739	771	16489
771	10473			773	8195	811	6168	773	7463
773	6977			780	26557	832	6412	780	26105
778	5914			795	7965			795	6188
780	26214			811	5617			811	6002
795	7799			848	5374			834	5179
811	7556							848	5156
834	5119							850	5563
848	6058								
850	6195								

Table S3. The list of *m/z* values and corresponding intensities for detected signals in chloroform fraction of B & D extract of *Staphylococcus warneri* collected with NALDI-MS

rep 1		rep 2		rep 3		rep 4		rep 5	
m/z	Intensity	*m/z*	Intensity	*m/z*	Intensity	*m/z*	Intensity	*m/z*	Intensity
409	72446	409	29859	409	31183	409	9771	409	43267
425	95707	425	44113	425	44400	425	10419	425	79895
437	7981	437	4144	437	11167	437	11030	437	7991
439	6265	467	5167	439	10312	439	9082	439	7047
465	8182	487	5402	444	5118	465	7527	444	6757
467	7655	493	10251	446	6089	467	8439	446	7309
487	8826	495	10418	465	12891	487	6057	465	7077
493	17652	551	4795	467	12033	493	11244	467	7803
495	14289	591	16006	487	5058	493	10258	487	5024
551	6375	607	5085	493	11082	495	9777	493	21858
563	11507	619	4757	495	14144	498	2728	495	18270
591	32218	675	5175	563	7072	551	10795	498	5760
605	9643	685	28658	591	25815	563	15064	551	5302
607	9271	701	32287	605	5930	591	15248	563	5969
619	11744	755	5210	607	6535	619	15784	591	19480
633	6067	761	11421	619	7434	685	15909	605	5734
675	8250	767	5610	675	8103	701	17186	607	8294
685	55548	769	9066	677	5803	761	14842	619	8496
701	61499	771	11505	685	57823	767	10646	675	6777
703	7566	783	10578	701	61379	769	16727	685	38706
733	9833	799	6315	733	6490	771	11945	701	53462
755	11238	887	10412	761	12905	783	16753	703	7773
761	21041	901	5374	767	5714	799	18454	733	5410
767	13788	903	8350	769	30658	887	20886	755	7136
769	12191	915	44051	771	28838	901	18010	761	14968
771	11987	929	7829	783	13513	903	22687	767	6712
783	24283	931	35419	799	9013	915	19117	769	19820
799	14423	943	6437	887	10037	929	22347	771	16938
887	16840	945	6483	903	10133	931	21091	783	18650
901	8030	957	3799	915	46170	943	11837	799	10473
903	14988	959	5666	929	7034	945	21045	887	10776
915	80565	999	3620	931	42577	959	20437	903	10533
929	14404			943	7246	1001	21770	915	49650
931	65983			945	7511			929	8602
943	13916			957	4237			931	48408
945	10479			959	6505			943	8738
957	8623			999	4775			945	8117
959	9148			1001	5057			957	4925
999	4748							959	8299
1199	4237							999	4145

Table S4. The list of *m/z* values and corresponding intensities for detected signals in chloroform fraction of B & D extract of *Lactobacillus plantarum* collected with NALDI-MS

rep 1		rep 2		rep 3		rep 4		rep 5	
m/z	Intensity	*m/z*	Intensity	*m/z*	Intensity	*m/z*	Intensity	*m/z*	Intensity
409	55343	409	49483	409	46184	409	33846	409	11372
425	93785	425	101912	425	87453	425	71481	425	9476
437	13380	437	12567	437	15497	437	10205	437	4934
439	12932	439	11415	439	14127	439	11436	439	73343
444	8004	465	13141	465	17844	465	13742	465	11158
446	7477	467	11749	467	15961	467	11603	467	5567
465	14614	493	25814	493	25704	493	15484	493	9016
467	12278	495	22788	493	9171	493	5872	495	31007
493	19111	495	6393	495	23032	495	12264	495	5455
495	17392	591	6402	495	7409	495	5966	591	24641
563	7339	631	6529	617	10010	617	8738	617	6866
589	8711	685	65188	655	8494	685	51486	631	5225
591	9812	701	79142	685	56783	701	69291	655	51923
617	17993	769	34148	701	84156	703	8432	685	10770
631	11556	771	32726	769	43186	769	28276	701	90103
655	7960	885	26563	771	41130	771	27512	769	81802
657	6863	887	64274	785	7439	885	24005	771	11198
685	85184	901	20736	787	9324	887	50257	785	5322
701	105700	903	50440	885	26871	901	22896	805	5703
769	37255	911	19779	887	59983	903	43035	807	8715
771	34991	913	74046	901	21908	911	14329	885	6394
885	32810	915	28069	903	52112	913	60524	887	5461
887	64646	927	33636	911	19755	915	24305	901	6872
901	23559	929	52354	913	70745	927	26222	903	9331
903	49199	931	23320	915	27945	929	53230	911	11338
911	23997	937	6631	927	30686	931	19164	913	7163
913	78290	939	30106	929	57135	937	6807	915	10916
915	31321	941	59542	931	24948	939	26414	927	5992
927	38396	943	26507	939	33048	941	49601	929	14565
929	57816	945	6507	941	59701	943	22698	931	6402
931	25940	953	15040	943	27965	955	25551	937	90426
939	37515	955	27360	955	29122	957	43456	939	165590
941	66678	957	49723	957	54400	959	9988	941	81159
943	27373	959	11008	959	7657	960	7511	943	6080
955	32382	983	11597	983	9761	999	7927	953	8897
957	53621	985	7400	985	7104	1025	7029	955	9454
959	12630	997	7366	997	5962			957	6268
981	8028	999	7513	1025	8922			960	41620
983	12417	1025	7547					981	94935
985	8111	1027	6259					983	10129
997	7960							985	87934
999	7060							999	24008
								1025	7545

Table S5. The list of *m/z* values and corresponding intensities for detected signals in chloroform fraction of B & D extract of *Enterococcus faecium* collected with NALDI-MS

rep 1		rep 2		rep 3		rep 4		rep 5	
m/z	Intensity	*m/z*	Intensity	*m/z*	Intensity	*m/z*	Intensity	*m/z*	Intensity
409	18202	409	24039	409	30148	409	24386	409	33268
425	25499	425	35438	425	53131	425	30908	425	52911
437	26904	437	30985	437	27620	437	28908	437	31737
439	24822	439	26994	439	20826	439	26003	439	30395
444	8135	444	9074	465	25963	465	29446	446	9624
446	7986	465	29097	467	26518	467	23808	465	32623
465	28315	467	26324	493	13366	493	12133	467	31026
467	24832	493	13973	493	16154	493	16032	493	14505
493	10606	493	17479	495	13732	495	12281	493	19541
493	16626	495	15704	495	14749	495	15568	495	16212
495	15748	571	10937	611	7652	569	8032	495	18484
569	8064	573	7907	613	12836	611	9229	571	9167
571	8315	611	8170	615	9883	613	18503	611	11105
597	7101	613	15722	655	14866	615	13414	613	16584
611	10501	615	12420	657	11550	631	8756	615	10631
613	14255	655	18974	685	67652	639	8703	631	13658
631	7723	657	11491	697	11712	655	20720	655	20703
655	17520	685	62282	701	84838	657	14840	657	15188
657	11357	697	14859	739	11989	685	68564	685	89291
685	54792	699	9969	769	57533	697	17155	697	17792
697	15437	701	65527	771	54630	701	64037	699	13993
699	10453	703	9558	779	16830	703	9354	701	93276
701	50949	739	15309	783	7772	739	13718	739	13426
739	10452	769	59900	785	8956	741	10204	741	10280
741	7800	771	58411	793	9715	769	67395	769	81050
769	55185	779	13119	839	9997	771	67462	771	74076
771	47748	785	12211	873	11961	779	13255	779	16100
779	8799	787	10124	875	10371	785	12355	785	12317
781	7658	823	8933	887	7621	787	10289	787	14275
785	6698	873	12672	901	7151	823	9718	839	9164
873	12319	875	11176	903	7294	839	7957	873	15866
875	9212	911	9997	911	14034	873	12504	875	14597
911	7070	913	30558	913	42864	875	11705	885	8014
913	22881	915	10978	915	17867	887	7637	887	9571
915	8355	927	12570	927	17120	911	12193	911	16126
927	9109	929	24434	929	39262	913	35781	913	47839
929	18041	931	12081	931	21563	915	16539	915	22190
931	9143	939	33427	939	44461	927	15189	927	19228
939	25388	941	64549	941	80980	929	24744	929	41671
941	50894	955	31428	943	21057	931	14054	931	20332
953	10610	957	52490	955	42344	939	42022	939	51801
955	21829	959	14312	957	78142	941	72026	941	98775

957	39743	983	9918	959	18282	943	16206	955	46752
959	9306	1025	11433	983	14959	955	30821	957	87830
983	9244	1027	8483	1025	11841	957	51704	959	20469
1023	5303			1027	9947	959	13457	983	15671
1025	7143			1085	5875	983	11574	1025	13792
1027	6576					1025	10415	1027	12440
						1027	8419	1069	6879

Table S6. The list of *m/z* values and corresponding intensities for detected signals in chloroform fraction of B & D extract of *Enterococcus durans* collected with NALDI-MS

rep 1		rep 2		rep 3		rep 4		rep 5	
m/z	Intensity	*m/z*	Intensity	*m/z*	Intensity	*m/z*	Intensity	*m/z*	Intensity
409	13145	409	11066	409	9765	409	11793	409	8536
425	31201	425	21843	425	17177	425	29774	425	21807
437	43713	437	36393	437	25985	437	34577	437	36523
439	38908	439	31829	439	22678	439	29001	439	33127
444	10415	444	7789	444	7060	444	8823	444	9569
446	10049	465	32420	465	23060	446	8060	446	8357
465	39331	467	29893	467	22724	465	30726	465	32744
467	39376	493	8915	493	7100	467	27612	467	31108
493	10587	493	10155	495	6317	493	10644	493	8879
493	10922	495	8042	685	31058	493	7570	493	9331
495	11896	495	9024	701	47587	495	9459	495	8487
495	9345	685	44091	768	28512	495	7831	495	10223
685	48605	701	69987	770	27792	685	46593	685	35794
701	83153	703	10468	779	7105	701	86565	701	56940
768	55069	768	57492	912	20586	768	56118	703	9359
770	52832	770	52747	914	8410	770	49942	768	51293
779	12365	784	11570	926	7031	779	12467	770	46961
784	12720	786	11745	928	14537	784	12002	779	7527
786	9711	822	12204	930	7136	786	12186	784	9527
838	8090	838	8148	938	22605	822	11196	786	9532
872	12902	872	10146	940	46913	838	11911	822	7044
874	11663	874	7298	952	8353	872	10686	872	14165
910	8140	910	10509	954	19927	874	8573	874	13255
912	35910	912	40182	956	38335	910	10245	912	24836
914	14634	914	13823	958	7891	912	36566	914	9846
926	11521	926	10496	982	8987	914	14305	926	8191
928	34620	928	33869	1023	9348	926	10314	928	23785
930	16129	930	13697	1025	7217	928	33238	930	11149
938	37389	936	7980			930	15760	938	27113
940	83356	938	40108			938	39581	940	61325
952	12980	940	87612			940	82242	952	9455
954	39724	942	18310			954	38101	954	29394
956	78210	954	39976			956	82317	956	56595

958	18211	956	77141			958	18735	958	15530
982	16630	958	18608			982	18094	982	12700
997	7832	982	16110			1021	8207	997	6465
1021	8340	995	7756			1023	17901	1021	6173
1023	16446	997	7509			1025	13466	1023	15428
1025	13637	1021	10516					1025	10400
		1023	19271						
		1025	16517						

Table S7. The list of *m/z* values and corresponding intensities for detected signals in chloroform fraction of B & D extract of *Lactococcus garvieae* collected with NALDI-MS

rep 1		rep 2		rep 3		rep 4		rep 5	
m/z	Intensity	m/z	Intensity	m/z	Intensity	m/z	Intensity	m/z	Intensity
409	11552	409	11900	409	8151	409	9071	409	6515
425	21053	425	30948	425	21085	425	16161	425	16572
437	27676	437	29283	437	26121	437	18753	437	19774
439	25846	439	26183	439	21511	439	16736	439	16434
465	28761	465	28489	465	25839	465	20049	465	19171
467	25440	467	27883	467	24464	467	16905	467	16580
493	8273	493	12070	493	7436	493	5417	493	4267
493	8547	495	9682	493	5476	493	4846	493	4603
495	7586	495	6022	495	6659	495	5249	495	5027
685	40074	685	43576	495	5266	685	39805	685	23765
701	52958	701	81846	685	39685	701	55734	701	40429
768	44001	703	9325	701	63205	768	31186	768	25214
770	41311	768	59432	768	48140	770	28038	770	24249
784	10767	770	52723	770	43356	784	7160	784	5574
786	8779	784	13064	784	10729	786	5566	786	5533
804	7288	786	11006	786	10753	804	8678	804	8263
806	9170	804	17579	804	13514	806	10579	806	9789
884	13111	806	16035	806	16194	822	5036	884	4729
886	37204	822	7756	822	5888	884	7389	886	18898
900	8451	838	6823	884	9801	886	23261	900	5970
902	26828	884	12919	886	32727	900	6410	902	17539
910	9613	886	35938	900	7849	902	22444	910	4863
912	39979	900	11406	902	26110	910	7365	912	17280
914	23976	902	41060	910	7388	912	25841	914	11078
924	7030	910	10264	912	31452	914	16129	926	14862
926	28614	912	38861	914	19987	926	19033	928	19301
928	30237	914	25480	926	25894	928	22345	930	11249
930	19765	926	32277	928	26436	930	12959	938	9280
938	18762	928	43440	930	18222	938	11798	940	25166
940	54711	930	27791	938	14375	940	35391	942	14402
942	24527	938	19014	940	43320	942	19690	952	4637
952	10381	940	54212	942	22628	952	7257	954	17612
954	32525	942	34484	952	7241	954	21002	956	26173

956	36493	952	8399	954	25552	956	29145	958	5931
958	8257	954	33283	956	37183	958	6801	980	7227
980	10453	956	55520	958	7345	980	8454	995	4223
982	9326	958	11141	980	9745	982	5505	1023	6050
984	6986	980	11209	982	6535	984	4599		
995	6180	982	10872	983	5054	996	4707		
997	6974	984	9309	985	5043	1023	5618		
1023	7858	995	8786	995	6702				
1025	6690	997	8616	997	8044				
		1023	11933	1023	9788				
		1025	10078	1025	7538				
				1037	4749				

Table S8. The list of *m/z* values and corresponding intensities for detected signals in chloroform fraction of B & D extract of *Staphylococcus epidermidis* collected with NALDI-MS

rep 1		rep 2		rep 3		rep 4		rep 5	
m/z	Intensity	*m/z*	Intensity	*m/z*	Intensity	*m/z*	Intensity	*m/z*	Intensity
409	33803	409	25940	409	27726	409	27032	409	23137
423	10297	425	41367	425	46072	425	43915	425	40448
425	46453	437	43853	437	32913	437	47914	437	45458
437	49745	439	38782	439	33495	439	44722	439	41038
439	49477	465	48768	451	7442	465	50378	465	48616
465	54800	467	40993	465	41986	467	52671	467	47238
467	49937	487	14993	467	34785	487	15740	487	12468
487	13769	493	14035	487	15293	493	18738	493	15309
493	17260	493	17062	493	15104	493	18111	493	14553
493	18678	495	14360	495	12147	495	16059	495	14280
495	16103	495	13394	498	15576	498	16824	495	13950
495	17751	498	16047	546	11374	546	12547	498	16262
498	14998	546	10309	551	12839	551	15815	546	9053
546	10421	551	16222	591	46355	565	10792	551	14556
551	16771	565	9443	605	26333	591	38237	565	8433
577	10481	591	34500	607	19903	605	21348	591	32596
591	56700	605	18487	619	21992	607	20503	605	18575
605	31726	607	13688	621	11721	619	21505	607	16467
607	23949	619	20917	633	14146	621	9183	619	18733
619	33639	633	12836	635	9249	633	14090	633	12044
621	11747	635	8563	675	13821	635	9586	675	14847
633	20437	675	14064	677	9924	675	15677	677	12702
635	11022	677	10458	685	82618	677	12016	685	74827
675	18509	685	75712	691	8900	685	77113	689	10749
677	16176	689	8692	701	92152	689	11425	701	89913
685	107484	701	88936	766	19630	701	91230	768	73610
689	12411	703	13598	768	51635	766	20260	770	66677
701	118949	766	17643	770	48368	768	68803	774	16128
703	18728	768	64215	774	17816	770	64997	782	31283

766	23418	770	64242	782	42068	774	19655	786	13984
768	71592	774	14888	788	11819	782	39661	788	13139
770	68483	782	34498	794	10576	786	13760	794	9742
774	20012	786	13515	796	24431	788	14785	796	18025
782	45405	788	10928	798	28695	794	11119	798	17964
786	14970	794	10359	810	19425	796	23049	810	14635
788	16021	796	20151	812	14871	798	26539	812	12502
794	15147	798	20576	824	14274	802	10454	824	12660
796	25397	810	16770	826	13454	810	18020	826	12103
798	26859	812	13052	840	8821	812	13224	900	8020
802	9803	824	12289	914	59723	824	13782	910	7519
810	19983	826	11556	928	35358	826	13698	914	42628
812	16855	840	8397	930	47315	840	9544	916	7977
824	17289	914	45738	942	33146	910	9197	928	29196
826	13966	916	8114	944	31458	914	55247	930	40365
840	11369	928	29670	956	29474	928	35771	942	25834
914	69207	930	43164	958	30464	930	54004	944	25969
916	10239	942	26314			942	33962	956	23483
928	47328	944	25655			944	36995	958	27490
930	59173	956	26661			956	27880	997	8210
942	46735	958	26964			958	29046		
944	40303	997	6972			997	7930		
956	35665	999	6549						
958	38320								
997	8689								

Table S9. The list of *m/z* values and corresponding intensities for detected signals in chloroform fraction of B & D extract of *Escherichia coli* collected with NALDI-MS

rep 1		rep 2		rep 3		rep 4		rep 5	
m/z	Intensity	*m/z*	Intensity	*m/z*	Intensity	*m/z*	Intensity	*m/z*	Intensity
437	20902	405	7428	405	5603	405	5646	403	5399
439	18634	409	9589	425	6981	437	27078	405	6173
465	20706	425	8878	437	29361	439	22976	425	5536
467	18168	437	39529	439	27902	465	23280	437	30394
563	22613	439	34406	444	5438	467	20886	439	28020
591	6221	465	35304	465	28273	563	21997	465	29316
669	6900	467	33374	467	28215	591	5265	467	24572
671	6830	538	7926	495	5533	669	8302	549	4945
685	6604	549	7665	563	24677	671	7959	563	24667
726	7662	563	41509	591	7780	726	5880	591	8508
728	5307	591	12373	669	10871	728	5432	655	5050
742	39200	669	17315	671	8144	742	25028	669	9464
763	21403	671	15503	685	10150	763	15194	671	7846
768	8138	685	20049	701	8178	768	9874	685	6963
770	10767	701	16841	706	6906	769	5723	701	6332
772	4570	706	12533	726	11115	770	9553	726	7080

779	15000	726	21328	728	10080	779	11999	728	6574
791	6033	728	15975	742	55196	791	4879	742	41768
807	4879	742	87468	763	35862	832	7636	763	28984
832	8623	744	9570	768	11354	834	9657	768	8825
834	11160	763	66641	769	13591			769	10069
847	5575	765	12227	770	12865			770	9006
849	4773	768	13240	777	6641			777	5056
		770	24112	779	28476			779	24923
		772	9876	791	9148			791	6883
		775	11610	793	6852			793	6751
		777	14854	807	8383			807	6513
		779	48884	832	13846			832	10473
		791	20629	834	17472			833	4562
		794	9285	847	7037			834	11216
		803	9062	849	7843			847	6382
		807	15121					849	4807
		810	10150						
		832	11976						
		834	16669						
		847	13883						
		849	12294						

Table S10. The list of *m/z* values and corresponding intensities for detected signals in methanol fraction of B & D extract of *Morganella morganii* collected with NALDI-MS

rep 1		rep 2		rep 3		rep 4		rep 5	
m/z	Intensity	*m/z*	Intensity	*m/z*	Intensity	*m/z*	Intensity	*m/z*	Intensity
409	35907	409	19983	409	54679	409	60802	409	51714
425	24723	425	21636	425	35760	425	57328	425	46491
437	12147	437	8928	437	15463	437	17701	437	18175
439	9919	439	6205	439	12724	439	16219	439	15946
465	12316	465	9226	465	18678	465	21616	465	16216
467	9820	467	8457	467	14414	467	17914	467	16483
493	15867	493	9084	493	25399	493	25281	493	22667
495	15687	495	7821	495	23442	495	26891	495	23232
764	7221	711	2898	708	7753	690	6203	674	6402
780	3712	764	4163	764	6727	708	7028	690	6718
		779	3061	780	5899	764	13184	764	12203
		795	2998	795	8277	779	7689	779	5133
				811	5849	795	10835	780	6703
						911	5987	795	8352
								811	5887

Table S11. The list of *m/z* values and corresponding intensities for detected signals in methanol fraction of B & D extract of *Staphylococcus warneri* collected with NALDI-MS

rep 1	rep 2	rep 3	rep 4	rep 5

m/z	Intensity	*m/z*	Intensity	*m/z*	Intensity	*m/z*	Intensity	*m/z*	Intensity
409	51409	409	78883	409	53079	409	88017	409	74160
425	28831	425	44236	425	35921	425	52326	425	40805
465	8007	493	20103	437	7243	465	10245	437	9286
493	21171	495	17342	439	6746	467	9094	465	11758
495	19377	661	11804	465	9006	493	24039	467	11887
510	6694	689	8378	467	8940	495	23870	492	29864
512	8002	739	16392	493	19412	510	7637	494	26744
661	8877	745	11909	495	20419	605	8076	510	8339
689	6540	753	5275	605	5173	633	12111	512	6729
717	6484	755	14426	633	5786	661	27211	633	6788
739	7580	761	11855	661	15023	677	10770	661	14776
745	5334	767	40865	675	4556	689	19397	675	5301
755	5550	769	6475	677	5372	690	6444	689	10741
761	5788	781	5193	689	9942	705	6887	708	5500
767	17703	783	34634	705	4749	717	14043	710	5401
773	4476	797	5195	708	4666	733	7398	717	8352
783	12453	799	9421	717	8611	739	13159	733	7554
915	12328	887	5424	739	8643	745	9486	739	13167
931	4323	915	36287	745	7013	747	5540	745	10583
999	3089	929	7213	755	7364	755	10980	755	10883
		931	12884	761	10259	761	15222	761	13059
		943	5341	767	23266	767	37088	767	28749
				773	4199	773	7802	769	4724
				783	17715	781	5450	773	5822
				799	4742	783	29710	783	20188
				887	3774	799	9299	799	6230
				915	22743	829	4630	887	5714
				929	4028	887	6570	915	27506
				931	8712	915	35863	929	3966
				943	3114	929	7425	931	9941
				999	3509	931	17447	999	4222
				1001	3771	943	6541	1001	4216
						999	4765		

Table S12. The list of *m/z* values and corresponding intensities for detected signals in methanol fraction of B & D extract of *Lactobacillus plantarum* collected with NALDI-MS

rep 1		rep 2		rep 3		rep 4		rep 5	
m/z	Intensity	*m/z*	Intensity	*m/z*	Intensity	*m/z*	Intensity	*m/z*	Intensity
409	106503	409	135851	409	73048	409	110951	409	136141
425	93073	425	126604	425	61014	425	105792	425	128261
493	33447	437	13060	492	19413	437	7636	492	41386
494	33664	439	12015	494	17865	444	8643	494	44776
527	167557	444	13828	527	200188	446	7648	527	199068
610	14065	446	14302	610	16989	465	11386	610	19456
612	11696	465	20450	612	15173	467	7629	612	18746

696	7952	467	17999	690	7595	492	54285	708	9900
710	7509	492	42058	696	8871	494	50467	710	8769
712	7555	494	40265	712	10840	527	107136	712	6903
764	19559	527	154273	748	7727	610	13223	734	7395
780	8944	610	14315	764	10219	612	10330	742	10957
887	7430	612	13187	780	6178	708	12182	764	33909
913	9395	675	10108	941	4948	710	9532	780	14713
927	4213	691	8184			726	4980	795	6238
939	5066	708	10890			742	7392	887	9096
941	11798	724	7510			764	22093	913	14273
955	4333	734	9147			780	10522	915	5564
		742	14501			885	3911	927	4947
		764	37789			887	8325	929	5669
		780	16943			913	10834	939	11466
		885	7371			939	6483	941	23439
		887	14064			941	14687	955	7215
		903	9110			955	5183	957	9658
		913	20275			957	7025		
		915	7910			1027	3443		
		927	7088						
		929	8362						
		939	13887						
		941	25671						
		957	11396						

Table S13. The list of *m/z* values and corresponding intensities for detected signals in methanol fraction of B & D extract of *Enterococcus faecium* collected with NALDI-MS

rep 1		rep 2		rep 3		rep 4		rep 5	
m/z	Intensity	*m/z*	Intensity	*m/z*	Intensity	*m/z*	Intensity	*m/z*	Intensity
457	10271	444	6975	437	46874	437	31195	437	33735
527	14219	468	7633	444	116545	444	26543	441	13513
712	5029	685	5170	446	114185	446	23627	444	44497
		696	5288	453	39281	453	19006	446	39277
		941	7341	521	11902	527	20929	453	31434
				527	16115	696	13522	457	12337
				660	13943	712	10874	527	26273
				662	13445			712	5731
				712	8047				
				823	6038				
				913	5684				
				941	11113				
				955	4448				
				1133	3841				
				1199	4320				

Table S14. The list of *m/z* values and corresponding intensities for detected signals in methanol fraction of B & D extract of *Enterococcus durans* collected with NALDI-MS

rep 1		rep 2		rep 3		rep 4		rep 5	
m/z	Intensity	*m/z*	Intensity	*m/z*	Intensity	*m/z*	Intensity	*m/z*	Intensity
409	8294	409	6281	409	10595	409	9414	409	9083
437	7574	437	15237	437	16283	437	16620	437	22544
465	7825	439	12087	439	15418	439	12626	439	19240
467	7380	465	16513	465	18776	465	16259	465	22999
663	8475	467	14806	467	15982	467	17996	467	20035
679	6814	468	5684	663	8471	468	9971	468	5116
685	8037	470	5910	679	4438	470	8333	675	4161
696	6944	663	4602	685	7055	527	7169	680	3913
701	8288	682	3908	696	4403	663	8812	685	4916
940	3566	685	5040	701	5194	679	5692	912	1917
		696	4879	746	4560	685	8435	940	3765
		701	3870	940	3956	701	5914		
		940	2537						

Table S15. The list of *m/z* values and corresponding intensities for detected signals in methanol fraction of B & D extract of *Lactococcus garvieae* collected with NALDI-MS

rep 1		rep 2		rep 3		rep 4		rep 5	
m/z	Intensity	*m/z*	Intensity	*m/z*	Intensity	*m/z*	Intensity	*m/z*	Intensity
437	59208	437	58460	437	6709	437	6932	409	8508
439	56092	439	55040	441	6789	439	6116	437	13200
465	48531	465	60752	527	10075	441	7239	439	11419
467	42619	467	54359	711	4453	457	7133	441	8751
468	9762	591	11356			527	10252	457	11460
527	16824	619	10443					465	9949
652	11344	685	10839					467	7735
680	8242	711	9206					527	10045
685	7009	886	12693						
768	6411	902	5412						
770	7008	912	7681						
902	3592	914	10142						
912	3595	926	7907						
940	9124	930	4190						
954	4797	940	20422						
956	3678	954	12638						
		956	8739						
		980	4218						

Table S16. The list of *m/z* values and corresponding intensities for detected signals in methanol fraction of B & D extract of *Staphylococcus epidermidis* collected with NALDI-MS

rep 1		rep 2		rep 3		rep 4		rep 5	
m/z	Intensity	*m/z*	Intensity	*m/z*	Intensity	*m/z*	Intensity	*m/z*	Intensity
437	32871	437	18819	437	32862	409	11056	409	19538
439	32627	439	15449	439	27315	437	107283	437	30864
465	37040	465	22562	465	36662	439	98788	439	29028
467	32055	467	18296	467	30061	446	9818	465	31370
682	4829	696	7218	574	8325	465	118675	467	30841
766	3613	714	6709	696	6258	467	118022	483	23516
		766	6776	714	6283	468	10541	497	21431
				766	5919	470	8931	499	20348
						497	13874	574	23110
						499	13603	590	14945
						510	13368	674	11406
						512	12057	692	15991
						654	16658	695	17514
						675	6758	711	11586
						678	10100	714	21247
						680	22602		
						682	20760		
						684	8273		
						766	14259		
						780	5900		
						782	8584		
						796	4132		
						914	6021		

Table S17. The list of *m/z* values and corresponding intensities for detected signals in methanol fraction of B & D extract of *Escherichia coli* collected with NALDI-MS

rep 1		rep 2		rep 3		rep 4		rep 5	
m/z	Intensity	*m/z*	Intensity	*m/z*	Intensity	*m/z*	Intensity	*m/z*	Intensity
404	20233	404	18550	404	20465	404	25221	404	24673
409	13787	409	13004	409	14996	409	17244	409	16682
437	64254	437	58447	437	51238	437	41357	437	47888
439	61676	439	50801	439	48164	439	35642	439	41877
465	71448	465	58174	465	58535	465	45660	465	54192
467	68722	467	52722	467	49930	467	39730	467	50249
487	12844	487	11445	654	9944	682	9531	680	10209
654	11429	654	9597	680	13160	696	10500	682	8969
680	15084	680	14225	682	12904	711	9913	696	10714
682	14507	682	12488	711	6841	763	15683	711	9636
711	8208	763	14135	763	16382	764	10416	763	12874
763	8022	764	8509	778	24609	778	28254	764	8899
764	7272	772	5831	780	10462	780	11704	778	22547
778	20175	778	26505	792	8118	792	10674	780	11381

780	7675	780	10802	794	28813	794	35108	791	7123
794	19792	792	7129	806	6615	806	7537	794	29765
808	6402	794	26832	808	5935	808	9052	806	6574
810	7764	806	6729	810	9558	810	11169	808	7627
822	6916	810	7645	822	7582	822	12310	810	9544
		822	7226					822	9064

Table S18. Comparison of the extraction performance of PPY@ZIF-8 and CAR/PDMS SPME fibers for standard mixture of VOCs by HS-SPME-GC-FID analysis

	PPy@ZIF-8			75 μm CAR/PDMS		
Compound	Intensity (a. u.)	SD	RSD, %	Intensity (a. u.)	SD	RSD, %
Methanol	1406.93	127.60	9.07	49.47	1.10	2.22
Benzene	93.17	10.10	10.84	185.93	10.24	5.51
Toluene	156.40	7.63	4.88	413.87	3.18	0.77
Ethylbenzene	262.23	9.94	3.79	576.17	38.32	6.65
p-xylene	434.30	17.82	4.10	589.23	8.04	1.36
BFB	377.13	28.15	7.46	1393.90	25.91	1.86
Phenol	224.40	12.40	5.53	69.63	2.80	4.02
Dodecane	1431.17	145.93	10.20	42.20	2.07	4.90

5. Conclusion and final remarks

The main aim of the presented research was to fabricate innovative analytical devices for the analysis of volatile and non-volatile low-molecular-weight compounds. After fabricating innovative analytical devices and characterizing them, this study investigated their potential for analyzing low-molecular-weight compounds and their complementary application in bacterial strain metabolic profiling.

The results of presented research can be summarized via the following points:

5.1. The results of modification of polypyrrole with the metal-organic framework (MOF) ZIF-8 demonstrated significantly enhanced extraction performance for selected volatile organic compounds (VOCs). Sensitivity has shown to be higher for fabricated PPy@ZIF-8 fiber as compared to pure polypyrrole coating, ranging from 5 to 16 times. Utilization of the newly fabricated PPy@ZIF-8 fiber with the film thickness ranging from 65 to 72 µm facilitated the extraction and identification of over 100 VOCs emitted by three species of bacteria (*Hafnia alvei*, *Proteus mirabilis*, and *Enterococcus faecalis*);

5.2. Anisotropic gold nanostars showed sensitivity towards low-molecular-weight compounds, such as adonitol and lipids at the nanomolar level (*lyso*-phosphatidylethanolamine, phosphatidylcholine, and *lyso*-phosphatidylinositol). The results showed a bright perspective for the future utilization of gold nanostars as an inorganic matrix for LDI-MS analysis of low molecular weight compounds;

5.3. Variation in the mass of (from 2.5 to 100 mg) $[Ag_5(O_2CC_2F_5)_5(H_2O)_3]$ used in chemical vapor deposition processes as precursor, yielded variations in the size and morphology of deposited silver nanostructures and subsequently, tunable LDI-MS efficiency for low molecular weight compounds. Fabricated LDI-MS substrates (stainless steel plates, surface modified with silver nanograins) showed enhanced sensitivity towards biologically active compounds, including lipids (at nano- and picomolar levels), in both ion-negative and positive modes;

5.4. The differences in the non-volatile profiles collected by silver nanostructures assisted LDI-MS substrates fabricated with the utilization of 5 mg of $[Ag_5(O_2CC_2F_5)_5(H_2O)_3]$ as a CVD precursor resulting in the deposition of silver grains with size 50 ± 10 nm were sufficiently enough for the differentiation between eight bacterial species. The differences in volatile profiles collected by PPy@ZIF-8 fiber with the film thickness ranging from 65 to 72 µm showed clear differentiation between Gram-positive (G+) and Gram-negative (G−) species. The

correlation between volatile and non-volatile profiles has also been observed. The obtained results potentially indicate on perspectives for utilization of fabricated devices as complementary, offering insights into bacterial metabolism and differentiation of bacterial species.

6. References

[1] https://www.nature.com/subjects/small-molecules, (n.d.).

[2] Council Directive 1999/13/EC of 11 March 1999 on the limitation of emissions of volatile organic compounds due to the use of organic solvents in certain activities and installations, 1999.

[3] S. Qiu, Y. Cai, H. Yao, C. Lin, Y. Xie, S. Tang, A. Zhang, Small molecule metabolites: discovery of biomarkers and therapeutic targets, Signal Transduct. Target. Ther. 8 (2023) 1–37. https://doi.org/10.1038/s41392-023-01399-3.

[4] M.W.Y. Southey, M. Brunavs, Introduction to small molecule drug discovery and preclinical development, Front. Drug Discov. 3 (2023) 1–8. https://doi.org/10.3389/fddsv.2023.1314077.

[5] Z. Ling, J. Yang, Y. Zhang, D. Zeng, Y. Wang, Y. Tian, H. Wang, Z. Xu, Y. Sun, Y. Shen, Applications of advanced materials in the pretreatment and rapid detection of small molecules in foods: A review, Trends Food Sci. Technol. 141 (2023) 104175. https://doi.org/10.1016/j.tifs.2023.104175.

[6] G.L. Yang, X.L. Jiang, H. Xu, B. Zhao, Applications of MOFs as Luminescent Sensors for Environmental Pollutants, Small. 17 (2021) 1–19. https://doi.org/10.1002/smll.202005327.

[7] G.G. Guilbault, M. Hjelm, Nomenclature for automated and mechanised analysis, Pure Appl. Chem. 61 (1989) 1657–1664.

[8] L. Liu, Z. Wang, Q. Zhang, Y. Mei, L. Li, H. Liu, Z. Wang, L. Yang, Ion Mobility Mass Spectrometry for the Separation and Characterization of Small Molecules, Anal. Chem. 95 (2023) 134–151. https://doi.org/10.1021/acs.analchem.2c02866.

[9] C.L. Arthur, J. Pawliszyn, Solid Phase Microextraction with Thermal Desorption Using Fused Silica Optical Fibers, Anal. Chem. 62 (1990) 2145–2148. https://doi.org/10.1021/ac00218a019.

[10] R.E. Shirey, SPME Commercial Devices and Fibre Coatings, Elsevier Inc., 2012. https://doi.org/10.1016/B978-0-12-416017-0.00004-8.

[11] M. Lashgari, Y. Yamini, An overview of the most common lab-made coating materials

in solid phase microextraction, Talanta. 191 (2019) 283–306. https://doi.org/10.1016/j.talanta.2018.08.077.

[12] K. Khodarahmian, A. Ghiasvand, A. Barkhordari, Exploring the optimal electropolymerization strategy for the preparation of solid-phase microextraction fibers using pyrrole-dopamine copolymers, J. Chromatogr. A. 1714 (2024) 464562. https://doi.org/10.1016/J.CHROMA.2023.464562.

[13] R. Mametov, G. Sagandykova, F. Monedeiro, B. Buszewski, Development of controlled film of polypyrrole for solid-phase microextraction fiber by electropolymerization, Talanta. 232 (2021). https://doi.org/10.1016/j.talanta.2021.122394.

[14] A. Omarova, N. Baimatova, H. Kazemian, MOF-199-based coatings as SPME fiber for measurement of volatile organic compounds in air samples: Optimization of in situ deposition parameters, Microchem. J. 185 (2023) 108263. https://doi.org/10.1016/J.MICROC.2022.108263.

[15] H. Javanmardi, M. Doosti, A. Abbasi, H. Bagheri, Synthesis and modification of MIL-101-NH2-based metal organic frameworks for preparation of SPME fibers using sol-gel methodology, Adv. Sample Prep. 7 (2023) 100075. https://doi.org/10.1016/J.SAMPRE.2023.100075.

[16] L.E.S. Nascimento, B. Thapa, W. da S. Oliveira, P.R. Rodrigues, H.T. Godoy, J.L. Anderson, Multivariate optimization for extraction of 2-methylimidazole and 4-methylimidazole from açaí-based food products using polymeric ionic liquid-based sorbent coatings in solid-phase microextraction coupled to gas chromatography–mass spectrometry, Food Chem. 444 (2024) 138593. https://doi.org/10.1016/J.FOODCHEM.2024.138593.

[17] W.A. Khan, M.B. Arain, M. Soylak, Nanomaterials-based solid phase extraction and solid phase microextraction for heavy metals food toxicity, Food Chem. Toxicol. 145 (2020) 111704. https://doi.org/10.1016/J.FCT.2020.111704.

[18] K. Tanaka, H. Waki, Y. Ido, S. Akita, Y. Yoshida, T. Yoshida, Protein and polymer analyses up to m/z 100 000 by laser ionization time-of-flight mass spectrometry, Rapid Commun. Mass Spectrom. 2 (1988) 151–153. https://doi.org/10.1002/rcm.1290020802.

[19] F. Fournelle, N. Lauzon, E. Yang, P. Chaurand, Metal-assisted laser desorption ionization imaging mass spectrometry for biological and forensic applications, Microchem. J. 185 (2023) 108294. https://doi.org/10.1016/J.MICROC.2022.108294.

[20] L. Chen, J. Ou, H. Wang, Z. Liu, M. Ye, H. Zou, Tailor-Made Stable Zr(IV)-Based Metal-Organic Frameworks for Laser Desorption/Ionization Mass Spectrometry Analysis of Small Molecules and Simultaneous Enrichment of Phosphopeptides, ACS Appl. Mater. Interfaces. 8 (2016) 20292–20300. https://doi.org/10.1021/acsami.6b06225.

[21] E. Maślak, A. Arendowski, M. Złoch, J. Walczak-Skierska, A. Radtke, P. Piszczek, P. Pomastowski, Silver Nanoparticle Targets Fabricated Using Chemical Vapor Deposition Method for Differentiation of Bacteria Based on Lipidomic Profiles in Laser Desorption/Ionization Mass Spectrometry, Antibiotics. 12 (2023). https://doi.org/10.3390/antibiotics12050874.

[22] G. Sagandykova, O. Pryshchepa, K. Rafińska, R. Mametov, P. Madajski, P. Pomastowski, LDI-MS performance of gold nanostars as an inorganic matrix for low molecular weight analytes, Int. J. Mass Spectrom. 478 (2022) 116872. https://doi.org/10.1016/J.IJMS.2022.116872.

[23] J. Sunner, E. Dratz, Y.C. Chen, Graphite Surface-Assisted Laser Desorption/Ionization Time-of-Flight Mass Spectrometry of Peptides and Proteins from Liquid Solutions, Anal. Chem. 67 (1995) 4335–4342. https://doi.org/10.1021/ac00119a021.

[24] Q. Zhang, H. Zou, Q. Zhang, Z. Guo, H. Jiang, J. Ni, X. Chen, Desorption/ionization mass spectrometry on porous silicon, Fenxi Huaxue. 29 (2001) 1368–1369.

[25] K.K. Murray, R.K. Boyd, M.N. Eberlin, G.J. Langley, L. Li, Y. Naito, Definitions of Terms Related to Mass Spectrometry (IUPAC Recommendations 2013), Pure Appl. Chem. 85 (2013) 1515–1609. https://doi.org/10.1515/ci.2004.26.3.23a.

[26] W.H. Müller, A. Verdin, E. De Pauw, C. Malherbe, G. Eppe, Surface-assisted laser desorption/ionization mass spectrometry imaging: A review, Mass Spectrom. Rev. 41 (2022) 373–420. https://doi.org/10.1002/mas.21670.

[27] J. Kratochvíl, V. Prysiazhnyi, F. Dyčka, O. Kylián, P. Kúš, P. Sezemský, J. Štěrba, V. Straňák, Gas aggregated Ag nanoparticles as the inorganic matrix for laser

desorption/ionization mass spectrometry, Appl. Surf. Sci. 541 (2021) 148469. https://doi.org/10.1016/J.APSUSC.2020.148469.

[28] S. Owega, E.P.C. Lai, A.D.O. Bawagan, etry, Anal. Chem. 70 (1998) 2360–2365. https://doi.org/10.1021/ac971166u.

[29] H. Bagheri, Z. Ayazi, M. Naderi, Conductive polymer-based microextraction methods: A review, Anal. Chim. Acta. 767 (2013) 1–13. https://doi.org/10.1016/j.aca.2012.12.013.

[30] S. Sadki, P. Schottland, N. Brodie, G. Sabouraud, The mechanisms of pyrrole electropolymerization, Chem. Soc. Rev. 29 (2000) 283–293. https://doi.org/10.1039/a807124a.

[31] M. Yaghi, O. M.; Li, Hailian; Eddaoudi, Mohamed; O'Keeffe, Design and synthesis of an exceptionally stable and highly, Nature. 402 (1999) 276–279.

[32] P. Rocío-Bautista, I. Pacheco-Fernández, J. Pasán, V. Pino, Are metal-organic frameworks able to provide a new generation of solid-phase microextraction coatings? – A review, Anal. Chim. Acta. 939 (2016) 26–41. https://doi.org/10.1016/J.ACA.2016.07.047.

[33] S.R. Hosseini, M. Omidkhah, Z. Mehri Lighvan, S. Norouzbahari, A. Ghadimi, Synthesis, characterization, and gas adsorption performance of an efficient hierarchical ZIF-11@ZIF-8 core–shell metal–organic framework (MOF), Sep. Purif. Technol. 307 (2023) 122679. https://doi.org/10.1016/J.SEPPUR.2022.122679.

[34] A. Arendowski, K. Ossoliński, A. Ossolińska, T. Ossoliński, J. Nizioł, T. Ruman, Serum and urine analysis with gold nanoparticle-assisted laser desorption/ionization mass spectrometry for renal cell carcinoma metabolic biomarkers discovery, Adv. Med. Sci. 66 (2021) 326–335. https://doi.org/10.1016/j.advms.2021.07.003.

[35] L. Huang, J. Wan, X. Wei, Y. Liu, J. Huang, X. Sun, R. Zhang, D.D. Gurav, V. Vedarethinam, Y. Li, R. Chen, K. Qian, Plasmonic silver nanoshells for drug and metabolite detection, Nat. Commun. 8 (2017). https://doi.org/10.1038/s41467-017-00220-4.

[36] H. Su, X. Li, L. Huang, J. Cao, M. Zhang, V. Vedarethinam, W. Di, Z. Hu, K. Qian,

Plasmonic Alloys Reveal a Distinct Metabolic Phenotype of Early Gastric Cancer, Adv. Mater. 33 (2021) 2007978. https://doi.org/10.1002/adma.202007978.

[37] M.O. Amin, M. Madkour, E. Al-Hetlani, Metal oxide nanoparticles for latent fingerprint visualization and analysis of small drug molecules using surface-assisted laser desorption/ionization mass spectrometry, Anal. Bioanal. Chem. 410 (2018) 4815–4827. https://doi.org/10.1007/s00216-018-1119-2.

[38] Y.T. Lai, K. Kandasamy, Y.C. Chen, Magnetic Graphene Oxide-Based Affinity Surface-Assisted Laser Desorption/Ionization Mass Spectrometry for Screening of Aflatoxin B1 from Complex Samples, Anal. Chem. 93 (2021) 7310–7316. https://doi.org/10.1021/acs.analchem.1c00878.

[39] H. Zhang, L. Zhao, J. Jiang, J. Zheng, L. Yang, Y. Li, J. Zhou, T. Liu, J. Xu, W. Lou, W. Yang, L. Tan, W. Liu, Y. Yu, M. Ji, Y. Xu, Y. Lu, X. Li, Z. Liu, R. Tian, C. Hu, S. Zhang, Q. Hu, Y. Deng, H. Ying, S. Zhong, X. Zhang, Y. Wang, H. Wang, J. Bai, X. Li, X. Duan, Multiplexed nanomaterial-assisted laser desorption/ionization for pan-cancer diagnosis and classification, Nat. Commun. 13 (2022) 1–11. https://doi.org/10.1038/s41467-021-26642-9.

[40] X. Li, X. Chen, J. Tan, X. Liang, J. Wu, Palladium modified porous silicon as multi-functional MALDI chip for serum peptide detection, Analyst. 142 (2017) 586–590. https://doi.org/10.1039/c6an02165d.

[41] C. Pei, C. Liu, Y. Wang, D. Cheng, R. Li, W. Shu, C. Zhang, W. Hu, A. Jin, Y. Yang, J. Wan, FeOOH@Metal–Organic Framework Core–Satellite Nanocomposites for the Serum Metabolic Fingerprinting of Gynecological Cancers, Angew. Chemie - Int. Ed. 59 (2020) 10831–10835. https://doi.org/10.1002/anie.202001135.

[42] K. Shibamoto, K. Sakata, K. Nagoshi, T. Korenaga, Laser Desorption Ionization Mass Spectrometry by Using Surface Plasmon Excitation on Gold Nanoparticle, J. Phys. Chem. C. 113 (2009) 17774–17779. https://doi.org/10.1021/jp9020432.

[43] G. Paramasivam, N. Kayambu, A.M. Rabel, A.K. Sundramoorthy, A. Sundaramurthy, Anisotropic noble metal nanoparticles: Synthesis, surface functionalization and applications in biosensing, bioimaging, drug delivery and theranostics, Acta Biomater. 49 (2017) 45–65. https://doi.org/10.1016/J.ACTBIO.2016.11.066.

[44] H. Wang, D.W. Brandl, P. Nordlander, N.J. Halas, Plasmonic Nanostructures: Artificial Molecules, Acc. Chem. Res. 40 (2007) 53–62. https://doi.org/10.1021/ar0401045.

[45] D. Dufour-Rainfray, M. Lambérioux, P. Boulard, M. Guidotti, J.B. Delaye, M.J. Ribeiro, A.S. Gauchez, A.C. Balageas, P. Emond, A. Agin, Metabolomics – an overview. From basic principles to potential biomarkers (part 2), Médecine Nucléaire. 44 (2020) 158–163. https://doi.org/10.1016/J.MEDNUC.2020.02.004.

[46] J. Walczak-Skierska, M. Złoch, K. Pauter, P. Pomastowski, B. Buszewski, Lipidomic analysis of lactic acid bacteria strains by matrix-assisted laser desorption/ionization time-of-flight mass spectrometry, J. Dairy Sci. 103 (2020) 11062–11078. https://doi.org/10.3168/JDS.2020-18753.

[47] K.A. Jurgen Schiller, Rosmarie Suss, Beate Fuchs, Matthias Muller, Olaf Zschornig, MALDI-TOF MS in lipidomics, Front. Biosci. 12 (2007) 2568–2579.

[48] B. Fuchs, J. Schiller, MALDI-TOF MS analysis of lipids from cells, tissues and body fluids, in: Subcell. Biochem., 2008: pp. 541–565. https://doi.org/10.1007/978-1-4020-8831-5_21.

[49] C. Breil, M. Abert Vian, T. Zemb, W. Kunz, F. Chemat, “Bligh and Dyer” and Folch methods for solid–liquid–liquid extraction of lipids from microorganisms. Comprehension of solvatation mechanisms and towards substitution with alternative solvents, Int. J. Mol. Sci. 18 (2017) 1–21. https://doi.org/10.3390/ijms18040708.

[50] M. Milanowski, F. Monedeiro, M. Złoch, I.A. Ratiu, P. Pomastowski, T. Ligor, B.S. De Martinis, B. Buszewski, Profiling of VOCs released from different salivary bacteria treated with non-lethal concentrations of silver nitrate, Anal. Biochem. 578 (2019) 36–44. https://doi.org/10.1016/j.ab.2019.05.007.

[51] K. Żuchowska, W. Filipiak, Modern approaches for detection of volatile organic compounds in metabolic studies focusing on pathogenic bacteria: Current state of the art, J. Pharm. Anal. (2023). https://doi.org/10.1016/J.JPHA.2023.11.005.

[52] K. Song, Q. Cheng, Desorption and ionization mechanisms and signal enhancement in surface assisted laser desorption ionization mass spectrometry (SALDI-MS), Appl. Spectrosc. Rev. 55 (2020) 220–242.https://doi.org/10.1080/05704928.2019.1570519.

7. Abstract

Low-molecular-weight (LMW) compounds play crucial roles in numerous biological, chemical, and environmental processes. Given the diverse roles and significance of LMW compounds, the development of innovative analytical techniques for their analysis is imperative. In this thesis, we present novel approaches for the analysis of LMW compounds, focusing on the fabrication of advanced analytical devices to meet the evolving needs of various scientific disciplines.

The primary objective of the research was to fabricate novel analytical devices and explore their capabilities in the analysis of volatile and non-volatile LMW compounds.

Innovative solid-phase microextraction (SPME) fibers were synthesized by modification of polypyrrole coating material with metal-organic frameworks (MOFs), specifically ZIF-8, enhancing their extraction performance for volatile organic compounds (VOCs).

For the analysis of non-volatile compounds, two types of LDI-MS targets were fabricated: gold nanostars as inorganic matrix and silver nanostructured substrates. Gold nanostars were synthesized using seed-mediated approach and characterized using XRD, DLS, SEM and TEM, UV-VIS spectroscopy, ICP-MS. At the same time, silver nanostructured substrates were synthesized using chemical vapor deposition. The effect of mass of silver precursor on particles morphology, size and distribution, and LDI-MS performance was investigated. Both LDI-MS targets demonstrated promising sensitivity towards LMW compounds, including lipids.

The potential of devices for differentiation of bacterial species has been investigated on eight bacterial strains such as *Morganella morganii* (MM), *Staphylococcus warneri* (SW), *Lactobacillus plantarum* (LP), *Enterococcus faecium* (EF), *Enterococcus durans* (ED), *Lactococcus garvieae* (LG), *Staphylococcus epidermidis* (SE), and *Escherichia coli* (EC). Statistical methods of data processing included principal component analysis, hierarchical cluster analysis, random forest model, and canonical correlation analysis. The results of the research indicated on potential of lab-made innovative devices for differentiation between bacterial strains.

Developed analytical devices demonstrated significant potential for analysis of LMW compounds and subsequent applications in various fields, including analytical chemistry, forensic sciences, food manufacturing, and environmental monitoring, offering cost-efficient alternatives to commercially available analogs.

8. Streszczenie

Związki o niskiej masie cząsteczkowej odgrywają kluczową rolę w licznych procesach biologicznych, chemicznych i środowiskowych. Z uwagi na ich różnorodność i znaczenie niezbędny jest rozwój innowacyjnych technik analitycznych służących ich analizie. W niniejszej pracy przedstawiono nowatorskie podejście do analizy związków niskocząsteczkowych, koncentrując się na wytworzeniu nowych, zaawansowanych podłoży analitycznych do zastosowania w znanych procedurach analitycznych, wychodząc naprzeciw potrzebom różnych dyscyplin naukowych.

Głównym celem przeprowadzonych badań było skonstruowanie nowatorskich podłoży analitycznych i zbadanie ich możliwości w analizie lotnych i nielotnych związków niskocząsteczkowych. Pierwsze z nich, innowacyjne włókna mikroekstrakcyjne w fazie stałej (SPME), zostały zsyntetyzowane w procesie modyfikacji powłok polipirrolu za pomocą złożonych struktur metaloorganicznych (MOF), w szczególności ZIF-8. Wykazały one zdecydowanie wyższą wydajność ekstrakcji w stosunku do lotnych związków organicznych (VOC). Dla potrzeb analizy związków nielotnych skonstruowano dwa rodzaje podłoży LDI-MS: modyfikowane powierzchniowo nanogwieździstymi strukturami złota oraz sferycznymi nanostrukturami srebra. Nanogwiazdy złota zostały zsyntetyzowane przy użyciu metodologii seed-mediated approach i scharakteryzowane przy użyciu XRD, DLS, SEM, TEM, spektroskopii UV-VIS i ICP-MS. Nanostruktury srebra zostały zsyntetyzowane przy użyciu techniki chemicznego osadzania z fazy gazowej, wykorzystując perfluorowany karboksylan srebra(I) jako prekursor. Zbadano wpływ masy prekursora CVD na morfologię, rozmiar i rozkład cząstek srebra na wytwarzanych podłożach, a następnie na wydajność procesów LDI-MS. Obie matryce LDI-MS wykazały obiecującą czułość w stosunku do niskocząsteczkowych związków, w tym lipidów.

Możliwości aplikacyjne wytworzonych podłoży (innowacyjnych włókien mikroekstrakcyjnych SPME oraz zmodyfikowanych powierzchniowo nanostrukturalnie matryc do analiz LDI -MS) do różnicowania gatunków bakteryjnych zostały sprawdzone na ośmiu szczepach bakterii, takich jak *Morganella morganii* (MM), *Staphylococcus warneri* (SW), *Lactobacillus plantarum* (LP), *Enterococcus faecium* (EF), *Enterococcus durans* (ED), *Lactococcus garvieae* (LG), *Staphylococcus epidermidis* (SE) i *Escherichia coli* (EC). Wyniki badań, poparte metodami

statystycznego przetwarzania danych, wskazały na wysoki potencjał wytworzonych w ramach niniejszej pracy innowacyjnych podłoży, do różnicowania szczepów bakteryjnych.

Wytworzone podłoża analityczne, wykazały znaczące możliwości aplikacyjne w analizie związków niskocząsteczkowych, dając tym samym możliwość ich zastosowania w różnorodnych dziedzinach, takich jak chemia analityczna, medycyna sądowa, produkcja żywności i monitorowanie środowiska i oferując ekonomiczne alternatywy dla komercyjnie dostępnych analogów.

9. Academic achievements

Education

Bachelor of Engineering Sciences in Chemistry in Al-Farabi Kazakh National University (2011 – 2015)
Master of Engineering Sciences in Nanomaterials and Nanotechnologies in Al-Farabi Kazakh National University (2015 – 2017)

Publications

1. **Mametov R**., Sagandykova G., Monedeiro F., Buszewski B. Development of controlled film of polypyrrole for solid-phase microextraction fiber by electropolymerization, *Talanta* 232, 122394 (2021). IF = 6.1 MP = 140.

2. **Mametov R**., Ratiu I.A., Monedeiro F., Ligor T., Buszewski B. Evolution and Evaluation of GC columns, *Critical Reviews in Analytical Chemistry* 51(2), 150-173 (2019). IF = 6.535 MP = 100.

3. Ratiu I.A., **Mametov R**., Ligor T., Buszewski B. Micro-Chamber/Thermal Extractor (μ-CTE) as a new sampling system for VOCs emitted by feces, *Scientific Reports* 11(1), 18780 (2021). IF = 4.6 MP = 140.

4. Ratiu I.A., Railean-Plugaru V., Pomastowski P., Milanowski M., **Mametov R**., Bocos-Bintintan V., Buszewski B. Temporal influence of different antibiotics onto the inhibition of Escherichia coli bacterium grown in different media, *Analytical Biochemistry*, 585, 113407 (2019). IF = 2.219 MP = 100.

5. Sagandykova G., Pryshchepa O., Rafinska K., **Mametov R**., Madajski P., Pomastowski P. LDI-MS performance of gold nanostars as an inorganic matrix for low molecular weight analytes, *International Journal of Mass Spectrometry*, 478, 116872 (2022). IF = 1.934 MP = 70.

6. Arendowski A., Sagandykova G., **Mametov R**., Rafińska K., Pryshchepa O., Pomastowski P. Nanostructured Layer of Silver for Detection of Small Biomolecules in Surface-Assisted Laser Desorption Ionization Mass Spectrometry, *Materials (Basel).* 2022, 15(12), 4076. IF = 3.748 MP = 140.

7. Sagandykova G.; Piszczek P.; Radtke A.; **Mametov R**.; Pryshchepa O.; Gabryś D.; Kolankowski M.; Pomastowski P. Silver Nanostructured Substrates in LDI-MS of Low Molecular Weight Compounds. *Materials (Basel).* 2022, *15* (13). IF = 3.748 MP = 140.

8. **Mametov, R**.; Sagandykova, G.; Monedeiro-Milanowski, M.; Gabryś, D.; Pomastowski, P. Electropolymerized Polypyrrole-MOF Composite as a Coating Material for SPME Fiber for Extraction VOCs Liberated by Bacteria, *Scientific Reports.* 2023, *13* (1), 1–10. IF = 4.6 MP = 140.

9. **Mametov** R.; Sagandykova G.; Monedeiro F.; Florkiewicz A.; Piszczek P.; Radtke A. and Pomastowski P. Metabolic Profiling of Bacteria with the Application of Polypyrrole-MOF SPME fibers and Plasmonic Nanostructured LDI-MS Substrates, *Scientific Reports.* 2024, *14, 5562.* IF = 4.6 MP = 140.

Conferences

1. 11th Congress Societas Humboldtiana Polonorum "Science in the age of globalization", Szczecin, Poland, 12-15 September 2019, poster session 'Volatile organic compounds associated with colorectal cancer biomarkers'
2. 15th International Student conference 'Modern analytical chemistry', Prague, Czech Republic with oral presentation 'Evolution and evaluation of GC-columns', 19-20 September 2019
3. 7th Scientific Conference of Polish Metabolomics Society, Bialystok, Poland, with oral presentation 'Polypyrrole based coating materials for SPME fibers to be used in analysis of VOCs as potential colorectal cancer biomarkers', 4-6th November 2020
4. International Conference on Innovative and Smart Materials ICISM Krakow, Poland, oral presentation 'SALDI plate based on an electrodeposited layer of silver for mass spectrometric analysis of low molecular weight compounds' December 11-13, 2021
5. 26th International Symposium on Separation Sciences & 25th International Symposium for High-Performance Thin-Layer Chromatography, Oral presentation of young scientist session entitled: 'Polypyrrole – metal organic frameworks as a coating material for SPME fibers for extraction VOCs emitted by bacteria', 28th June - 1st July, 2022, Ljubljana, Slovenia

Projects

1. *Executor* of the project 'Synthesis of refractory powder materials from boric raw materials of the Republic of Kazakhstan' (2012-2015)
2. *Executor* of the project 'Development of scientific foundations of ceramic materials based on borides of transition metals in mode of solid flame combustion' (2015-2017)
3. *Executor* of the project 'Airborne Biomarkers for Colorectal Cancer', grant ERA-NET TRANSCAN/02/2018 (2018-2021)
4. *Principal investigator* of the Preludium project 'Development of selective coating materials based on conductive polymers for SPME fibers for analysis of VOCs as potential colorectal cancer biomarkers' funded by National Science Center, Poland (Nr. 2019/35/N/ST4/04363) (2020-2023)
5. *Executor* of the Preludium project 'Development of NALDI plates with application of chemically synthesized nanoparticles of metals and metal oxides for analysis of low molecular weight natural compounds' funded by National Science Center, Poland (2020-2021)
6. *Member* of Toruń Center of Excellence 'Towards Personalized Medicine' operating under Excellence Initiative-Research University (Torun, Poland) (2021-2023)

7. *Executor* of the project: ‘Establishment of a Research and Development Center and conducting research and development activities in the field of welding at EwiKor Construction Ltd.’ https://bioserv.pl/index.php/projekt-spawanie-hybrydowe/ (2022)

Patent applications

‘Sposób przygotowania podłoża ze stali nierdzewnej do elektroosadzania powłok PPy-MOF dla włókien SPME, roztwór do elektropolimeryzacji oraz sposób jego otrzymywania’, application number is **P.445714**.

Internships

1. *Internship* in laboratory ‘Ecology of Biosphere’ in Center of Physical Chemical Methods of Research and Analysis in the project: ‘Monitoring concentrations of organic pollutants in ambient air of Almaty (Kazakhstan) using GC-MS and SPME’ (2017-2018);
2. *Internship* in framework of TRANSCAN project in Fraunhofer Institute for Process Engineering and Packaging, department of Sensory Analytics and Technologies (Munich, Germany) under supervising of dr. *Jonathan Beauchamp* (April-May, 2019).

Prizes and awards

1. Award from Rector of Nicolaus Copernicus University for publication of research paper in *Scientific Reports* journal (2021) entitiled: ‘Micro-Chamber/Thermal Extractor (µ-CTE) as a new sampling system for VOCs emitted by feces’
2. Award from Rector of Nicolaus Copernicus University for publication of research paper in *Scientific Reports* journal (2023) entitiled: ‘Electropolymerized Polypyrrole-MOF Composite as a Coating Material for SPME Fiber for Extraction VOCs Liberated by Bacteria’

10. Statements

UNIWERSYTET
MIKOŁAJA KOPERNIKA
W TORUNIU
Interdyscyplinarne Centrum
Nowoczesnych Technologii

Toruń, 2024

PhD Gulyaim Sagandykova

Centre for Modern Interdisciplinary Technologies

Nicolaus Copernicus University in Toruń

Wileńska 4, Toruń, 87-100

STATEMENT

I hereby declare that, as co-author of the following publications:

1. Mametov, R.; **Sagandykova, G.**; Monedeiro-Milanowski, M.; Gabryś, D.; Pomastowski, P. "Electropolymerized Polypyrrole-MOF Composite as a Coating Material for SPME Fiber for Extraction VOCs Liberated by Bacteria". *Sci. Rep.* 2023, *13* (1), 1–10.

2. **Sagandykova G.**, Pryshchepa O., Rafinska K., Mametov R., Madajski P., Pomastowski P. "LDI-MS performance of gold nanostars as an inorganic matrix for low molecular weight analytes. *International Journal of Mass Spectrometry.* Volume 478, August 2022, 116872

3. **Sagandykova, G.**; Piszczek, P.; Radtke, A.; Mametov, R.; Pryshchepa, O.; Gabryś, D.; Kolankowski, M.; Pomastowski, P. Silver Nanostructured Substrates in LDI-MS of Low Molecular Weight Compounds. *Materials (Basel).* 2022, *15* (13).

4. Mametov, R.; **Sagandykova, G.;** Monedeiro, F.; Florkiewicz, A.; Piszczek, P.; Radtke, A.; Pomastowski, P. Metabolic Profiling of Bacteria with the Application of Polypyrrole-MOF SPME fibers and Plasmonic Nanostructured LDI-MS Substrates. *Scientific Reports.* (2024) 14:5562

Being a part of the doctoral dissertation of MSc Radik Mametov, I declare that my contribution was participation in conceptualization, data collection and interpretation, validation, visualization, writing of the original draft, review and editing in publications (1-4) and funding acquisition & project administration in publications (2) and (3).

15.04.2024

UNIWERSYTET
MIKOŁAJA KOPERNIKA
W TORUNIU
Interdyscyplinarne Centrum
Nowoczesnych Technologii

Toruń, 2024

Dr. hab. Katarzyna Rafinska Prof. NCU

Department of Environmental Chemistry and Bioanalysis

Faculty of chemistry

Nicolaus Copernicus University in Toruń

Gagarina 7, Toruń, 87-100

STATEMENT

I hereby declare that, as co-author of the following publications:

1. Sagandykova G., Pryshchepa O., **Rafinska K.**, Mametov R., Madajski P., Pomastowski P. "LDI-MS performance of gold nanostars as an inorganic matrix for low molecular weight analytes. *International Journal of Mass Spectrometry.* Volume 478, August 2022, 116872

Being a part of the doctoral dissertation of MSc Radik Mametov, I declare that my contribution was microscopic characterization of gold nanostars, participation in investigation, validation, and visualization.

15.04.2024 Katarzyna Rafinska

NICOLAUS COPERNICUS UNIVERSITY IN TORUŃ
Faculty of Chemistry

RESEARCH UNIVERSITY
EXCELLENCE INITIATIVE

Toruń, 15.04.2024

Dr. hab. Aleksandra Radtke, Prof. NCU
Department of Inorganic and Coordination Chemistry,
Faculty of Chemistry
Nicolaus Copernicus University in Toruń
Gagarina 7, Toruń, 87-100

STATEMENT

I hereby declare that, as co-author of the following publications:

1. Sagandykova, G.; Piszczek, P.; **Radtke, A.**; Mametov, R.; Pryshchepa, O.; Gabryś, D.; Kolankowski, M.; Pomastowski, P. Silver Nanostructured Substrates in LDI-MS of Low Molecular Weight Compounds. *Materials (Basel).* 2022, *15* (13)

2. Mametov, R.; Sagandykova, G.; Monedeiro, F.; Florkiewicz, A.; Piszczek, P.; **Radtke, A.;** Pomastowski, P. Metabolic Profiling of Bacteria with the Application of Polypyrrole-MOF SPME fibers and Plasmonic Nanostructured LDI-MS Substrates. *Scientific Reports.* (2024) 14:5562

Being a part of the doctoral dissertation of MSc Radik Mametov, I declare that my contribution was the synthesis of silver nanostructures for LDI-MS substrates and their characterization, writing of the part of the original draft, participation in the conceptualization, review & editing, co-supervising.

Aleksandra Radtke

NICOLAUS COPERNICUS UNIVERSITY IN TORUŃ Faculty of Chemistry
Gagarina Street 7, 87-100 Toruń, Poland, tel. +48 56 611 43 02, e-mail: wydzial@chem.umk.pl
chem.umk.pl/en

UNIWERSYTET
MIKOŁAJA KOPERNIKA
W TORUNIU
Interdyscyplinarne Centrum
Nowoczesnych Technologii

Toruń, 2024,04-11

Dr. hab. Pawel Pomastowski, Prof. NCU

Centre for Modern Interdisciplinary Technologies

Nicolaus Copernicus University in Toruń

Wileńska 4, Toruń, 87-100

STATEMENT

I hereby declare that, as co-author of the following publications:

1. Mametov, R.; Sagandykova, G.; Monedeiro-Milanowski, M.; Gabryś, D.; **Pomastowski, P.** Electropolymerized Polypyrrole-MOF Composite as a Coating Material for SPME Fiber for Extraction VOCs Liberated by Bacteria. *Scientific Reports.* 2023, *13* (1), 1–10
2. Sagandykova G., Pryshchepa O., Rafinska K., Mametov R., Madajski P., **Pomastowski P.** LDI-MS performance of gold nanostars as an inorganic matrix for low molecular weight analytes. *International Journal of Mass Spectrometry.* Volume 478, August 2022, 116872
3. Sagandykova, G.; Piszczek, P.; Radtke, A.; Mametov, R.; Pryshchepa, O.; Gabryś, D.; Kolankowski, M.; **Pomastowski, P.** Silver Nanostructured Substrates in LDI-MS of Low Molecular Weight Compounds. *Materials (Basel).* 2022, *15* (13)
4. Radik Mametov, Gulyaim Sagandykova, Fernanda Monedeiro, Aleksandra Florkiewicz, Piotr Piszczek, Aleksandra Radtke and **Pawel Pomastowski**. Metabolic Profiling of Bacteria with the Application of Polypyrrole-MOF SPME fibers and Plasmonic Nanostructured LDI-MS Substrates. *Scientific Reports.* (2024) 14:5562

Being a part of the doctoral dissertation of MSc Radik Mametov, I declare that my contribution was scientific supervising, reviewing of the original draft of publications, providing of the part of the resources for the study.

UNIWERSYTET
MIKOŁAJA KOPERNIKA
W TORUNIU
Wydział Chemii

UCZELNIA BADAWCZA
INICJATYWA DOSKONAŁOŚCI

Toruń, 2024

Dr. hab. Piotr Piszczek, Prof. NCU
Department of Inorganic and Coordination Chemistry,
Faculty of Chemistry
Nicolaus Copernicus University in Toruń
Gagarina 7, Toruń, 87-100

STATEMENT

I hereby declare that, as co-author of the following publications:

1. Sagandykova, G.; **Piszczek, P.**; Radtke, A.; Mametov, R.; Pryshchepa, O.; Gabryś, D.; Kolankowski, M.; Pomastowski, P. Silver Nanostructured Substrates in LDI-MS of Low Molecular Weight Compounds. *Materials (Basel).* 2022, *15* (13)

2. Mametov, R.; Sagandykova, G.; Monedeiro, F.; Florkiewicz, A.; **Piszczek, P.;** Radtke, A.; Pomastowski, P. Metabolic Profiling of Bacteria with the Application of Polypyrrole-MOF SPME fibers and Plasmonic Nanostructured LDI-MS Substrates. *Scientific Reports.* (2024) 14:5562

Being a part of the doctoral dissertation of MSc Radik Mametov, I declare that my contribution was synthesis of silver nanostructures for LDI-MS substrates analyses and their characterization, writing of the part of the original draft, participation in the review & editing, conceptualization, validation, visualization.

UNIWERSYTET MIKOŁAJA KOPERNIKA W TORUNIU Wydział Chemii
ul. Gagarina 7, 87-100 Toruń, Polska, tel. +48 56 611 43 02, e-mail: wydział@chem.umk.pl
chem.umk.pl

UNIWERSYTET
MIKOŁAJA KOPERNIKA
W TORUNIU
Interdyscyplinarne Centrum
Nowoczesnych Technologii

Toruń, 2024

PhD Oleksandra Pryshchepa

Centre for Modern Interdisciplinary Technologies

Nicolaus Copernicus University in Toruń

Wileńska 4, Toruń, 87-100

STATEMENT

I hereby declare that, as co-author of the following publications:

1. Sagandykova G., **Pryshchepa O.**, Rafinska K., Mametov R., Madajski P., Pomastowski P. "LDI-MS performance of gold nanostars as an inorganic matrix for low molecular weight analytes. *International Journal of Mass Spectrometry.* Volume 478, August 2022, 116872

2. Sagandykova, G.; Piszczek, P.; Radtke, A.; Mametov, R.; **Pryshchepa, O.**; Gabryś, D.; Kolankowski, M.; Pomastowski, P. Silver Nanostructured Substrates in LDI-MS of Low Molecular Weight Compounds. *Materials (Basel).* 2022, *15* (13).

Being a part of the doctoral dissertation of MSc Radik Mametov, I declare that my contribution was participation in investigation, characterization of gold nanostars by DLS, writing of the part of the original draft, participation in review & editing, conceptualization, visualization.

15.04.2024 O. Pryshchepa

Toruń, 2024

PhD Maciej Monedeiro-Milanowski

Centre for Modern Interdisciplinary Technologies

Nicolaus Copernicus University in Toruń

Wileńska 4, Toruń, 87-100

STATEMENT

I hereby declare that, as co-author of the following publications

1. Mametov, R.; Sagandykova, G.; **Monedeiro-Milanowski, M.**; Gabryś, D.; Pomastowski, P. "Electropolymerized Polypyrrole-MOF Composite as a Coating Material for SPME Fiber for Extraction VOCs Liberated by Bacteria". *Scientific Reports*. 2023, *13* (1), 1–10.

Being a part of the doctoral dissertation of MSc Radik Mametov, I declare that my contribution was isolation and identification of bacteria, participation in data analysis, review & editing of the manuscript, validation.

Maciej Monedeiro-Milanowski

Toruń, 2024

MSc Piotr Madajski

Department of Chemistry of Materials Adsorption and Catalysis

Faculty of chemistry

Nicolaus Copernicus University in Toruń

Gagarina 7, Toruń, 87-100

STATEMENT

I hereby declare that, as co-author of the following publications:

1. Sagandykova G., Pryshchepa O., Rafinska K., Mametov R., **Madajski P.**, Pomastowski P. "LDI-MS performance of gold nanostars as an inorganic matrix for low molecular weight analytes. *International Journal of Mass Spectrometry.* Volume 478, August 2022, 116872

   Being a part of the doctoral dissertation of MSc Radik Mametov, I declare that my contribution was analyses by microscopic techniques (SEM, TEM) and data interpretation.

Piotr Madajski

Gliwice, 15 April 2024

MD, PhD, MSc Dorota Gabryś, prof. NIO-PIB

Radiotherapy Department,
Maria Sklodowska-Curie National Research Institute of Oncology,
Gliwice Branch, Wybrzeże Armii Krajowej 15 Str.
44-102 Gliwice, Poland

STATEMENT

I hereby declare that, as co-author of the following publications:

1. Mametov, R.; Sagandykova, G.; Monedeiro-Milanowski, M.; **Gabryś, D**.; Pomastowski, P. "Electropolymerized Polypyrrole-MOF Composite as a Coating Material for SPME Fiber for Extraction VOCs Liberated by Bacteria". *Scientific Reports.* 2023, *13* (1), 1–10

2. Sagandykova, G.; Piszczek, P.; Radtke, A.; Mametov, R.; Pryshchepa, O.; **Gabryś, D.;** Kolankowski, M.; Pomastowski, P. Silver Nanostructured Substrates in LDI-MS of Low Molecular Weight Compounds. *Materials (Basel).* 2022, *15* (13)

Being a part of the doctoral dissertation of MSc Radik Mametov, I declare that my contribution was to collect the samples from the patients, participation in conceptualization and investigation, interpretation of the obtained data, review and editing of the manuscripts.

MD, PhD, MSc Dorota Gabryś, prof. NIO-PIB

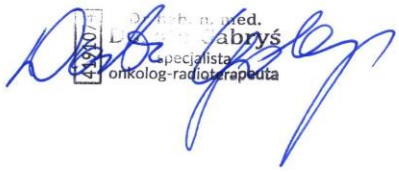

Toruń, 2024

PhD Fernanda Monedeiro

Department of Chemistry, Faculty of Philosophy,

Sciences and Letters of Ribeirão Preto,

University of São Paulo, Av. Bandeirantes 3900,

Ribeirão Preto, 14040-901, Brazil

STATEMENT

I hereby declare that, as co-author of the following publications

1. Radik Mametov, Gulyaim Sagandykova, **Fernanda Monedeiro**, Aleksandra Florkiewicz, Piotr Piszczek, Aleksandra Radtke and Pawel Pomastowski. Metabolic Profiling of Bacteria with the Application of Polypyrrole-MOF SPME fibers and Plasmonic Nanostructured LDI-MS Substrates. *Scientific Reports.* (2024) 14:5562

   Being a part of the doctoral dissertation of MSc Radik Mametov, I declare that my contribution was data analysis and interpretation, writing of the part of the original draft, review & editing, participation in investigation, validation.

Fernanda F. Monedeiro

UNIWERSYTET
MIKOŁAJA KOPERNIKA
W TORUNIU
Interdyscyplinarne Centrum
Nowoczesnych Technologii

Toruń, 2024

PhD Aleksandra Florkiewicz

Centre for Modern Interdisciplinary Technologies

Nicolaus Copernicus University in Toruń

Wileńska 4, Toruń, 87-100

STATEMENT

I hereby declare that, as co-author of the following publications:

1. Mametov, R.; Sagandykova, G.; Monedeiro, F.; **Florkiewicz, A.;** Piszczek, P.; Radtke, A.; Pomastowski, P. Metabolic Profiling of Bacteria with the Application of Polypyrrole-MOF SPME fibers and Plasmonic Nanostructured LDI-MS Substrates. *Scientific Reports.* (2024) 14:5562

   Being a part of the doctoral dissertation of MSc Radik Mametov, I declare that my contribution was isolation and identification of bacteria, lipids extraction and writing of the part of the original draft of paper, participation in review & editing.

15.04.2024
A. Florkiewicz

UNIWERSYTET
MIKOŁAJA KOPERNIKA
W TORUNIU
Interdyscyplinarne Centrum
Nowoczesnych Technologii

Toruń, 2024

MSc Radik Mametov

Centre for Modern Interdisciplinary Technologies

Nicolaus Copernicus University in Toruń

Wileńska 4, Toruń, 87-100

STATEMENT

I hereby declare that, as co-author of the following publications being a part of my doctoral dissertation, I declare below that my contribution was as follows:

1. **Mametov, R.**; Sagandykova, G.; Monedeiro-Milanowski, M.; Gabryś, D.; Pomastowski, P. "Electropolymerized Polypyrrole-MOF Composite as a Coating Material for SPME Fiber for Extraction VOCs Liberated by Bacteria". *Sci. Rep.* 2023, *13* (1), 1–10.

   I have carried out all experiments regarding synthesis and characterization of the composite material and fabrication of the SPME fibers, their application for standard solutions and collection of VOCs emitted by bacteria. I prepared conceptualization of the study and experimental design. I have written and prepared the original draft of the publication, edited draft and prepared answers for reviewers comments, submitted paper for the publication. I was responsible for the finding acquisition & project administration, providing the resources for the study.

2. Sagandykova G., Pryshchepa O., Rafinska K., **Mametov R.**, Madajski P., Pomastowski P. "LDI-MS performance of gold nanostars as an inorganic matrix for low molecular weight analytes" International Journal of Mass Spectrometry, 478, 116872 (2022).

   I have carried out the synthesis of gold nanostars, participated in conceptualization & experimental design, data collection, analysis and interpretation, visualization, writing of the original draft, review & editing, preparation of the answers for reviewers' comments. I was responsible for cutting and polishing of stainless steel substrates, fabrication of the spots and design of the template for spots' fabrication.

3. Sagandykova, G.; Piszczek, P.; Radtke, A.; **Mametov, R.**; Pryshchepa, O.; Gabryś, D.; Kolankowski, M.; Pomastowski, P. Silver Nanostructured Substrates in LDI-MS of Low Molecular Weight Compounds. *Materials (Basel).* 2022, *15* (13).

   I was responsible for cutting and polishing of stainless steel substrates, fabrication of the spots and design of the template for spots' fabrication, cleaning of the substrates prior to synthesis.

I participated in design of the experiments, data collection and analysis, writing of the original draft, editing, preparation of the answers for reviewers' comments.

4. **Mametov, R.;** Sagandykova, G.; Monedeiro, F.; Florkiewicz, A.; Piszczek, P.; Radtke, A.; Pomastowski, P. Metabolic Profiling of Bacteria with the Application of Polypyrrole-MOF SPME fibers and Plasmonic Nanostructured LDI-MS Substrates. *Scientific Reports.* (2024) 14:5562
I have performed synthesis, characterization and fabrication of the SPME fibers, extraction of VOCs emitted by bacteria, chromatograms integration and interpretation. I participated in the experiment for curation of the bacterial growth curves and interpretation of data. I was responsible for conceptualization of the study and experimental design, writing of the original draft, summarization of results and formation of conclusions, editing and preparation of the answers for reviewers' comments, preparation for submission and submission of the manuscript. I was responsible for funding acquisition & project administration, providing the resources for the study.

15.04.24